On an approach to provide space diversity to an ultra wideband time hopping pulse position modulated wireless communication system

Peter James Vial
University of Wollongong

On an approach to provide space diversity to an Ultra Wideband Time Hopping Pulse Position Modulated wireless communication system.

Doctor Of Philosophy (PhD)

from

UNIVERSITY OF WOLLONGONG

by

Peter James Vial,
BE (Hons 2 (i)), ME (Hons), DipEd

School of Electrical, Computer and Telecommunications Engineering

2009

Abstract

The hypothesis question, which is addressed in this PhD dissertation, is how to use two transmission antennas in an Ultra Wide Band Time Hopping Pulse Position Modulation system to take advantage of space diversity in such a way as to not significantly degrade the communication link compared to using only one transmit antenna. In answering the hypothesis question, this dissertation proposes a novel technique, based on Space Time Spreading, to allow an Ultra Wideband Time Hopping Pulse Position Modulation system to obtain full advantage from space diversity using two transmit antennas and one receive antenna, showing how such a Multiple Input Multiple Output system is designed. This is achieved with the added advantage of transmitting the same two symbols simultaneously on each antenna link. This means that for the proposed system, should a fade occur on one of the two antenna links, the two symbols transmitted will still be received with a slight increased cost in average Bit Error Rate (BER) performance as Signal to Noise Ratio (SNR) or measured E_b/N_o is increased.

Results are first provided for wideband Space Time Spreading in the presence of Multiple Access Interference when using two, four and eight transmit antennas. A system is developed in simulation using modules provided by MATLABs Simulink program. It is then shown that using low correlation Wysocki spreading code set results in an improved BER performance compared to the more often used Walsh Hadamard spreading code set. A Simulink Ultra Wide Band Pulse Position Modulation Single Input Single Output system is developed and validated against published peer reviewed material. This is then modified to consider the use of Space Time Spreading in a Single Input Single Output system and it is shown that improved performance over an Ultra Wide Band Pulse Position Modulated Single Input Single Output is possible. It is also shown that this improvement allows the transmission of two symbols in the same time that the original system only transmits one symbol.

The thesis also investigates a system which uses two transmit antennas but a hard decision is made on a chip by chip basis. Its performance, compared to an equivalent Single Input Single Output comparable system, is suboptimal. It does, however, have the advantage that it sends two symbols in the same time that the equivalent Single Input Single output Ultra Wide Band Pulse Position Modulation system sends one, and its implementation is simpler to codify. Also, it has the feature that both symbols are sent simultaneously on each antenna link.

The simulator is then modified to make a hard decision after all chips of a spreading sequence for two antennas are received and it is shown that this system, in simulation and analysis, has a similar performance to that for a comparable Single Input Single Output system with the added advantage that both antenna links send the same two symbols simultaneously. It is further demonstrated in simulation and analysis that such systems can be affected by Multiple Access Interference. In addition, it is shown, using simulation, that the choice of spreading sequence set does have an impact on the average BER performance of the proposed Space Time Spreading Time Hopping Ultra Wideband Pulse Position Modulation system. The thesis finally proposes some extensions using the developed simulator which are outlined in future work.

Statement of Originality

I Peter James Vial swear that this thesis, where attribute is not given to others, is solely my work and my research and no others. I personally wrote all the code or made modifications to existing code where attribution is provided via the codes comments, developed the proposed systems and undertook all associated studies including the analysis of the proposed system.

Signed: Mr Peter James Vial

Dated: 21st of May 2009

Acknowledgements

I wish to acknowledge all my supervisors who have assisted me in this work over the course of my studies. In particular Professor Tad Wysocki who started me on this path and who was my direct supervisor for most of my candidature for a PhD, Dr Beata Wysocki who helped and assisted with the published material and provided encouragement, Dr David Stirling for assisting at the end of my candidature with Dr Montse Ros, and my other two co-supervisors Dr Philip Ciufo and Professor Salim Bouzerdoum who were involved for brief periods of time in my candidature. I also acknowledge the assistance provided in Buffalo (New York, USA) by Dr Kylie Keshav (aka MacKenzie) who advised me on aspects of my PhD layout and who suggested the use of Reference Manager for the referencing as an alternative to that provided directly by Word 2007 (which does not provide correct IEEE referencing).

I would also like to acknowledge my family and friends who provided assistance while I undertook this study. My father, Dr Kenneth J Vial, who encouraged me to pursue academic matters when he was alive. My mother, Dr Denise Wallis, who has also encouraged me in my studies over these many years. My parents in law, Marie and Brian Bourke who have provided support and assistance when needed, especially with my children as they have grown up. My children John Francis Steven Vial and Alanna Heather-Therese Vial who have provided many hours of entertaining conversation. Finally, in particular, my wife Mrs Kathrine Anne Vial who provided loving support and encouragement while I made a significant contribution to the area of UWB communications. Without Kathrine this thesis would not have been possible.

Peer reviewed Publications of this thesis

[1] P. Vial, I. Raad, and T. Wysocki, "On the effect of adjacent sector Multiple Access Interference on Space Time Spreading Systems," *in Conference Proceedings of DSPCS'03,* Coolangatta, Queensland, Australia,pp. 543-548,December, 2003.

[2] P. J. Vial, I. S. Raad, and T. A. Wysocki, "On the Design and Validation of a Space Time Spreading System using Simulink," *in Conference Proceedings of the 14th International Czech-Slovak Scientific Conference Radioelektronika,* Bratislava, Slovak Republic,pp. 480-483,April, 2004.

[3] P. Vial, B. Wysocki, I. Raad, and T. Wysocki, "Space time spreading with modified Walsh-Hadamard sequences," *in Conference Proceedings of the Eighth IEEE International Symposium on Spread Spectrum Techniques and Applications,* Sydney, Australia,pp. 943-946,August, 2004.

[4] P. Vial, B. Wysocki, and T. Wysocki, "An Ultra Wideband Simulator Using MATLAB / Simulink," *in Conference Proceedings of DSPCS'05 & WITSP'05,* Noosa Heads, Queensland, Australia, December, 2005.

[5] P. Vial, B. Wysocki, and T. Wysocki, "Direct Sequence Modified Time Hopping PPM over Ultra Wideband S-V Channel," *in Conference Proceedings of the 5th Workshop on the Internet, telecommunications and Signal Processing (WITSP'06),* Hobart, Tasmania, Australia,December, 2006.

[6] P. Vial, B. Wysocki, and T. Wysocki, "Optimal receiver for Space Time Spreading across a Time Hopping PPM over Ultra Wideband Saleh-Valenzuela MIMO Channel," *in Conference Proceedings of the International Conference on Signal Processing and Communication Systems, 2007 (ICSPCS '2007),* Gold Coast, Queensland, Australia,pp. 56-61,December, 2007.

[7] P. Vial, B. Wysocki, and T. A. Wysocki, "Non-optimal receiver for space time spreading across a Time Hopping over Ultra Wideband PPM," *in Conference Proceedings of the third International Symposium on Communications, Control and Signal Processing, 2008 (ISCCSP 2008),* Malta,pp. 990-993,March, 2008.

Submitted to Journal for peer reviewed Publication

P. Vial, B. Wysocki, M. Ros, T.A. Wysocki, and D. Stirling, "On the effect of Multiple Access Interference in a Space Time Spreading Time Hopping PPM UWB System", submitted to IEEE Transactions on Wireless Communications on the 5th of February 2009.

Table of Contents

List of Figures

List of Tables

List of Abbreviations

AWGN	Additive White Gaussian Noise
BER	Bit Error Rate
BPSK	Binary Phase Shift Keying
BS	Base Station
CDF	Cumulative Distribution Function
CDMA	Code Division Multiple Access
CFO	multicarrier offsets (carrier frequency offsets)
CSI	Channel State Information
DS	Direct Sequence
DSP	Digital Signal Processing
FCC	Federal Communications Commission
FET	Field Effect Transistor
FFT	Fast Fourier Transform
FH	Frequency Hopping
H-R	Hurwitz-Radon
ICI	Inter Carrier Interference
IEEE	Institution of Electrical and Electronic Engineers
IFFT	Inverse Fast Fourier Transform
ISDN	Integrated Services Digital Network
ISI	Inter-symbol Interference
IS-OFDM	Interference Suppressing OFDM
I-UWB	Impulse based Ultra Wideband
LAN	Local Area Network
MAC	Medium Access Control
MAI	Multiple Access Interference
M-ALOHA	Multi-channel ALOHA
Mcps	Mega chips per second
MFSK	M-ary Frequency Shift Keying
MIMO	Multiple Input Multiple Output
MMRC	Maximal Ratio Receiver Combining
MOFDM	Multiband OFDM
M-PSMA	multi-channel pulse sense multiple access
MRC	Maximum Ratio Combining

MS	Mobile Station
MUI	Multiple User Interference
NLOS	Non Line of Sight
OFDM	Orthogonal Frequency Division multiplexing
OFDMA	Orthogonal Frequency Division Multiple Access
OOK	On-off keying
OTD	Orthogonal Transmit Diversity
PA	Power Amplifier
PAM	Pulse Amplitude Modulation
PAPR	Peak to Average Power Ratio
pdf	probability density function
PG	Processing Gain
PPM	Pulse Position Modulation
PRF	Pulse Repetition Frequency
PRI	Pulse Repetition Interval
PSK	Phase Shift Keying
QPSK	Quadrature Phase Shift Keying
RTW	Real Time Workshop (from MATLAB/Simulink)
SDMA	Space Division Multiple Access
SER	Symbol Error Rate
SINR	Signal in Noise Ratio
SISO	Single Input Single Output
SNR	Signal to Noise Ratio
ST	Space Time
STS	Space Time Spreading
SV	Saleh-Valenzeula
TH	Time Hopping
UWB	Ultra Wideband
WCDMA	Wideband Code Division Multiple Access
WSN	Wireless Sensor Network

Chapter 1: Introduction

1.1 Introduction

The last twenty years in wireless communications systems have seen advances in both coding gain (for example turbo and Gallagher codes) and in the use of space diversity in the form of multiple antennas. These systems have been outlined in the literature and formed into reference texts on the application of these signal processing techniques to wireless communication systems [1-5]. The last ten years have seen the development and interest in Ultra Wideband (UWB) systems. Particularly, these systems are for low power communications in a small room or offices with non-line of sight wireless communication. These systems, potentially, will provide access speeds of the order of tens of megabits per second using short pulses which span an ultra large segment of the available frequency bandwidth [6].

The application of space diversity using multiple transmit and receive antennas has been well developed over the last two decades (see Chapter 2). It is, however, unclear how these techniques could be applied to the Ultra Wideband systems being proposed in the early 21st century to allow the use of multiple antennas. When using pulse based systems to communicate wirelessly, results reported in [7] indicated that the channel had clusters of arriving rays separated by small time intervals that were random in nature. To handle such situations Rake receivers were developed (for example see [3]). These gathered some or all of the energy of the arriving rays. They use perfect knowledge or good estimates using pilot signals of each arriving rays known time of arrival at the receiver, its location in time relative to some synchronised time point, combined with the amplitudes of the arriving rays. This allows demodulation of the encoded symbols. If orthogonal spreading codes are used, the channel gains are used in the Rake receiver over the entire number of chips for each spreading code that represents one symbol. For example, in this thesis spreading codes with 128 chips and 32 chips are used.

1.2 Research Questions

This thesis attempts to answer the first research question of how to design an UWB Time Hopping (TH) pulse based system employing the non-linear pulse position modulation (PPM) single input single output (SISO) system to one which uses two transmit antennas and one receive antenna (that is, a multiple input multiple output (MIMO) system) and transmit two symbols in the same time that the equivalent SISO system uses to transmit one symbol. This provides a space diversity gain over the equivalent SISO system. This enhances the utility of the physical UWB wireless communication transmission by providing diversity on multiple transmission paths where a major fade on one antenna link is unlikely to occur at the same time as a major fade on the other antenna link. In the case of UWB this is further enhanced by the high coding gain associated with the relatively large number of resolvable multipath available in each antenna links channel realisations.

Further, in the second research question it is asked how to design this system in such a way which does not significantly degrade the overall system performance given the constraint of the large number of multipath signals observed in an UWB PPM based communication channel. The answer to both these research questions is the application of Space Time Spreading (STS) to the UWB PPM channel when using two transmit antennas as the signaling on each antenna in terms of the time positioning of each transmitted pulse will always be different.

An initial contribution to the first research question of how to use multiple antennas in an UWB PPM system (though they did not use Time Hopping which serves the purpose of providing a mechanism for multiple users and smoothing significantly the UWB PPM spectra which would be impulsive without the use of Time Hopping) was provided by Yang and Giannakis [8]. Yang and Giannakis [8] tried to provide a system which could incorporate the diversity provided by using two transmit antennas instead of a single one. Many of the results relevant to this thesis are reviewed in Section 2.10 which examines SISO and MIMO based UWB PPM systems. However, their MIMO systems uses only one spreading code (it is shown that this is the case in Section 8.2), with the other MIMO system proposed using each antenna in different symbol periods to send the same symbol. The techniques provided in [8] when combined with the Space Time Spreading technique outlined in [9] by Hochwald et al.

provides a way of sending two symbols simultaneously. Further, the same two symbols are coded in such a way that they are sent on both antennas over the same period of time. The advantage of this approach is that if one of the antennas does suffer a deep fading event, it is highly unlikely that the other antenna will simultaneously experience another deep fading event, and the use of Maximum Ratio Combining (MRC) [4] will still be able to recover the transmitted symbols, but at the expense of a moderate increase in instantaneous Bit Error Rate (BER) or in other words with a reduced instantaneous Signal to Noise Ratio (SNR).

The approach outlined in this thesis to answer the question of how to use multiple antennas in a Time Hopping UWB PPM system is founded on the fact that with the Space Time Spreading technique neither antenna will have the same position delay to transmit at the same instant in time. This was an observation that was only possible as a result of implementing the studies undertaken in Chapter 3 and Chapter 4, where this relationship was first noted. This means that, unlike if M-ary PPM were employed across two or more antennas (see below), the chances are that (even if the channels were highly correlated) their multipath arriving rays at the receiver would be unlikely to coincide in time, allowing the Rake receiver to distinguish between the two transmissions. The Rake receiver would then use the perfect channel state information (CSI) available within the simulations (where in a realisable systems pilot signals would be deployed to estimate these CSI), to demodulate the transmitted symbols. This contrasts to the MIMO UWB system which applies M-ary PPM between two (or more) transmit antennas where each pulse is coded to its location in time and on which individual antenna each UWB pulse is transmitted. In the M-ary PPM system it is quite possible that the pulses on each antenna are transmitted at the same time epoch and then it is required that the channels be uncorrelated for the Rake receiver to distinguish between the arriving UWB pulses multipath. In addition, the STS UWB PPM system encodes two symbols on each antenna link whereas the M-ary PPM system would encode one symbol on each antenna link.

1.3 Contributions of this thesis

The major contributions of this thesis are the presentation of new techniques which allows Ultra Wideband to effectively use the space diversity provided by deploying two transmit antennas in a environment which has a large number of multipath. This diversity allows the

transmission of two symbols or bits in the same time that a SISO based system would only transmit one symbol or bit. In this thesis multiple spreading codes are employed, as the Space Time Spreading technique requires two spreading codes per transmission; however these two spreading codes are used in such a way that they permit the transmission of two bits of data. These two bits of data could be from the same data stream (odd or even) or from different data streams depending on the application. The contribution and location in the thesis of these contributions are as follows:

- The construction of a Space Time Spreading simulator using MATLAB for the case of two, four and eight transmit antennas, the description of the designed simulation is provided in Chapter 3 beginning on page 79.
- Using the constructed Space Time Spreading simulator, an investigation of the effect of multiple access interference (MAI) caused by multiple un-synchronised Space Time Spreading sources which may arise in a system using Space Time Spreading as the wireless communication link of a cellular system deploying sectorised segments. This is provided in Section 4.3 page 97.
- Results of an investigation into the effect on the constructed Space Time Spreading system when deploying low correlation codes and have shown that the use of such codes reduces the effect of Multiple Access Interference in terms of a significant reduction in the BER performance of the system as more interferers are added. This is provided in Section 4.7 on page 101.
- The construction and validation of a SISO based UWB PPM system using Time Hopping in Simulink which is described in Chapter 5 starting on page 105 using the Saleh-Valenzuela (SV) multipath channel.
- Presentation of the discovery that the Saleh-Valenzuela multipath channel can cause bit errors to occur when there is no noise present and outlined the causation of this in the simulator. This effect has not been reported in any other study. It is provided in Section 5.5 on page 112.
- A new UWB communications system is proposed, designed and validated for a modified Direct Sequence (DS) TH UWB PPM SISO system that uses the Space Time Spreading schema and three pulse positions and it is shown that it has an improved BER performance over an equivalent system employing two pulse positions. It also transmitted two symbols in the same period that the compared SISO system transmits one symbol. This is provided in Chapter 6 starting on page 119.

- A new UWB communications system is proposed, designed and validated for a MIMO based UWB PPM TH non-optimal system that incorporated a chip by chip decision process using Space Time Spreading which showed that MIMO UWB PPM systems were realisable and that for the performance was comparable, but not an improvement on the corresponding SISO system. An advantage is it transmitted two symbols in the same period that the compared SISO system transmits only one symbol. The demodulator for such a system, however, has less complexity than one which is used to demodulate over an entire symbol period using perfect knowledge of the CSI. The designed system is provided in Chapter 7 starting on page 128.
- A new UWB communications system is proposed, designed and validated for a MIMO based Space Time Spread TH UWB PPM system which used a demodulator that considered all the CSI over an entire symbol period (optimal) and the received signals from both antennas in the decision metric, implementing Maximum Ratio Combining (MRC). This system showed an improved BER performance compared to the corresponding SISO system and provided two symbols in the same period that the SISO system would transmit one. It also has the advantage that two symbols are transmitted in each of the separate antenna channels. If one of these multipath channels experienced a significant fade the other channel would still have both transmitted data bits which could be demodulated but at the expense of a higher BER. The designed system is provided in Chapter 8 starting on page 140.
- Results of an investigation into the effect of Multiple Access Interference on the MIMO based Space Time Spread TH UWB PPM system and found that when there were five and ten interferers that in the case of both the Walsh-hadamard and the low correlation spreading codes employed that the BER performance was degraded. The use of low correlation codes for these systems appeared to have no significant effect, compared to the Walsh-Hadamard codes. However, it was noted that marginal improvement is possible using some low correlation code sets in comparison to that attained using Walsh Hadamard spreading sequences. It was also noted that randomly choosing any spreading code sets can provide very poor BER performance as the most degraded BER performance was found to be for the randomly selected spreading sequence set. These results are shown in Chapter 9 starting on page 152.

- A model is developed and analysed for the STS-TH-UWB-PPM system with and without the presence of Multiple Access Interference. The analysis and resultant theoretical plots are provided in Chapter 10 starting on page 174.

1.4 Outline of this thesis

Chapter 2 provides a review of the literature pertaining to MIMO systems and Space Time coding, and also Ultra Wideband pulsed systems. In particular, it examines the works on Space Time Spreading which [9] provides and on Ultra Wideband analog pulsed waveforms, as well as the Saleh-Valenzuela channel upon which the Simulink simulations of this thesis are based.

Chapter 3 and Chapter 4 present the simulations of Space Time Spreading validating them against results found in [9] and using them to investigate the effect of Multiple Access Interference. In Chapter 4 it is shown that mitigation against the effects of Multiple access interference is achieved by employing a low cross correlation spreading code sequence with improved properties compared to the more commonly employed Walsh-Hadamard orthogonal spreading sequences.

Chapter 5 provides a simulator of a UWB PPM system which is validated against results found in [8]. Further, Chapter 5 outlines an error mechanism which can occur in using the Saleh-Valenzuela multipath channel model.

Chapter 6 provides results for a modified three pulse position SISO system which is designed based on Space Time Spreading and shows improved performance over the corresponding two pulse position equivalent SISO system.

Chapter 7 provides a non-optimal MIMO system employing two transmit antennas and show that it has comparable, but degraded, BER performance but is simpler to implement than the system which is presented in Chapter 8.

Chapter 8 presents the MIMO system based on the Space Time Spreading technique where the decoding is done using all the CSI over a symbol period in which case two bits are transmitted simultaneously on both antenna channels.

Chapter 9 undertakes an investigation into Multiple Access Interference and shows that Multiple Access Interference can occur when over five other un-synchronised and overlapping MIMO STS-TH-UWB-PPM systems are encountered in the UWB wireless channel. Further, Chapter 9 investigates the use of different spreading sequence sets and their mitigation effects, if any, in the presence of MAI.

Chapter 10 provides a mathematical model and analysis of the STS-TH-UWB-PPM system with and without MAI sources, confirming the trend of measured results in the simulations of Chapter 9.

In Chapter 11 a summary and conclusion of this research on UWB multiantenna transmission is made together with a perspective on areas of possible future research.

Chapter 2: Literature Review

2.1 Introduction

There have been very many papers and books written in the last ten years on space time coding using different means of transmit and receive diversity. This literature review will outline many of these papers, their contributions and how, in particular, Space Time Spreading (STS) can be extended to the application of MIMO (Multiple Input Multiple Output) to Time Hopping Ultra Wideband Pulse Position Modulation systems.

2.2 MIMO and block orthogonal codes

Ganesan and Stoica [10] apply space time block codes with multiple transmit and receive antennas. Their block codes use the theory of amicable orthogonal designs developed in 1979 [11]. The ideas presented in [10] are very important and promising, building on previous papers which had similar concepts but this paper shows that using such block codes, using the Hurwitz-Radon (H-R) family of matrices in orders m=2, 4, and 8 provides minimal delay and maximum SNR. This work is initially examined in detail as these results are important to the understanding of STS.

Ganesan and Stoica [10] model a system with **m** transmitter antennas and **n** receiving antennas. All antennas are considered isotropic (ie they transmit equal power in all directions), with diversity being achieved through space time coding. The channel is modeled with different channel coefficients and no multipath reflections. These channel coefficients are measured in the presence of Additive White Gaussian Noise (AWGN), where the statistics are well known. The work in [10] considers the use of non-selective Rayleigh fading, which is also known as flat fading. Thus, the system is actually simplified by these assumptions, and in a room or enclosed area with a transmitter and receiver, one would expect that multiple reflections, Inter-Symbol interference phenomena would be experienced. In such situations a Rake receiver would be used, as is explained in [2],[9]. The paper does not have a specific frequency for the transmission, with the analysis being highly mathematically based on the theory of amicable orthogonal designs. This is typical of space time coding techniques.

The paper [10] models each receiver/transmitter pair with their own channel transfer coefficients, which would be expected to be complex with amplitude and phase. This is illustrated in the following diagram taken from [10]:

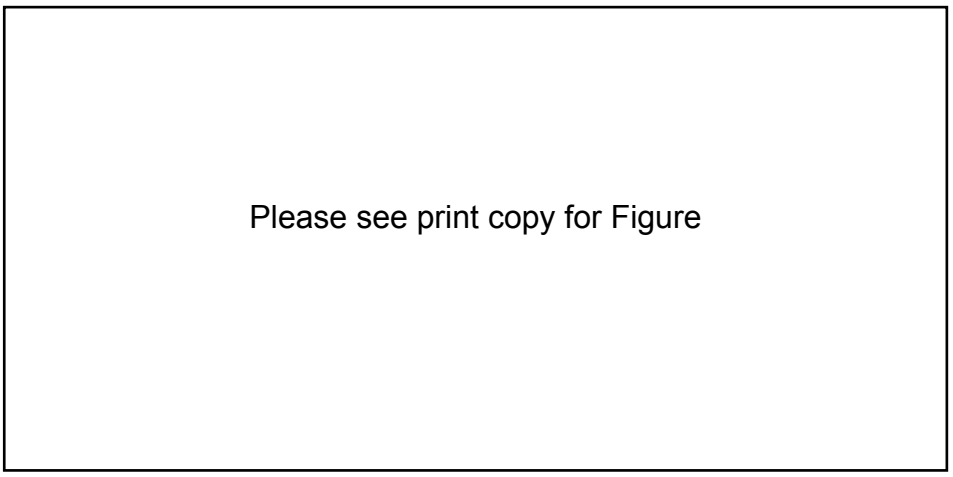

Figure 2.2-1: transmit receive setup for space-time diversity reproduced from [10].

Ganesan and Stoica assume that the coefficients do not change for N symbol periods (which is a function of the unstated frequency) and then are allowed to change to different values that are held constant for the next period of N symbols. Ganesan and Stoica describe this as 'quasi-static fading'. Ganesan and Stoica then transmit a scaled version of the transmitted symbol, s, from each transmitter and this is repeated N times so that they can achieve time diversity. Ganesan and Stoica multiplied each transmitter by a scaling factor, called x_k. This x_k is an $\mathbf{m} \times 1$ vector called the transmit weight vector whose "i^{th} element denotes the scaling factor used by the i^{th} transmitter antenna during the k^{th} symbol period" [10] (obviously k is a number between 1 and N, over which the channel coefficients are held constant). The vector x_k is allowed to change from one symbol period to another, but it is held constant during each symbol period (ie flat fading). They assumed that the receiver used a matched filter and that the channel was corrupted by AWGN. Using this topology Ganesan and Stoica suggest that the output of the matched filter, after appropriate sampling, at the k^{th} symbol period is an $\mathbf{n} \times 1$ vector (since there are **n** receiving antennas) called r_k given by the expression:

$$r_k = Ax_k s + \eta_k, \qquad k = 1,\ldots,N \qquad (2.2\text{-}1)$$

The added term is a noise term, A is an $\mathbf{n} \times \mathbf{m}$ matrix of channel coefficients (called the gain matrix in [10]) and x_k are the individual scaling elements which each transmit antenna is multiplied by.

The paper [10] outlines how linear processing is done at the receiver to limit computational complexity, a sensible approach due to limited capabilities that typically exist in mobile receivers. The receiver then takes a weighted sum of the outputs at different antennas and averages them over the N symbol periods over which the symbol is transmitted the N times. The authors then go on to show that the linear combiner used by the receiver at the k^{th} time period (being a value between 1 and N, inclusive) is an $\mathbf{n} \times 1$ vector where the complex conjugate of the i^{th} element is used to weight the output of the i^{th} antenna at the receiver [10]. This is denoted by the symbol z_k, and the decision is then based on the observation given by the expression:

$$D_{avg} = \frac{1}{N} \sum_{k=1}^{N} z_k^* [Ax_k + \eta_k] \qquad (2.2\text{-}2)$$

where '*' is used to indicate complex conjugate of the $\mathbf{n} \times 1$ vector z_k. Clearly, the decision is based on both space coding and time diversity considerations.

The paper [10] goes on to show how the SNR is maximal for the linear combiner by choosing the x_k and the z_k such that:

$$\frac{\left| E\left\{ z_k^* A x_k \right\} \right|^2}{E\left\{ z_k^* z_k \right\}} \qquad (2.2\text{-}3)$$

is a maximum, and they show that this is a maximum if the following equality is satisfied:

$$z_k = \alpha A x_k \qquad (2.2\text{-}4)$$

with any scalar factor which does not include zero. This is the optimum weight vector for the receiver. They go on to show that the choice of alpha does not affect the maximum value of the SNR. It is stated that in order to implement the optimal linear combiner at the receiver requires perfect knowledge of the channel at the receiver end, which can be estimated using pilot signals but appears to be known perfectly in many simulation based studies (including in this thesis).

Further description of the design of the transmit weight vector, x_k, is provided but under the condition that the transmitter does not know the channel and thus the decision is made to allow the transmitter to transmit the signal in all directions. A reasonable way to do this is to constrain the maximum eigenvalue of $R_{xx} = E\{x_k z_k^*\}$ to unity. They then use some well known relationships to show that under this constraint, but using R_{xx}=I, the maximum SNR is given by:

$$SNR_{\max} = N\frac{tr(A^*A)}{\sigma^2}E_s \qquad (2.2\text{-}5)$$

It is then pointed out that if the constraint is changed so that the maximum eigenvalue is now constrained to α, where α is a positive real number, then the SNR maximum becomes:

$$SNR_{\max} = \alpha N\frac{tr(A^*A)}{\sigma^2}E_s \qquad (2.2\text{-}6)$$

Looking at the receiver and, forming a matrix expression for the received signal as:

$$R = AXs + \eta \qquad (2.2\text{-}7)$$

where R is the received matrix which has the size $\mathbf{n} \times \mathbf{N}$, A is the channel coefficient matrix (no multipath) of size n by m, X is the beamforming matrix of size m by N which is formed by stacking the N vectors x_k, each of length m, on top of each other, s is the transmitted symbol and the last term is the noise matrix of size n by N.

The receiver uses optimal linear filtering which is based on the statistic:

$$D = tr(X^*A^*R) = tr(A^*AXX^*)s + tr(X^*A^*\eta) \qquad (2.2\text{-}8)$$

which is said to have a maximum SNR when $XX^* = I$, where I is the $\mathbf{m} \times \mathbf{m}$ identity matrix. The conclusion is that when orthogonal codes are used with optimal linear filtering at the receiver the best SNR is achieved. It is shown that the SNR in the presence of AWGN is:

$$SNR = \frac{tr(A^*A)}{\sigma^2}E_s \qquad (2.2\text{-}9)$$

and since the elements of A are independent and identically distributed (iid) complex Gaussian random variables it is pointed out that the SNR is a chi-squared random variable with **2mn** degrees of freedom, resulting in a diversity of order **mn**.

To compensate for the fact that time diversity is used, rather than send only one symbol repeatedly N times, they send N symbols, s_1 through s_N simultaneously. Thus each symbol s_i has a beamforming matrix X_i associated with it. With this setup the receiver has N parallel detectors with the i^{th} detector getting the following:

$$D_i = tr(A^* A X_i X_i^*) s_i + \sum_{j=1, j\neq i}^{N} tr(A^* A X_i X_j^*) s_j \qquad (2.2\text{-}10)$$

Clearly, with the careful choice of X_i, it may be possible to remove the second term and leave the desired first term. The paper suggests that the appropriate way to do this is to choose $X_i X_i^* = I$, to achieve maximum SNR but also choose $X_i X_j^* = -X_j X_i^*$, $i \neq j$ which results in $tr(A^* A X_i X_j^*) s_j$, $i \neq j$ being imaginary, and the desired output can be recovered by simply obtaining the real part of the complex component D_i [10].

The situation is such that the system has N different symbols being transmitted over N symbol periods giving a unity data rate. Also, while N can be equal or greater than m, a minimal delay design would, in fact, have N equal to m. The proposed solution for the X_i is to use an amicable orthogonal design composed of only three elements, 1, 0 and -1. This also reduces the complexity of the detector for this system. The theory for amicable orthogonal designs states that there exists an $\mathbf{m} \times \mathbf{m}$ matrix set of orthogonal submatrices which have the desired properties. It however, states that there are only m-1 such matrices, so the authors cleverly suggest that the $\mathbf{m} \times \mathbf{m}$ unity matrix I can be used as the m^{th} matrix to make a set of $\mathbf{m} \times \mathbf{m}$ beamforming matrices with the desired properties. The problem with this solution is that using H-R matrices, full rate solutions are known to only exist for m=2, 4 and 8. This limits the usefulness of the maximal SNR with minimum delay solution they propose.

Further analysis is provided in [10] for non minimal designs (where N>m), using further results from amicable orthogonal designs and also consider complex symbols, which are sent over a period of 2N. The scheme proposes the sending of Real and imaginary components separately as in the real symbol case, recovering the information at the receiver, reforming the complex symbol and this reformed symbol is used to detect the sent complex symbol. It is shown that such a scheme is better in terms of decoding delay compared to a previously

proposed technique which had the same rate, ½, where they could not start decoding until all 2N terms were received [12].

Table 2.2.1: A summary of the schemes for Real and Complex symbols for different values of m, adapted from a similar table shown in [10].

Type of Symbols	m	N	Date Rate
Real	2,4, or 8	2, 4, or 8	1
	3	4	1
	5,6, or 7	8	1
	m>8	N chosen such that $m \leq \rho(N)$	1
Complex	2	2	1
	3 or 4	4	¾
	m>4	N chosen such that $m \leq \rho(N)$	½

They investigate if a complex minimal delay, full rate solution exists, and using the theory of amicable orthogonal designs, once again with H-R matrices [11], they find that the only case which can exist is m=2. They further investigate if it is possible to achieve rates higher than ½ using complex symbols. Indeed, it was discovered that a ¾ rate solution for m=4 with complex symbols exists. The paper also gives the set of orthogonal matrices which accomplishes this (one of which is again the identity matrix). The paper leaves as an open question for further research whether it is possible to find a set of codes with higher data rates greater than ¾ for m=3, 4 and greater than ½ for m>4 if they let N>m [10]. Table 1 in this paper details the schemes which it proposes in a summarised form, and it is reproduced here as Table 2.2.1.

2.3 MIMO and Block coding with Quasi-orthogonal codes

Jafarkhani [13] proposes a hybrid space time block coding which uses pairs of codes which are orthogonal to each other. For this he terms the word quasi-orthogonal. Thus, instead of

making a decision based on a symbol by symbol case, it is proposed that quasi-orthogonal relationships are used and a decision is made on pairs of symbols, that are chosen to maximise their distance from each other but only some of which are in fact orthogonal in space and time (space-time). They do this by having pairs of columns orthogonal to each other rather than having each column orthogonal, thus leading to an increased transmission rate at the cost of lower diversity. The paper [13], through simulation, looks at the implementation of these quasi-orthogonal codes and compares them to space time block codes which use full diversity but at partial transmission rate. This section elucidates the contribution from [13].

Once again the channel is considered quasi-static, with the channel coefficients changing only after a time period T in which K symbols are transmitted. Using a signalling constellation of order 2^b and N transmit antennas, the encoder takes Kb bits with K the number of variables in the transmission matrix. At time t, where t is a value between 1 and T inclusive, the n^{th} element of the t^{th} row is transmitted on all N antennas. This is denoted C_{tn} in [13] which is an element of the resultant matrix C. The transmission matrix, G, is composed of indeterminates labelled x_k, where k is from 1 to K. The relationship for G is then a $T \times N$ transmission matrix such that :

$$G^* G = \left(|x_1|^2 + \cdots + |x_K|^2 \right) I \qquad (2.3\text{-}1)$$

Where here, * , indicates the Hermitian of G and I is the $N \times N$ identity matrix. The elements of G are linear combinations of the indeterminates and their complex conjugates which will thus mean that encoding only requires linear processing.

The received signal at the receiver antenna m at time t is thus given by the transmitted constellation, denoted C here, times the complex path gain, here termed $\alpha_{n,m}$ (from antenna n to antenna m) plus a noise term (assumed gaussian with complex variance N/(2 SNR)):

$$r_{t,m} = \sum_{n=1}^{N} \alpha_{n,m} C_{tn} + \eta_{t,m} \qquad (2.3\text{-}2)$$

The paper [13] assumes perfect channel knowledge (which can be estimated using pilot signals) and computes the decision metric:

$$\sum_{m=1}^{M}\sum_{t=1}^{T}\left|\mathrm{r}_{\mathrm{t,m}}-\sum_{n=1}^{N}\alpha_{\mathrm{n,m}}G_{tn}\right|^{2} \qquad (2.3\text{-}3)$$

which is done over all indeterminates $x_k=s_k$ elements of A which denotes a signal constellation of size 2^b ($s_1 \ldots s_K$). Taking the Alamouti scheme [14] and using a construction technique to create a 4 by 4 space time block code for N=T=K=4 they obtain the following space time block code:

$$A = \begin{pmatrix} x_1 & x_2 & x_3 & x_4 \\ -x_2^* & x_1^* & -x_4^* & x_3^* \\ -x_3^* & -x_4^* & x_1^* & x_2^* \\ x_4 & -x_3 & -x_2 & x_1 \end{pmatrix} \qquad (2.3\text{-}4)$$

They point out that the minimum rank of matrix $A\left(s_1-\tilde{s}_1, s_2-\tilde{s}_2, s_3-\tilde{s}_3, s_4-\tilde{s}_4\right)$ is 2, and thus a diversity of 2M is achieved when the transmission rate of the code is 1 (R=1). They then define a new variable ν_i, where i is from 1 to 4 and represents the i^{th} column of A, and using the inner product which is column i times column j's complex transpose that the following is true:

$$\langle \nu_1, \nu_2 \rangle = \langle \nu_1, \nu_3 \rangle = \langle \nu_2, \nu_4 \rangle = \langle \nu_3, \nu_4 \rangle = 0 \qquad (2.3\text{-}5)$$

It is stated that "the subspace created by ν_1 and ν_4 is orthogonal to the subspace created by ν_2 and ν_3" [13]. This allows the suggestion that the minimisation of the detection statistic, using a maximum likelihood decision metric, is achievable by simply minimising the terms $f_{14}(x_1+x_4)$ and $f_{23}(x_2+x_3)$ independently as they are independent of each other. This is done by selecting the pair (s_1, s_4) which minimises $f_{14}(x_1+x_4)$ and the same for the other term. Now pairs of transmitted symbols are used which gives the quasi-orthogonal flavour to this space time code.

Jafarkhani [13] then proceeds to present a ¾ rate 8×8 transmission matrix using a similar formation. The simulations of these schemes are performed using only one receive antenna.

They use four transmit antennas and use the ½ full diversity orthogonal code from [13], uncoded 4-PSK (Phase Shift Keying) and the proposed rate one quasi-orthogonal scheme. The plotted results show that for high SNR and thus low BER, full diversity is the better choice whereas for very low SNR and high BER it is better to have full transmission rate. That is, there is a cross over region at about 18dB when using space time block codes of 3 bits per second per Hertz, and about 22dB when using space time block codes of 2 bits per second per Hertz. There is no comparison to full rate full diversity as it is stated bluntly that no advantage can be gained (so this excludes 1 bit per second per Hertz). In the paper Hamid indicates that there is an slight increase in decoding complexity for quasi-orthogonal coding (since it is done in pairs). They also indicate that they expect that an open problem for future research is determination of the maximum possible rate for a given number of transmit antennas using quasi-orthogonal space time block codes. They finally "conjecture that the rate of a complex code which provides half of the full diversity and works with pairs of symbols cannot be more than one" [13].

2.4 Alamouti on simple transmit diversity

Alamouti [14] proposes a simple two transmitter and one receiver space time setup. This paper has been referenced by many papers within the last ten years as a seminal contribution, so it has had a major influence on the area of space time coding. Thus it seems that a review of its findings should be included in any literature review of this area. The idea behind the paper is that often there is only one receiving antenna on the mobile station, but two transmitting antennas are available for diversity on the fixed base station. The paper also outlines the use of two transmit antennas and M receive antennas which they show achieves a diversity order 2M. The diversity obtained using the two transmit and one receive antenna is shown to be the same as that obtained using Maximal Ratio Receiver Combining (MMRC) used in a one transmitter and two receiver antenna situation (which is the situation going from the mobile to the base station). One of the advantages of the proposed system is that fading is reduced at the receiver due to the use of multiple antennas and thus different paths to the receiver (with multipath included). In this section an examination of the results of [14] and the technique are provided.

The paper [14] starts with a description of a classical MRRC scheme, defining variables used in the presentation. Once again, the channel is modelled as a Line Of Sight channel with no delayed components (possible in multipath and wireless communications within indoor environments, for example a hall way). The noise on the channel is modelled as Gaussian and with the channel gains modelled as complex quantities:

$$h_0 = \alpha_0 e^{j\theta_0}$$
$$h_1 = \alpha_1 e^{j\theta_1} \qquad (2.4\text{-}1)$$

The signal received at the two receiver antennas is then given by:

$$r_0 = h_o s_0 + n_0$$
$$r_1 = h_1 s_1 + n_1 \qquad (2.4\text{-}2)$$

Figure 2.4-1 is taken from [14] and shows the setup for the MMRC case.

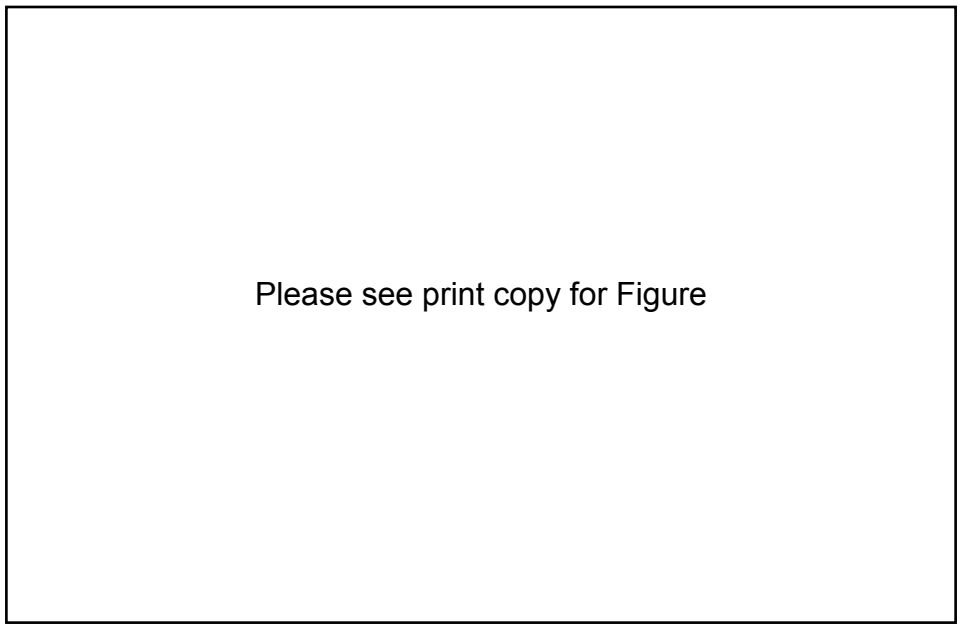

Figure 2.4-1: MMRC setup from [14].

It is shown that for PSK signal constellation, the decision rule derived reduces to choose $\mathbf{s_i}$ if and only if:

$$d^2(\tilde{s}_0, s_i) \leq d^2(\tilde{s}_0, s_k), \forall i \neq k \qquad (2.4\text{-}3)$$

And the reconstruction is shown in Figure 2.4-1.

Alamouti [14] proposes the use of a two branch and one receiver space model as shown in Figure 2.4-2. In this scheme two transmit antennas transmit two signals simultaneously, the signal from antenna 0 is called s_0 and the signal from antenna 1 is called s_1. In the next symbol or time frame the signal transmitted from antenna 0 is $-s_1^*$ and from antenna 1 the signal s_0^*. They point out that this coding is space time in nature, but it would also be possible to perform the same coding using two adjacent frequencies, which are not so far apart that the estimates for the channel coefficients would be different.

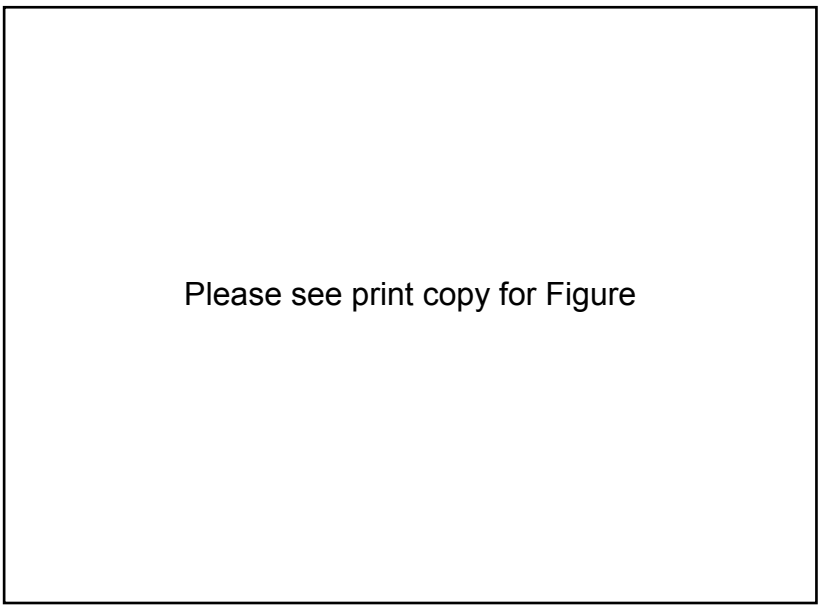

Figure 2.4-2: proposed system in [14].

They assume that fading is constant (flat) across the two consecutive symbol periods to give the following relationship for channel coefficients:

$$h_0(t) = h_o(t+T) = \alpha_0 e^{j\theta_0}$$
$$h_1(t) = h_1(t+T) = \alpha_1 e^{j\theta_1} \qquad (2.4\text{-}4)$$

with T being the symbol period. With this the received symbols can be expressed as:

$$r_0 = r(t) = h_0 s_0 + h_1 s_1 + n_0$$
$$r_1 = r(t+T) = -h_0 s_1^* + h_1 s_0^* + n_1 \qquad (2.4\text{-}5)$$

the noise terms being complex random variables representing receiver noise and interference. The combining scheme which is sent to the maximum likelihood detector is given by:

$$\tilde{s}_0 = h_0^* r_0 + h_1 r_1^*$$
$$\tilde{s}_1 = h_1^* r_0 - h_0 r_1^* \qquad (2.4\text{-}6)$$

which can be shown to be equivalent to (after some simple substitution of the previous third and second expressions into the last expression) as:

$$\tilde{s}_0 = \left(\alpha_0^2 + \alpha_1^2\right) s_0 + h_0^* n_0 + h_1 n_1^*$$
$$\tilde{s}_1 = \left(\alpha_0^2 + \alpha_1^2\right) s_1 - h_0 n_1^* + h_1^* n_0 \qquad (2.4\text{-}7)$$

These combined signals are sent to the maximum likelihood detector which uses the decision rule, if using PSK, that was shown for the MMRC case. It is concluded that this has the same diversity order as the MMRC case.

Further consideration is given to the case where there are two transmit and M receiver antennas, focusing on the situation where M=2. Figure 4 shows the setup from [14] for this situation. In this case for PSK they show that the estimates are:

$$\tilde{s}_0 = \left(\alpha_0^2 + \alpha_1^2 + \alpha_2^2 + \alpha_3^2\right) s_0 + h_0^* n_0 + h_1 n_1^* + h_2^* n_2 + h_3 n_3^*$$
$$\tilde{s}_1 = \left(\alpha_0^2 + \alpha_1^2 + \alpha_2^2 + \alpha_3^2\right) s_1 - h_0 n_1^* + h_1^* n_0 - h_2 n_3^* + h_3^* n_2 \qquad (2.4\text{-}8)$$

and the decision statistic reduces to choose s_i if and only if:

$$d^2(\tilde{s}_1, s_i) \leq d^2(\tilde{s}_1, s_k), \forall i \neq k \qquad (2.4\text{-}9)$$

which means that the two receiver case provides the equivalent of a four branch MMRC (or M=2, diversity = 2*M=4). It was suggested that this can be extended to M receivers and diversity is increased by an order 2M, with the combined signal from all receivers being simply added (as indicated in Figure 2.4-3). Thus they suggest that adding an antenna to the transmitter doubles the order of diversity that can be achieved with one transmitter and antenna and M receive antennas.

In [14] many factors are assumed, such as perfect channel knowledge, Rayleigh fading, and the power of two transmit antennas is the same as that of one (so the comparison can be similar). The curves are shifted by 3dB from the MRRC case, but if the power of each transmitter is increased to the same as one transmitter, this 3dB shift vanishes and it is pointed out that the curves follow each other.

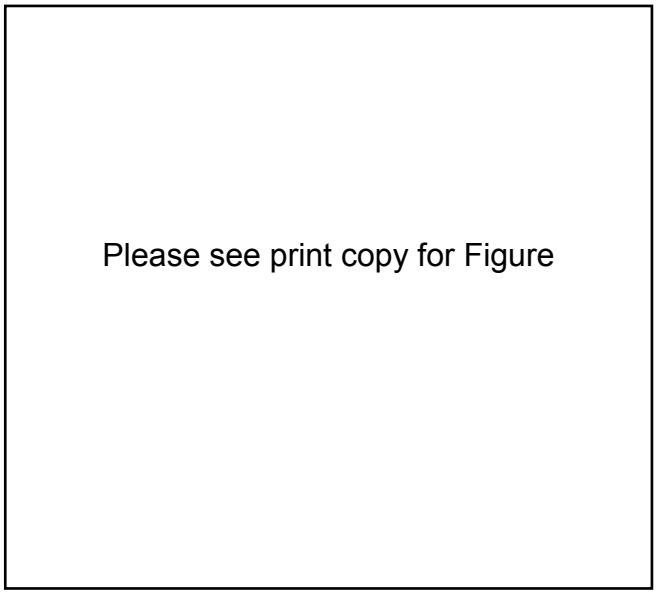

Figure 2.4-3: Two by two setup from [14].

Alamouti [14] also acknowledges some areas of difficulty with their scheme. This includes the use of pilot signals or insertion of known symbols to get close to perfect channel estimation for the scheme to work [15;16]. For each grouping of transmit and M receive antennas, requires M times as many pilot signals. Also, as the symbols are sent over two time symbol periods, the delay to decoding is two symbol periods, but the average rate is unity

(two symbols are sent over the two symbol periods, average one symbol per symbol period). The separation of the antennas is also important, studies [1] (pp. 102-103) indicate that for uncorrelated signals requires the antennas to be about ten wavelengths apart (if using diversity through number of directional antennas text books indicate that a spacing of half a wavelength is used, eg smart antenna design [5] p. 132). An advantage of the space-time scheme is that if one receive antenna fails or has a deep fade, soft failure is possible in that the signal may still be recovered but at the expense in a loss of diversity gain. It is also noted that interference from two transmitting antennas, transmitting different symbols may be of concern if the interference is not Gaussian in nature. This may be especially the case where interference cancellation schemes are used (such as array processing techniques).

In the introduction [14] refers to some papers in the early 1990's which used synthetic multipath to provide diversity [17-20]. In these schemes (according to Alamouti [14]) the symbols were transmitted at different times and then the multipath components recovered at the receiver (probably using a Rake receiver or similar construct) and the diversity over the channel was achieved this way. These results were found by Wittneben [17;18] and Winters [19;20] independently of each other.

2.5 Wideband CDMA systems based on Space Time Spreading

In [9] Hochwald et al. suggested a very interesting technique to provide transmit diversity for CDMA systems. Once again there is a basis in amicable orthogonal designs as outlined in [11]. The technique they outline is called or termed by them Space Time Spreading which reflects that it uses space-time coding but using special spreading codes as well. The technique is compared to other space time Code Division Multiple Access (CDMA) techniques such as Orthogonal Transmit Diversity (OTD), and the advantages of the newer technique are outlined. Diversity is expressed in this paper in terms of the chi-squared distribution for the extra orders of diversity that the authors claim. This section examines this paper in detail and considers the techniques contribution to space time coding in CDMA systems.

The technique outlined in [9] is an open loop transmit CDMA downlink system. It has been adopted as part of the IS-2000 Wideband CDMA (WCDMA) standard for the case of a two transmitter antenna / single receiver antenna setup as an optional diversity mode in release A of this standard. A closed loop technique involves transmission of known channel coefficients back to the transmitter using the reverse link. This information is then used to form beams in the forward link. They suggest that the success of such systems depends on many factors such as [9]:

- Quality of the channel estimates (which will likely be complex).
- Quality of the feedback channel (links in one direction do not always indicate that the wireless link exists in the reverse direction).
- Mapping between the two links.
- And the dynamical nature of the signal and any interference.

They argue that such closed loop techniques suffer from reduced uplink capacity because of this extra channel data that is transmitted. The other technique possible is to use transmit diversity at the base station, providing a diversity gain at the mobile station. This transmit diversity according to [9] is simpler to implement as it can operate in an open loop mode. By open loop they mean the transmitter does not have any knowledge of the channel characteristics (which it needed for the closed loop scenario). This does not mean that the receiver doesn't need such knowledge, so channel estimates are still required via the use of pilot signals.

In [9] it is argued that diversity due to temporal gains, resulting from motion, which are exploited by using coding and interleaving, are not likely to be present in most third generation wireless scenarios where the receiver and transmitter are likely to be stationary or very slowly moving. This is particularly the case when the mobile is located in a slow fading channel with a deep fade. It is pointed out that dependence on such factors should be reduced.

There is a cost associated with extra transmit antennas, apart from the direct hardware expense. Other techniques need extra orthogonal codes and/or extra bandwidth to achieve diversity. The Space Time Spreading code that [9] proposes does not need extra orthogonal codes and the bandwidth used is the same. The transmitter power is normalised so that the

total power is the same as that which would be used in the single transmitter antenna case. While not requiring extra orthogonal codes, it does need pairs of users or groups to be used, so that if odd numbers of users or groups are used, effectively an extra code is required (which could be taken advantage of by splitting the extra users or groups data into two streams, as is suggested in terms of odd and even symbols). The authors of [9] also argue that the technique is simple to implement, from an algebraic and complexity point of view. The initial analysis does not consider multipath, but later in the paper multipath considerations are included and it is deduced that the two diversity techniques are complementary from the presented simulation results.

Hochwald et al. [9] begins by describing different scenarios which have been proposed by others and which are also extreme cases on space time techniques. The difference between this paper and previous reviewed work is the inclusion of orthogonal spreading codes. The notation is defined as follows. Denote that the kth user has a data stream of real symbols $\{b_k(i)\}$, where the user's ith symbol $b_k(i)$ is spread by its own spreading code which has dimensions $P \times 1$ called $\underline{c}_k$. These spreading codes are assumed to then be orthogonal and also to have a unit norm such that:

$$\underline{c}_k^H \underline{c}_l = \delta_{kl} \qquad (2.5\text{-}1)$$

where H denotes the complex conjugate transpose or Hermitian transpose (the paper uses a different symbol which has this meaning) and δ_{kl} is the kronecker delta. The length P is defined as the spreading gain and, as is usually the case for CDMA, the elements of $\underline{c}_k$ are sent at the chipping rate. They claim that for this proposal the "exact spreading codes, gains and pulse shapes" [9] are unimportant. They then define the equation for one transmitter at the base station for the received signal at user k as:

$$\underline{r}_k = h_k \sum_n b_n \underline{c}_n + n_k, \mathrm{k} = 1,2,... \qquad (2.5\text{-}2)$$

In this equation the h_k is the complex channel coefficient, which is assumed to have a Rayleigh distributed amplitude and a uniformly distributed phase, between the transmit

antenna and the k[th] user. The term n_k is a $P \times 1$ vector of additive zero mean complex Guassian receiver noise samples. After despreading the received signal is mapped to:

$$d_k = \underline{c}_k^H \underline{r}_k = h_k b_k + \nu_k, \mathrm{k} = 1,2,... \qquad (2.5\text{-}3)$$

where $\nu_k = \underline{c}_k^H \underline{n}_k$. They assume that the receiver of the k[th] mobile knows h_k. It is pointed out that good decoding of the data symbols, b_k, is very dependent on a reasonably large channel gain, $|h_k|$. This cannot be guaranteed in most situations. A description of some diversity schemes is provided which attempt to provide large channel gain assuming that the transmitting antenna are widely separated, so the signals are uncorrelated as illustrated in other reviewed papers in this chapter.

The first schema that is described is the scheme where the same signal is transmitted from the two widely separated antennas. In this case both antennas transmit the signal:

$$\left(1/\sqrt{2}\right)\sum_n b_n \underline{c}_n \qquad (2.5\text{-}4)$$

This is then received at the k[th] mobile after despreading as:

$$d_k = \left(1/\sqrt{2}\right)\left(h_{1k} + h_{2k}\right)b_k + \nu_k \qquad (2.5\text{-}5)$$

The term h_{1k} represents the complex channel coefficient between antenna 1 and mobile k's receiver and the term h_{2k} represents the complex channel coefficient between antenna 2 and mobile k's receiver. The factor $1/\sqrt{2}$ is used to normalise the power so that it has the same total power as one transmitter. They then say that the wide separation between the transmitting antennas makes the channel coefficients independent giving this de-spread signal the same distribution that either one or the other channel coefficients would have had, thus resulting in no increase in diversity, that is no diversity gain is realised by this configuration.

The next scheme considered has the transmitter knowing the propagation coefficients and uses Maximal Ratio Weighting. This corresponds to a closed loop scheme, with the

disadvantages already mentioned by the authors. In this case antenna m could be fed the weighted signal:

$$\sum_n \left[\frac{h_{mn}^*}{\sqrt{|h_{1n}|^2 + |h_{2n}|^2}} \right] b_n \underline{c}_n \qquad (2.5\text{-}6)$$

And the k[th] mobile receives:

$$r_k = \sum_{m=1}^{2} h_{mk} \cdot \sum_n \left[\frac{h_{mn}^* b_n \underline{c}_n}{\sqrt{|h_{1k}|^2 + |h_{2k}|^2}} \right] + \underline{n}_k \qquad (2.5\text{-}7)$$

This is then despread so that the kth mobile calculates:

$$d_k = \left(\sqrt{|h_{1k}|^2 + |h_{2k}|^2} \right) b_k + \nu_k \qquad (2.5\text{-}8)$$

This, Hochwald et al. [9] highlight, has an instantaneous SNR which is proportional to $|h_{1k}|^2 + |h_{2k}|^2$. It is noted that this statistical distribution is proportional to a chi-squared random variable, χ_4^2, which is claimed to have two fold diversity with an expected value which is twice that which can be obtained from the single antenna case, at the same power. Thus this scheme does increase the diversity but at the expense of the transmitter needing to have knowledge of the complex channel coefficients.

The next scheme reviewed was proposed by [21] and [22]. In this scheme each user is assigned a different orthogonal code for each transmitter antenna. In this case, says [9], the transmitted signal on antenna m is given by:

$$\left(1/\sqrt{2}\right) \sum_n b_n \underline{c}_{mn} \qquad (2.5\text{-}9)$$

It is once again assumed that there are two transmit antennas, thus the received signal at the k[th] mobile becomes:

$$r_k = \left(\frac{1}{\sqrt{2}} \right) \left[h_{1k} \sum_n b_n \underline{c}_{1n} + h_{2k} \sum_n b_n \underline{c}_{2n} \right] + \underline{n}_k \qquad (2.5\text{-}10)$$

Once again the first factor normalises the power, then the two terms represent the signals from the two transmit antennas with each antenna having its own spreading code. The k[th] user then separately despreads using orthogonal codes $\underline{c}_{1k}$ and $\underline{c}_{2k}$, which they indicate yields two received signals at user k:

$$\begin{aligned} d_k^{(1)} &= \left(1/\sqrt{2}\right) h_{1k} b_k + \underline{c}_{1k}^H \underline{n}_k \\ d_k^{(2)} &= \left(1/\sqrt{2}\right) h_{2k} b_k + \underline{c}_{2k}^H \underline{n}_k \end{aligned} \qquad (2.5\text{-}11)$$

They then form simple matrices to express this relationship in matrix notation, such that, for the k[th] user:

$$\underline{d}_k = \begin{bmatrix} d_k^{(1)} \\ d_k^{(2)} \end{bmatrix} = \begin{bmatrix} d_k^{(1)} & d_k^{(2)} \end{bmatrix}^{\mathrm{T}} \qquad (2.5\text{-}12)$$

which can be then expressed as:

$$d_k = \left(1/\sqrt{2}\right) \underline{h}_k b_k + \underline{\nu}_k \qquad (2.5\text{-}13)$$

where the following matrices are defined:

$$\underline{\mathrm{h}}_k = \begin{bmatrix} h_{1k} \\ h_{2k} \end{bmatrix} \qquad \underline{\nu}_k = \begin{bmatrix} \underline{c}_{1k}^H \underline{n}_k \\ \underline{c}_{2k}^H \underline{n}_k \end{bmatrix} \qquad (2.5\text{-}14)$$

It is stated that using a simple receiver for user k, called the maximum ratio combiner can demodulate b_k by multiplying $\underline{d}_k$ on the left side by h_k^H which has the following outcome:

$$\underline{h}_k^H \underline{d}_k = \left(1/\sqrt{2}\right)\left(|h_{1k}|^2 + |h_{2k}|^2\right) b_k + \underline{h}_k^H \underline{\nu}_k \qquad (2.5\text{-}15)$$

At this point either hard or soft decoding may be performed to decode the individual symbol b_k. The statistical distribution of $|h_{1k}|^2 + |h_{2k}|^2$ is proportional to the chi-squared distribution χ_4^2 which obtains a two-fold diversity increase over the single transmit antenna case.

Comparing this case to that obtained when the channel coefficients are known at the transmitter there is a 3dB loss in SNR, simply because the channel is not known.

Hochwald and colleagues [9] then generalise this to the case where there are M transmitter antennas and state that the instantaneous SNR is:

$$SNR_{dist} = \left(\frac{\underline{h}_k^H \underline{h}_k}{\sqrt{M}} \right) \cdot \frac{1}{\left(\underline{h}_k^H \underline{h}_k \right) \sigma_k^2} = \frac{\underline{h}_k^H \underline{h}_k}{M \sigma_k^2} \qquad (2.5\text{-}16)$$

with $\sigma_k^2 = E\{\nu_k^2\}$, and they point out that the $E\{\underline{h}_k^H \underline{h}_k\} = M$ and hence the SNR remains at $1/\sigma_k^2$. It is highlighted that the advantage of more antennas is that the probability distribution has shorter tails and conclude that the instantaneous SNR, in general, is proportional to a chi-squared χ_{2M}^2 distribution which caters for an M-fold diversity.

Hochwald et al. [9] highlight that this scheme has very attractive diversity improvements, but there is a cost of two spreading codes per user, which is a severe penalty considering that spreading codes are limited in number (depending on the number of chips). If there are M transmitter antennas then each user needs M spreading codes, which reduces the number of possible users in the system at any one time.

The next technique considered is known as Orthogonal Transmit Diversity (OTD) proposed in [23;24] and which was included earlier as an option in the IS-2000 standard. In Orthogonal Transmit Diversity each users data stream is split into odd and even substreams. The odd substream is then denoted $\{b_{k1}(i)\}$ and the even substream is denoted by $\{b_{k2}(i)\}$. The authors subsequently drop the index k, for user k, and the time index i and denote these odd and even streams as simply $\{b_1\}$ and $\{b_2\}$. In this technique, the first antenna transmits the odd substreams of user data (b_1) in the odd symbol period and nothing in even symbol periods and vice-a-versa for the even substream but for antenna 2. The technique uses the same spreading code for even and odd substreams so this technique does not require additional spreading codes. As a result of this schema, the two antennas have the form:

$$t_1 = b_1 \underline{c}_1$$
$$t_2 = b_2 \underline{c}_2 \qquad (2.5\text{-}17)$$

where the spreading codes are defined as:

$$\underline{c}_1 = \begin{bmatrix} \underline{c} \\ \cdots \\ 0_{P\times 1} \end{bmatrix} \quad ; \qquad \underline{c}_2 = \begin{bmatrix} 0_{P\times 1} \\ \cdots \\ \underline{c} \end{bmatrix} \qquad (2.5\text{-}18)$$

where the 0_{PX1} represents a series of zeros (P of them). Both spreading codes, it is noted, have a length of 2P chips and are mutually orthogonal but only one spreading code is needed to do this. In OTD the received signal is now given as:

$$r = b_1 h_1 \underline{c}_1 + b_2 h_2 \underline{c}_2 + \underline{n} \qquad (2.5\text{-}19)$$

and then this signal is despread with the codes above to give:

$$\begin{aligned} d_1 &= h_1 b_1 + \nu_1 \\ d_2 &= h_2 b_2 + \nu_2 \end{aligned} \quad \text{where } \nu_1 = \underline{c}_1^H \underline{n} \quad and \quad \nu_2 = \underline{c}_2^H \underline{n} \qquad (2.5\text{-}20)$$

and the recovered substreams are recovered as:

$$\begin{aligned} \hat{b}_1 &= h_1^* d_1 = |h_1|^2 b_1 + h_1^* \nu_1 \\ \hat{b}_2 &= h_2^* d_2 = |h_2|^2 b_2 + h_2^* \nu_2 \end{aligned} \qquad (2.5\text{-}21)$$

Using this technique, they point out that the instantaneous SNR is then given by:

$$SNR_{OTD}(q) = |h_q|^2 / \sigma^2 \,, \sigma^2 = E\{\nu_1^2\} = E\{\nu_2^2\} \qquad (2.5\text{-}22)$$

for the q^{th} substream.

Comparing this scheme to that which uses an orthogonal code per transmitter per user, they noted that Orthogonal Transmit Diversity provides an unbalanced diversity to each of the users substreams. Thus, in a long fade on one of the transmit antennas, half of the users data is lost, whereas in the previous scheme a fade on one transmit antenna can still recover odd and even substreams provided that a long fade does not occur on both antennas (the notation

of channel gains is used to express the fades, after all this is the quantity that these techniques are trying to improve). They point out that it is more likely for either but not both channels to be in a long fade. In the case of very fast fading the performance of OTD is similar to that obtained using an orthogonal code per transmit antenna per user as:

$$SNR_{dist} = \frac{1}{2\left(SNR_{OTD}(1) + SNR_{OTD}(2)\right)} \qquad (2.5\text{-}23)$$

with diversity being obtained temporally, but as they pointed out earlier this type of diversity cannot be relied on as often transmitter and receiver will be stationary with respect to each other.

This finally brings the authors to their proposal which is the Space Time Spreading technique. Using this technique they have two transmitters and one receiver. Once again the system splits the users substream into odd and even parts as was done in the OTD technique. The proposal is that the following signals be transmitted on the two antennas:

$$\begin{aligned} t_1 &= \left(1/\sqrt{2}\right)\left(b_1 \underline{c}_1 + b_2 \underline{c}_2\right) \\ t_1 &= \left(1/\sqrt{2}\right)\left(b_2 \underline{c}_1 - b_1 \underline{c}_2\right) \end{aligned} \qquad (2.5\text{-}24)$$

This is shown in Figure 2.5-1, taken from [9]. In this case $\underline{c}_1, \underline{c}_2$ are any set of orthogonal unitary (or unit-norm) spreading sequences such that $\underline{c}_1^H \underline{c}_2 = 0$.

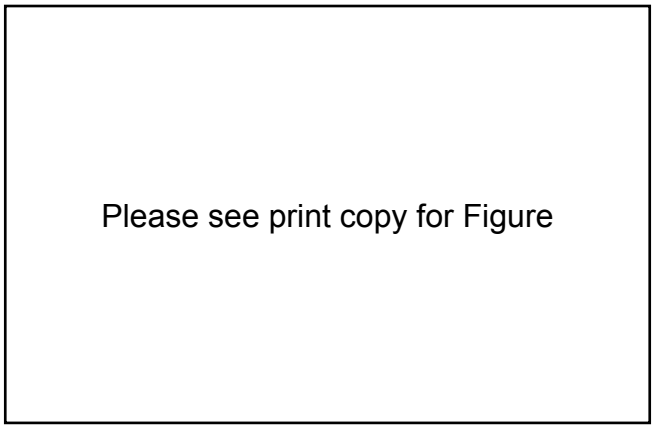

Figure 2.5-1: Proposed Space Time Spreading setup from [9].

The system uses two codes of length 2P, but now each code is used with both data symbols, so this technique shares the advantage of OTD that no extra spreading codes are needed, though it should be pointed out that OTD needed only one spreading code which was then shared between odd and even substreams. At the receiver, after despreading with the two orthogonal codes it obtains:

$$\begin{aligned} d_1 &= \left(1/\sqrt{2}\right)\left(h_1 b_1 + h_2 b_2\right) + \underline{c}_1^H \underline{n} \\ d_2 &= \left(1/\sqrt{2}\right)\left(-h_2 b_1 + h_1 b_2\right) + \underline{c}_2^H \underline{n} \end{aligned} \qquad (2.5\text{-}25)$$

The following is defined (where superscript T denotes matrix transpose):

$$\underline{d} = \begin{bmatrix} d_1 \\ d_2 \end{bmatrix} = \begin{bmatrix} d_1 & d_2 \end{bmatrix}^{\mathrm{T}} \qquad (2.5\text{-}26)$$

and let

$$H = \begin{bmatrix} h_1 & h_2 \\ -h_2 & h_1 \end{bmatrix} \quad \underline{b} = \begin{bmatrix} b_1 \\ b_2 \end{bmatrix} \quad \underline{\nu} = \begin{bmatrix} \underline{c}_1^H \underline{n} \\ \underline{c}_2^H \underline{n} \end{bmatrix} \qquad (2.5\text{-}27)$$

to give:

$$\underline{d} = \frac{1}{\sqrt{2}} H \underline{b} + \underline{\nu} \qquad (2.5\text{-}28)$$

The algorithm then left multiplies this by H^{H} to obtain:

$$H^{\mathrm{H}} \underline{d} = \frac{1}{\sqrt{2}} \begin{bmatrix} |h_1|^2 + |h_2|^2 & h_1^* h_2 - h_2^* h_1 \\ h_2^* h_1 - h_1^* h_2 & |h_1|^2 + |h_2|^2 \end{bmatrix} \underline{b} + H^{\mathrm{H}} \underline{\nu} \qquad (2.5\text{-}29)$$

Taking the real part of this the authors obtain:

$$\begin{aligned} \Re e\left\{H^{\mathrm{H}} \underline{d}\right\} &= \frac{1}{\sqrt{2}} \begin{bmatrix} |h_1|^2 + |h_2|^2 & 0 \\ 0 & |h_1|^2 + |h_2|^2 \end{bmatrix} \underline{b} + \Re e\left\{H^{\mathrm{H}} \underline{\nu}\right\} \\ &= \frac{1}{\sqrt{2}} \begin{bmatrix} \left(|h_1|^2 + |h_2|^2\right) b_1 \\ \left(|h_1|^2 + |h_2|^2\right) b_2 \end{bmatrix} + \Re e\left\{H^{\mathrm{H}} \underline{\nu}\right\} \end{aligned} \qquad (2.5\text{-}30)$$

This is simplified by letting $\underline{h}_q$ represent the q$^{\mathrm{th}}$ column of H so that:

$$\Re e\left\{\underline{h}_q^H \underline{d}\right\} = \left(1/\sqrt{2}\right)\left(\left|h_1\right|^2 + \left|h_2\right|^2\right)b_q + \Re e\left\{\underline{h}_q^H \underline{v}\right\} \qquad (2.5\text{-}31)$$

Hochwald et al. [9] then state that this "possesses the optimum two fold diversity gain with respect to the single transmitter expressed" [9] in the case where each transmit antenna for each user had M orthogonal codes (if M transmitters are present) where here M=2. In this system the mobile of interest only needs to multiply its despread signal, denoted by $\underline{d}$ with h_1^H and h_2^H to recover the odd and even symbol substreams. After this hard or soft decoding can be used on this data.

In these works the authors further discuss two modes of operation. One mode they refer to as "subuser grouping" and the other as "user grouping". The subuser grouping is the technique described above where the users data is divided into odd and even substreams. The user grouping is where two different users streams are used to replace the odd and even substreams. This will mean each user sees a lower data rate compared to the case where subuser grouping is used. It is briefly pointed out that user grouping only requires the channel to be invariant over one symbol period, whereas the subuser grouping technique requires this over two symbol periods (for two transmit antennas). The draw back or disadvantage for user grouping is the need for a companion user stream. One area of possible future research is to combine these two schemes in a rate adaptive manner so that full advantage may be taken of the link capacity using the space time technique [25] however this is not undertaken in this thesis. They finish this section by indicating that they believe that sub-user grouping is the more useful situation and the paper continues on this theme.

To this point in [9] attention has been drawn to two transmit antennas and one receive antenna. They now start to consider the more general case, where the theory of amicable orthogonal designs [11] is introduced into the methodology. They ask if the two transmit antennas can be generalised to use M transmit antennas using STS. First they define Q to be the total number of subtreams into which each user is split, thus in the initial version Q was 2. They then say let L be the number of spreading codes per Q substreams, and L is allowed to be equal to Q and greater than Q ie $L \geq Q$. Thus the scheme which was initially proposed was one where M=L=Q=2.

Much of the material that [9] presents has already been presented in [10] (see Table 2.2.1). The only difference is in [9] a presentation is based on orthogonal spreading codes, whereas the presentation in [10] is a strict space time coding setup. In [9] they briefly look at the effect of having N receive antennas, expected to be more practical as frequencies get higher (such as 60 GHz [26]). They show that using extra receiver antennas with their scheme increases the SNR and adds an extra two degrees of freedom to the chi-squared distribution. The rest of the analysis and simulation of the paper reflects only one receive antenna.

In [9] they consider first the transmission of real data symbols. They let the spreading codes now have length of 2P so the two spreading codes required form 2P by 1 vectors. Then they let S be the 2P by 2 matrix formed from the spreading codes of both transmit antennas. In this mathematical formation the "p^{th} row of S represents the baseband representation of the signals on the two antennas at chip p" [9]. Proceeding by forming the following relationship:

$$S = C \cdot B \tag{2.5-32}$$

where:

$$C = \begin{bmatrix} \underline{c}_1 & \underline{c}_2 \end{bmatrix}, \quad B = \begin{bmatrix} b_1 & b_2 \\ b_2 & -b_1 \end{bmatrix} \tag{2.5-33}$$

at which point one removes the power normalisation factor. The baseband signal S is received at the mobile as:

$$S\underline{h} + \underline{n} = CB\underline{h} + \underline{n} \tag{2.5-34}$$

Left multipling by C^H to despread it gives:

$$\begin{bmatrix} \underline{c}_1^H & \underline{c}_2^H \end{bmatrix}(S\underline{h} + \underline{n}) = B\underline{h} + \begin{bmatrix} \underline{c}_1^H \underline{n} \\ \underline{c}_2^H \underline{n} \end{bmatrix} = \begin{bmatrix} b_1 & b_2 \\ b_2 & -b_1 \end{bmatrix}\begin{bmatrix} h_1 \\ h_2 \end{bmatrix} + \underline{\nu} = \begin{bmatrix} h_1 & h_2 \\ -h_2 & h_1 \end{bmatrix}\begin{bmatrix} b_1 \\ b_2 \end{bmatrix} + \underline{\nu} = H\underline{b} + \underline{\nu}$$

(2.5-35)

The authors then obtain the q^{th} substream by left multiplying this expression by the q^{th} row of H^H. It is observed that the general M fold diversity with M transmitter antennas one can use the identity to decode each substream as:

$$\Re e\left\{H^{\mathrm{H}} H\right\} = \underline{h}^{H}\, \underline{h \cdot I}, \quad \underline{h} = \begin{bmatrix} h_1 \\ \vdots \\ h_M \end{bmatrix} \tag{2.5-36}$$

Attempting to satisfy this equation is achieved "by grouping Q substreams at a time with L spreading codes on M antennas, where $L \geq Q$ and $L \geq M$ " [9]. From this the ratio of L to Q is used, with the preferred ratio being that of one, which has been referred to as the minimal delay scenario in [10] in terms of space time coding scenario. Consideration is given to the situation where L=Q=M=2 as found in previous studies [12;21;27]. They proceed to show that "if the entries of the $L \times Q$ matrix H depend linearly on $\underline{h}$ through real coefficients and if " [9]:

$$H^T H = \underline{h}^T \underline{h} \cdot I \tag{2.5-37}$$

then

$$\Re e\left\{H^{\mathrm{H}} H\right\} = \underline{h}^{H}\, \underline{h \cdot I}, \quad \underline{h} = \begin{bmatrix} h_1 \\ \vdots \\ h_M \end{bmatrix} \tag{2.5-38}$$

is true. The proof is located in [9], but during the proof they show that the real coefficient matrices that are the coefficients such that:

$$H = \begin{bmatrix} A_1 \underline{h} & A_2 \underline{h} & \cdots & A_Q \underline{h} \end{bmatrix} \tag{2.5-39}$$

where the A_i matrices are L by M matrices. Further showing the requirement is that the matrices be skew symmetric such that:

$$A_i^T A_j = -A_j^T A_i \text{ with } i \neq j = 1, \ldots, Q \tag{2.5-40}$$

and also that:

$$A_1^T A_1 = \ldots = A_Q^T A_Q = I \tag{2.5-41}$$

Now defining the j^{th} column of A_i to be symbolised by $\underline{a}_{ij}$ such that:

$$A_i = \left[\underline{a}_{i1} \quad \underline{a}_{i2} \quad \cdots \quad \underline{a}_{iM} \right] \qquad i = 1,\ldots,Q \tag{2.5-42}$$

Hochwald et al. [9] then define a new L by Q matrices called $\widetilde{A}_1,\ldots,\widetilde{A}_M$ with the jth column of $\widetilde{A}_i$ is $\underline{a}_{ji}$ which means that:

$$\widetilde{A}_i = \left[\underline{a}_{1i} \quad \underline{a}_{2i} \quad \ldots \quad \underline{a}_{Qi}\right], \quad i = 1,\ldots,M \tag{2.5-43}$$

And defining B to equal:

$$B = \left[\widetilde{A}_1 \underline{b} \quad \widetilde{A}_2 \underline{b} \quad \cdots \quad \widetilde{A}_M \underline{b}\right] \quad where \quad \underline{b} = \begin{bmatrix} b_1 \\ \vdots \\ b_Q \end{bmatrix} \tag{2.5-44}$$

It is highlighted that B is an L by M matrix which satisfies:

$$B\underline{h} = H\underline{b} \tag{2.5-45}$$

Hochwald et al. [9] proceed to prove that B has similar properties to H such that:

$$B^T B = \underline{b}^T \underline{b} \cdot I \tag{2.5-46}$$

Also showing that $\widetilde{A}_i^T \widetilde{A}_j = -\widetilde{A}_j^T \widetilde{A}_i$ with $i \neq j$ and also that $\widetilde{A}_1^T \widetilde{A}_1 = \ldots = \widetilde{A}_M^T \widetilde{A}_M = I$.

It is stated that "B matrices that obey $B^T B = \underline{b}^T \underline{b} \cdot I$ yield H matrices that obey $H^T H = \underline{h}^T \underline{h} \cdot I$" [9]. The transmitted signal to yield the desired M Fold diversity is as defined earlier, that is $S = C \cdot B$ but here $C = \left[\underline{c}_1 \quad \underline{c}_2 \quad \cdots \quad \underline{c}_L\right]$, with B being an L by M matrix which obeys the relation $B^T B = \underline{b}^T \underline{b} \cdot I$.

It is suggested that to design a M-fold diversity transmitter system it is possible to start with either B or H, they suggest that H be used as the mobile has the most difficult problems related to processing power and system complexity. They then point out that orthogonal designs as proposed in [28] obey the desired properties such as the following H for a L=Q=M=4 transmit diversity scheme:

$$H = \begin{bmatrix} h_1 & h_2 & h_3 & h_4 \\ -h_2 & h_1 & -h_4 & h_3 \\ -h_3 & h_4 & h_1 & -h_2 \\ -h_4 & -h_3 & h_2 & h_1 \end{bmatrix} \qquad (2.5\text{-}47)$$

Using the equations provided to work out the set of $\{A\}$ and $\{\tilde{A}\}$, which are matrices with elements composed only of -1, 0, and 1, which results in a B matrix:

$$B = \begin{bmatrix} b_1 & b_2 & b_3 & b_4 \\ b_2 & -b_1 & b_4 & -b_3 \\ b_3 & -b_4 & -b_1 & b_2 \\ b_4 & b_3 & -b_2 & -b_1 \end{bmatrix} \qquad (2.5\text{-}48)$$

From this the transmitted signal across the four antennas is given by:

$$S = \begin{bmatrix} \underline{c}_1 & \underline{c}_2 & \underline{c}_3 & \underline{c}_4 \end{bmatrix} \begin{bmatrix} b_1 & b_2 & b_3 & b_4 \\ b_2 & -b_1 & b_4 & -b_3 \\ b_3 & -b_4 & -b_1 & b_2 \\ b_4 & b_3 & -b_2 & -b_1 \end{bmatrix} \qquad (2.5\text{-}49)$$

They indicate that it is possible to generate M=3 from an M=4 solution by replacing h_4 by zero, which results in a B matrix:

$$B = \begin{bmatrix} b_1 & b_2 & b_3 \\ b_2 & -b_1 & b_4 \\ b_3 & -b_4 & -b_1 \\ b_4 & b_3 & -b_2 \end{bmatrix} \qquad (2.5\text{-}50)$$

where the last column is removed from the previous B. Pointing out that it does not matter if they use 3 or 4 transmit antennas as here they have 4 subuser groups and 4 spreading codes (L=Q=4). One, thus, does not need extra spreading codes to achieve three or four fold diversity. However, looking at the case where M=Q=L=3 and they indicate that such a system does not exist, which result is found in [11] that designs of this type (for real matrices) only exist for M=2,4,8 (which is also observed in [10]). Thus, any research pursued in this area (still using orthogonal designs) will need to concentrate on values of M with L=Q>M (ie rates less than unity). This thesis only considers MIMO systems with unity rate (ie M=2, 4 and 8). It is further noted that their technique adds extra complexity in the despreader (which will typically be a Rake receiver) but not in the decoder.

In [9] they also look at the situation with Complex Data Symbols. They do not develop a comprehensive theory for complex data symbols, leaving this open to further research and development, but from a pure orthogonal designs view point, using results in [11] again, they show that for the case L=Q=M, only the two transmit case can be used. This is started by representing the complex data symbols as $b_1, \cdots, b_Q$ and then require the L by Q matrix H to satisfy:

$$H^{\mathrm{H}} H = \left(|h_1|^2 + \cdots + |h_2|^2 \right) I = \underline{h}^H \underline{h} \cdot I \qquad (2.5\text{-}51)$$

Then they show a case, M=2, where

$$H = \begin{bmatrix} h_1 & h_2 \\ -h_2^* & h_1^* \end{bmatrix} \qquad (2.5\text{-}52)$$

which the authors claim satisfies the relationship above, so looking at the product:

$$\begin{aligned} H\underline{b} &= \begin{bmatrix} h_1 & h_2 \\ -h_2^* & h_1^* \end{bmatrix}\begin{bmatrix} b_1 \\ b_2 \end{bmatrix} \\ &= \begin{bmatrix} h_1 b_1 + h_2 b_2 \\ -h_2^* b_1 + h_1^* b_2 \end{bmatrix} \end{aligned} \quad (2.5\text{-}53)$$

And one looks for a B which satisfies the relation $B\underline{h} = H\underline{b}$, which cannot be found. However if the second entry of the product is conjugated so that:

$$\left(-h_2^* b_1 + h_1^* b_2\right)^* = -h_2 b_1^* + h_1 b_2^* \quad (2.5\text{-}54)$$

Then the following was shown:

$$\begin{aligned} \begin{bmatrix} h_1 b_1 + h_2 b_2 \\ -h_2 b_1^* + h_1 b_2^* \end{bmatrix} &= \begin{bmatrix} b_1 & b_2 \\ b_2^* & -b_1^* \end{bmatrix}\begin{bmatrix} h_1 \\ h_2 \end{bmatrix} \\ &= B\underline{h} \end{aligned} \quad (2.5\text{-}55)$$

They then have a $B = \begin{bmatrix} b_1 & b_2 \\ b_2^* & -b_1^* \end{bmatrix}$ which gives the transmitted signal:

$$\begin{aligned} S &= C \cdot B \\ &= \begin{bmatrix} \underline{c}_1 & \underline{c}_2 \end{bmatrix}\begin{bmatrix} b_1 & b_2 \\ b_2^* & -b_1^* \end{bmatrix} \end{aligned} \quad (2.5\text{-}56)$$

The mobile despreads this signal using (as in the real symbol case):

$$C^{\mathrm{H}}\left(S\underline{h} + \underline{n}\right) = B\underline{h} + \begin{bmatrix} \underline{c}_1^H \underline{n} \\ \underline{c}_2^H \underline{n} \end{bmatrix} \quad (2.5\text{-}57)$$

The difference, they state, is then to conjugate the second entry of the result which yields:

$$H\underline{b} + \begin{bmatrix} \underline{c}_1^H \underline{n} \\ \left(\underline{c}_2^H \underline{n}\right)^* \end{bmatrix} \quad (2.5\text{-}58)$$

From this they say that the qth substream is obtained by multiplying on the left by the qth row of H^{H}. In the complex data symbol case both the real and imaginary parts of the data symbol carry information and this scheme has achieved the L=Q=M=2 desired situation. From other

results reported in [10] [11] it is stated that the case M>2 does not exist such that L=Q=M for complex data symbols. Also in [9] a design where M=Q=3 and L=4 which provides three fold diversity is illustrated.

Hochwald and colleagues in [9] proceed to calculate theoretically the probability of error for their scheme which uses log-likelihood ratios and is beyond the current scope of this literature review. Plots of the probability of error versus expected SNR for the cases where they have M=1,2,3, and 4 transmit antennas are provided. Generally, as SNR increases the probability of error improves as the number of transmit antennas is increased. However, for low SNR using multiple antennas can actually lead to a poorer performance compared to a lower number of antennas. It is claimed that there is, in fact, a tradeoff between diversity gain and reduction in the SNR. With higher SNR the gain in diversity is due to the increased number of propagation paths between the transmitters and receiving antenna, whereas when the SNR is reduced there is an increase in crosstalk which is a result of the lack of knowledge of the propagation coefficients (the h_i) which is needed for this technique.

A discussion on multipath is provided, which is lacking from most other papers in space time that are included in this literature review. It is observed that the conditions that lead to good design of a Rake receiver are complementary to those that lead to good design of a STS system. Some impressive simulation results are provided using their STS scheme and comparing it to systems that use only single path and also systems with two multipath components. They plotted results for one and two transmitter antennas situations, with significant improvement being shown by the two transmitter case, under the use of pilot signals with 10dB stronger power than the transmitted information signal, using QPSK (Quadrature Phase Shift Keying) transmission. The results they present for multipath use perfect knowledge of the fading propagation coefficients. From these results a 6dB improvement in SNR is seen for the two transmitter case over the single transmitter case at a probability of error of 0.01. It is noted that when using a RAKE receiver in flat fading this improvement drops to 4.3dB which they attribute to mutual interference. However, favourable multipath conditions may not always exist and in such cases using their STS scheme will improve the performance of the system. On the other hand, adding extra transmitter antennas requires the addition of extra pilot signals so that the receiver can have

estimates of the different propagation coefficients. These pilot signals power will then need to be inversely proportional to the number of transmit antennas so that leakage of power between cells does not increase (in a cellular based system for Space Divison Multiple Access (SDMA) schemes). They also point out that lower powered signals may mitigate the power control problem that CDMA systems are known for. Another advantage of using extra spreading codes is that the interference may appear more gaussian in nature, though many papers seem to assume flat fading and gaussian noise.

2.6 A Brief description of other works on Space Time Techniques

Marzetta and Hochwald in [29] (which is referenced in [10]), consider the effect of increasing the number of transmitter and receiver antennas in a flat Rayleigh fading channel. This study assumes that the receiver does not use any training symbols (blind system). They show that very little gain is achieved if the number of transmitter antennas exceeds the coherence interval, with in fact capacity for a slow fading channel which can transmit M symbols before new fading coefficients are necessary being reached when the number of transmit antennas equals the value of the coherence interval, M. A consequence of this is that if the coherence interval is only one symbol, then there is no advantage in terms of capacity in having two transmitting antennas.

In [30] and [31] Tarokh et al examine various methods of Space Time coding, array processing and coding. In [30] they provide design codes which provide both diversity and coding gain assuming slow fading and frequency non-selective channels. They provide performance criteria for designing such codes and use these to design trellis codes for high data rate wireless transmission. In [31] a linear array processing technique is employed with Space Time techniques and groups of antennas at the transmitter to minimise signals transmitted by other antenna groups by treating them as interference. The technique outlined in [31] using array processing at the receiver and groups of transmit antennas is shown to be effective over a narrowband wireless channel.

In [32] Kohno et al. propose a signal cancellation and directional antenna system to remove signals that are not in the same direction (through angle of arrival filtering) and interfering

signal cancellation for different users arriving from the same direction in a Direct Sequence spread spectrum environment.

In [33] Naguib et al show that using multiple antennas at the base station for both receive and transmit in a CDMA system can increase the capacity of the wireless link, this being done in 1994. This study did not include multipath, which they followed up in another study. In [34] Paulraj and Papadias provide a thorough review of space time techniques, explaining the different areas within wireless diversity techniques concentrating on space time, as is done in the reference book by Pieter van Rooyen et al [5]. In [35] Gerbach and Paulraj outline a system that connects to multiple targets with feedback to estimate channel coefficients is presented. They find that their system, which was used at 900 MHz, requires slow moving targets (vehicles) in order to work well, even though this is a closed loop type system where the feed back from receiver to transmitter allows the transmitter to get estimates of the channel fading coefficients.

In [36] Raleigh et al. provide a scheme for beamforming using a blind adaptive transmit antenna. This shows that the technique proposed is feasible and they indicate that it would also be applied to CDMA systems in a later study.

In [37] Rashid-Farrokhi and Tassiulas and in [38] Ligdas and Farvardin examine techniques for transmit power control in a slow fading environment. In [37] they propose multiple transmit antennas, power control and Rake receivers at the mobile and attempting to minimise the Signal in Noise Ratio (SINR) they show that significant improvements in BER can be achieved. In [38] they design a power adaptive system which uses the probability density function (pdf) of the slow fading channel and other feed back information, such as channel capacity, delay and the number of states of the bit error rate performance of their proposed policies.

In [39] Soni et al. examine space time spreading techniques which are contrasted with Orthogonal Transmit diversity in the presence of punctured codes and at different information coding rates, specifically ¼ and ½ convolutional coders. This is performed with different length spreading codes (64 Walsh codes and 128 Walsh codes), a bit rate of 9600 bps, a chipping rate of 1.2288 Mcps (Mega chips per second) (IS-2000), a frequency of 1.9 Ghz, a

Rayleigh fading channel, and a frame duration of 20 ms. They find that STS outperforms OTD under varying conditions and both techniques outperform no transmit diversity systems. The difference in performance between STS and OTD is greater at low transmission speeds compared to high transmission speeds (they used a 9.6kbps for low and a 76 kbps for high in their study) and also greater with 128 Walsh codes compared to 64 Walsh codes.

In [40] Jafarkhani and Tarokh provided a multiple transmit antenna differential detection scheme from Generalised orthogonal designs. This was a generalisation of a two transmitter antenna differential detection scheme which they previously had proposed. This uses space time block coding and develops an encoding/decoding technique on this basis using results from orthogonal design theory using results from [12].

In [41] and [25] space time block coding is applied to Orthogonal Frequency Division Multiplexing (OFDM) based systems. In [25] block coded Orthogonal Frequency Division Multiple Access (OFDMA) with linear precoding is reported. It provides for the possibility of multiuser and multirate services which can be used in Integrated Services Digital Network (ISDN) type systems. It uses transmit and receive antenna diversity in its design. They use a three level approach to achieve their gains. At the highest level they use OFDMA which caters for Multi User Interference (MUI). At the intermediate level they use space time block coding which results in the diversity gain that is observed in other studies. At the lowest level they use linear precoding in order to mitigate Intersymbol Interference (ISI). Their simulation studies show that using these techniques leads to an improvement in BER.

2.7 Ultra Wideband Systems

Ultra Wideband (UWB) systems are proposed as wireless access systems which are potentially able to provide broadband access speeds using large frequency spectrum bandwidths at low power over short distances (about 0-100 metres, also called pico cells in cellular systems). Over larger distances communication is possible but at lower access speeds. Even though the spectrum is wideband and will extend over frequencies which have been auctioned off to various commercial companies by governments, it is so low power that it appears as background radiation and forms part of the noise floor. The possible applications

range from the radio used in the formation of Ad Hoc network low power devices in a Wireless Sensor Network (WSN) scenario (comprised of small radio devices termed motes) [42] to the access of the internet using wireless transceivers in a LAN (Local Area Network).

Two main classifications of UWB are referred to in the literature. One uses multiband orthogonal frequency division multiplexing (MOFDM) where spectra is sliced into relatively large widths of broadband frequency (as distinct from narrowband) and time hopping between frequency slices may be employed across the larger UWB spectrum available. The other technique is the use of Gaussian pulses whose bandwidth extends into many GHz in terms of its spectrum. This is determined by the time duration of the pulses that are emitted by the UWB transmitter.

Ultra Wideband systems are defined as either systems using more than 500MHz of bandwidth or a minimum of twenty percent of the available bandwidth using the formula [43;44]:

$$B_f = 2\left(\frac{f_H - f_L}{f_H + f_L}\right) \qquad (2.7\text{-}1)$$

Where the values of the upper and lower frequencies are the -10dB bandwidths, as per the ruling of the Federal Communications Commission (FCC) in April 2002. This document also provided a template of radiation limits for indoor and outdoor UWB which applied to the operation of UWB systems in the United States of America (USA)(see [43] pages 5-6). This thesis uses a Gaussian pulse which does not comply with the FCC template as the template has significant radiation limits in the one to three GHz frequency band. The reason is the requirement to validate the UWB simulator against results reported in [8].

2.8 Multiband Orthogonal frequency division multiplexing

As Ultra Wideband systems span many MHz of bandwidth but at low power levels so as to appear as background noise to other licensed spectrum users, a technique which has been proposed, as well as pulse based systems (see Section 2.9 and Section 2.10), is to separate the total available bandwidth into narrower bandwidth segments which are orthogonal in frequency to each other (hence the name Multiband Orthogonal Frequency Division

Multiplexing or MOFDM or multiband UWB). This technique uses the Fast Fourier Transform (FFT) and Inverse Fast Fourier Transform (IFFT) to send signals combined with a form of spread spectrum known as Frequency hopping (FH - as used in Bluetooth radios). As stated in [45], another advantage of MOFDM systems over pulse based systems (which have spectra spanning the entire frequency space in GHz and are baseband systems) is that the bands of spectra which coincide with narrowband users who have licensed the spectra can be avoided. MOFDM systems, like narrowband OFDM systems, also need to have guard bands to ensure they are orthogonal [44;46], they suffer from phase noise which introduces Inter Carrier Interference (ICI), if the frequency hopping is very fast then timing issues associated with changing the frequency band to another can provide system design issues, and also, like OFDM, they require a large dynamic range in the signal processing circuitry which leads to the often researched high peak to average power ratio (PAPR) especially for the Power Amplifier (PA) used in the transmitters of OFDM modems [45].

One of the contributions in the area of MOFDM was a study on the use of residue number systems to assist with Fast Frequency synchronous ultra wideband spread spectrum which allowed for multiple access [47]. They used an M-ary frequency shift keying (MFSK) non-coherent system with multistage frequency hopping. They were able to reduce multiuser interference by combining users into smaller groups. The groups were split into sub-groups of from two users through to twenty four users (Figures 5 through 7 in [47]) when there were up to 32760 users in the proposed system (the lowest BER being reported, of 10^{-3} ,when there were fewer total users, for between 3780 to 5940 total users in the system). The system they propose assumes synchronous transmission from the base station to the mobile, and they point out that one advantage of FH is that detection of the signal has to be performed during each hop, but that this is not as complicated as demodulating of chip interval in the case of DS-CDMA and each hop change in frequency band is at a lower rate than that required for chip level demodulation in a DS-CDMA system [47].

In [48] Gerakoulis and Salmi describe the use of Interference Suppressing OFDM (IS-OFDM) where they use orthogonal Hadamard sequences to divide the frequency bins into groups. It is targeted at a wireless home network to provide very high access rates (of the order of 500Mbps and centred with a carrier frequency near 6GHz (5.25GHz)). Using this

technique they suppress the influence of narrowband signals and also it uses low power transmission so that it does not emit radiation significantly outside of the home.

In [49] a good summary of the state of UWB different modulation techniques (including a reference to the multi-antenna system described in [8]) are provided. It shows the FCC spectral mask for UWB in Table 1 and Figure 1 of [49]. They discuss the use of different pulse shapes to allow for different subbands of the FCC mask to be used. Such systems are referred to as multiband UWB. The advantage of multiband UWB is that the subbands could be designed (with appropriate frequency guard bands) to adapt to the FCC mask. These typically involve subbands of 500-800MHz in frequency span, and interference of narrowband systems could be achieved by eliminating certain subbands if the UWB system detects significant radiation from narrowband systems (though the FCC mask is designed so that the UWB signal should appear as background radiation). They point out that such systems will rely on analog carriers and need complex circuitry to adapt to multicarrier offsets (CFO). They will also need to synchronise the carrier frequencies and phases for coherent demodulation, which is a challenging task. They also indicate that if frequency hopping is required this also complicates the physical communication link as well as estimating the multiple channels being used by the multiband UWB system [49].

In [50] Mehbodniya and Aissa point out that two standards have been proposed to the UWB communication standards group IEEE (Institute of Electrical and Electronic Engineers) 802.15.3a (TG3a). The two proposals are using MOFDM and DS-UWB. According to [50], this standards body was not able to decide which would prevail. The authors of [50] then provide an investigation for the coexistence of both forms of UWB. They found that DS-UWB users cause more interference than TH-UWB users to the MOFDM system studied. They also designed a modulated multiband signal using thirteen smaller frequency bands and found that when in the presence of DS-UWB or TH-UWB this mitigated against interference over the three frequency bands examined in their study. This study illustrates that future systems will, most likely, involve both multiband UWB and pulse modulated systems [50].

This thesis is concerned with pulse position modulated systems, so multiband UWB or MOFDM is only of interest in that it is an alternative technique to deliver Ultra Wideband

services to the radar like pulse based systems. It also has the advantage that the frequency mask of the FCC can be more closely utilised. There will be no further consideration of multiband UWB/ MOFDM systems in this thesis.

2.9 Ultra Wideband Pulse Position Modulation SISO systems

This thesis uses the non-linear PPM technique to provide a MIMO based system (two transmit antennas to a single receive antenna) using the Space Time Spreading technique which has its basis in orthogonal designs. Our technique uses the Space Time Spreading approach to signal different pulse positions (See Chapter 6, Chapter 7, and Chapter 8) representing the underlying values observed in implementing the narrowband systems described in Chapter 3 and Chapter 4. This approach is related closely to the technique of using M-ary PPM. However, this work uses one less pulse position to encode the same data symbol. Further, this thesis can be extended to implement this for systems with four and eight antennas, though such simulation studies were not carried out due to the extra complexity required in the simulator. This study suggests that the simulations performed in Chapter 3 for four and eight antennas indicate that similar systems could be developed for the Ultra Wideband MIMO system developed later. This, of course, relates to the major advantage of the approach proposed in this thesis which demonstrates how to effectively use multiple antennas to take advantage of space diversity in an Ultra Wideband MIMO system.

In [51] an analysis of M-ary PPM systems is provided in the presence of multiple access (but without any multipath). They include a Time Hopping pattern, as this thesis does, but they allow the Time Hopping pattern to be random. The M-ary PPM is modeled as a sequence of timing offsets to represent each of the M symbols of the M-ary symbol set, which they express mathematically as [51]:

$$S_i(t) \triangleq \sum_{k=0}^{N_s-1} w\left(t - kT_f - \delta_i^k\right) \qquad (2.9\text{-}1)$$

Where i=1,2,…,M, δ_i^k is the shift for the kth frame, and T_f is the period of frame. They further indicate that the design of the shifts, the pulse waveform and whether the system uses

orthogonal, equally correlated, or N-orthogonal (where N is the number of signals in each orthogonal dimension) is used to define different M-ary systems. They look at the effect of multiple access using different M-ary designs and compare this to the analytical analysis providing numerical examples of different M-ary designs. They conclude, that in a system using M-ary PPM in the absence of multipath, the "analysis shows that impulse radio modulation is theoretically able to provide multiple access communications in a Gaussian channel with a combined transmission capacity of hundreds of megabits per second at BERs in the range 10^{-4} to 10^{-7} using receivers of moderate complexity" [51].

In [44] Di Benedetto and Giancola provide a description of the use of the different SISO based pulse techniques which include Pulse Amplitude Modulation (PAM) and PPM, in the absence of multipath over an AWGN channel. Different schemes are examined and the use of signal correlators and optimum receivers are employed. They consider binary orthogonal systems and provide a demodulator that is an optimum receiver for 2PPM. Essentially a template of the two received waveforms is formed and this is then compared to the actual noisy received waveform with the correlator output with the largest energy being used (or one correlator can be used with the template signal being the difference between the two pulse waveforms representing a shifted and unshifted received pulse waveform). These schemes are also extended to PAM systems where the energy and phase of the pulse is used to form the communication across the UWB channel and a single correlator is used to form the optimum receiver. This is extended in the M-ary case to a set of M correlators with the largest energy output being selected for the estimated M-ary symbol transmitted. An alternative design is shown in [44] which utilises a single correlator but a series of thresholds are used to detect the transmitted symbol. For M-ary PPM the optimum receiver provided in [44] is shown in Figure 2.9-1. Each of the M symbols has its own correlator and as the pulse shapes are orthogonal (that is they have different delays for each symbol) the demodulator chooses the M-ary symbol whose output has the largest value. This needs adaptation for the multipath by using a Rake receiver with perfect knowledge of the channel gains of each multipath and the arriving time epoch of each multipath. The M-ary demodulator for SISO requires M correlators. Extending this to two antennas with M-ary schema would still require multiple pulses on each antenna which, while passing through uncorrelated channels and hence would unlikely overlap at the receiver, could have the same pulse position on both antennas. The schema proposed in this thesis will always have pulses on each antenna with different pulse

delays. This is because the Space Time Spreading scheme always produced a position value on either antenna which never has the same positional value.

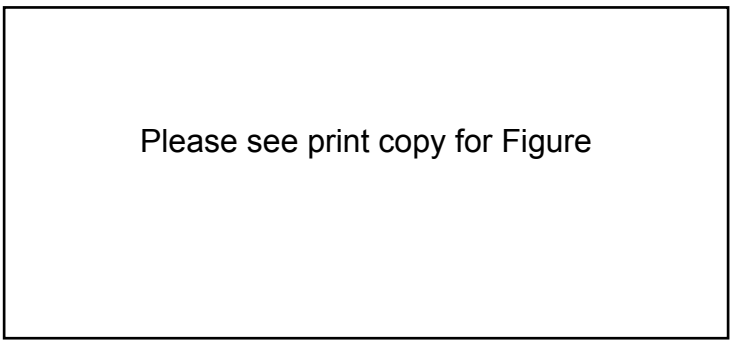

Figure 2.9-1: Optimum receiver for orthogonal M-ary PPM with TH as reproduced from [44].

The SISO system for PPM is analysed in Section 2.10 which leads onto the analysis for a MIMO system based on the work reported in [8]. For this reason it is left to that section to provide the mathematical foundation to the SISO and MIMO systems. Another work on SISO systems applied to the Medium Access Control (MAC) layer of an UWB pulse based system is provided in [52]. They indicate that an important criterion for an UWB PPM or Impulse-based UWB (I-UWB) is the pulse repetition interval (PRI). They indicate that the PRI can range from microseconds to nanoseconds. Systems with PRI's in the range 1μs to 10ns are described by them as moderate. Our system, including the effect of the TH pattern, has a PRI of between 100-1600ns (100ns times 8 slots for each TH pattern position, and considering that the TH pattern can be anywhere in the eight 100ns time slots, including the end and beginning of the eight slots). Hence the system proposed in this thesis would be classified as moderate (the mean PRI for this system would be approximately 800ns). They then describe the effect of a changing PRI. If a system has a shorter PRI than their moderate range the system will suffer from degradation due to ISI. In addition, they suggest, if the FCC's average power limit mask is to be satisfied, then the system with a shorter PRI than moderate will need to use lower power pulses. Further, they say, the amplitude of the spectral lines in comparison to the mean power will get larger as the PRI decreases [6]. They indicate that the inverse of the PRI is the pulse repetition frequency (PRF) and that the system designer of a system with a PRI less than 10ns cannot continue to increase the PRF in order to improve the throughput without the extra costs to the system that they outlined.

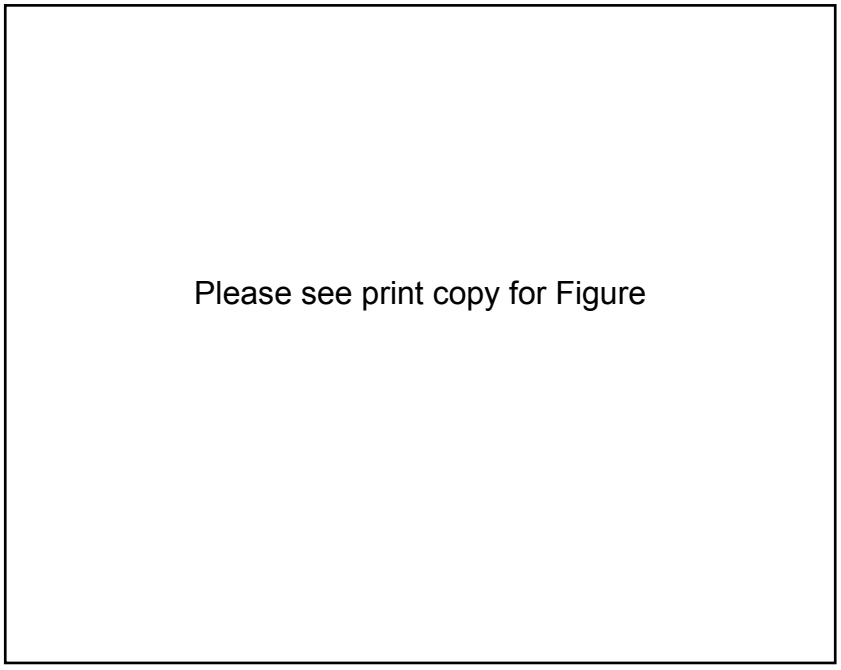

Figure 2.9-2: Multichannel MAC operation as reproduced from [6]

In [6], August and Ha continue, by examining systems with PRI's greater than 1ms suggesting that these systems, in bandwidth, begin to approach the bandwidth of narrowband systems and once again the average power limit of the FCC mask needs to be observed. So outside the moderate range for larger PRI (or smaller PRF), the designer is limited in options and cannot arbitrarily increase the SNR of the system. As they are largely interested in the MAC protocol they point out that operation in a multi-channel ALOHA (M-ALOHA) or multi-channel pulse sense multiple access (M-PSMA) multi-access MAC environments, where they indicate that the maximum delay spread for their systems of interest is 25ns (our system spans 100ns), that there is a lot of dead time between pulse emissions. This dead time can be used to send other data streams. Also, as nodes may be spaced at different distances the individual propagation delays may vary allowing pulses to be transmitted at the same time at individual transmitters but received at different times at the receiver, also over uncorrelated channels. They illustrate the operation of a multi-access/multi-channel MAC operation in Figure 2 of [6] which is reproduced in Figure 2.9-2. They indicate that for their systems a collision may occur (as even in the UWB channel there are gaps between individual rays within the same multipath channel) only when the individual pulse channels PRI overlay at the receiver. They then develop some analysis on the probability of collision at the MAC layer. They indicate that with pulse based system which they propose as the M-ALOHA, and

where there are large periods of no transmissions or dead bands in the wireless medium, that such multichannel systems have a reduced chance of collision as compared to the use of a single channel protocol, such as ALOHA. The investigation of MAC protocols for the UWB MIMO system is not further studied in this thesis. Such systems will need to be developed for successful application of UWB MIMO communication links and some are described in [43].

2.10 Ultra Wideband Pulse Position Modulation MIMO systems

The other major technique proposed in the literature to provide transmission using pulses with very small duration (in the order of hundreds of picoseconds to nanoseconds) which in the frequency domain have very large bandwidths (in the order of GHz)([43] pages 1-3). Most proposed systems in the literature prior to 2004 were concerned with SISO UWB PPM systems. In 2004 a paper was published which described the use of the Analog Space Time Coding for a MIMO based system and provided some possible scenarios for deployment [8].

In [8] Yang and Giannakis model a UWB system without any super-imposed Time Hopping pattern. They consider a more generic case where the system can be shown to be a combination of PAM and PPM. They start by providing the model of a SISO peer to peer UWB system. They define the system as one which uses a stream of pulses to provide this peer to peer communication. These pulses, though, have extremely short duration (hence the large bandwidth), which they suggest is typically between 0.2ns and 2ns. This pulse duration is denoted by them as T_w using a pulse waveform or shape denoted as w(t). They denote N_t as the number of transmit antennas and N_r as the number of receive antennas (which in this thesis is always one but they did allow for two receive antennas). These pulses are modulated in some way (amplitude or position) determined by the value of the symbol being transmitted (-1 or 1), and then they are transmitted over the channel using repetition a total of N_f times with each channel transmission, or frame, having a duration of T_f, they say. They lead on to point out that if the individual path gains are denoted $\alpha_g(l_g)$, where l_g is the path number of the g^{th} arriving ray, then the physical multipath channel can be mathematically expressed as:

$$g(t) = \sum_{l_g=0}^{L_g-1} \alpha_g(l_g)\, \delta\left(t - \tau_g(l_g)\right)$$

(2.10-1)

Where they specifically order the arrival time of the arriving multipath rays such that the arriving times are sequential and that the time of the arrival of each ray meets the criteria that [8]:

$$\tau_g(l_g) > \tau_g(l_g - 1) \quad , \quad \forall l_g \in [1, L_g - 1] \qquad (2.10\text{-}2)$$

Yang and Giannakis [8] state that convolution can be utilised to find the overall channel h(t) by simply convolving the "pulse shaper" [8] or realistically the continuous time expression of the pulse shape within a single channel time frame duration (T_f), with the physical multipath channel described by Equation 2.10-1 to get:

$$h(t) = g(t) * w(t) = \sum_{l_g=0}^{L_g-1} \alpha(l_g) w\left(t - \tau_g(l_g)\right) \qquad (2.10\text{-}3)$$

Yang and Giannakis [8] note that the maximum delay spread of the dense multipath is given basically as the arriving time of the last arriving ray or:

$$T_g = \tau_g(L_g - 1) \qquad (2.10\text{-}4)$$

Hence, to avoid the possibility of Intersymbol interference, the channel frame duration, T_f, simply must exceed the sum of the maximum delay spread and the duration of a typical pulse shape, w(t) ie:

$$T_f \geq T_g + T_w \qquad (2.10\text{-}5)$$

Yang and Giannakis [8] then go on to model the multipath fading channel as being quasi-static which they claim is typical of indoor environments. At a wireless workshop in 2005 [53] it was explained that realistic UWB signals will stay quasi-static for approximately 300 milliseconds which would in fact be many symbol periods. In [8] they continue by saying that the assumption is that the channel remains quasi-static for at least one symbol, with the channel allowed to vary between symbols. In their model this means that the channel multipath coefficients are static for a period of $N_f T_f$, seconds.

A Rake receiver is then needed to sift through the received multipath signal and a template signal is developed which is then used to recover the transmitted symbol [54]. A Rake receiver is composed of individual matched filter detectors for each distinct multipath. Each of these multipaths is referred to as a finger. This gives the receiver its name where the receiver uses each multipath to 'rake' up the energy of each detected multipath as if raking up leaves on a lawn in the Autumn. The number of multipath in the receivers Rake receiver is denoted L in [8] and also in this thesis. Using the L paths of the Rake receiver and adjusting for time of arrival for each of the paths used they then form a decision statistic. Using the decision statistic a decision is made to determine if the transmitted symbol is -1 or 1. They then go on to suggest in the case where a single transmit antenna is deployed sending a binary signal '**s**' in the set {-1,1} with energy ε providing the transmitted symbol waveform [8]:

$$s(t) = s\left(\sqrt{\frac{\varepsilon}{N_f}}\right)\sum_{n_f=0}^{N_f-1} w\left(t - n_f T_f\right), \qquad s = \pm 1, \tag{2.10-6}$$

This signal is conditioned in that the pulse shaper $w(t)$ has unit energy, ie [8]:

$$\int_0^{T_f} w^2(t)dt = 1 \tag{2.10-7}$$

Yang and Giannakis [8] highlight that for a single receiver, and after appropriately adjusting for the time of each arriving ray (that is the timing offsets), the signal received or seen at the receiver is then given by [8]:

$$r(t) = s(t) * g(t) + \eta(t) \tag{2.10-8}$$

Here $\eta(t)$ is additive white Gaussian noise (AWGN) with zero mean, and variance σ^2, $N(0,\sigma^2)$. They then combine Equation 2.10-1, Equation 2.10-6, Equation 2.10-7, and Equation 2.10-8 to give:

$$r(t) = s\left(\sqrt{\frac{\varepsilon}{N_f}}\right)\sum_{n_f=0}^{N_f-1} h\left(t - n_f T_f\right) + \eta(t) \qquad (2.10\text{-}9)$$

They continue on that this resulting signal contains a large number of multipaths, and these are resolvable, as they are ultra short and can be harvested by an appropriately designed Rake receiver [8].

In [8] Yang and Giannakis indicate that using the pulse shaper, $w(t)$, as a basis for a reference waveform and a Rake receiver with L fingers it would result in a correlation of the received waveform $r(t)$ with L delayed versions of basic pulse shaper waveform composed of appropriately delayed times or epochs corresponding to the multipath rays which are used in the Rake receiver's sweep of the received radiated energy. That is, the reference signal is the set of time ordered waveforms [8]:

$$\left\{w\left(t - \tau(l)\right)\right\}_{l=0}^{L-1} \qquad (2.10\text{-}10)$$

But with the condition that they are ordered such that:

$$0 \le \tau(0) < \tau(1) < \tau(2) < \cdots < \tau(L-1) \le T_g \qquad (2.10\text{-}11)$$

These being the epochs at which each ray arrives at the receiver in time increasing order. They note that the times at which rays arrive are not restricted by discrete intervals (ie it is a continuous arrival process). However, they observe that the rays which are used in the Rake receiver are chosen completely at the discretion of the receivers design based on some criteria. Clearly, if the rays arrive within a time span less than a pulse width, T_w, the Rake receiver will be unable to distinguish between the arriving rays. If rays are chosen, that are used in the Rake receiver, such that they satisfy the criteria that follows, the Rake receiver should be able to resolve the outputs of the matched filters used by the receiver. Firstly, for

the outputs of the Rake's matched filters to be uncorrelated implies that the individual channel gains, $\{\alpha_g(l_g)\}_{l_g=0}^{L_g-1}$, are also uncorrelated. If this first condition is satisfied (as it should be), then the second condition they suggest is that the selected rays should satisfy:

$$\tau(l) - \tau(l-1) \geq 2T_w, \ \ \forall l \in [1, L-1] \qquad (2.10\text{-}12)$$

Where L is the number of multipaths chosen in the L fingers that are used to form the decision statistic. They highlighted that the designer of the Rake receiver can choose the necessary paths which satisfy the criteria of Equation 2.10-12.

Yang and Giannakis [8] continue with their analysis, further, simplifying it by using the epochs of the arriving rays to satisfy the condition that:

$$\tau(l) = 2lT_w, \qquad \forall l \in [0, L-1] \qquad (2.10\text{-}13)$$

Where L is less than or equal to L_g. Continuing they explain that the output of the l[th] finger during each frame duration is given by [8]:

$$x(l) = s\left(\sqrt{\frac{\varepsilon}{N_f}}\right)\alpha(l) + \zeta(l), \qquad \forall l \in [0, L-1] \qquad (2.10\text{-}14)$$

Here they defined the following relations for Equation 2.10-14 [8]:

$$\zeta(l) = \int_0^{T_f} \eta(t) w\big(t - \tau(l)\big) dt \qquad (2.10\text{-}15)$$

And

$$\alpha(l) = \int_0^{T_f} h(t) w\big(t - \tau(l)\big) dt \qquad (2.10\text{-}16)$$

So that:

$$\alpha(l) = \sum_{l_g=0}^{L_g-1} \alpha_g(l_g) R_w\left(\tau(l) - \tau_g(l_g)\right) \qquad (2.10\text{-}17)$$

Where:

$$R_w(\tau) = \int_0^{T_f} w(t) w(t-\tau) dt \qquad (2.10\text{-}18)$$

is, in fact, the autocorrelation function of the pulse shaper. They indicate that the expression for $\zeta(l)$ in Equation 2.10-15 has zero mean and variance σ^2 since the assumed pulse shaper has unit energy, and the finger delays satisfy Equation 2.10-12. Thus they suggest that $\zeta(l)$ is also white [8].

It is also pointed out in [8] they point out that one can maximise the SNR using an MRC combined at different levels, one at the L fingers per frame of the employed Rake receiver and the other over the N_f frames that correspond to a transmitted symbol. They suggest that to use the MRC they require knowledge of the individual channel coefficients (gains and delays), usually achieved by deploying pilot signals. They symbolise these coefficients involving the gains and delays by using the symbol $\{\alpha(l)\}_{l=0}^{L-1}$ containing knowledge of the multipath gains, $\{\alpha_g(l_g)\}_{l_g=0}^{L_g-1}$ and the multipath delays, $\{\tau_g(l_g)\}_{l_g=0}^{L_g-1}$, and hence the output of the MRC per received frame then becomes [8]:

$$y(n_f) = \sum_{l=0}^{L-1} x(l)\alpha(l) = s\left(\sqrt{\frac{\varepsilon}{N_f}}\right)\sum_{l=0}^{L-1}\alpha^2(l) + \sum_{l=0}^{L-1}\alpha(l)\zeta(l) = s\left(\sqrt{\frac{\varepsilon}{N_f}}\right)\varepsilon_g + \xi(n_f)$$

(2.10-19)

Where Equation 2.10-19 is valid for $\forall n_f \in [0, N_{f-1}]$. Clearly for Equation 2.10-19 we have $\varepsilon_g = \sum_{l=0}^{L-1}\alpha^2(l)$ and $\xi(n_f) = \sum_{l=0}^{L-1}\alpha(l)\,\zeta(l)$, and they suggest that ε_g represents the energy captured by the Rake receiver with L fingers [8]. This captured energy, for L constant, is then determined by the channel as the pulse shaper has unit energy. They also note that the noise term has zero mean (white Gaussian noise) but it now has a variance given by $\varepsilon_g\sigma^2$. Since they assume that the channel remains invariant over $N_f T_f$ seconds, the MRC of the N_f frames, they suggest, is simply the summation of all the received waveforms described by Equation 2.10-19 over N_f frames. They go on to suggest that the resulting decision statistic is based on the symbol *s* and they indicate this is given by:

$$z = s\left(\sqrt{(N_f\varepsilon)}\right)\varepsilon_g + \sum_{n_f=0}^{N_f-1}\xi(n_f) \qquad \text{(2.10-20)}$$

They also note that the noise term of Equation 2.10-20 has zero mean (white Gaussian noise) but it now has a variance given by $N_f \varepsilon_g \sigma^2$, from which they deduce that when one uses a maximum likelihood detector the BER is given by the equation:

$$P\left(e|\{\alpha(l)\}_{l=0}^{L-1}\right) = Q\left(\sqrt{(\rho\varepsilon_g)}\right) \tag{2.10-21}$$

Where

$$\rho = \frac{\varepsilon}{\sigma^2} \tag{2.10-22}$$

Which denotes the transmit SNR. For the simulations used in this thesis the received SNR at the receiver is considered, rather than the transmit SNR, as some energy radiates away from the receiver. This may account for the minor variations in simulation results that were observed in Section 5.5. The function Q(x) is the Gaussian tail function defined as:

$$Q(x) = \left(\frac{1}{\sqrt{2\pi}}\right) \int_x^{\bowtie} e^{-\left(t^2/2\right)} dt \tag{2.10-23}$$

It is suggested that if it is conditioned on ε_g, using the Chernoff bound, then the probability of error is found as [2;8;55]:

$$P\left(e|\{\alpha(l)\}_{l=0}^{L-1}\right) \leq e^{-\left(\frac{\rho\varepsilon_g}{2}\right)} \tag{2.10-24}$$

Yang and Giannakis [8] then use Equation 2.10-19 and Equation 2.10-24 to get:

$$P\left(e|\{\alpha(l)\}_{l=0}^{L-1}\right) \leq e^{\left(-\rho\left(\sum_{l=0}^{L-1}\left(\frac{\alpha^2(l)}{2}\right)\right)\right)} \tag{2.10-25}$$

Or

$$P\left(e|\{\alpha(l)\}_{l=0}^{L-1}\right) = \prod_{l=0}^{L-1} e^{-\left(\frac{\rho\alpha^2(l)}{2}\right)} \qquad (2.10\text{-}26)$$

In [8] they also note that in indoor environments in the presence of multiple reflections and refractions, the gain of each path can be represented by a Rayleigh distributed random variable and its phase can be represented as a uniformly distributed random variable in the range 0 through 2π (excluding the point 2π) [7]. They then point out that UWB systems only involve real signals, so the system is only concerned with the real part of each path gain [8]. In fact, they indicate that the real parts of the gains can be represented by a gaussian distributed variable with zero mean (Real part of Rayleigh distributed complex gains) since, they say, that the combination of gaussian random variables, in this case the $\alpha(l)$'s, will also result in a gaussian distribution [8;56].

Yang and Giannakis continue in [8] by once again highlighting that provided the time between selected fingers is chosen such that the time difference is greater than twice the width of a pulse, T_w, for all l an element of the interval 1 through L-1. In that case, they continue, if the expectation operator, E, is taken of the product of any two of the selected $\alpha(l)$'s they would find that the result would be zero. This implies that the waveforms (which were carefully chosen in the Rake receiver) are orthogonal to each other or mathematically [8]:

$$E[\alpha(l_1)\alpha(l_2)] = 0, \qquad \forall l_1 \neq l_2 \qquad (2.10\text{-}27)$$

Yang and Giannakis [8] further emphasise this by saying that these waveforms are uncorrelated for all instances or fingers such that $\forall l_1 \neq l_2 \in [0, L-1]$.

Yang and Giannakis [8] then define the $\beta(l)$ to be the expectation of the square of the individual $\alpha(l)$'s such that:

$$\beta(l) = E[\alpha^2(l)] \qquad (2.10\text{-}28)$$

Yang and Giannakis [8] then average the conditional BER over independent Gaussian distributions of $\alpha(l)$ where they then establish the first proposition, which they label proposition 1 which is as follows [8]:

"The average BER of a single-antenna UWB system employing a L-finger Rake receiver is upper bounded at high SNR ($\varepsilon \gg \sigma^2$), by:

$$P(e) \leq (\rho B_L)^{-\frac{L}{2}} \qquad (2.10\text{-}29)$$

With diversity gain given by $L/2$, and coding gain given by:

$$B_L = \left(\prod_{l=0}^{L-1} \beta(l)\right)^{1/L} \text{"} \text{ [8]} \qquad (2.10\text{-}30)$$

Yang and Giannakis [8] suggest that Equation 2.10-29 provides confirmation to the notion that as the number of fingers used in the Rake receiver, L, is increased that the order of diversity is also improved. They further indicate that it can be proved that if the $\alpha(l)$'s are, in fact, independent complex Gaussian random variables with a variance of $\frac{\beta(l)}{2}$ per dimension the BER upper bound can be shown to be [8;30]:

$$P(e) = \left(\frac{\rho B_L}{2}\right)^{-L} \qquad (2.10\text{-}31)$$

Yang and Giannakis [8] further elucidate that the difference is due to the fact that the UWB transmissions are real.

In [8] the authors then consider the effects of the Rake receiver on the designed system. They point out that a higher diversity gain is achieved by increasing the number of fingers, L, used in the Rake receiver. This can be achieved by choosing denser finger delays or spreading the fingers out within the channel sounding and using larger finger delays. They point out if the choice is for denser finger delays then the fingers will be packed closer in time and then the likelihood is that the channel $\alpha(l)$'s will become more correlated which would challenge the independence assumption for the $\alpha(l)$'s in the Rake receiver. On the other hand, using fingers separated in time from each other within a channel sounding (or instance) risks the use of fingers which have lower real amplitudes (decreasing power profile as multipath path lengths

are increased) and hence the coding gain, B_L , is seriously depreciated. They then point out that the diversity order is a function of the energy capture capability of the Rake receiver. This energy capture, unfortunately, will not increase linearly as the number of fingers used in the Rake receiver is increased. They then highlighted that tragically large L does not, consequently, improve the performance but simply increases the implementation complexity of the designed Rake receiver. Thus, they suggest, that there is an engineering tradeoff even in the design of the number of Rake receiver fingers. On one hand a larger number of fingers is undesireable due to complexity, on the other hand there is a need to increase the diversity order (ie use more multipath or more of the total energy available at the receiver). It is this engineering tradeoff which inspired [8] to suggest the Analog Space Time (ST) Coding schemes which they proceeded to describe and which also inspired the application of Space Time Spreading to a similar system proposed and studied in this thesis. However, our proposed system uses multiple spreading codes and thus allows for the presence of multiple users.

In [8] Yang and Giannakis then describe their Analog ST Coding. Two systems are proposed. The ST Coding Scheme II uses transmission from each antenna at different time epochs, thus taking advantage of Space diversity using each antenna at alternative times (time diversity). This technique does not transmit data on both antennas at the same time. As such it does not directly compare to the proposed system in this thesis and wastes the resources of having two antennas while still having a diversity advantage as both antennas should experience uncorrelated channels. They also investigate the use of a ST Coding Scheme I system which does transmit on both antennas simultaneously. This system is further described in Section 8.2. As this is the case, in this chapter, a review of the analysis provided in [8] for the ST Coding Scheme I system is provided next. In Section 8.2 of this thesis it is highlighted that this scheme is using a form of direct sequence spreading.

In [8] they then proceed to consider the case of a UWB system with two transmit and one receive antenna. They introduce the notation that the m^{th} transmit antenna to the single receive antennas impulse response for the coupled multipath fading channel should be denoted by:

$$g_m(t), \quad m = 0,1 \qquad (2.10\text{-}32)$$

Yang and Giannakis [8] indicate that the individual impulse responses, $g_0(t)$, and $g_1(t)$ are assumed to be quasi-static and mutually independent over a symbol duration of $N_f T_f$. Thus, they say, that the multipath channel from the m[th] transmit antenna to the single receive antenna can be expressed as the following convolution:

$$h_m(t) = g_m(t) * w(t) \qquad (2.10\text{-}33)$$

Yang and Giannakis [8] then denote the maximum delay spread of $g_m(t)$ to be symbolized by T_{gm}. Hence, they indicate, the maximum overall delay spread must be given by the maximum delay spread of antenna 0 or antenna 1 or mathematically:

$$T_g = max(T_{g0}, T_{g1}) \qquad (2.10\text{-}34)$$

Yang and Giannakis [8] then indicate that Inter Symbol Interference is avoided simply by choosing a frame duration which satisfies the SISO equivalent as expressed by Equation 2.10-5, ie the frame duration should be greater or equal to the sum of the maximum delay spread and the width of the shaper pulse.

Yang and Giannakis [8] then indicate that the value of N_f is chosen to be even (when using spreading codes they are usually powers of two and hence are even). They then describe the ST coding Scheme I system indicating that for such a system during each symbol duration $N_f T_f$ they transmit from antenna 0 the waveform given by (reproduced from [8] equation 10):

$$s_o(t) = s\left(\sqrt{\frac{\varepsilon}{2N_o}}\right)\sum_{n_f=0}^{N_f-1}(-1)^{n_f}\, w\left(t - n_f T_f\right) \qquad (2.10\text{-}35)$$

And from the 1[st] antenna they transmit the waveform given by (reproduced from [8] equation 11):

$$s_1(t) = s\left(\sqrt{\frac{\varepsilon}{2N_o}}\right)\sum_{n_f=0}^{N_f-1} w\left(t - n_f T_f\right) \qquad (2.10\text{-}36)$$

The factor of two in the denominator is used to normalise the transmitted power so that it is equivalent to a SISO based system. They indicate that only one symbol is transmitted over N_f frames as is the case for a SISO based system. They then indicate that the received noisy waveform seen at the receiver is given by the expression:

$$r(t) = s_o(t) * g_0(t) + s_1(t) * g_1(t) + \eta(t) \qquad (2.10\text{-}37)$$

Or using Equation 2.10-33, Equation 2.10-35 and Equation 2.10-36, they get:

$$r(t) = s\left(\sqrt{\frac{\varepsilon}{2N_f}}\right)\sum_{n_f=0}^{N_f-1}\left[(-1)^{n_f}h_0\left(t-n_fT_f\right)+h_1\left(t-n_fT_f\right)\right]+\eta(t) \qquad (2.10\text{-}38)$$

Yang and Giannakis [8] then proceed to remove the even and odd indexed frames of each symbol and these are then given the names $r_e(t)$ and $r_o(t)$ and using this, they then re-express the received waveform as:

$$r(t) = \sum_{n_f=0}^{N_f'-1}\left[r_e\left(t-2n_fT_f\right)+r_o\left(t-2n_fT_f-T_f\right)\right] \qquad (2.10\text{-}39)$$

Where Yang and Giannakis [8] define:

$$N_f' = N_f/2 \qquad (2.10\text{-}40)$$

And Yang and Giannakis [8] define:

$$r_e(t) = s\left(\sqrt{\frac{\varepsilon}{2N_f}}\right)[h_0(t)+h_1(t)]+\eta_e(t) \qquad (2.10\text{-}41)$$

And:

$$r_{\boldsymbol{o}}(t) = s\left(\sqrt{\frac{\varepsilon}{2N_f}}\right)[h_{\boldsymbol{1}}(t)-h_{\boldsymbol{0}}(t)]+\eta_{\boldsymbol{o}}(t) \qquad (2.10\text{-}42)$$

Yang and Giannakis [8] then indicate that these quantities are fed into the Rake receiver with L fingers in which case the output of the l^{th} finger for even frames is given by:

$$x_e(l) = s\left(\sqrt{\frac{\varepsilon}{2N_f}}\right)[\alpha_0(l) + \alpha_1(l)] + \zeta_e(l) \quad (2.10\text{-}43)$$

And the output of the l^{th} finger for odd frames is given by:

$$x_o(l) = s\left(\sqrt{\frac{\varepsilon}{2N_f}}\right)[\alpha_1(l) - \alpha_0(l)] + \zeta_o(l) \quad (2.10\text{-}44)$$

Where Yang and Giannakis [8] define the quantity:

$$\alpha_m(l) = \int_0^{T_f} h_m(t)w\big(t - \tau(l)\big)\,dt\ ,\ m = 0{,}1 \quad (2.10\text{-}45)$$

Yang and Giannakis [8] then highlight that the output of the MRC for evenly indexed frames is:

$$y_e(n_f) = s\left(\sqrt{\frac{\varepsilon}{2N_f}}\right)\sum_{l=0}^{L-1}[\alpha_0(l) + \alpha_1(l)]^2 + \xi_e(n_f) \quad (2.10\text{-}46)$$

And for oddly indexed frames is:

$$y_o(n_f) = s\left(\sqrt{\frac{\varepsilon}{2N_f}}\right)\sum_{l=0}^{L-1}[\alpha_1(l) - \alpha_0(l)]^2 + \xi_o(n_f) \quad (2.10\text{-}47)$$

Yang and Giannakis [8] then note that the even noise term is given by:

$$\xi_e(n_f) = \sum_{l=0}^{L-1}[\alpha_0(l) + \alpha_1(l)]\,\zeta_e(l) \quad (2.10\text{-}48)$$

And the odd noise term is given by:

$$\xi_o(n_f) = \sum_{l=0}^{L-1}[\alpha_1(l) - \alpha_0(l)]\,\zeta_o(l) \quad (2.10\text{-}49)$$

The noise terms in Equation 2.10-48 and Equation 2.10-49, they indicate, are white gaussian noise terms with zero mean. The variance of the even noise term is stated, by them to be:

$$\sigma_{\xi_e}^2 = \sigma^2 \sum_{l=0}^{L-1} [\alpha_0(l) + \alpha_1(l)]^2$$

(2.10-50)

And for the odd noise term it has variance:

$$\sigma_{\xi_o}^2 = \sigma^2 \sum_{l=0}^{L-1} [\alpha_1(l) - \alpha_0(l)]^2$$

(2.10-51)

With Equation 2.10-50 and Equation 2.10-51 conditioned on:

$$\forall n_f \in [0, N_f' - 1]$$

(2.10-52)

Yang and Giannakis [8] then proceed to sum up the even and odd MRC outputs described by Equation 2.10-46 and Equation 2.10-47 over N_f frames which then corresponds to one symbol, s. They then form the decision variable z, such that z is defined as:

$$z = s\left(\sqrt{\frac{N_f \varepsilon}{2}}\right)(\varepsilon_{g0} + \varepsilon_{g1}) + \sum_{n_f=0}^{N_f'-1} \left(\xi_e(n_f) + \xi_o(n_f)\right)$$

(2.10-53)

Where Yang and Giannakis [8] define:

$$\varepsilon_{gm} = \sum_{l=0}^{L-1} \alpha_m^2(l)$$

(2.10-54)

And Yang and Giannakis [8] indicate that the zero mean noise has a variance given by the formula:

$$N_f\sigma^2(\varepsilon_{g0}+\varepsilon_{g1}) \qquad (2.10\text{-}55)$$

Yang and Giannakis [8] then indicate that for channels $g_0(t)$ and $g_1(t)$ the BER attached to the Maximum-Likelihood (ML) detector is:

$$P\{e|\{\alpha_0(l),\alpha_1(l)\}_{l=0}^{L-1}\} = Q\left(\sqrt{\rho\frac{(\varepsilon_{g0}+\varepsilon_{g1})}{2}}\right) \qquad (2.10\text{-}56)$$

Where $\rho = \frac{\varepsilon}{\sigma^2}$, the transmit SNR, and the Q function is given by Equation 2.10-23. Yang and Giannakis [8] then suggest that if the Chernoff bound is applied one gets:

$$\begin{aligned} P\{e|\{\alpha_0(l),\alpha_1(l)\}_{l=0}^{L-1}\} &\le exp\left(-\rho\left(\varepsilon_{g0}+\varepsilon_{g1}\right)/4\right) \\ &= exp\left(-\frac{\rho\varepsilon_{g0}}{4}\right)\cdot exp\left(-\frac{\rho\varepsilon_{g1}}{4}\right) \end{aligned} \qquad (2.10\text{-}57)$$

Yang and Giannakis [8] then suggest that if this is averaged over all the channel gains, $\{\alpha_0(l),\alpha_1(l)\}_{l=0}^{L-1}$ they obtain their second proposition which is that if the channel coherence time is N_fT_f and an L-finger rake is implemented the mean BER of a UWB system which uses two transmit and one receive antenna, for high SNR, is upper bounded by the equation [8], for a ST coding Type I system:

$$P(e) \le \left(\frac{\beta_L}{2}\rho\right)^{-L} \qquad (2.10\text{-}58)$$

Which indicates that the diversity is of order L and the coding gain is $\beta_L/2$. They observe that this ST coding Type I scheme doubles the diversity order but with a trade off of 3dB loss in the coding gain and the resource of using one extra antenna when compared to Equation 2.10-29.

Yang and Giannakis [8] continue by describing the Analog ST Coding II scenario which requires a coherence time of $2N_fT_f$ but achieves twice the diversity of the Analog ST Coding I but at a cost of higher latency (twice that of Analog ST Coding I) and smaller coding gain (half that of Analog ST Coding I). The Analog ST Coding II scheme transmits on either antenna at different time periods, thus it is not simultaneous transmission and if multiple users are present may degrade significantly. The Analog ST Coding II scheme is not investigated in this thesis as this thesis compares its proposed system to Analog ST Coding I schema to which it is closest in function.

Yang and Giannakis [8] proceed by discussing various aspects of their Analog ST Coding schemes. Of particular interest is their discussion on Analog ST coding for PPM. They also consider ST Coding schemes which are non-coherent (ie there is no need for channel state information). These non-coherent schemes are not of interest to this thesis as it proposes a coherent system whereby it has perfect knowledge of the channel state information within its simulations. In terms of the discussion on Analog ST coding PPM systems are modelled using the timing of the pulse or its position in time (see Section 2.9) . They indicate that a binary PPM can be used to represent the symbol -1 using the pulse shaper, $w(t)$, with no offset in time whereas the symbol +1 would use a pulse shaper offset in time by a value Δ such that the pulse shaper used is in fact $w(t-\Delta)$. They indicate that the choice of this offset time, Δ, is entirely up to the discretion of the system designer. If this is the case then Equation 2.10-5 needs to be slightly modified to become:

$$T_f \geq T_g + T_w + \Delta \qquad (2.10\text{-}59)$$

Yang and Giannakis [8] indicate that this is a necessary condition to avoid ISI. The Δ represents the modulation index of our PPM system. In [57] they indicate that this delay can be selected to minimise the correlation, and the minimum of $\int_0^{T_f} w(t)w(t-\Delta)dt$ is found in [57] according to [8] as Δ =0.156ns. In [8] they continue by pointing out that the value of Δ can be selected such that $\int_0^{T_f} w(t)w(t-\Delta)dt = 0$. That is the -1 pulse shaper $w(t)$ is selected to be orthogonal to the +1 pulse shaper $w(t-\Delta)$. They indicate that to satisfy this condition one could obviously choose the situation where $\Delta \geq \mathrm{T_w}$ which results in orthogonal PPM. At an extreme, they suggest, choosing the delay to be:

$$\Delta = T_g + T_w \qquad (2.10\text{-}60)$$

Which will provide a communication system equivalent to block coded on-off keying (OOK). They indicate that in such a system -1 is observed by transmitting pulses during frames with an even index and +1 is observed by transmitting pulses during frames with an odd index [58]. While OOK guarantees modulation even when the signal experiences propagation through a frequency selective channel with a maximum delay spread up to T_g, they say, it provides only half the rate of transmission of a PAM system or a PPM system which employ small Δ. They then point out that for arbitrary Δ, their Analog ST Coding I schema can be applied without modification, requiring only the use at the Rake receiver's correlators of the template signal $w(t-\tau(l)-\Delta)-w(t-\tau(l))$ instead of $w(t-\tau(l))$ [8].

In [8] Yang and Giannakis form simulations using channels described according to [59] and [7]. These channels describe rays arriving in clusters. Section 2.11 describes these channels in some detail and Section 5.2 briefly describes the channel. They set up their simulations using the parameters provided which are also used for the proposed system simulations of this thesis as indicated in Section 5.3. They chose, as the systems proposed in this thesis do, the frame duration to be 100ns and the maximum delay spread was set to 99ns. They chose their pulse shaper to be the second derivative of the Gaussian function, as this thesis describes in Section 5.2 which is mathematically described in Equation 5.2-2. They then simulated their Analog ST Coding I schema with two transmit antennas and one receive antenna. They used L=1, 4 and 16 fingers in their simulations (in this thesis it uses L=1 and L=4). They then proceeded to compare the BER performance of a single antenna system with that of their two proposed Analog ST Coding techniques. The results plot of Figure 2 in [8] are reproduced in Figure 2.10-1. They found from their simulations that better BER performance occurred as SNR is increased, due to higher diversity orders, for their Analog ST coding techniques.

In [8] for test case 5 they looked specifically at using PPM. They contrasted the BER performance of the SISO system with their Analog ST Coding Type I scheme. They used a delay, Δ, of 0.156ns and 1ns. The best performance was achieved using the 0.156ns delay (this thesis compares our system to the 1ns results as it did not employ the 0.156ns delay in our simulator). The use of a delay of 1ns corresponded to orthogonal PPM since the pulse width was set to 0.7ns. The results plot of Figure 7 for one finger (L=1) and Figure 8 for four

fingers (L=4) in [8] are reproduced in Figure 2.10-2 and Figure 2.10-3. They observed that for both L=1 and L=4 that a higher diversity order advantage can be seen for high SNR over the SISO based system.

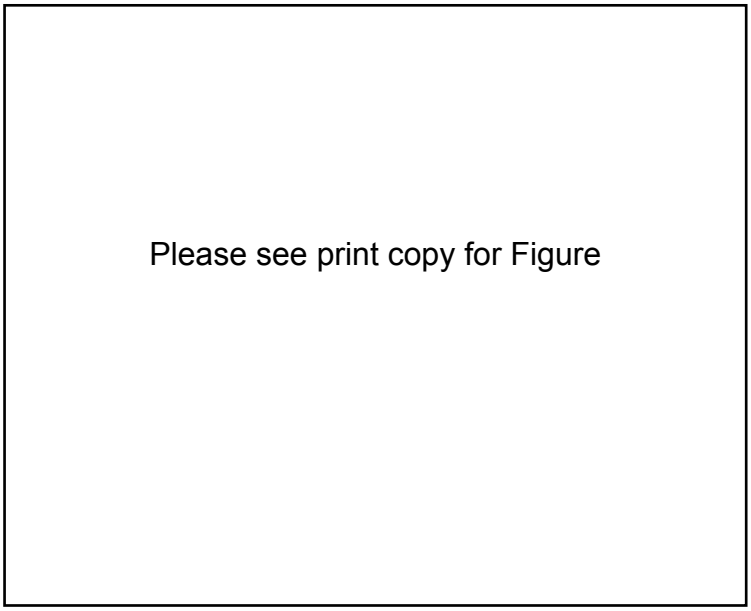

Figure 2.10-1: Results of BER performance versus SNR for single and multiple antenna Analog Coding Type I and II reproduced from [8].

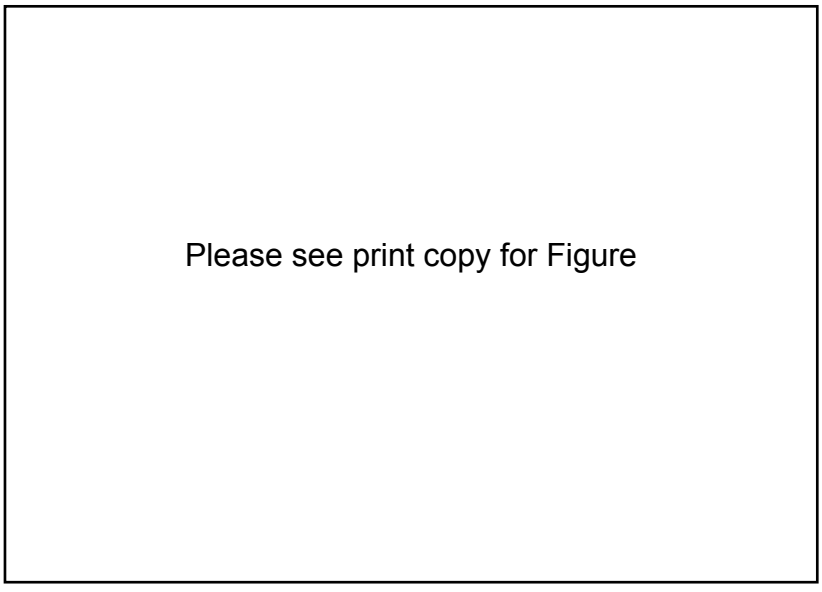

Figure 2.10-2: Results of BER performance versus SNR for single and multiple antenna Analog ST Coding Type I scheme using L=1 for PPM reproduced from [8].

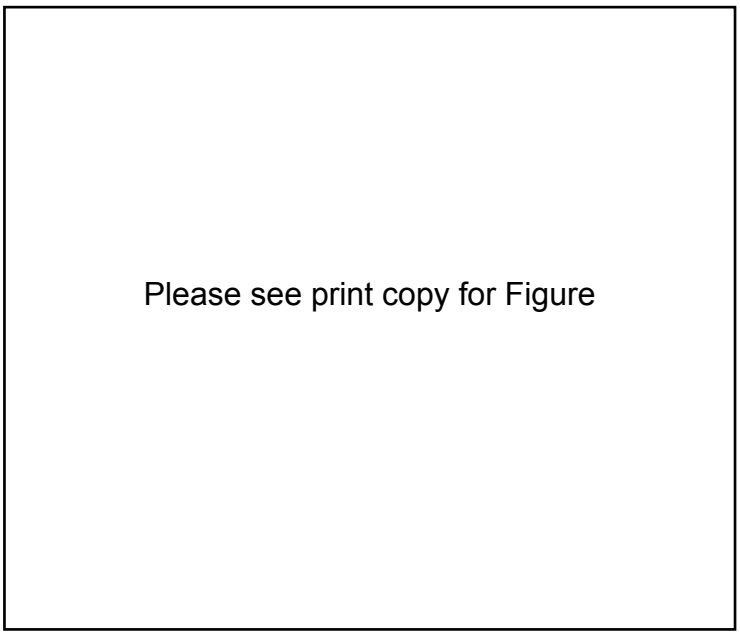

Figure 2.10-3: Results of BER performance versus SNR for single and multiple antenna Analog ST Coding Type I scheme using L=4 for PPM reproduced from [8].

In Section 5.5 this thesis compares the results for the SISO based system of [8] with the Simulink Simulation it constructed and describes in Chapter 5. In Section 8.5 it does the same, but this time for the Analog ST Coding Type I scheme described in this section and contributed by [8]. It then proceeds to compare these systems to the proposed Space Time Spreading adaptations proposed in this thesis.

2.11 The Saleh-Valenzuela multipath channel

The Saleh-Valenzuela multipath channel is used in simulations in [8] to model the UWB multipath channel (see Section 2.10). It was originally proposed by Saleh-Valenzuela in [7] as a result of measurements conducted in the middle 1980's in office space within a city building. In the study conducted by Saleh-Valenzuela they employed a radar like low power 1.5GHz pulse with width about 10ns and time resolution measurements of 5ns over a time duration of 600ns. From their physical measurements they proposed a model which has become known as the Saleh-Valenzuela statistical model. It is adopted in the work described in [8] with a pulse width of 0.7ns over a 100ns channel duration, against which the Simulink simulations of this thesis were validated. Even though in [7] they made measurements across

a time duration of 600ns, the channel observed were mainly located before 200ns. The measurements were conducted in offices, and the floor plan of these offices is reproduced in Figure 2.11-1. They indicated that they only used the rooms in their measurements as the corridors were longer (and hence had multipath with long arrival times), and also had direct line of sight which is not normal for an office environment. As a result the Saleh-Valenzuela model is known as a non line of sight model.

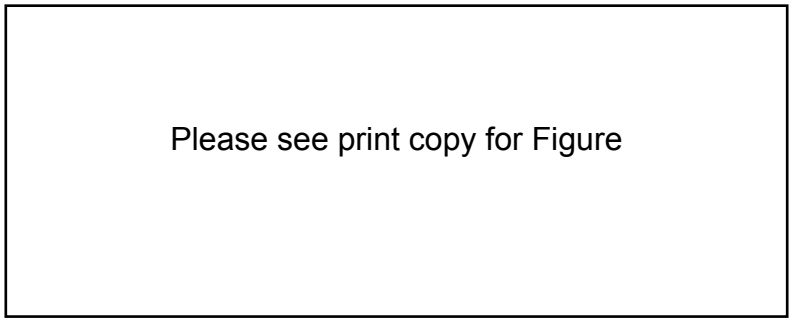

Figure 2.11-1: Plan of floor used in measurements of radar-pulse like communication upon which Saleh-Valenzula statistical model is based, reproduced from [7].

The measurement equipment used in [7] is shown in the reproduced figure from [7] as Figure 2.11-2. They used a vertically polarised Discone antenna which they stated had an omnidirectional radiation pattern in horizontal plane for both the transmitter and receiver. The receiver had a low noise Field Effect Transistor (FET) amplifier chain with a 3dB noise figure operating over the frequency range of 1 to 2GHz, centred on 1.5GHz. They then used a square law envelope detector which they connected directly to a computer controlled digital storage oscilloscope. They claimed that the dynamic range of their equipment exceeded 90dB, accessing this range by manually adjusting the step attenuator at the transmitter and the vertical scale on the oscilloscope [7].

Saleh-Valenzuela [7] indicated that when a measurement was taken those within close proximity to the transmitter and the receiver, or in the hallway were asked to be stationary. They found that those who were in their offices moving around had a insignificant effect on the multipath channel measured.

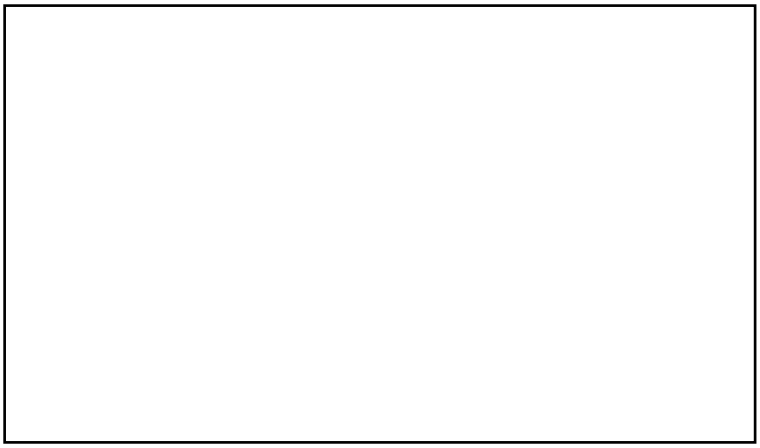

Figure 2.11-2: Shows the measurement setup used in 1987 to develop the Saleh-Valenzuela model as reproduced from [7].

Presented in Figure 2.11-3 are some frequency averaged power profiles measured and reproduced from [7]. This figure has seven averaged power profiles. They indicate that the vertical axis is not in dB but is linear, and the dB value recorded on each figure refers to the attenuation setting (in dB) of the transmitters step attenuator. The time axis in all figures of Figure 2.11-3 is in 10ns increments. According to [7] the figures in Figure 2.11-3 go from left to right in alphabetically increasing order (a-g). The first figure they refer to as (a) is actually the connection of a coaxial cable directly from the transmitter to the receiver and hence is a measure of the power profile of a radar-like pulse. The second figure, (b), was the measurement when the transmitter and receiver are one metre apart (a line of sight measurement of the channel). The third figure, (c), is a measurement taken when the transmitter and receiver were separated by a distance of sixty metres. In the third figure , (c), they noted that a strong multipath was seen at 60ns due to the location of a metallic door and they noted that the signal strength decreased from 60dB as shown in (b) for the one metre separation down to 30dB as shown in (c) for the sixty metre separation. In Figure 2.11-3 for figures (d) through (g) the signal strength decreased another 25dB down to 5dB and the multipath or averaged frequency power profile now extended out to 100ns. Also of importance is that the strongest multipath in Figure 2.11-3 for figure (e) and figure (g) occurs not as the earliest arriving signal but at 60ns (which they indicate is still due to close proximity to the door), which is typical of a non-line of sight channel (as this was, as in this case the receiver was located in one of the offices).

Saleh-Valenzuela [7] observes that the measured frequency-averaged power profiles of Figure 2.11-3 for figures (d) through (g) appear to exhibit a clustering of arriving rays. The other observation is that these arriving rays are, on average, decreasing amplitude but that they also can have the strongest arriving ray occur in time many nanoseconds after the first arriving ray has been seen. From these observations they proposed a model for the channel which has become known as the Saleh-Valenzuela statistical model and which is employed in this thesis and in [8] to model the UWB channel, using the real part of this model (as UWB signals are real).

Saleh-Valenzuela [7], after justifying the determining factors of a model for the proposed channel, proceed to define their model in a statistical sense. They formulated the basis for their model by proceeding as follows from first principles. They modelled each RF radar-like pulse using the complex domain mathematical description:

$$x(t) = p(t)e^{j(wt+\phi)} \qquad (2.11\text{-}1)$$

Here they defined $p(t)$ as the baseband pulse shape which they indicated for their setup has a width of 10ns (as distinct to 0.7ns in [8]) and the variable w represented the angular frequency, which in their experiment was $2\pi \times 1.5GHz$ and ϕ is an arbitrary phase. They nominate the multiple arriving rays to each have a path index which they give the symbol, *k*. The value of *k* can span from 0 to infinite, however most real channels will reach a point where the amplitudes of the multipath have effectively reached a negligible value (in the simulations provided in this thesis, this is done by truncating the channels at 100ns).

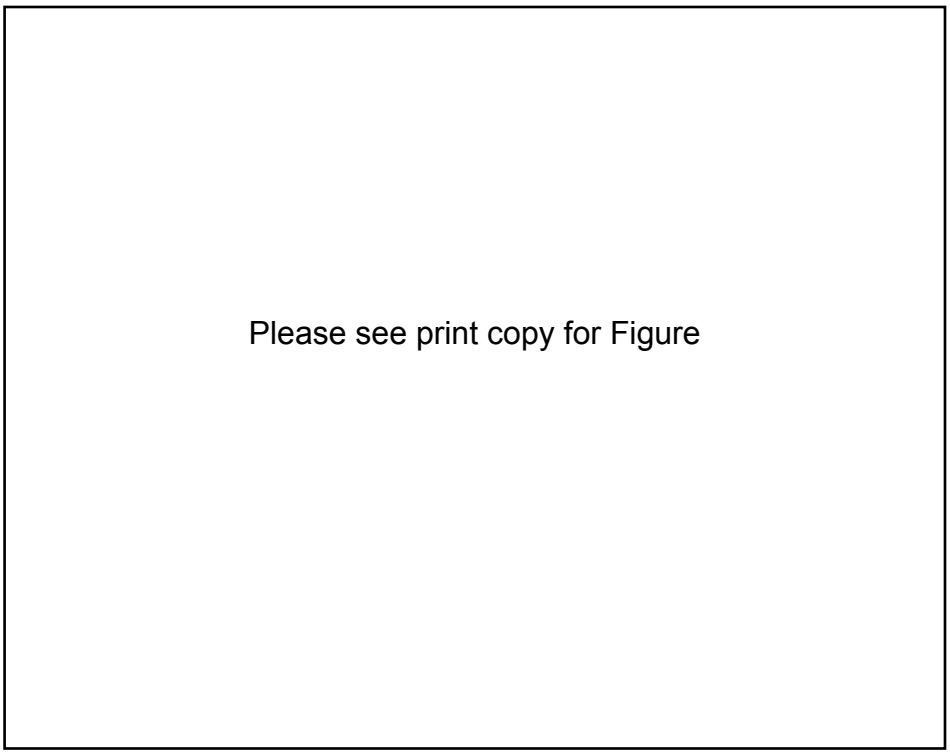

Figure 2.11-3: Some sample averaged power profiles observed and reproduced from [7].

Saleh-Valenzuela [7] indicate that they can represent the channel as being composed of multiple paths or arriving rays that have real positive gains, which they denote as $\{\beta_k\}$ and with propagation delays or time of arrival epochs denoted by $\{\tau_k\}$. They also indicate that the phase of the arriving rays can be denoted by $\{\theta_k\}$. From the definition of these parameters they form the low-pass channel impulse response as:

$$h(t) = \sum_k \beta_k e^{j\theta_k} \delta(t - \tau_k) \qquad (2.11\text{-}2)$$

with $\delta(\cdot)$ denoting the Dirac Delta function [7].

Saleh-Valenzuela [7] then convolve the signals in Equation 2.11-1 and Equation 2.11-2 to get:

$$y(t) = \sum_k \beta_k p(t - \tau_k) e^{j[w(t-\tau_k)+\phi+\theta_k]}$$

(2.11-3)

Saleh-Valenzuela [7] then input this signal into the square-law envelope detector and, they suggest, the oscilloscope displays the power profile signal given by:

$$|y(t)|^2 = \sum_k \sum_l \{\beta_k \beta_l p(t - \tau_k) p(t - \tau_l) e^{j[\theta_k - \theta_l + w(\tau_l - \tau_k)]}\}$$

(2.11-4)

Saleh-Valenzuela [7] indicate that if the pulses do not overlap (which in their experiments required the difference between the different arriving rays to equal or exceed 10ns) then Equation 2.11-4 would be simplified to the expression:

$$|y(t)|^2 = \sum_k (\beta_k)^2 p^2(t - \tau_k)$$

(2.11-5)

Saleh-Valenzuela [7] proceed to indicate that even in the case of pulse overlap, if the realistic assumption that the phases are uniformly distributed in the range between 0 and 2π (excluding 2π) and statistically independent is made, then Equation 2.11-4 reduces upon using the mathematical expectation operator, *E*, with respect to θ, to:

$$E_\theta\{|y(t)|^2\} = \sum_k (\beta_k)^2 \, p^2(t - \tau_k)$$

(2.11-6)

Saleh-Valenzuela [7] then indicate that Equation 2.11-6 is equivalent to Equation 2.11-5 but it now allows overlap of pulses. They proceed to explain that taking the expectation with respect to the phases of the arriving rays was accomplished in their experiments by using the digital oscilloscope to average the power waveform over multiple sweeps of the channel using multiple pulses. They continue by indicating that if the frequency bandwidth, Δf, is large enough then it can be shown that the frequency average power profile is found as [7]:

$$s(t) = \frac{1}{\Delta f}\left(\int_{-\Delta/2}^{\Delta/2} |y(t)|^2 \, df\right) = \sum_k (\beta_k)^2 p^2(t - \tau_k) \qquad (2.11\text{-}7)$$

In their particular experiment they indicated that their frequency bandwidth was 200MHz and this permitted resolution of pulses that arrived more than 4ns apart in time, any closer than this could not be resolved. For their experiment this meant that if two arriving rays were separated by less than 4ns then these arriving rays would be considered to belong to the same path.

Saleh-Valenzuela [7] then observe that given the frequency averaged power profile described by Equation 2.11-7 and knowing the pulse shape, $p(t)$, the task of developing a channel model becomes finding the pairs $\{(\tau_k, (\beta_k)^2), k = 1,2,3,\cdots\}$ which fit best the measured frequency average power profile for some minimum error criteria, such as mean squared error.

Saleh-Valenzuela [7], after further discussion of alternative models and their advantages and disadvantages, propose the model used in this thesis and also in [8]. Their first observation is that the rays arrive in clusters, so they need to model cluster as well as ray arrival times. They then suggest that the arrival of clusters be modelled using a poisson arrival process. They suggest that clusters arrive with a poissonian arrival process with some fixed rate, Λ. Within clusters rays, they suggest, are also modelled to arrive with a fixed poissionian arrival rate, which they denote as λ. They suggest that typically the clusters consist of many arriving rays which then implies that:

$$\lambda \gg \Lambda \qquad (2.11\text{-}8)$$

Saleh-Valenzuela [7] then proceed by defining the arrival time of the l[th] cluster as $T_l, l = 0,1,2,\cdots$, and they let the arrival time of the k[th] ray measured from the beginning of the l[th] cluster be represented by the time epoch $\tau_{kl}, k = 0,1,2,\cdots$. They indicate that by definition we have the first cluster at $T_0 = 0$ and the first arriving ray of the l[th] cluster is given by $\tau_{0l} = 0$. As the arrival process is poisson in their model then they indicate that the quantities T_l and τ_{kl} can be modelled using an independent interarrival exponential pdf, such that [7]:

$$p(T_l|T_{l-1}) = \Lambda e^{[-\Lambda(T_l - T_{l-1})]}, \ \ l > 0 \qquad (2.11\text{-}9)$$

and

$$p(\tau_{kl}|\tau_{(k-1)l}) = \lambda e^{[-\lambda(\tau_{kl} - \tau_{(k-1)l})]}, \ \ k > 0 \qquad (2.11\text{-}10)$$

They then define the gain of the k[th] ray of the l[th] cluster as β_{kl} and its phase is defined as the quantity θ_{kl}. They then define a low pass channel impulse response (comparable to Equation 2.11-2) for their proposed model as:

$$h(t) = \sum_{l=0}^{\infty}\sum_{k=0}^{\infty} \beta_{kl} e^{j\theta_{kl}} \delta(t - T_l - \tau_{kl}) \qquad (2.11\text{-}11)$$

Where, they highlight, that the phases, $\{\theta_{kl}\}$, are uniformly distributed random variables over the range 0 through 2π (excluding the exact value 2π). Also in their model they point out that the $\{B_{kl}\}$ are statistically independent positive random variables which they later show have Rayleigh distribution, and are monotonically decreasing functions of the random variables $\{T_l\}$ and $\{\tau_{kl}\}$, where they can be expressed as [7]:

$$\overline{(\beta_{kl})^2} = \overline{\beta^2(T_l, \tau_{kl})} = \overline{\beta^2(0,0)} e^{-T_l/\Gamma} e^{-\tau_{kl}/\gamma} \qquad (2.11\text{-}12)$$

And where:

$$\overline{\beta^2(0,0)} \ = \ \overline{(\beta_{00})^2} \qquad (2.11\text{-}13)$$

Which they indicate is the average power gain of the first cluster of arriving rays. They indicate that the quantity Γ is the power delay time constant for the arriving clusters and γ is the power delay time constant for the arriving rays. They provide a figure to illustrate their proposed model which is reproduced in Figure 2.11-4. They note that the clusters generally overlap, however as each new cluster arrives, even though the old cluster will be infinite in extent, the old clusters magnitudes will tend quickly towards a negligible magnitude. They observed from their measured data that rays and clusters outside a window of 200ns, even though they exist, were generally too small to be detected by their experimental setup [7].

In [7] they then form the expected value of the ray power as a function of time measured from the time of arrival of the first ray of the first cluster, given that there are L clusters with arrival time of clusters denoted by $T_0, T_1, T_2, \cdots, T_L$, then they provided the formula:

$$\overline{\beta^2(t)} = \overline{\beta^2(0,0)} \sum_{l=0}^{L} e^{-T_l/\Gamma} e^{-(t-T_l)/\gamma} u(t-T_l)$$

(2.11-14)

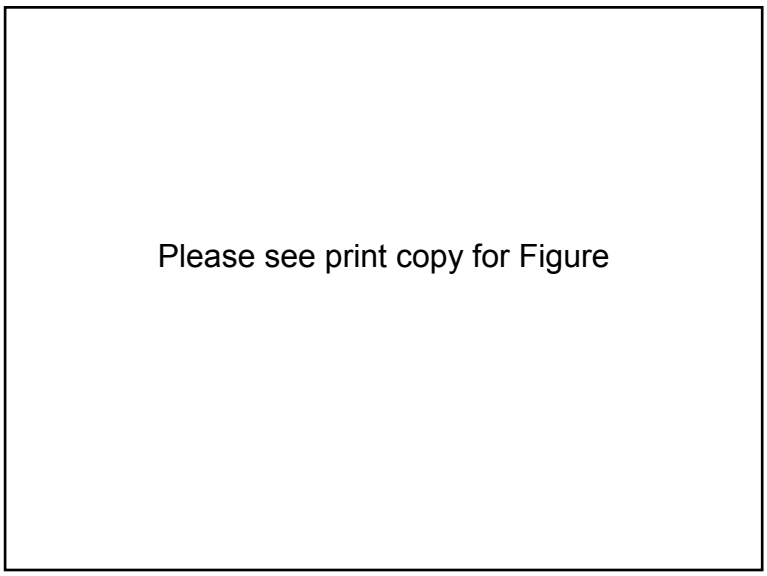

Figure 2.11-4: Figure reproduced from [7] which shows an envelope and ray representation of their proposed model.

Where u(t) (as distinct from U(t) in [7]) is used to represent the unit step function (ie a function which has amplitude unity for time greater than and equal to zero, and has zero amplitude when time is negative). Saleh-Valenzuela [7] provided a sketch of Equation 2.11-14 in Figure 7 of [7] which is reproduced in Figure 2.11-4. They estimated the value of $\overline{\beta^2(t)}$ by aligning the time origin and taking the mean of a large number of measured power profiles within the same room. These figures show actual measurements against the exponential power decay profile of the arriving clusters and rays within clusters against the exponential model expressed in Equation 2.11-14. They further model the path voltage gain (ie the amplitudes of the arriving rays) using a Rayleigh pdf such that [7]:

$$p(\beta_{kl}) = \left(\frac{2\beta_{kl}}{\overline{\beta_{kl}^2}}\right) e^{-\left(\beta_{kl}^2/\overline{\beta_{kl}^2}\right)} \qquad (2.11\text{-}15)$$

From this Rayleigh distribution the multipath voltage gains of each ray can be drawn randomly in a simulation of the channel. Such a system was implemented to generate the multipath channel instances used in the UWB Simulink simulations and also as described in [8]. Our multipath channel instances used in our Simulink simulations were generated by modifying MATLAB code provided with [44]. Appendix 6 shows the channel generating code written in MATLAB employed in these thesis simulations for the channel model deployed for the UWB PPM systems.

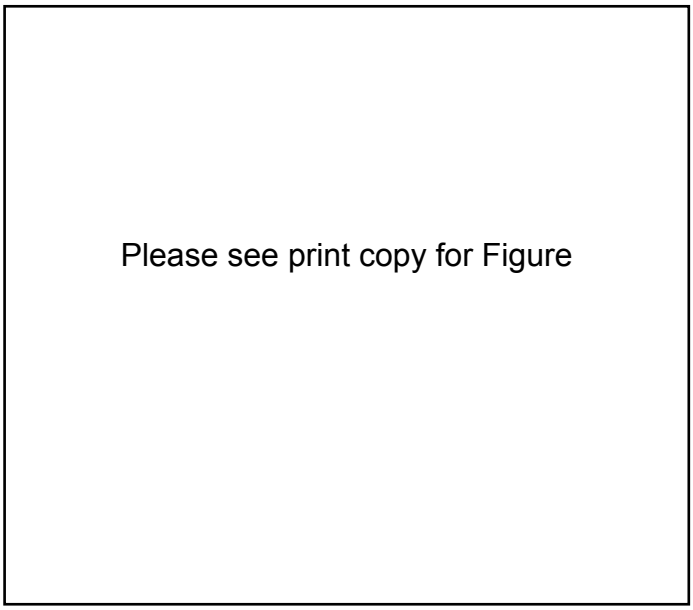

Figure 2.11-5: averaged power profiles reproduced from [7].

2.12 Methodology

The methodology adopted in this thesis is based on the approach of simulation. We chose to use MATLABs' Simulink and the Real Time Workshop executables (available for both Windows and Linux based platforms) for the reasons outlined in Section 3.5(page 93). The simulations were validated against known results reported in this literature review, specifically for the wideband simulations in Chapter 3 and Chapter 4 we validated our system against results reported in [9]. For the UWB PPM TH SISO and MIMO systems we validated against results reported in [8]. We used the Saleh-Valuenzuela channel as it was used in [8] and the model is outlined in Section 2.11. Once the simulators were validated against results in these papers, studies of the effects of Multiple Access Interference were carried out. We also modeled in simulation our proposed novel STS TH UWB PPM two transmit antenna to single receive antenna MIMO technique. The results were then analysed and presented in this thesis (which is based on multiple peer-reviewed publications as outlined on page vi and vii). Simulation of the proposed models is an often used method of approach in studies conducted on multiple antenna systems being used in [51], [8], and [9] among many other studies.

2.13 Conclusion

This chapter considered the literature related to diversity techniques applied to multiple antenna systems. Different techniques were reviewed, as outlined in the literature and the use of the channel coefficients were highlighted particularly for systems based on the use of multiple antennas. One of the techniques that was examined was the application of Space Time Spreading using two, four and eight transmit antennas. This technique is based on the theory of orthogonal designs and allows for the efficient transmission of individual symbols not just on either antenna but both symbols are encoded and transmitted on both antennas simultaneously. This leads to the studies conducted in Chapter 3 and Chapter 4 on narrowband MIMO systems where the wideband simulation (as distinct from ultra wideband) using Simulink was validated and then used to investigate multiple access interference and the use of low correlation codes to mitigate against this.

This chapter also looked at Ultra Wideband systems. In particular concentrating on Pulse Position Modulated systems and provided from the literature an analysis of such systems. The combining of these pulse based systems with the Space Time Spreading technique and noting that using a Rake receiver in the presence of multipath and different (ie uncorrelated) multipath channels diversity gains are available. This then leads onto the Ultra wideband systems developed in this thesis. These are based on the observation that the pulse positions can be modeled on the discrete values observed on each channel which allows for a more efficient transfer of the data. It also takes advantage of the diversity available on two multipath channels as a fade is unlikely to occur on both antenna links at the same time.

The next two chapters continue by looking at simulations of the Space Time Spreading wideband system and investigate the effect of multiple access interference on its performance. It was from this study and the study of the literature reported on UWB in this chapter that lead to the novel combination of UWB PPM TH and Space Time Spreading provided in the final chapters of this thesis.

Chapter 3: Modeling and Validation of STS system in Simulink

3.1 Introduction

Space Time Spreading systems are proposed as a method to enhance communications between the Base Station (BS) and Mobile Station (MS) by using multiple transmit antennas at the Base Station. This provides a form of transmit diversity when there are more than one transmitting antennas. This chapter shows how such a system was built using the Digital Signal Processing and Communications Blocksets of MATLAB's Simulink environment. Simulink has advantages over other simulation environments which are highlighted in this chapter (see Section 3.5). The system was tested and validated against the original Space Time Spreading work of Bertrand Hochwald et al. [9]. The finer details associated with such simulations are highlighted and it is shown how Simulink can be used in the simulation of communications system environments. The development of the Space Time Spreading narrowband system leads onto the specific development in Chapter 8 of the Ultra Wideband MIMO system which allows for the deployment of multiple antennas achieving a diversity gain of two using the Time Hopping Ultra Wideband Pulse Position Modulation system which is proposed in this thesis dissertation.

In [9] Hochwald et al. propose a novel transmit diversity technique called Space Time Spreading (see Section 2.5). This technique is classified as an open loop transmit diversity system in that there is no knowledge at the transmitter, received from the reverse link, about the form of the channel between the transmitter and the receiver. This information is only needed at the receiver, and estimates of the complex channel coefficients can be found from associated pilot signals sent by the BS (Base Station) to the MS (Mobile Station). In [9] Space Time Spreading systems were shown to be efficient in their use of the limited number of orthogonal spreading sequences and to provide a diversity gain. In the case of two transmitter antennas at the BS and one receiving antenna at the MS the gain is of order two. The technique requires that the antennas be uncorrelated, which means in practice that the antennas should be at least ten wavelengths in terms of separation [5;60]. A Simulink model

of this system with two transmit and one receive antenna has been successfully developed. This chapter details the developed model and provides a case study of how the DSP Blockset and Communications Blockset of Simulink can be used to develop such systems.

This chapter is organised as follows, first a description is provided of the algorithm used in the Space Time Spreading System which follows closely the description given by the authors in [9] and provided in Wideband CDMA systems based on Space Time Spreading. This is followed by a detailed description of how this system is modeled in the MATLAB Simulink modeling language. The results of validation experiments are then described and provided in graphical (Figure 3.4-1 and Figure 3.4-2) and tabular (Table 3.4.1 and Table 3.4.2) form. These results are very close to results obtained from experiments in [9] for BPSK (Binary Phase Shift Keying) transmission hence validating the developed Simulink simulation. In Section 3.5 a brief description of the problems and advantages of using Simulink are provided and, in particular, suggestions are provided for the modeling of CDMA systems using Simulink. Finally, the Design and Validation chapter of the Simulink STS is concluded leading onto the Multiple Access Interference study of Chapter 4.

3.2 Space Time Spreading

The Space Time Spreading system that this study looks at is the case where there are two transmit antennas (at the BS) and one receive antenna (at the MS). The Space Time Spreading schema starts by separating a bit stream into odd and even symbols. These are then identified as b_1 and b_2. These are then mixed at the two transmitting antennas as follows:

$$\begin{aligned} t_1 &= \left(1/\sqrt{2}\right)\left(b_1\underline{c_1} + b_2\underline{c_2}\right) \\ t_2 &= \left(1/\sqrt{2}\right)\left(b_2\underline{c_1} - b_1\underline{c_2}\right) \end{aligned} \qquad (3.2\text{-}1)$$

Here $\underline{c_1}$ and $\underline{c_2}$ are the orthogonal spreading codes with processing gain equal to their length. In this study the length of the orthogonal codes was chosen as 128 chips. While this is not considered crucial in [9] and typically for data transmission lower values for processing gain (PG) are used, this was chosen for this study as it does not affect the results obtained. The constant $1/\sqrt{2}$ is used to normalise the power for comparison to a single antenna system. Figure 3.2-1a illustrates in block diagram form the Space Time Spreading technique for two antennas as described by Equation 3.2-1.

These are then transmitted through the channel to one receiver, each path experiencing a different complex coefficient or gain (since they are uncorrelated) and these gains are considered in this system as fading coefficients, but they are flat fading. That is, over a symbol period they remain the same value. They are faded using a Rayleigh pdf with mean unity and uniform phase distributed between zero and 2π. Figure 3.2-1b illustrates the system between the BS and the target MS, with the channel coefficient from antenna t_1 labeled as h_1 and that from antenna t_2 labeled as h_2.

The received signal at the target MS is then de-spread by the two orthogonal codes giving received signals:

$$\begin{aligned} d_1 &= \left(1/\sqrt{2}\right)\left(h_1 b_1 + h_2 b_2\right) + \underline{c_1}^H \underline{n} \\ d_2 &= \left(1/\sqrt{2}\right)\left(-h_2 b_1 + h_1 b_2\right) + \underline{c_2}^H \underline{n} \end{aligned} \qquad (3.2\text{-}2)$$

where the superscript H stands for the Hermitian transpose and $\underline{n}$ is a 128 by 1 vector of additive zero mean complex Gaussian receiver noise samples.

In [9] this is re-written using the following:

$$\underline{d} = \begin{bmatrix} d_1 \\ d_2 \end{bmatrix} = \begin{bmatrix} d_1 & d_2 \end{bmatrix}^{\mathrm{T}} \qquad (3.2\text{-}3)$$

, and

$$H = \begin{bmatrix} h_1 & h_2 \\ -h_2 & h_1 \end{bmatrix} \quad \underline{b} = \begin{bmatrix} b_1 \\ b_2 \end{bmatrix} \quad \underline{\nu} = \begin{bmatrix} \underline{c_1}^H \underline{n} \\ \underline{c_2}^H \underline{n} \end{bmatrix} \qquad (3.2\text{-}4)$$

, so that:

$$\underline{d} = \frac{1}{\sqrt{2}} H \underline{b} + \underline{\nu} \qquad (3.2\text{-}5)$$

In [9] they show that if h_q represents the q^{th} column of H (in this case q=1 or 2 only) then the following is true:

$$\Re e\left\{\underline{h_q}^H \underline{d}\right\} = \left(1/\sqrt{2}\right)\left(|h_1|^2 + |h_2|^2\right)b_q + \Re e\left\{\underline{h_q}^H \underline{\nu}\right\} \qquad (3.2\text{-}6)$$

It is then a simple matter to use this to decode for either b_1 or b_2 by using Equation 3.2-6 and knowledge of the channel coefficients and hence the H matrix at the receiver. In [9] the authors note that this has the required two-fold diversity gain, expected for this system. The results of our simulation confirm these expected results.

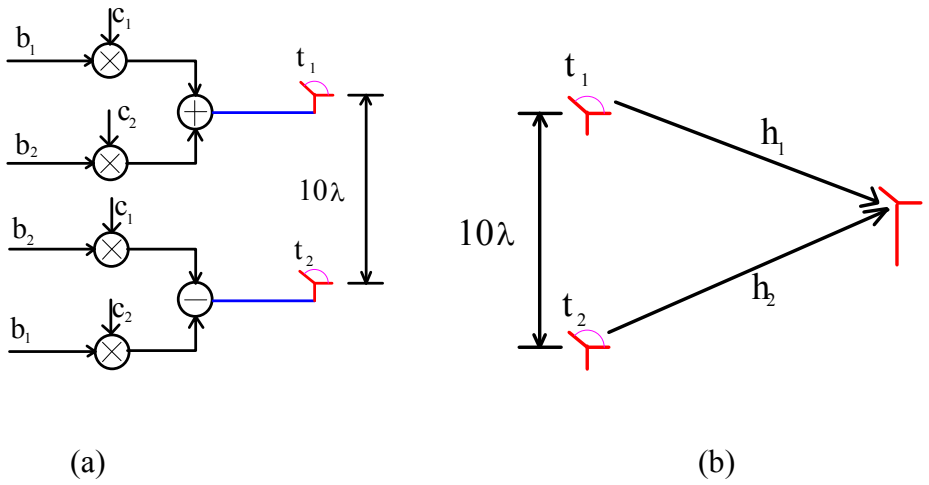

Figure 3.2-1: (a) The computations done on b_1 and b_2 before being transmitted on t_1 and t_2 antennas [9]. (b) Shows complex fading coefficients for STS system.

3.3 Description and Design of Model

The Simulink model consists of a series of sub-systems which are modeled in Simulink. It is shown in functional form in Figure 3.3-1. For the validation experiments the symbol rate was chosen as 50 Mbps, though across the Space Time Spreading simulator with two symbols being transmitted at the same time, the apparent symbol rate was 100 Mbps. The chip rate used was 128 times that used for the actual symbol rate. Every 32 symbols transmitted (that is, every actual symbol transmission periods) the flat fading complex coefficients for each path were changed using a Rayleigh pdf with mean unity (1) and a uniformly distributed phase over 2π. The received power was normalised so that the expected SNR was achieved at

the de-spreading stage used to demodulate the individual symbols which were then fed into the demodulator. The demodulator then used perfect knowledge of the complex fading coefficients to form exact representations of the H matrix (formed from channel complex coefficients). The estimates for individual symbols are described by Equation 3.2-3, Equation 3.2-4 and Equation 3.2-5. The underlying assumption within the simulation was that each signal contributed the same mean received power at the receiver antenna. The processing gain, which here was 128, was involved in normalising the received powers on each path. The simulation was tested initially with no noise and the delay through the Simulink model was found to be 22 symbols. This was initially found from trial and error, but further examination of the developed model confirmed that in fact a delay of 22 symbols was correct. The analysis is as follows. Two symbols of this delay were due to the delay incurred in using the Simulink Digital Signal Processing (DSP) Blockset **Buffer** module to segment the symbols into odd and even symbol streams (see Figure 3.3-2). The simulation had nine (9) symbols per path (due to a modeled 50 metres separation between transmitters and receiver) and one symbol per path for the Symbol Matched Filter used in the despreading stage. This amounts to another 20 symbols, totaling the 22 Symbols found in the simulation. Using a delay of 22 symbols and no noise resulted in perfect reception of the transmitted Bernoulli based distribution binary symbol train. The **Bernoulli** Simulink module was setup to have a 50% probability of transmitting a '0' and a 50% probability of transmitting a '1'. After showing that the no-noise case had perfect reception, gaussian noise was added to both signal paths which were complex with zero mean and some fixed variance. The variance was chosen depending on whether one signal path or two signal paths were available within the Simulink simulation. These cases corresponded to setting m=1 or m=2 where m represents the number of transmit antennas. These are used in the validation experiments which are described in Section 3.4 (page 90). In this simulation orthogonal 128 length Walsh-Hadamard codes were used, formed from 64 length Walsh codes using a schema described in [9]. These were validated using MATLAB and found to be orthogonal to each other.

It was found early in the simulation build process that the simulator needed to be in Variable-Step and Discrete under the Simulation Parameters configuration panel. Also, as is typical for other Simulink models, many needed MATLAB parameters were exported to the MATLAB workspace from within the Simulink modules initialisation framework Model Properties.

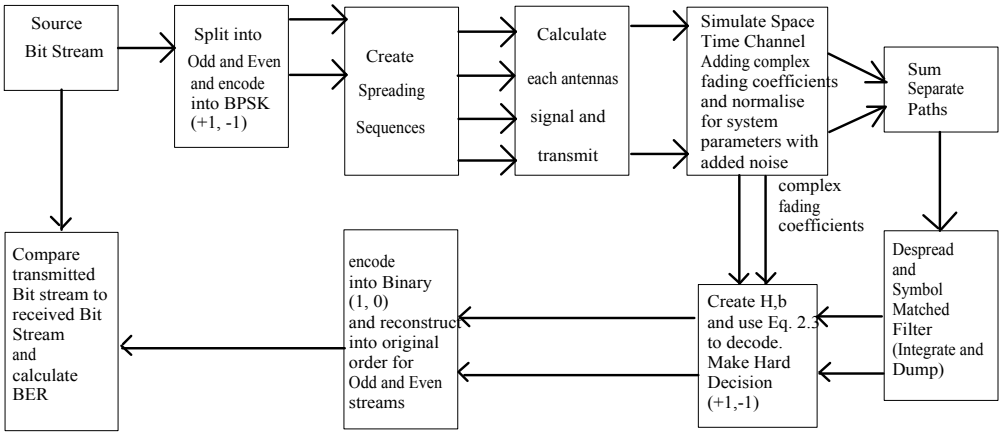

Figure 3.3-1: Space Time Spreading Simulink Model.

The first stage after generating the symbol train (bit stream) in the model was to convert the single symbol stream into odd and even symbol streams. This was essentially done using the DSP Blocksets **Buffer** module followed by a **Demux** module as shown in Figure 3.3-2. The **Buffer** module converted the symbols stream into odd and even components, the **Unbuffer** and **Buffer** modules which follow this actually only prepare the signal to be converted into a format acceptable to the **U(:)** module which is equivalent to the vectorisation operation that can be used in MATLAB proper.

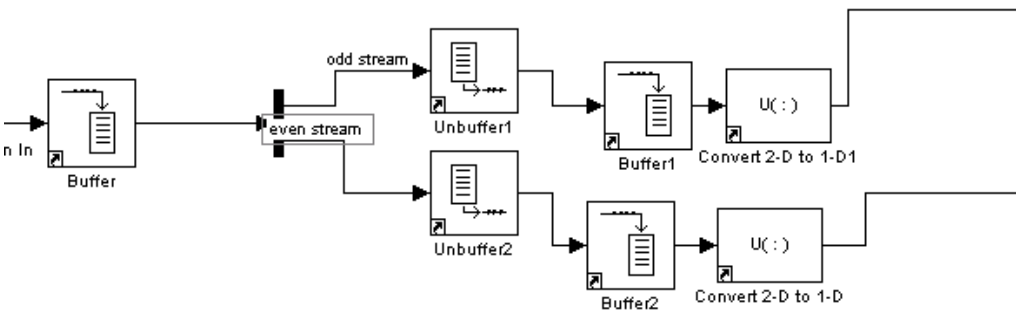

Figure 3.3-2: Splitting streams into odd and even components.

The next stage is to create the individual spread streams. An orthogonal set of two Walsh codes called c1 and c2 were calculated and then saved in the MATLAB workspace (using the Model Properties referred to above). These were then retrieved in a cyclic manner from the MATLAB workspace at the simulated chip rate within the simulation using the **Signal from Workspace** Simulink module. The Walsh codes were 128 chips in length which corresponds to the number of chips per symbol and were already in the requisite {0,1} mapped to {-1,1} form. These were subsequently mixed with the odd and even streams after these streams had been converted also from {0,1} to {-1,1} giving the baseband equivalent of BPSK. This formed four new spreaded streams called boddc1, bevenc1, boddc2, and bevenc2. Figure 3.3-3 indicates the modules involved. The mixer modules used the **.*** scalar element by element multiply in its operation. These signals were then added and subtracted as per Figure 3.2-1a.

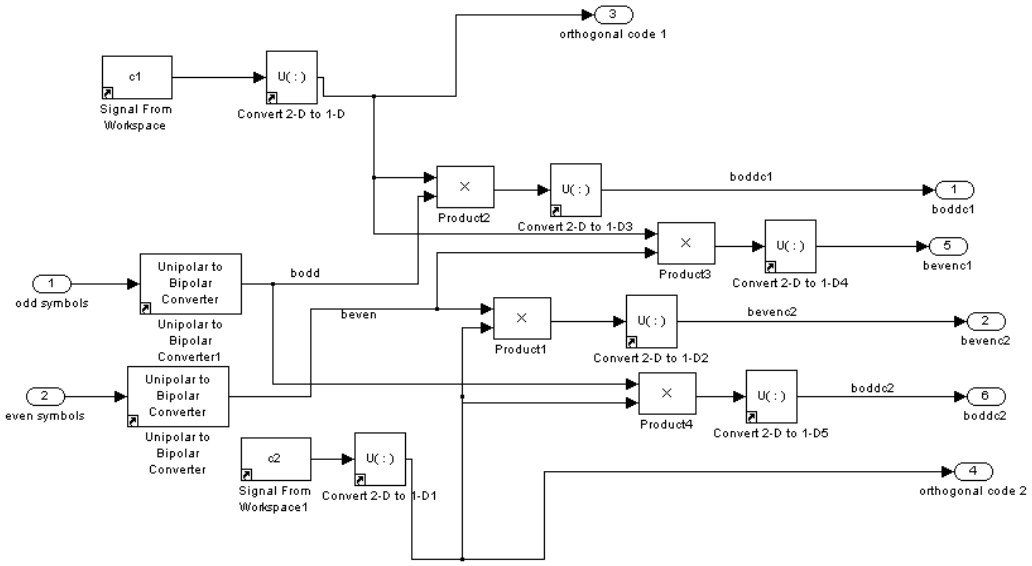

Figure 3.3-3: Spreading stage of simulation.

The transmitted baseband antenna signals are then exposed to the module that simulates the channel through which the electromagnetic waveforms would propagate in a real scenario. The channel here is modeled as flat fading as it was in [9]. The signal was normalised depending on whether there were two paths or one path in the simulation. When one path was used the gain was set to unity, when two paths were used each path had a multiplier of $1/\sqrt{2}$ applied so as to normalise the received signal strength to that seen for a single, m=1, case. Proceeding by examining the case where m=2 in this description. The sub-system that

simulated the channel was called the **STS Channel** within the Simulink model. Each path had identical components but drawn from different modules so it will also show only one path, as shown in Figure 3.3-4. The integer delay modules are used to correctly align the individual orthogonal codes which are sent on from the spreading stage and which are also used in the de-spreading stage. The signal is then split into absolute value and angle parameters. The absolute value is subsequently modulated with the individual Rayleigh pdf generated fading values that are stochastically determined inside the Magnitude sub-system. The Rayleigh pdf was generated inside the Magnitude sub-system using analytical calculations and a Uniform distribution as follows:

For Rayleigh pdf with mean value unity (1) the following describes the distribution [55;56]:

$$f(\chi) = \frac{\pi\chi}{2} e^{-\pi\chi^2/4} U(\chi) \qquad (3.3\text{-}1)$$

Where $U(\chi)$ is the unit step function. The Cumulative Distribution Function (CDF) is then [55]:

$$F_X(\chi) = 1 - e^{-\pi\chi^2/4} \qquad (3.3\text{-}2)$$

where $\chi > 0$

Then $\Gamma = Fx(X)$ is a Uniform Distribution over the range 0 to 1, and X is the Rayleigh Distribution [55].

Thus this provides:

$$\Gamma = 1 - e^{-\pi X^2/4} \qquad (3.3\text{-}3)$$

Hence rearranging and taking the natural logarithm of both sides yields:

$$-\frac{\pi X^2}{4} = \ln(1-\Gamma) \qquad (3.3\text{-}4)$$

Clearly, if Γ is Uniform in the range 0 to 1 so is $1-\Gamma$. Proceeding by replacing $1-\Gamma$ with Γ to get:

$$-\frac{\pi X^2}{4} = \ln(\Gamma) \qquad (3.3\text{-}5)$$

and rearranging in terms of X, the Rayleigh distribution to obtain:

$$X^2 = -\left(\frac{4}{\pi}\right)\ln(\Gamma) \qquad (3.3\text{-}6)$$

Since Γ is in the range 0 to 1, then $\ln(\Gamma) \le 0$ and hence

$$X = \sqrt{\left(\frac{4}{\pi}\right)|\ln(\Gamma)|} \qquad (3.3\text{-}7)$$

where $|\ln(\Gamma)|$ is the absolute value of $\ln(\Gamma)$

Thus, Figure 3.3-5 shows the series of Simulink modules which perform the mathematical operations based on Equation 3.3-7 to generate the Rayleigh pdf for the magnitudes. The Phase is simply a Uniform Random Generator over 0 to 2π. The main path in Figure 3.3-4 has two gain elements. The first gain element is set to the factor $1/16$. This is composed of multiplying $1/\sqrt{2}$ times $1/\sqrt{128}$ and then noting that $1/\sqrt{256}$ is this factor. The first term is the power normalisation factor needed to normalise the two transmitter case to that used in a single transmitter system. The second term is the first of two normalisation constants needed in the simulation to get the correct values for the expected SNR in the simulation, taking into account the effect of the processing gain in the de-spreading/symbol matched filter stage. The second gain element is then modified to obtain different values of expected SNR over which Bit Error Rates are plotted. Simulink has a **dB** module which could also have been used at this location. Each path has complex gaussian noise added as suggested in Section 3.4 and is summed and sent to the de-spreading stage. Again there is a need to align some of the signals to the correct location considering delays added to simulate propagation delay across the path (assuming 3×10^8 m/s for the speed of light). The initial section of the de-spreading

stage is shown in Figure 3.3-6. There is the normalisation factor in a gain element of $1/\sqrt{128}$ to complete the normalisation of the systems processing gain. If this is not done then the system will not simulate the required expected SNR in the demodulation which follows in the Symbol Matched Filter (Figure 3.3-7) and the matrix manipulation described by Equation 3.2-6 on page 82. This brings the output into the decoding stage which follows Equation 3.2-6 and is shown in Figure 3.3-8.

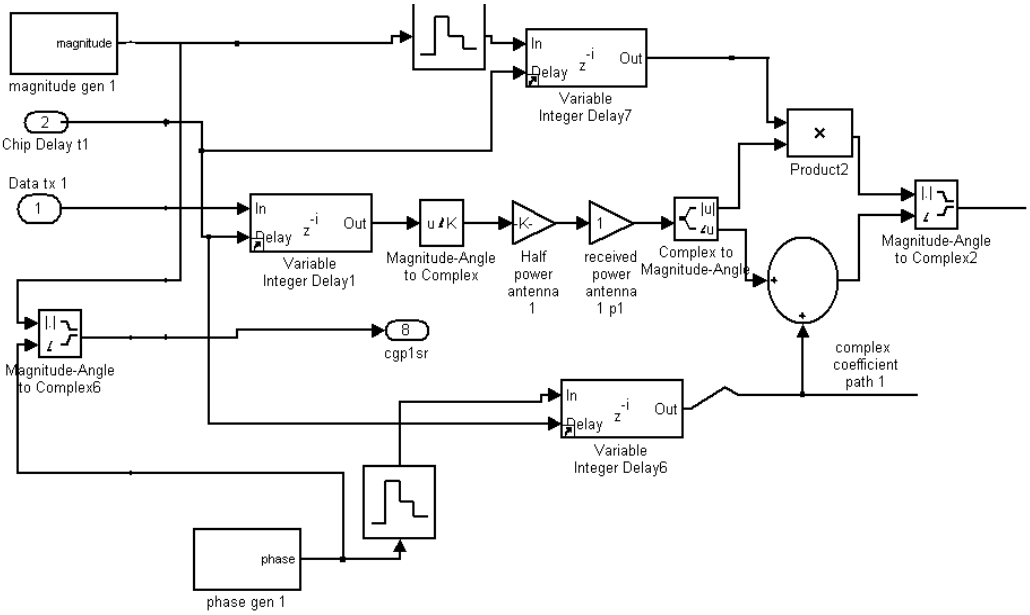

Figure 3.3-4: Single path modelling STS channel.

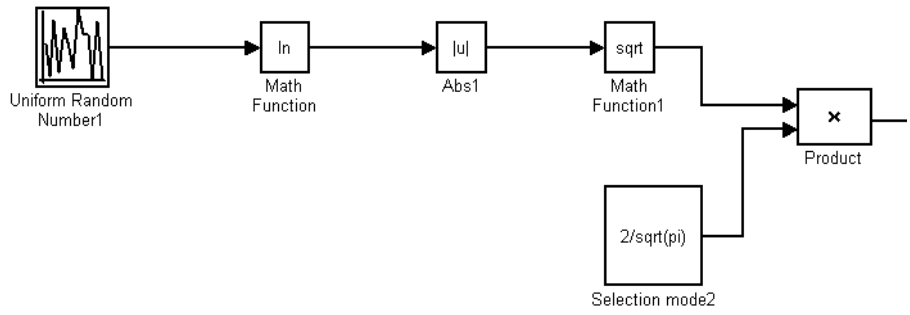

Figure 3.3-5: Generation of Rayleigh pdf.

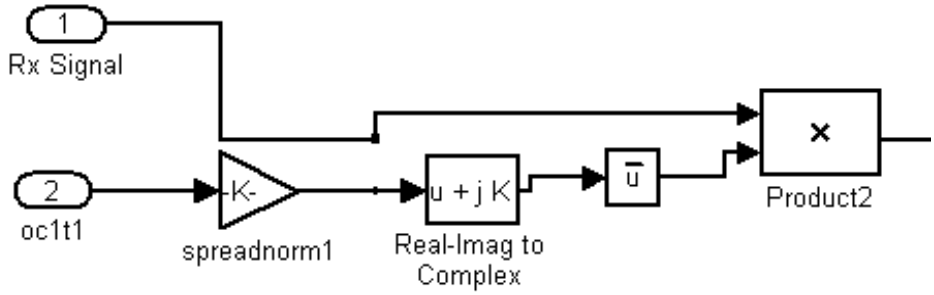

Figure 3.3-6: despreading with normalisation gain element.

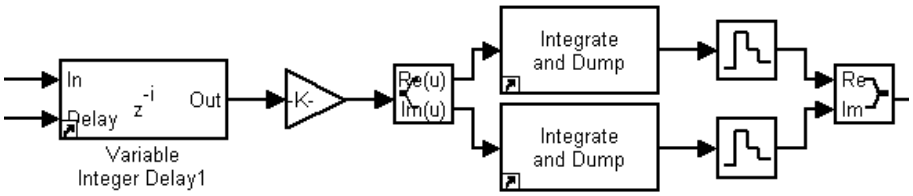

Figure 3.3-7: Symbol Matched Filter, Integration done at actual symbol rate.

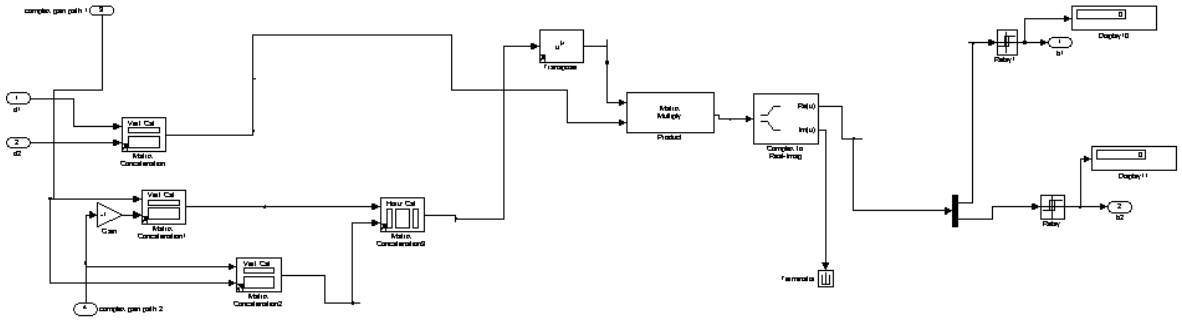

Figure 3.3-8: STS Decoder sub system.

The STS Decoder sub-system starts by retrieving the correctly aligned and perfectly known channel coefficients. These are then formed into the required matrices as per the description of Equation 3.2-5 and Equation 3.2-6 which are multiplied and finally the Real part of the expression is taken depending on whether the individual symbol values are negative or positive a hard decision is taken to decide if a –1 or a 1 was transmitted. The two outputs of this stage are then reassembled into a single symbol stream and converted from –1 or 1 to 0

or 1 for comparison with the original transmitted symbol stream from which Bit Error Rates are calculated and results produced in the validation experiments obtained in Section 3.4.

3.4 Validation of SIMULINK model

In [9] Hochwald and colleagues provide results for a BPSK system for systems with a diversity of 1 and 2 for two transmit antenna system. The Simulink model described in Section 3.3 has been developed and has been validated using results found in [9] (the figure used for comparison was Figure 4 of [9]). To emulate a system with a diversity gain of unity, one of the paths was given coefficients which had a magnitude of zero. The other path was allowed to vary with a Rayleigh pdf of unity mean and uniform distribution over 2π for the phase. The flat fading coefficients were perfectly reproduced at the receiver as was also the case in the corresponding data provided in [9]. Also, there was no multipath but this was also the case in the two plots with which the data provided here was compared. The results for this simulation are provided with 95% confidence intervals and they are plotted as the m=1 curve in Figure 3.4-1. They are plotted with BER versus expected SNR as outlined in [9]. The complex gaussian noise added at the receiver for these results used a mean of zero and a variance for each of real and imaginary components of $1/\sqrt{2}$. The receiver then made a hard decoding decision on the received bit streams. These results showed very close agreement with the corresponding results in [9]. The tabulated results for m=1 with 95% confidence intervals as measured in the Simulink simulator are given in Table 3.4.1.

Table 3.4.1: Measured values from m=1 Simulink simulation of Space Time Spreading System.

Exp. SNR (dB)	**Lower 95% value**	**Average Mean BER**	**Upper 95% value**
0	0.15580	0.15595	0.15610
2	0.11649	0.11666	0.11683
4	0.083535	0.083612	0.083688
6	0.0577641	0.0578706	0.0579770
8	0.0388098	0.0388938	0.0389778
10	0.0255275	0.0255871	0.0256467
12	0.0165672	0.0166182	0.01666929
14	0.0106397	0.0106858	0.01073188
16	0.0067820	0.0068267	0.00687146

Further, the other path was then allowed to follow a Rayleigh pdf of unity mean and uniform distribution over 2π for the phase, again with perfect knowledge at the receiver of these flat fading coefficients. Once again there was no multipath within this simulation as was the case in [9]. The complex gaussian noise added at the receiver for these results used a mean of zero and a variance for each of real and imaginary components of $1/\sqrt{8}$. As shown in Figure 3.3-8, a Hard decoding decision was made at the receiver. The results for these simulations with 95% confidence intervals are plotted for the m=2 case in Figure 3.4-1. Once again there was very close agreement with the corresponding results in [9]. The tabulated values of the 95% confidence intervals for m=2 are shown in Table 3.4.2.

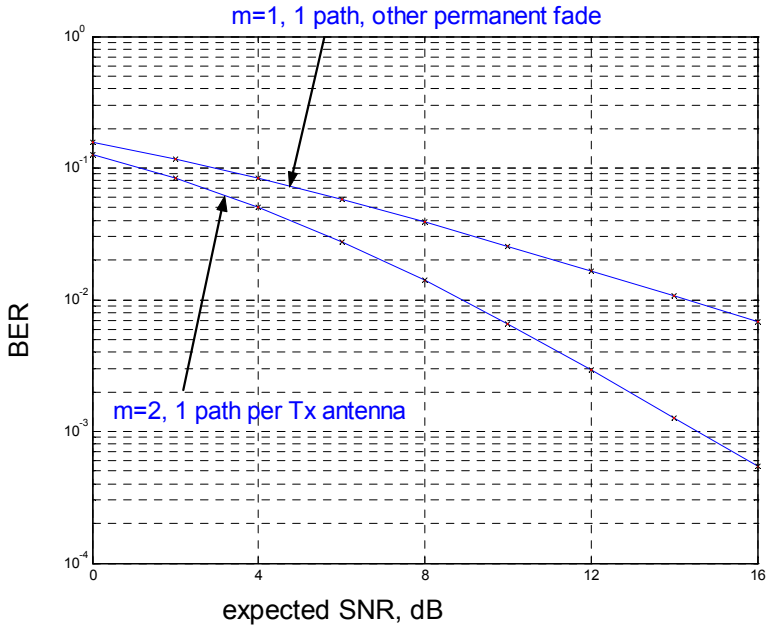

Figure 3.4-1: Plot for m=1 and m=2 with perfect knowledge of the flat fading complex coefficients and no multipath for BPSK system using Simulink.

The Simulink STS simulator was extended to simulate the use of four and eight transmit antennas. This followed the use of the material presented in Section 2.5 (page 21) and Equation 2.5-49 (page 35) where the four antenna (m=4) case is presented. The eight antenna analysis was also done but is not presented in this thesis. The results are shown in Figure 3.4-2, showing the different diversity gains for m=1, 2, 4 and 8 (See Appendix 5 for the MATLAB scripts used). The main difference between m=2 and m=4, 8 is that there needed to be more Simulink modules to simulate the different antenna complex coefficients and the STS encoder and decoder needed to be suitably adjusted. These results were presented in an

invited seminar at Warsaw University in April-May 2004. Appendix 2 shows the measured simulation results for m=4 and m=8 with 95% confidence intervals.

Table 3.4.2: Measured values from m=2 Simulink simulation of STS System.

Exp. SNR (dB)	Lower 95% value	Average Mean BER	Upper 95% value
0	0.1252665	0.125378	0.1254898
2	0.0831215	0.8322366	0.08332581
4	0.0502437	0.0503287	0.05041376
6	0.0276203	0.0276945	0.02776882
8	0.0139458	0.0139903	0.01403474
10	0.0065782	0.0066009	0.00662362
12	0.0029317	0.0029446	0.00295742
14	0.0012654	0.0012712	0.00127689
16	0.0005373	0.00054065	0.00054400

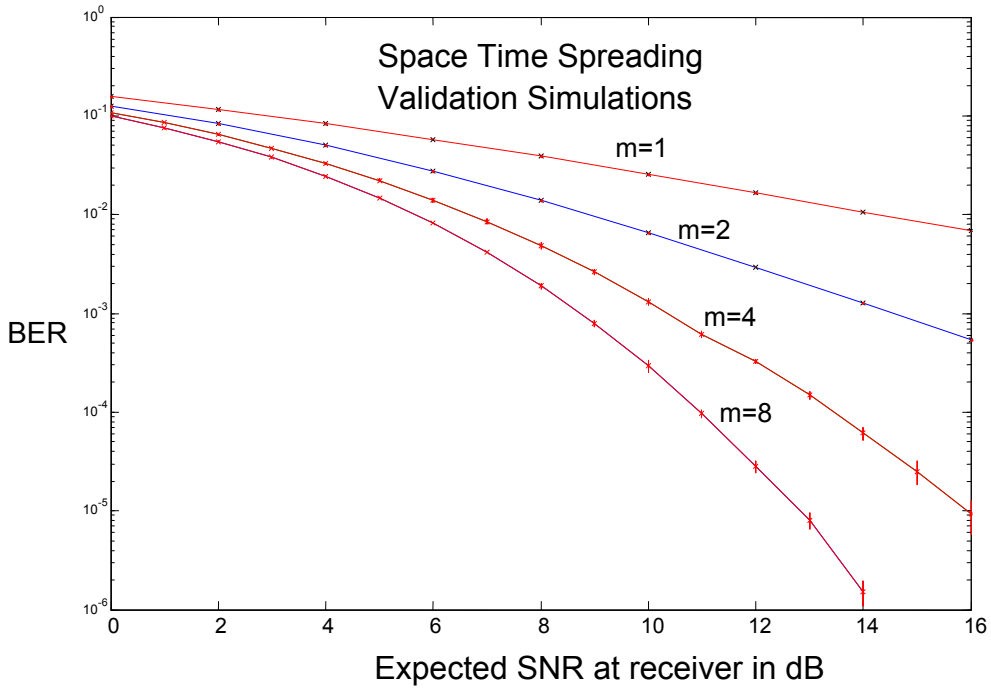

Figure 3.4-2: Plot for m=1, 2, 4 and 8 with perfect knowledge of the flat fading complex coefficients and no multipath for BPSK system using Simulink with 95% confidence intervals for m=4 and m=8 cases [presented to Warsaw university April-May 2004].

3.5 Observations

Simulink was chosen for this study because of its similarity to real communication systems. Most communication systems are composed of basic modules and sub-modules which build up an overall communication system. Simulink, with its graphical interface, allows the system to be displayed as it would be if a physical communications system were built. On top of that, access is still provided to the underlying MATLAB engine so that when algorithms and modules are needed that are not available in a Simulink library, they can be emulated by using MATLAB code or by developing new Simulink library modules (though more difficult), or using Embedded MATLAB (as per Chapter 5 simulations). Also, Simulink provides various simulated test equipment such as a simulated Oscilloscope or Eye Diagram generator. When testing and validating the initial module, usage was made of the Oscilloscope 'sink' module. On top of this it is possible to send and receive data generated by Simulink and MATLAB. The orthogonal codes c_1 and c_2 were retrieved from the MATLAB workspace using this feature. The Simulink model can also be paused and re-started from where it left off. It was also found, that during the debugging stage, leaving various signal to workspace (modules) in the simulation resulted in Simulink generated array's which eventually dramatically slowed down the simulation. It was found that adding extra computer memory alleviated this problem. However, in production runs it is recommended that only those modules needed for the experiment should be used or that one should use Simulinks Real Time Workshop (RTW), as presented in Chapter 5, to reduce the simulation time of experiments. This is not a major problem when computer memory is now very affordable. Simulations for each simulation run took over two days for the simulated transmission of two million bits. This was on an Intel Pentium-3 700MHz running Windows 2000 Professional, which is now quite slow (these simulations were run in 2003 and early 2004). With increasing computing capacity run times continue to decrease. For example, in 2004, the author of this thesis obtained an Intel Pentium-4 2.4GHz Personal Computer running Microsofts' Windows XP which performed the same simulation in only 8 hours. Computers have improved since then but these particular simulations have not been re-run so times for these experiments on more modern computing infrastructure are not available, but expected to have further decreased in duration. Later MAI experiments introduced more Simulink modules which increased simulation complexity and slowed down the simulations even further. Overall, it was found that Simulink is an effective way to model communication

systems, and in particular the Space Time Spreading System communication system this study was based upon.

3.6 Conclusion

This chapter has presented an Simulink model of a Space Time Spreading wideband system (as distinct from ultra wideband). It described how the simulator was constructed using the Simulink blocksets available in MATLABs Simulink simulation environment. It compared the results for one and two transmit antennas to similar systems described by Hochwald et al. in [9] and was able to validate the Simulink simulation against the results also provided in [9]. The study now proceeds to use the Simulink simulator validated in this chapter to undertake studies in the effect of Multiple Access Interference in Chapter 4. This chapter together with Chapter 4 provided the basis for the Ultra Wideband two transmit antenna systems proposed in Chapter 7 and Chapter 8. They also provide the basis for the SISO UWB PPM system proposed and studied in Chapter 6.

Chapter 4: Multiple Access Interference in STS systems

4.1 Introduction

Hochwald et al. [9] propose a novel transmit diversity technique which they named Space Time Spreading. This technique is classified as an open loop transmit diversity system in that there is no knowledge at the transmitter, received from the reverse link, about the quality of the channel between the transmitter and the receiver. This information is only needed at the receiver, and estimates of the complex channel coefficients can be found from the associated pilot signals sent by the BS to the MS. Within this work Hochwald and colleagues establish that Space Time Spreading systems are efficient in their use of the limited number of orthogonal spreading sequences and to provide a diversity gain, which in the case of two transmitter antennas at the BS and one receiving antenna at the MS, is of order two. They also describe the more general case of having multiple antennas at the transmitter (BS) and the receiver (MS). The technique requires that the antennas be uncorrelated, which means in practice that the antennas should be at least ten wavelengths apart [5;60].

Having a diversity gain means that if one path is in a very deep fade, it is unlikely that the other path will also be in a very deep fade and the system would then default back to a single diversity system [9]. This system also moves away from diversity gains that would occur through temporal factors such as mobility between the BS and MS. Wireless LANs are one of the expected application areas of Space Time Spreading systems. Wireless LAN based networks will have low or no motion between the transmitter and receiver(s) involved. Further, it is probable that SDMA systems would be deployed using sectorised cells for each Access Point. The MAC technique used would thus be a combination of SDMA and CDMA [3]. A common use for Wireless LANs is to provide communications between a computer using wireless in an office or lecture theatre and a fixed Access Point (BS). There is low to no relative motion in this case. This then does not allow for gains in diversity that can be obtained via the use of temporal factors as often used in the literature (such as coding and interleaving – as stated in [9]). Space Time Spreading systems do not depend on such diversity techniques and thus have a major potential advantage in this segment of the wireless

communications market. Space Time Spreading is described in Section 2.5 in Chapter 2 and in Section 3.2 in Chapter 3.

SDMA can be used with CDMA systems by sectorising the cells within which different users may be located. For example, a cell can be split into three segments divided into 120 degree arcs as shown in Figure 4.1-1. With mobile scatterers being placed within these sectors it is possible for signals from one sector to be reflected or scattered into adjacent sectors. This is expected to cause the orthogonal codes used to separate signals to become unsynchronized and to result in Multiple Access Interference.

This chapter is organised as follows, first it refers to the description of STS previously presented as described in [9]. This is followed by a description of how the simulator was modified specifically for MAI experiments as modeled in the MATLAB Simulink modelling language. Then a description of the MAI scenario is presented with reasons provided for specific choice of parameters. Then it describes a scenario which introduces MAI from communications to another MS in an adjacent sector. The results of STS in the presence of MAI using 128 chip Walsh-Hadamard orthogonal codes are then presented. Finally a set of codes with improved cross-correlation properties, but with 32 chip length, are incorporated into the MAI simulations and the observed performance is then compared to the 128 chip Walsh-Hadamard performance observed in initial MAI investigation.

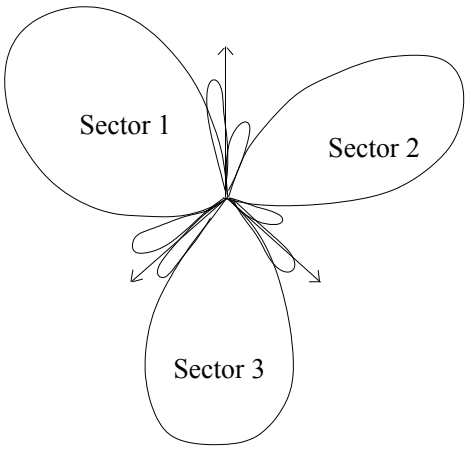

Figure 4.1-1: A cell sectorised into three 120 degree segments [1].

4.2 Description of SIMULINK model

The Simulink model used is described in Section 3.3 (page 82) and validated in Section 3.4 (page 90). For the validation experiments the symbol rate was chosen as 50 Mbps, resulting in a rate across the Space Time Spreading simulator with two symbols being transmitted at the same time of 100 Mbps. Due to the fact that this would represent a very large bandwidth in an actual system, the actual symbol rate was changed to 1 Mbps in the simulation used to investigate adjacent MAI. The chip rate used was 128 times that used for the actual symbol rate. Every 32 symbols transmitted, the flat fading complex coefficients for each path were changed using a Rayleigh pdf with mean 1 and a uniformly distributed phase over 2π. The received power was normalised so that the expected SNR was achieved at the output of the STS decoder. The STS decoder was provided with perfect knowledge of the fading coefficients which allowed for formation of the exact representation of the H matrix over each channel period. This was used by the STS decoder to provide estimates of the transmitted symbols as described by Equation 3.2-5 (page 81). The receive antenna was assumed to be equidistant from the transmit antennas, and that mean (average) received power for both transmitters was the same.

4.3 Adjacent Multiple Access Interference (MAI)

When sectoring is applied different but orthogonal codes would be used in each of the sectors. When transmitted by a single antenna these codes would be synchronised and cause no MAI to different MS's in that particular sector. However, some signal could be deflected by scatterers from one sector to other MS's in another sector. These scatterers could also move about causing the mis-alignment of otherwise orthogonal codes to occur. An example of moving objects may be a crowd of people in range of the sectorised BS or localised rain that falls in one sector but not in another. In this situation one or more multipath signals from one sector could impinge upon the received signal experienced by another MS in a different sector.

The interference following from this mis-alignment leads to Adjacent MAI errors in the received bit stream for the target MS in the Adjacent sector. Figure 4.4-1 shows a possible scenario for one multipath component that is deflected from one sector to another.

It is possible for the related interferer to have a signal power that is stronger to very much weaker than that transmitted by the BS in sector 1 under the following conditions:

- The distance between BS and Sector 1's Target MS is about 300 metres.
- Assuming that approximately one symbol period is the time taken normally for a signal to propagate from the BS to target MS.
- The multipath taken from sector two's scatterers to the Target MS in Sector 1 is less than approximately 900 metres.
- Assuming that power controls in adjacent sectors are not correlated.

Simple calculations based on this scenario and using a Bit rate of 1 Mbps per antenna pairing and considering the speed of light as being 3×10^8 m/s reveals that the interfering signal can be unsynchronised with the Line of Sight signal from Sector 1's BS by a factor that varies between 0 and 127 chips, resulting in the MAI. Only when the signals are synchronised (zero chip variation) will there be no interference when using orthogonal code sets. The individual paths due to the two antenna transmitter in each Sector will have the same number of chip offset due to the distance and chip rate involved at 128 times the 1 Mbps rate of the symbol (a variation of 300/128 = 2.344 metres). The validated Space Time Spreading simulator (see Section 3.4) was modified to model an extra multipath received from a different user in another sector using two paths that will flow across a similar distance (in terms of chip periods). The target MS was set to experience an expected SNR of 0dB and 4dB. The interfering MS from the adjacent sector had its expected SNR varied between -5dB and 1dB. The simulator was modified so that both signals were added together and then complex Gaussian noise was introduced as was done in the original validated models. Individual decoding stages decoded the streams for User 1 and User 2, but only User 1 is considered from the BER calculations. The flat fading complex coefficients were changed every 2346 symbols actually transmitted and the chip delay was varied every 18768 symbols transmitted. These numbers were chosen as they represent the Maximum Transmission Unit

of a Medium Access Control packet of an IEEE802.11 system for the chip delay variation and one eighth of this for the changing of the flat fading complex coefficients.

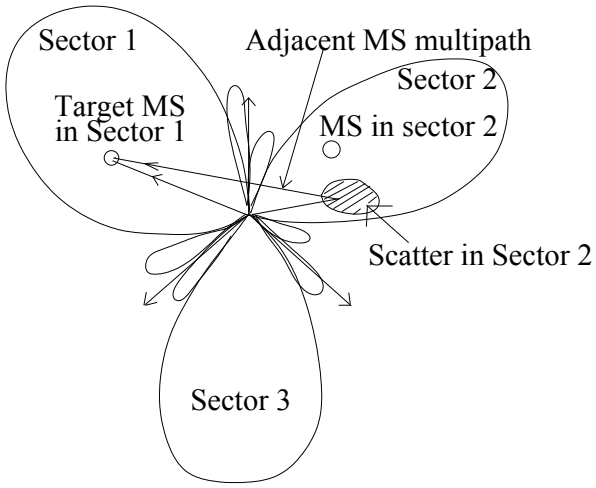

Figure 4.4-1: System with scatter in Sector 2 producing MAI in Sector 1.

4.4 Effect of Adjacent MAI

The effects of adjacent MAI are shown in Figure 4.5-1 and Figure 4.5-2. In Figure 4.5-1 the target MS (called User 1) receives an expected SNR of 0dB whereas in Figure 4.5-2 the same MS receives an expected SNR of 4dB. The flat line in both graphs indicates the measured BER when no adjacent MAI is present. Clearly, in both Figure 4.5-1 and Figure 4.5-2 the presence of adjacent MAI increases the BER experienced by the target MS's received signal. Tabulated data of the results for the case where User 1's received strength is kept constant at a SNR of 0dB, while User 2's signal SNR varies is provided with 95% confidence intervals in Appendix 3. Also, in Appendix 3, this thesis provides single seed values of the tabulated data for the case of fixing User 1 at an SNR of 0dB and fixing another MAI user at 0dB and letting the second MAI user vary its SNR. It also provides tabulated data using a single seed value of the case of fixing User 1dB to 4dB and letting the MAI source User 2 vary its SNR.

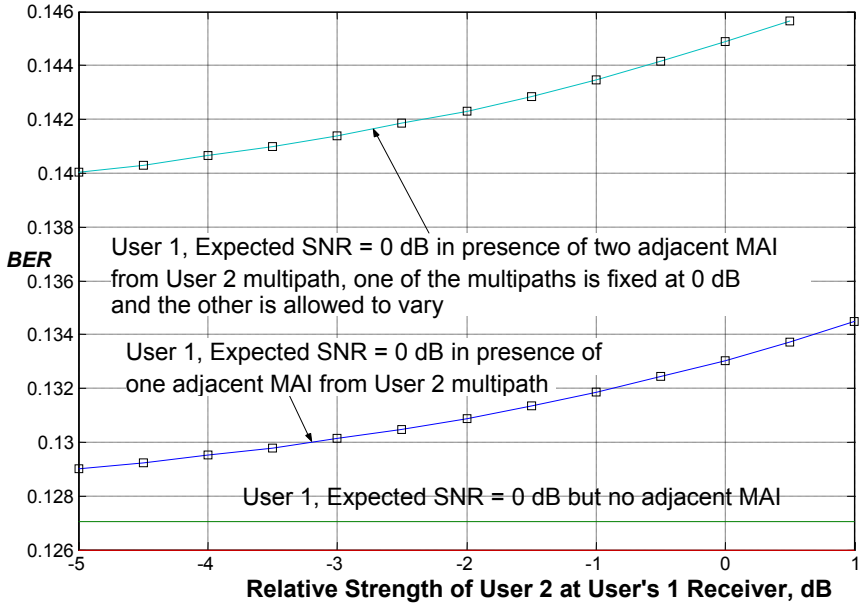

Figure 4.5-1: Effect of MAI on an adjacent sectors CDMA based user with User 1 received strength constant at 0dB, User 2 signal varies (single seed set used only).

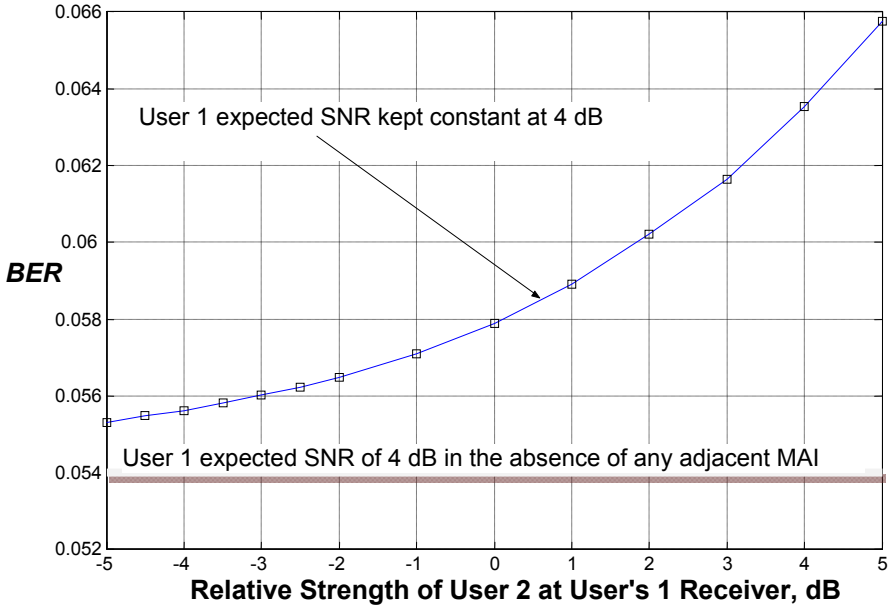

Figure 4.5-2: Effect of MAI on an adjacent sectors CDMA based user with User 1 received strength constant at 4dB, User 2 signal varies (single seed set used only).

4.5 On the effect of low correlation codes on MAI in STS

In Section 4.4 it was shown that the performance of a STS system with two transmit antennas at the BS is degraded in the presence of mutual interference from adjacent sectors in the same cell. These simulation experiments were conducted using a set of four orthogonal Walsh-Hadamard codes with the varying alignment of code boundaries. It was shown that significant degradation occurred compared to the case where no adjacent sectors existed. Other studies have indicated that better sets of orthogonal codes can be found which mitigate the effects of MAI [61]. The next section uses simulation to carry out an investigation into the use of these codes as they are applied to a Space Time Spreading System as proposed in [9].

4.6 Improved Orthogonal Codes

In [61], the authors establish that better choices in the orthogonal codes can result in improved cross-correlation performance which potentially mitigates the effects of MAI. It has been shown that different H-equivalent Hadamard matrices can be used to obtain different sets of spreading sequences having different correlation properties. The H-equivalent Hadamard matrices are obtained by multiplying whole column(s) by +/-1 or by using different permutations of the columns. The sequences used here are derived from the Sylvester-Hadamard matrix of order 32 (Sylvester-Hadamard construction leads to the Walsh-Hadamard sequences) and then by multiplying it by a diagonal matrix with a diagonal equal to [61]:

$$\text{Diag Matrix} = [++--+-+--+---++++--++++++++++++]$$

Where ‘ + ‘ and ‘ – ‘ denote ‘+1’ and ‘-1’ respectively. These modified sequences are characterised with a peak value in the magnitude of aperiodic cross-correlation function between any pair of two sequences C_{max} equal to 0.4063, compared to C_{max}=0.9688 for the original Walsh-Hadamard sequences. This peak value is very important in considering the MAI for the case where the chosen sequences do not change for the duration of the whole frame (at least) and when the number of active users is low [61].

4.7 Simulation results using improved orthogonal codes

Using the same scenario and simulation as described in Section 4.3 except the length of the orthogonal codes was changed from 128 chip length to 32 chip length. The simulation was run using the 32 chip Modified Walsh-Hadamard code set [61] described in Section 4.6, with

two codes kept constant for the target user (User 1) and then a random sequence of code pairs was generated. This sequence was kept the same for all simulations, with the seed value of noise sources and bit stream sources changed. In another experiment, to compare directly to the case described in Section 4.3 where only four (4) orthogonal 128 chip Walsh-Hadamard codes were used, only four of the improved codes were used for the entire simulation. Seed values used were the same between the different simulation runs (a set of three (3) seed value sets were used for the results in Section 4.4 and a set of four (4) were used for the simulations using the Modified Walsh-Hadamard code set, three of which were the same as in the values used in Section 4.4).

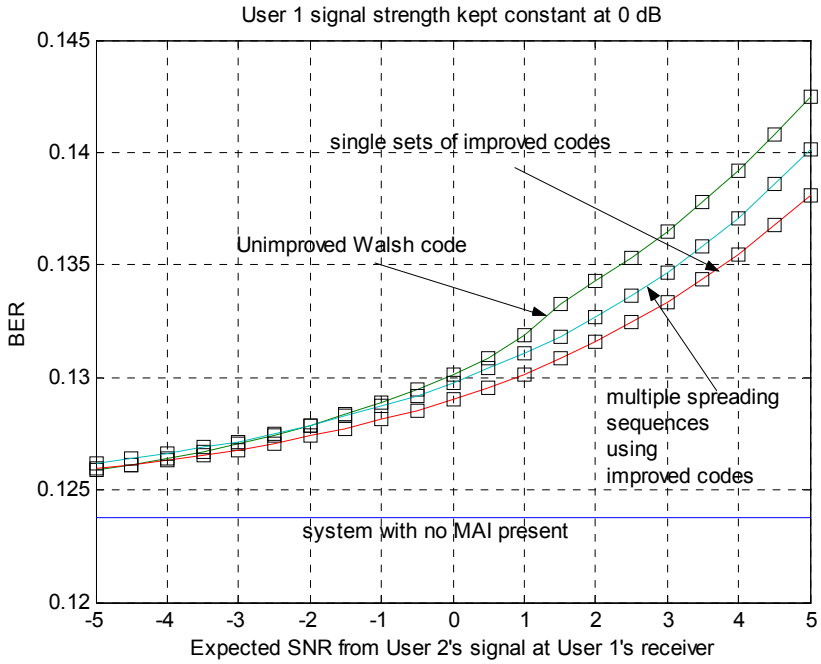

Figure 4.8-1: Bit Error Rate versus Expected SNR from User 2's signal at User 1's receiver comparing the results from Section 4.4 and those obtained using the improved Modified Walsh Hadamard codes proposed in [61].

Three curves are shown in Figure 4.8-1. The curve with the worst BER performance is from the results obtained in Section 4.4 with the Walsh-Hadamard codes. The curve with the best BER performance was also obtained in this study, using only four improved 32 chip orthogonal codes which were kept constant for the entire simulation. This is the same

situation, which was simulated in Section 4.4 with 128 chip Walsh-Hadamard codes. The curve, which lies between the worst and best performance, was the BER performance for the more practical situation where the pairs of codes used in the adjacent sector are different over time. This corresponded in the simulation to 100 different pairs of these codes during the period of the simulation. As different coding pairs will interact in a similar but slightly different manner in terms of their statistical effect of the cross correlation, auto-correlation, and aperiodic cross-correlation (see Figure 1 in [61]) this worse performance is expected. An improvement of between 0.5 – 2 dB is seen in comparison between the results reported in Section 4.4 and the results obtained using the proposed Modified 32 chip Walsh-Hadamard codes of these simulations. It should be noted that when the signal from User 2 has low power there is very little difference between the use of these codes, but as the signal strength of User 2's interference increases at User 1's receiver, the improved codes show a clear improvement in performance in terms of BER. Tabulated data of these results with 95% confidence intervals are provided in Appendix 4.

4.8 Conclusion

This chapter presented a simulation of a simple Space Time Spreading system in the presence of MAI. It was used to investigate how a Space Time Spreading system in adjacent sectors would behave in the presence of multipath from adjacent scatters. It was found that such multipath from adjacent sectors, called adjacent MAI, does in fact degrade the performance of Space Time Spreading systems. The chapter then proposed the use of low correlation orthogonal code sets proposed in [61]. The simulator was modified so that a comparison could be made of the use of orthogonal Walsh-Hadamard codes in a STS system with two transmit antennas with the use of the improved Modified Walsh Hadamard codes described in Section 4.6 and found in [61]. It was found that when the MAI is significant the improved codes improve the BER performance by 0.5 – 2 dB over the unimproved code (128 chip) Walsh-Hadamard codes used in the first MAI simulations. Moreover, that improvement has been achieved despite using four times shorter spreading codes resulting in a smaller processing gain.

This chapter leads on to the investigation in Chapter 9 of the effect of MAI in the developed STS-TH-UWB-PPM system, which uses two transmit antennas to take advantage of space diversity, and which is designed and simulated in Chapter 8. As the results in this chapter indicate that low correlation codes can mitigate against MAI and provide improved BER performance, similar effects may be encountered in applying these codes to the UWB equivalent system. The results of this application are provided in Chapter 9.

Chapter 5: Simulation and Validation of a SISO UWB-PPM system using Simulink

5.1 Introduction

In order to implement a MIMO STS-TH-UWB-PPM system it is necessary to initially undertake an implementation of a SISO UWB-PPM system. This basic system can then be modified to provide the basis for the techniques which allow UWB to take full advantage of the space diversity offered by STS as outlined in Chapter 2, Section 2.5. It is noted here that UWB is a promising technology for sensor networks, broadband wireless data access and location finding applications [43;44]. This chapter outlines the development and validation of a single transmitter and receiver system across the multipath channel proposed by Saleh-Valenzuela [7]. This chapter also discusses how the channel instances of Saleh-Valenzuela multipath were generated and how these were incorporated into the Simulink model developed. This entails the design and testing of a UWB simulator using MATLAB's Simulink in combination with the RTW Tool box for Simulink using the Fixed Step Discrete Solvers of RTW which is required to produce executable simulations on multiple computers (both Linux and Microsoft based devices). In addition this chapter also outlines the basic design and modules chosen for the simulation and compares our results to those published in the literature to validate the designed simulation. It was found that our simulator provides similar performance to the reported results in [8]. We also found that an error floor occurs at high signal to noise ratio when the Saleh-Valenzuela channel is used and the assumption is made that the channel changes every symbol period. Using time traces from the simulation this chapter shows the mechanism behind this phenomenon. This has not been reported by any of the available literature.

UWB is an area of interest to researchers interested in the areas of sensor networks and wireless broadband data access in particular. There are various forms of this proposed technology. Direct Sequence systems can be classified into PPM and PAM. Mathematical expressions have been provided in the published literature which include both types of

systems in the same mathematical analysis, for example Yang and Giannakis do so in [8]. Our simulator is designed to consider only PPM so PAM systems will not be considered further here (see [8] for analysis). It also assumes a system with perfect knowledge of the CSI, where all the phases and gains of the channel are known. Since UWB signals are real, it only considers the real part or in-phase component of the channel setting the imaginary or quadrature component to zero. It also limits the channel to 100 nano-seconds, truncating any further multipath that the Saleh-Valenzuela channel may have generated to zero thus ignoring any possible ISI. For the simulator described in this chapter, it uses only one Gaussian pulse to represent a symbol and the CSI changes for each such pulse. This is not typical in a real UWB system where a channel is slow flat fading and changes approximately every 300 milliseconds [53]. It does not implement any spreading or time hopping which will result in a very peaked and discrete power spectrum which would also not be implemented in a real system. Time Hopping is implemented in subsequent chapters.

This chapter is organised as follows. Section 5.2 describes the Gaussian pulse used and defines the signal and CSI used in the Simulator. Section 5.3 describes how the CSI was generated and what parameters were used in its generation. Section 5.4 describes the developed Simulink model and how MATLAB's RTW was used to generate Monte Carlo based simulations of the UWB PPM system. Section 5.5 compares the results of our study to those found in Yang and Giannakis [8] and uses a time trace to explain the observed error floor inherent in high SNR values. Section 5.6 provides conclusions and how this simulator was used to form the basis for the study into systems implementing Time Hopping, whose implementation is covered in Chapter 6 onwards.

5.2 UWB Signals and the Saleh-Valenzuela multipath Channel

To develop a UWB simulator initially requires definition of a pulse shape. In order to compare results we adopted the pulse shape seen at the receiver suggested in [8]. This pulse shape, called $\omega(t)$, was suggested by [8] to be the second derivative of the Gaussian function:

$$g(t) = \left(\sqrt{\frac{\tau^3}{3}}\right)\left(\frac{2}{\pi}\right)^{1/4} e^{\left(-t^2/\tau^2\right)} \qquad (5.2\text{-}1)$$

Which was calculated to be:

$$\omega(t) = 2\left(\sqrt{\frac{\tau^3}{3}}\right)\left(\frac{2}{\pi}\right)^{1/4}\left(\frac{1}{\tau^2}\right)\left[\frac{2t^2}{\tau^2}e^{\left(-t^2/\tau^2\right)} - e^{\left(-t^2/\tau^2\right)}\right] \quad (5.2\text{-}2)$$

Here $\tau = 0.1225\, ns$ which [8] points out gives a pulse width of 0.7ns. Figure 5.2-1 shows a plot of the squared value of the pulse, which was shown using Mathematica and MATLAB to have a unit area under the curve and hence unit energy (as suggested by [8]). Figure 5.2-2 shows a plot of the expression in Equation 5.2-2 which was the modeled received waveform $\omega(t)$ [8].

The simulator uses the Saleh-Valenzuela channel model [7] which was accepted as a sound model for the UWB channel [43] at least until 2004. The simulations of this thesis continued to use this channel so as to compare and contrast our simulation to those available in the literature. This was chosen to validate our simulator using results found in [8] where the Saleh-Valenzuela model was used. The simulator does allow for the channel model to be changed by generating different multipath 100ns spans using different statistical models, but this is not done for this study for the reason just provided.

In our model the channel multipaths arrive in clusters within the observation window of 100ns. It has a cluster arrival rate with Poissonian mean Λ, while within clusters it possesses a ray arrival rate with Poissonian mean λ. These values determine the time of arrival of each ray within the channel. The amplitude of each arriving ray is then chosen from a Rayleigh distributed random variable which is now dependent on which cluster the ray arrives in and then on another Rayleigh distributed variable within the cluster. That is, one Rayleigh variable is assigned which determines all the clusters amplitudes and the other is assigned on an individual basis within the arriving rays within the cluster. These are then denoted (in nano-seconds) as Γ for the cluster and γ for the individual rays within the cluster. These values determine the rate of decay of the amplitudes over time which conforms to results found in [7].

Appendix 6 details the code developed from [44] to generate the channel multipath using the Saleh-Valenzuela statistical description. This conformed to that for the Saleh-Valenzuela model suggested by [7] and used in [8]. It produced the real and imaginary components of the channel, but as UWB is a real signal it only used the real values of the channel as input to our simulink model. To generate this data a threshold was selected which limited the number of possible multipath to between 100 and 300 paths. The real part of the multipath channel coefficients were taken and the resulting channel instances were written into a larger MATLAB variable with multipath between 100 and 300 per 100ns channel. In most cases there were not 200 such multipaths in the individual channel instances and so this data was further truncated to 200 multipath for the simulink simulations. A snap shot of one 100ns channel is shown in Figure 5.2-3.

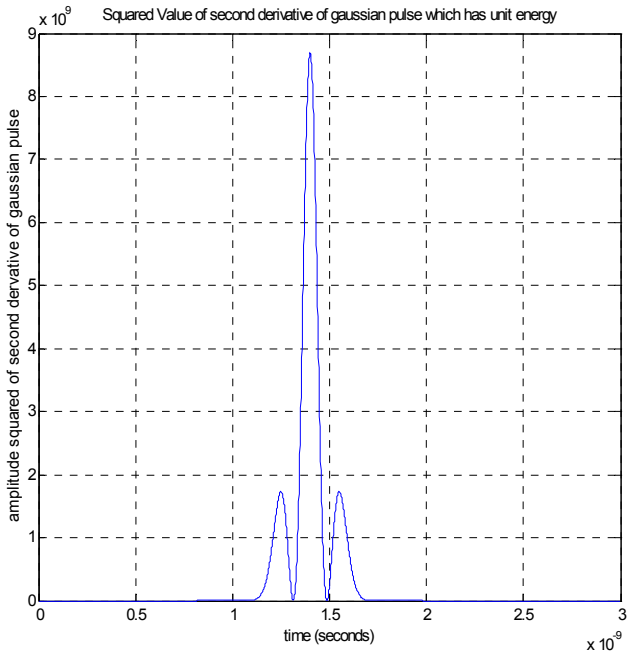

Figure 5.2-1: Squared value of second derivative of Gaussian pulse.

If any multipath component was more than one nanosecond away from another multipath in the same channel, this was noted using a flag in the MATLAB array used to represent the multipath. As stated by Yang and Giannakis in [8] the multipath used in the Rake receivers is entirely the choice of the designer of the receiver, so this marking of the multipath essentially provides a pre-filter or selective filtering of the usable multipath in any one particular

instance of a channel realisation. These MATLAB variables were then read in at the initialisation of the Simulink simulation into the MATLAB/Simulink workspace and then referenced at the required instances in simulated time. An embedded MATLAB/Simulink block then converted the data from the individual channel instances into a continuous series of pulses with appropriate amplitudes for the real part of the signal which was then transmitted onto the receiver section of the Simulink implementation of the UWB PPM system.

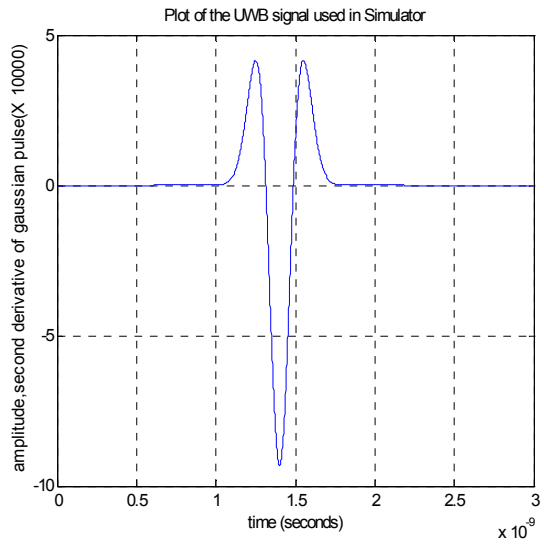

Figure 5.2-2: Time plot of second derivative of Gaussian pulse.

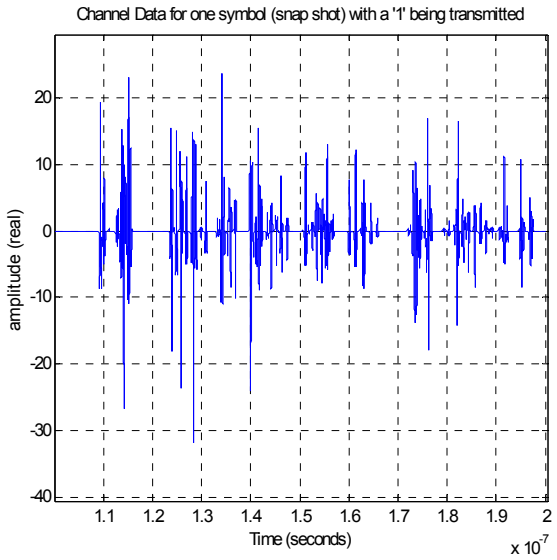

Figure 5.2-3: Snap shot of a single channel over 100ns.

5.3 Channel Definition and modeling

As indicated in Section 5.2, using some modified MATLAB files from [44] (see Appendix 6) a significant number (in the order of thousands) of different channel state information sets, were generated to ensure that the channel behaved as per the description in [8]. These were then used to generate different seed values for different monte-carlo simulations of the systems developed and proposed in this thesis. For the simulations in this chapter these channels were changed every symbol and there was no spreading or time hopping patterns used (simply only a peer to peer single user system was examined). A symbol in this context was simply one Gaussian pulse. This also means that the system was changing at a faster rate than would be expected in an actual UWB channel, where as a rule of thumb the channel changes every 300 milliseconds [53].

Once the channel data set was generated and stored into an array with such information as time of multipath arrival with respect to the line of sight path and using a NLOS (Non Line of Sight) models as suggested in [8] and [7]. To generate this data it used the parameters $\Gamma = 33\ ns,\ \gamma = 5ns,\ 1/\Lambda = 2\,ns$ and $1/\lambda = 0.5\ \ ns$. These parameters were used by [8] for their results as per the description in [7]. The simulation of the channel was done with a sampling rate of 1×10^{12} samples per second so that one channel span of $100ns$ would have 100000 samples. One such channel is shown in Figure 5.2-3. In later simulations this value was lowered to reduce simulation run time with no significant variation in results (to ensure this, a test of the system using the same parameters was run and the results were essentially the same).

The array which was produced by the MATLAB code was then input via the Simulink block "Matrix Channel Data" which at the start of the simulation loads the entire matrix into Simulink data space. This was followed by a Variable Selector and an embedded MATLAB function which randomly chose a channel matrix to use for generating the channel. Figure 5.3-1 illustrates the technique employed to do this.

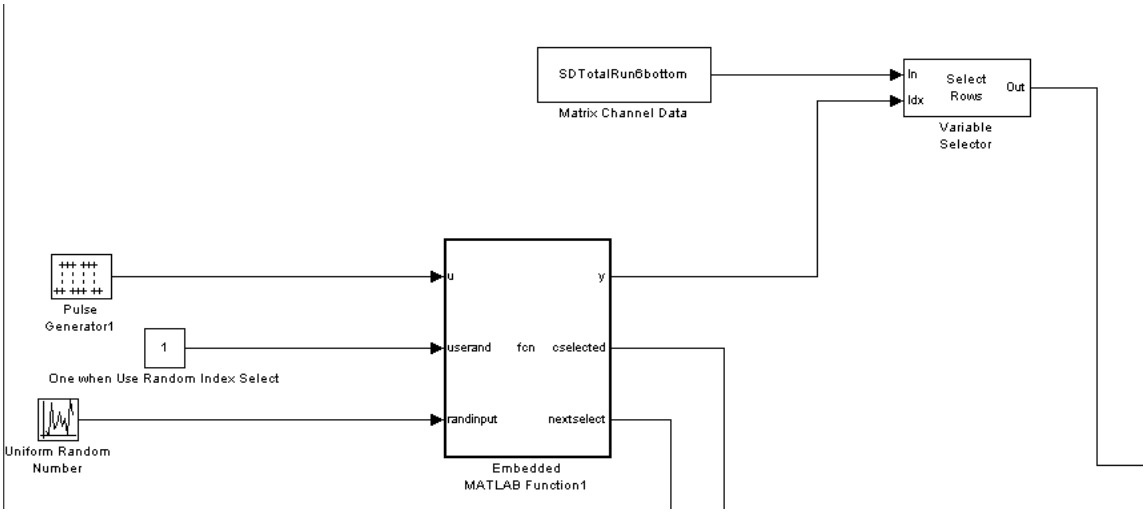

Figure 5.3-1: Selecting the Channel in Simulink.

5.4 Design of Simulink UWB-PPM Model

The Simulink model uses the data from the channel matrix and embedded MATLAB to generate a sequence of pulses with different amplitudes but zero phase (for real UWB signals). Embedded MATLAB provides a cut down or reduced set of MATLAB functions. Using embedded MATLAB and RTW compilations it was possible to have multiple simulations with different seed values in a reasonable time frame. Also, it allowed the author of this thesis to access the available clusters of computers to run multiple simulations in parallel without needing any MATLAB or Simulink licenses. This allowed the results reported to include 95% confidence intervals, as shown in Figure 5.5-1 (which compares results found in [8] to outputs from the simulink simulation of the same set of system parameters as reported in [8]).

The Simulink Model itself used a section to generate the case where a '1' was sent and a section to generate the case where a '0' was sent. In this simulation it used Orthogonal PPM with a spacing of 1ns to conform to the simulations in [8]. These were generated simultaneously even though only one of the two was transmitted. The energy of the signal and the energy of the noise as per the description in [8] was calculated. The Expected SNR was calculated based on the ratio of received signal strength (for all received paths) to the received noise power multiplied by channel gains. The system implemented a partial Rake

using the L^{th} best arriving (useful) rays but rejecting rays that had multipath too close (within 1ns) of each other . A Maximal Ratio Combining decision was made to decide for a '1' or a '0'.

In our model it assumed that 100% of the power is detected by the receiver (in [8], it is assumed that 10% of the power is lost). We used the case where we had the template using '1' path (L=1) and '4' paths (L=4). Figure 5.4-2 illustrates some of the modules used in the 'correct value sent' communication link.

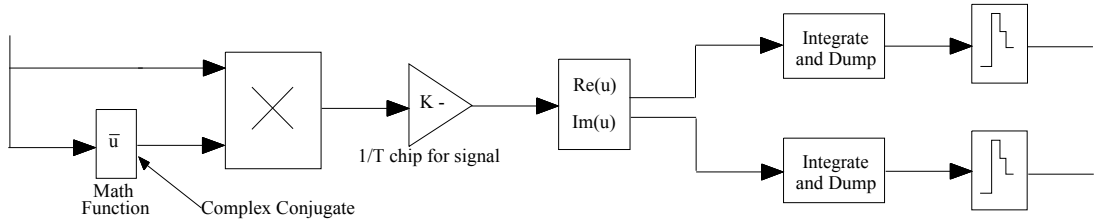

Figure 5.4-1: Main communication link in simulator.

5.5 Model Validation

Using the data reported in [8] the author of this thesis obtained estimates of the simulation when orthogonal PPM with spacing between the '0' and '1' being one nanosecond was used for the case the number of paths in the template was '1' and the case where the number of paths was '4'. Figure 5.5-1 shows the data that the Simulink simulation/RTW produced compared to that from the published Figures 7 and 8 in [8]. The tabulated data for the Simulink simulation data shown in Figure 5.5-1 is provided in Appendix 7. It can be seen that our data is very close to that reported in [8] with BER's versus Expected SNR either within error bars or close to the estimated (by eye) data from [8], especially for Expected SNR less than 22dB. Above 22dB, for L=4, it was found that our system had a slightly smaller BER than that reported in [8] until it was increased above 28dB where it was found that an error floor developed. All results for L=4 above 22dB were measured until 100 error events occurred to ensure that the data was statistically reliable (using the law of large numbers). Above 20dB for L=1 it was found that our system experienced a smaller BER. The explanation for this is the conservative selection of the number of multipaths that were included, an example of which is shown in Figure 5.2-3. The error events used to generate the data in Figure 5.5-1 for L=1 had a minimum value of 200 errors (which was more than the

minimum used of 100 error events chosen for L=4 measurements). Figure 5.5-2 and Figure 5.5-3 show the results from the Simulink simulator for the case L=1 and L=4 respectively when the first set of arriving rays is used, a Partial Rake is implemented and a Selective Rake is implemented. The tabulated data for the Simulink simulation data shown in Figure 5.5-2 and Figure 5.5-3 is provided in Appendix 7 and Appendix 8.

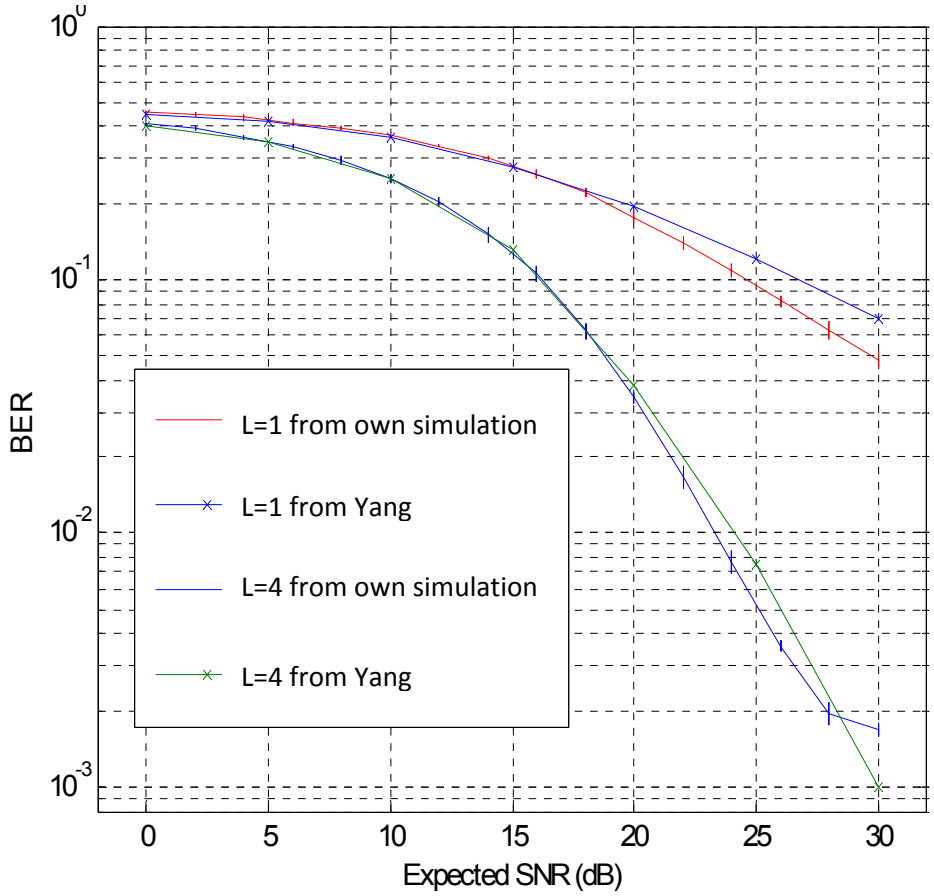

Figure 5.5-1: Comparison of measurements from Simulink model to estimates from Figures 7 and 8 from [8].

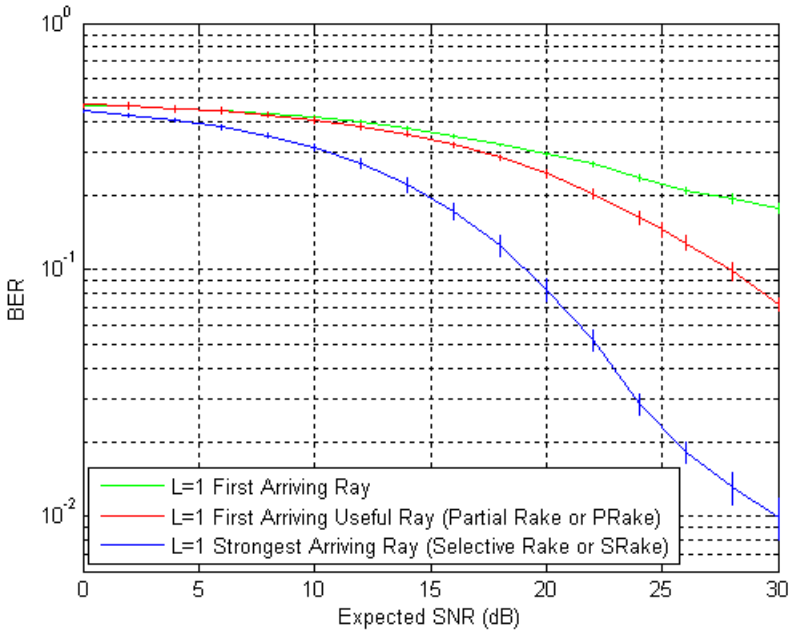

Figure 5.5-2: BER versus Expected SNR (dB) for first arriving ray, first useful (PRake) arriving ray and strongest arriving ray (SRake) for Simulink Simulation.

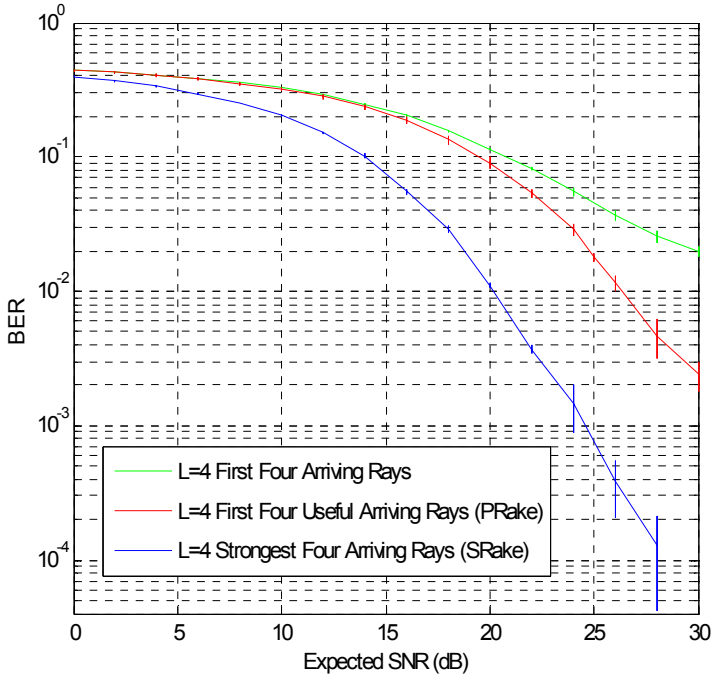

Figure 5.5-3 : BER versus Expected SNR (dB) for the case first 4 arriving rays, first 4 useful (PRake) arriving rays and strongest 4 arriving rays (SRake) for Simulink Simulation.

Plotting the BER in Figure 5.5-4 for a single seed value, the observed data shows that the curve flattens out at high SNR. Interestingly it was discovered that when the simulator using the UWB channel model and no noise was run, various errors occurred. The Simulator with multipath was then run with no noise to locate where the first error occurred and a time trace was recorded. Figure 5.5-5 shows a snapshot of the results from probe signals inside the simulation. It indicates the location of the pulse sent for a zero and then the location of a series of pulses close to each other which combine to 'appear' to be the correct symbol sent (using MRC).

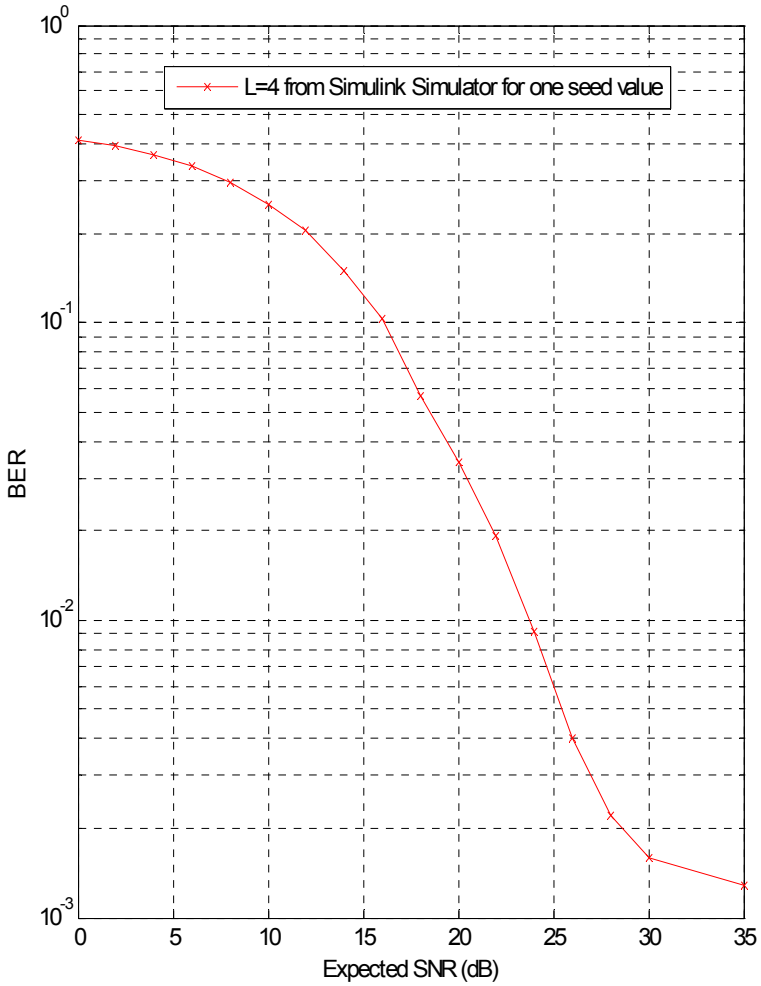

Figure 5.5-4: Plot of a single seed for L=4 showing an error floor appearing after 28dB in Simulink Simulation.

Table 5.5.1 details the data that was used to form the channel at the location where the error occurred. The first column in Table 5.5.1 indicates the magnitude of the real part of the multipath at the time index appearing in column 2 of Table 5.5.1. The third column in Table 5.5.1 represents the time elapsed since the start of the current symbol's period (which is a total of 100*ns*). The fourth column of Table 5.5.1 is an internal simulation flag used to indicate if a multipath is present or not (there is a maximum of 200 such paths, but in many instances there are less than 200). The fifth column of Table 5.5.1 is also a flag. This flag indicates if the individual multipath element has a significant magnitude compared to other multipath and is simultaneously located at a distinctly different time, determined by the pulse width, from any other multipath with significant magnitude generated by the SV channel model. If both of these criteria are satisfied then this flag is set (1), otherwise it is reset (0). Multipath with this flag set are termed 'useful' multipath for the purposes of this thesis.

From Table 5.5.1 the magnitude of the surrounding pulses to the main pulse were of opposite phase and comparable magnitude. More importantly the two multipaths that were 0.4ns and 1ns away from the correct decision point (bottom two entries in Table 5.5.1) were nearly as large and had the same phase reinforcing each other and creating the error condition. Better choice of simulation data set would alleviate this problem, but in a real system this would correspond to ignoring a complete channel set or choosing pulses which had smaller magnitude decreasing the expected SNR of the system.

Table 5.5.1: Data used to form the channel around the location of the error.

Magnitude	Time Index	Time (secs)	Present	Useful Number
3.7774e-005	16889	1.6888e-008	1	0
-0.00035181	17647	1.7646e-008	1	1
8.5502e-005	17672	1.7671e-008	1	0
0.00022275	18112	1.8111e-008	1	0
4.9095e-005	18352	1.8351e-008	1	0

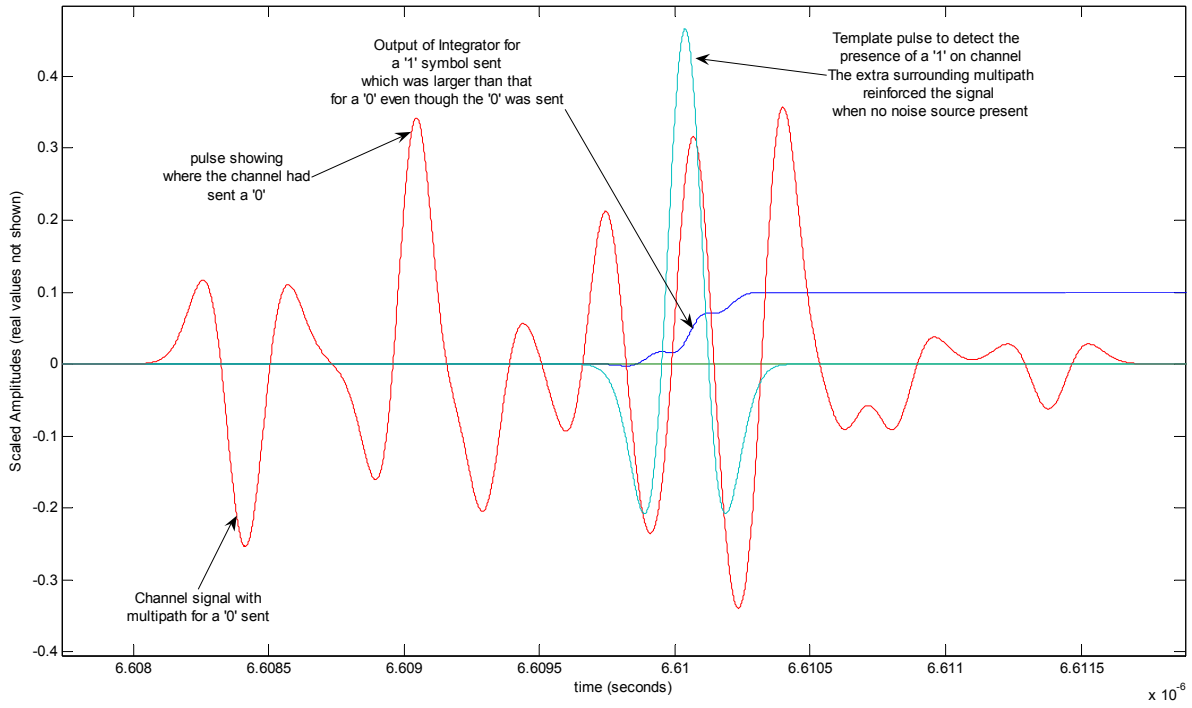

Figure 5.5-5: Snapshot of a small segment of channel signal at the point where error occurs without any noise.

5.6 Conclusion

This chapter presents the development and validation of a UWB simulation using Simulink which shows comparable results to those reported in [8]. This was for a Saleh-Valenzula channel using the same parameters as [7]. It was also found that for our randomly generated data set, with the channel changing every symbol transmitted, an error floor became evident at an expected SNR of approximately 28dB. This was found to be a result of the multipath around the incorrect decision point.

This chapter has described the development of a model which can be modified such that the rate of fading can be changed relatively easily. The shape of the received pulse can also be changed with some effort. Chapter 6 will add time hopping followed by direct sequence spreading to our simulator. It was expected, and found to be the case, that if the channel state information is changed less often that the simulation time will decrease as there will not be a requirement for the embedded MATLAB to be called as often to modify the channel state

information. The developed model is flexible in that it can also use its framework to model other channel models by generating the channel state information separately and importing these into our simulinks channel data array (see Figure 5.4-1). This allows the simulator to be used for other datasets (ie. for other UWB channel models proposed in the literature [44]).

The model described in this chapter leads onto the development of a modified SISO system which is developed and investigated in Chapter 6. This system adds the use of spreading and Time Hopping. Chapter 7 employs a MIMO system which uses a decoder that makes hard decisions on a chip by chip basis at the receiver. This system is much less complex than the system developed and investigated in Chapter 8 and Chapter 9. Both of these systems provide an answer to how to use two transmit antennas to transmit two symbols in the time that a SISO equivalent, using UWB, would transmit one symbol. The system developed in Chapter 8 shows how to do this without degrading the system (ie decision is performed on a symbol by symbol basis, where a symbol in this sense represents two binary data bits). All these systems were developed on the work studied and described and validated in this chapter.

Chapter 6: DS Modified TH PPM over UWB SISO S-V Channel

6.1 Introduction

The simulator developed in Chapter 5 is now modified to incorporate Time Hopping and a spreading sequence is implemented so that it has a two-position PPM system using Ultra Wideband transmission. This system is then modified further to use a three position PPM scheme which is proposed for a Direct Sequence Time Hopping Ultra Wideband wireless communication SISO system. The channel is based on the Saleh-Valenzuela model outlined in Chapter 5 Section 5.2 . This chapter will show that by adapting the Space Time Spreading technique seen in Chapter 3 and Chapter 4 to be used in our UWB PPM system that it can use three pulse positions in a single input single output system representing -2,0,2 resulting in an improvement in Bit Error Rate compared to sending the same bits using two pulse positions only. In addition, this system that is proposed provides a bit access rate that is doubled as two bits can now be successfully sent in the same time using our proposed system at the expense of only one extra pulse position.

In the study reported by August and Dong [6] I-UWB is described for distributed MAC (Medium Access Control) protocols. In this paper the authors describe a UWB system which is applicable in the moderate range of PRI of between 1μs to 10μs. They suggest that this moderate range is an adequate representation due to the challenges that occur with intersymbol interference, increased frequency of pulses (need to meet FCC criteria in the United States of Americas) and increased magnitude of spectral lines with decreased PRI [6]. These authors go on to point out that, due to the channel characterisation, advantage can be taken of the dead time between pulses, which can be interleaved with other sub-channels (as needed in a shared MAC media). This interleaving of channels allows us to consider a system which uses DS-TH-UWB (Direct Sequence-Time Hopping-Ultra Wide Band) in a similar way. This idea also is expressed in [62] which looked at a comparison of Orthogonal Transmit Diversity and Space Time Spreading systems for IS-2000 (not a UWB based system).

Choi and Stark [63] analyse PPM UWB orthogonal, overlapped and OOK employing binary block coded modulation over a indoor multipath channel for a single user SISO system using MRC at the Rake receiver. They show that the choice of interval and multipath used for individual re-combinations at the Rake receiver is up to the receivers' choice and can be considered dependent on the channels characteristics. This is done by careful selection of the used multipath as a function of their location in time relative to other multipath considering the time shifts (for different pulse positions) and the duration (time based width) of a single ultra wideband pulse (typically in nanoseconds). This further implies the importance of time between received pulses and their multipath. This concept is then further extended, in this thesis, by applying the use of the STS code to the pulse position mechanism.

Chapters 3 to 5 covers the development of STS systems in the presence of Multiple Access Interference and the development of a PPM UWB simulation using MATLAB's Simulink. This chapter seeks to combine these two systems across a SISO wireless link using simulation and show that in the presence of multipath and with perfect knowledge of the channel coefficients the BER performance normalised for energy per bit for a three position pulse position scheme, which is described below, is equal or superior to the two position pulse position scheme when using DS-TH-UWB technique. Moreover, by doing so the data rate can be doubled as two bits of information can be transmitted in the same time slot instead of a single bit that can be sent using only a two position technique as done in Chapter 5.

The inspiration for this technique, which this thesis calls Direct Sequence Modified Time Hopping Pulse Position Modulation, was from the earlier work in building a STS MIMO system as outlined in Chapter 3. This was simulated in Chapter 3 and showed how low correlation spreading codes (proposed in [61]) can be used to reduce the effects of MAI in Multiple Access Direct Sequence Spread Spectrum systems as shown in Section 4.7.

This chapter is organised as follows. Section 6.2 outlines the simulation of the DS-TH-UWB two pulse position simulation. Section 6.3 proposes how the two pulse position simulation can be modified to three pulse positions using the Space Time Spreading Technique proposed in [9] as applied across a Saleh-Valenzuela channel using UWB PPM. Section 6.4 compares

the BER performance of the two systems using simulation in the presence of Gaussian noise on an energy per bit to noise ratio. Section 6.5 concludes the chapter and outlines its relationship to the other sections of this thesis.

6.2 DS-TH-UWB with Two pulse Positions

The work in this chapter uses the simulator described in Chapter 5 from which a Direct Sequence Time Hopping Ultra Wideband simulation is constructed using MATLAB/ Simulink. Specifically, a Direct Sequence outer loop is added based on a simple thirty two bit Walsh-Hadamard code and a Time Hopping bit pattern. A frame with eight one hundred nano-second slot positions was defined where during one of these eight slots a Gaussian pulse (as illustrated in Section 5.2) would be transmitted. A time hopping pattern was then superimposed on this to add further time dithering and hence smooth out the spectrum of our system. The Time hopping pattern chosen (purely randomly) was [6 0 5 3 6 4 5 3] and this was not varied during the simulations for either two or three pulse position modulation. To further elucidate, each frame was split into eight one hundred nano-second time frames. For the first such frame at the sixth slot a Gaussian UWB pulse was transmitted with a zero shift to represent a '0' and a one nano-second shift (delay) to represent a '1' (dependent on the value being transmitted and the Walsh-Hadamard spreading sequence). These shifts corresponded to those imposed in the simulations described in Chapter 5.

It was assumed here that only the energy received at the demodulators' receiver was considered (as was done in Chapter 5). Prior to generating the SV channel coefficients the received Gaussian pulses were ranked in order of strongest to weakest useful multipath. Usefulness was decided on whether there were any other significant multipaths in the near vicinity of the signal in time. The simulations were then conducted for the first useful ray (L=1, Partial Rake) and the best useful ray (L=1, Selective Rake), the first four useful rays (L=1, Partial Rake) and the best four useful rays (L=4, Selective Rake). The measured results are shown in Figure 6.2-1 with 95% confidence interval error bars. The tabulated data with 95% confidence intervals for this system are provided in Appendix 9.

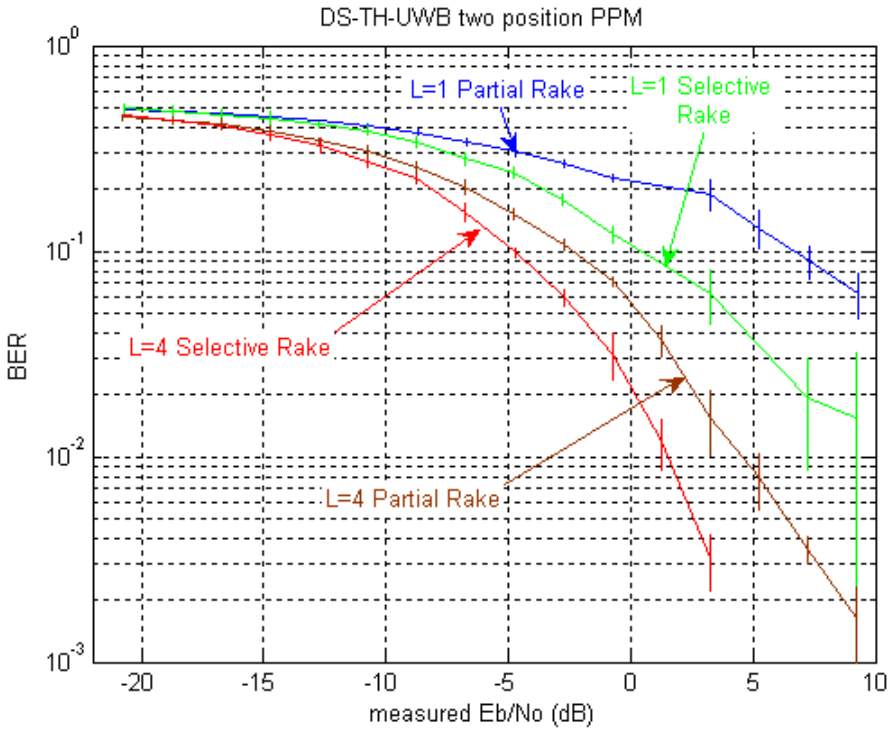

Figure 6.2-1: DS-TH-UWB simulations for two position PPM.

6.3 DS Modified-TH Pulse Position Modulation

While developing the Space Time Spreading simulation described in Chapter 3 it was observed that the values being sent per stream could be represented by -2, 0, or 2. These could correspond to three different time shifts in a UWB PPM scheme. At the computational expense of one extra shift in time within a slot (an extra nanosecond), it is recognised that this modified system could send one symbol representing two chips of data instead of one and use the space time spreading demodulator described in Chapter 3 to demodulate the received signal. This is implemented with perfect timing and channel coefficients knowledge at the receiver. The receiver then makes a decision in the presence of noise as to which symbol has been transmitted by comparing the received signal with three possible received symbols but with no noise (as done in Chapter 5).

The stream sent could be the summation of two bits multiplied by the 32 bit spreading sequence. This study now represents the individual chips of the spreading sequence by $c_1[j]$ and $c_2[j]$ where these are the two Walsh-Hadamard spreading sequences used in Space Time Spreading and j is the counter for the individual chips within that sequence which here is a

integer in the range {1,2,..,32}. If b_1 and b_2 are the two bits to be transmitted across the UWB channel, then for the addition stream it is described by:

$$b_1 c_1[j] + b_2 c_2[j] = \left\{ \begin{matrix} 2 \\ 0 \\ -2 \end{matrix} \right\} \quad for \quad j = 1,...,32 \qquad (6.3\text{-}1)$$

While for the difference stream is described by:

$$b_2 c_1[j] - b_1 c_2[j] = \left\{ \begin{matrix} 2 \\ 0 \\ -2 \end{matrix} \right\} \quad for \quad j = 1,...,32 \qquad (6.3\text{-}2)$$

Either of these streams can then be transmitted and demodulated at the receiver using the Space Time Spreader demodulation technique used in Chapter 3. This means that one symbol now represents two bits instead of the one bit represented per symbol transmitted in Section 6.2. Using the same UWB channels as described in Section 6.2 this study conducted the simulations for the first useful ray (L=1, Partial Rake) and the best useful ray (L=1, Selective Rake), the first four useful rays (L=1, Partial Rake) and the best four useful rays (L=4, Selective Rake). The measured results are shown in Figure 6.3-1. The tabulated data with 95% confidence error intervals is provided in Appendix 10.

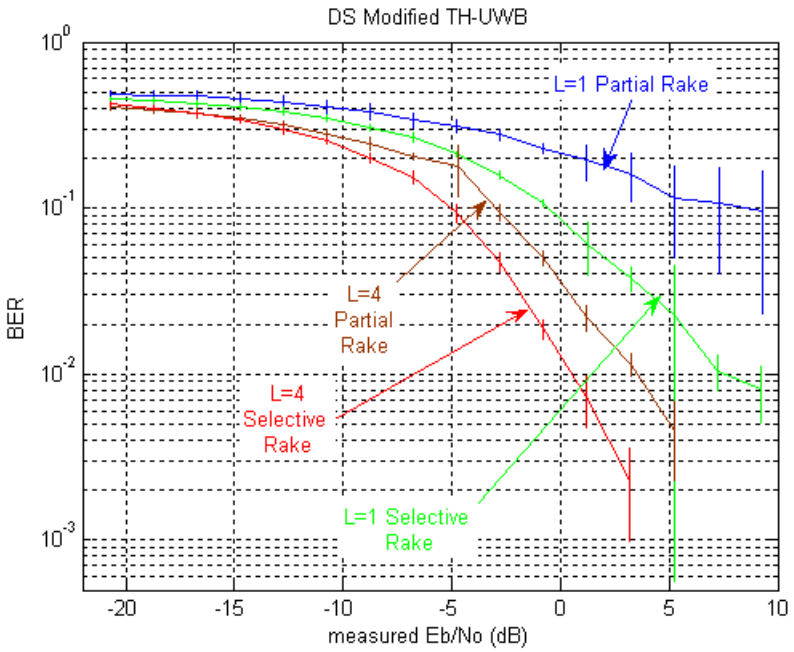

Figure 6.3-1: DS Modified-TH-UWB simulations for three position PPM 95% confidence intervals for this system are provided in Appendix 10.

6.4 Comparison of DS-TH-UWB with DS-Modified-TH-UWB

This study now compares the results obtained using the two pulse position UWB and the modified three pulse position UWB based on the Space Time Spreading technique. Figure 6.4-1 shows the modified and un-modified method developed in Section 6.3 and Section 6.2, respectively for the first useful arriving ray (L=1, Partial Rake). For the Measured E_b/N_o (the ratio of bit energy to noise energy) in the middle range the two methods appear to work nearly the same. For lower and higher measured E_b/N_o values the un-modified methods performance in terms of BER is superior. For this middle range of values for measured Eb/No it would be better to choose the modified method as two bits are sent in the same time taken to transmit one bit with the un-modified method with no loss in the BER.

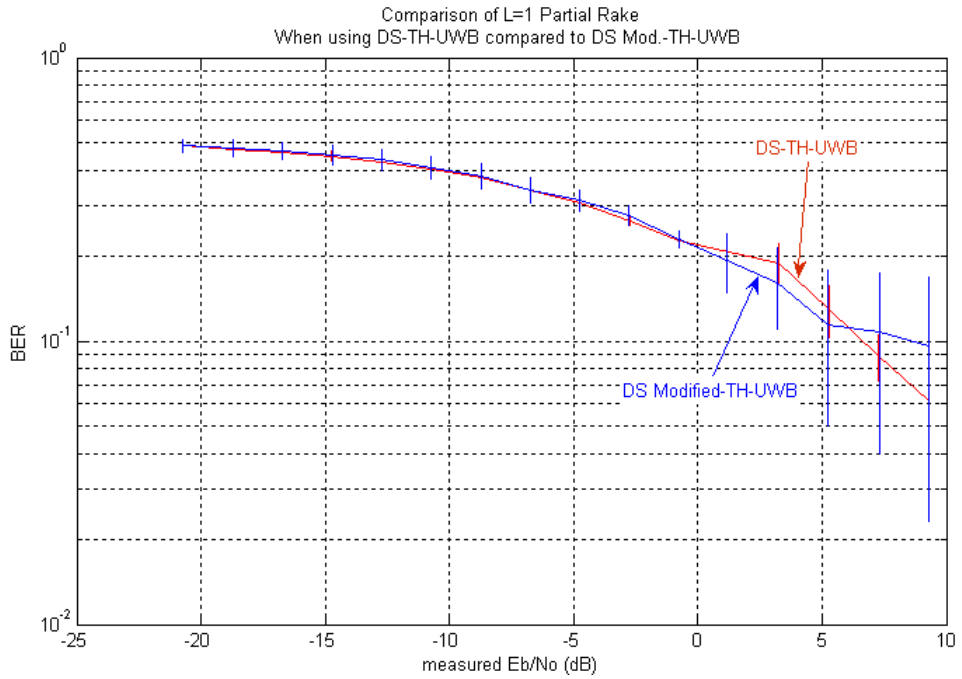

Figure 6.4-1: Comparison of L=1 Partial Rake with DS-TH-UWB and DS-Modified-TH-UWB.

Figure 6.4-2 shows the modified and un-modified method developed in Section 6.3 and Section 6.2, respectively for the first four useful arriving rays (L=4, Partial Rake). Examination of the plotted data indicates that there is a significant improvement in the modified methods performance over the un-modified methods performance in terms of BER. For low values of measured E_b/N_o the modified method has a slightly better performance than the un-modified method. For higher values of measured E_b/N_o there is a significant

improvement of BER over the unmodified method, for example at a BER of 0.03 there is approximately a 3dB difference in measured E_b/N_o between the two methods.

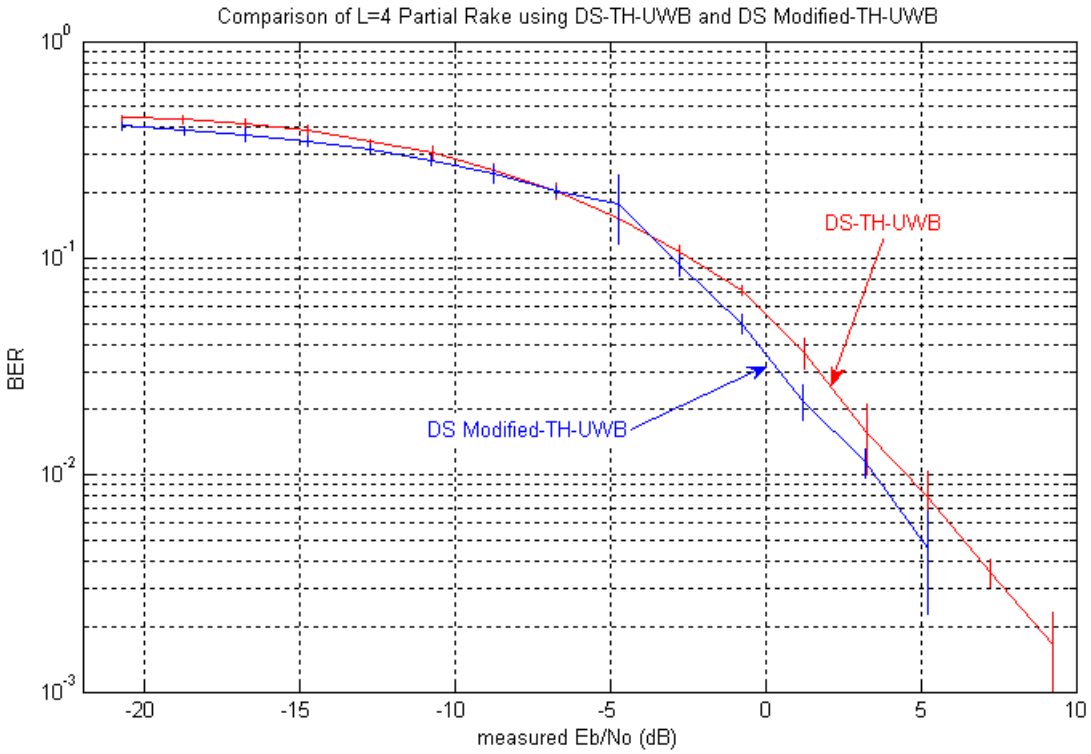

Figure 6.4-2: Comparison of L=4 Partial Rake using DS-TH-UWB and DS-Modified-TH-UWB.

Figure 6.4-3 shows the modified and un-modified method for the best arriving ray (L=1, Selective Rake). The modified method shows significant improvement in BER over the un-modified method for all values of measured E_b/N_o. Once again a more significant improvement is seen for higher values of E_b/N_o than lower. This contrasts with Figure 6.4-1 where the two techniques performed in a similar manner for the middle set of E_b/N_o values. For the case of selective rake this performance improvement clearly favours the modified method.

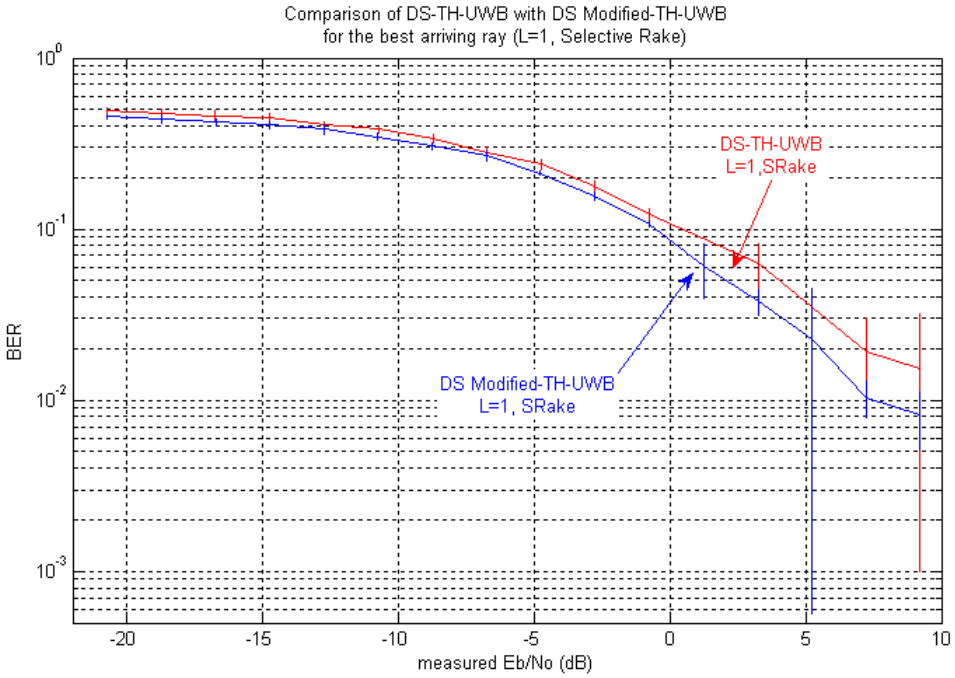

Figure 6.4-3: Comparison of L=1 Selective Rake using DS-TH-UWB and DS-Modified-TH-UWB.

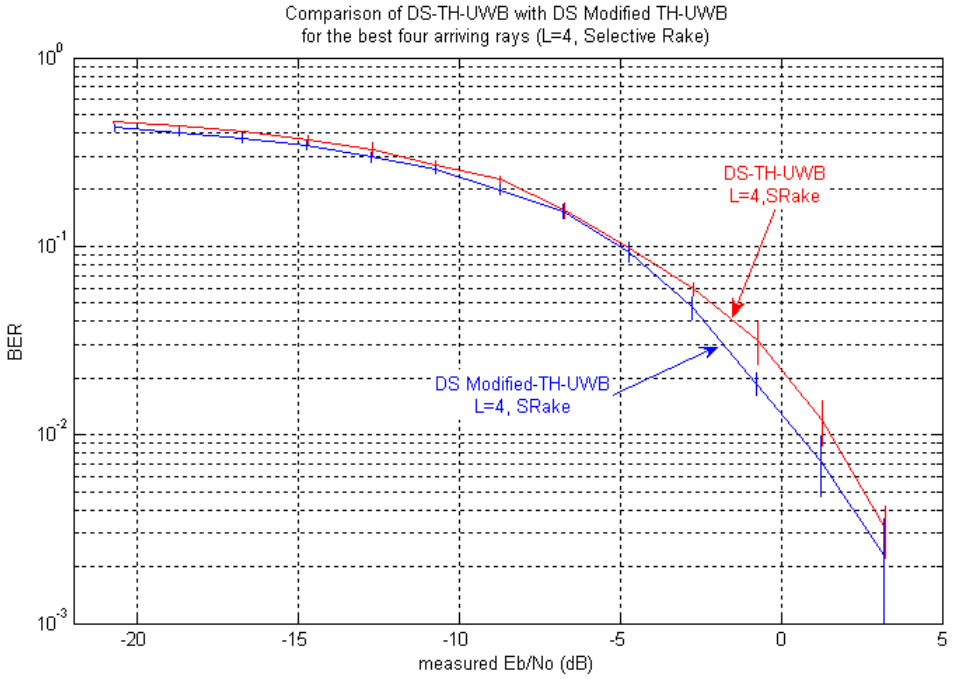

Figure 6.4-4: Comparison of L=4 Selective Rake using DS-TH-UWB and DS-Modified-TH-UWB.

Figure 6.4-4 shows the results for the two methods when the best four arriving rays are used (L=4, Selective Rake). Once again there is significant improvement in the BER for the same measured E_b/N_o, which improves as the measured Eb/No increases.

6.5 Conclusion

The simulation described in Chapter 5 has been modified to include Direct Sequence and Time Hopping. It was then proposed to modify this technique using the sum or difference approach described in space time spreading which this thesis terms DS-Modified-TH-UWB. It was found that for three out of the four studies conducted DS-Modified-TH-UWB performed with a better BER than DS-TH-UWB at the same measured E_b/N_o values in our simulation. In the case where there was no performance advantage it was shown that for middle values of E_b/N_o the systems performed similarly. Even in this case, the added advantage higher data rate would warrant usage of the DS-Modified-TH-UWB method.

The SISO system for TH-UWB-PPM presented in this chapter shows how the application of the Space Time Spreading system to UWB PPM can enhance the data rate. As only one antenna is used to transmit, if a deep fade occurs, the data will be likely received in error. The system proposed in the next three chapters use two transmit antennas. They will show how Space Time Spreading can be applied to the UWB PPM system to take advantage of the space diversity provided when using two antennas with uncorrelated multipath. The system provided in this chapter was merely a necessary stage of development to the system which was proposed and investigated in Chapter 8. Chapter 9 will proceed to investigate the effect of Multiple Access Interference on the system proposed in Chapter 8.

Chapter 7: Non-Optimal receiver for STS - TH over UWB PPM MIMO S-V Channel

7.1 Introduction

The application of STS to an TH-DS-UWB-PPM to use two transmit antennas, and hence take advantage of space diversity in a MIMO system, was first achieved with a non-optimal technique. This technique is simpler to implement and involves deciding which chip has been sent. As will be highlighted in this chapter, this involves identifying which pulse position was sent on which antenna. In building an STS system to study MAI effects in STS systems, it was the observation that each antenna sends a different signal level at the same instance in time, and at no stage does it send the same signal value. In the case of two transmit antennas this correlates with the discrete values -2, 0 or 2. It is proposed that these could be translated into pulse positions and hence used to transmit data in the STS schema across the UWB PPM system. In this chapter the decision is made on a chip basis using a MRC at the receiver. Chapter 8 looks at this same scenario but instead retains the advantage of the CSI coefficients until after one symbol period when a hard decision is made. The advantage of the system described in this chapter is that the decoder is simpler than that required in Chapter 8 and for some situations this simpler decoder may be an advantage provided a poorer BER performance is acceptable.

In this chapter, a novel non-optimal chip based technique is also proposed to use two antennas to transmit data across a Direct Sequence Time Hopping Ultra Wideband dual antenna wireless communication system to a single receiver. The spread data is sent over the independent channels using the Space Time Spreading technique to encode the chips which are sent on each antenna simultaneously. A hard decision is made at each chip of the spreading code received based on the known Channel State Information which Pulse Position Modulated signal was received from each antenna. This chapter shows that by adapting the Space Time Spreading technique to use three pulse positions in a dual input single output system one can transmit data at a lower Bit Error Rate for high E_b/N_o. Three receive

techniques are considered; the use of the first arriving rays, the first set of useful arriving rays and the best set of arriving rays for each symbol period. The proposed receiver is less complex than that of the optimal system where a Maximum Ratio Combiner is used across the entire spread signal space (per symbol rather than per chip), requiring more memory storage in the receiver. In addition, two symbols are transmitted during the period of one symbol period for a single antenna system. This is achieved at the expense of a higher measured BER compared to single antenna systems.

Previous chapters have covered the development of STS systems (Chapter 3 and Chapter 4) in the presence of MAI and the development of a Direct Sequence Time Hopping Ultra Wideband Pulse Position Modulation simulation using MATLAB's Simulink (Chapter 5). This chapter combines these two systems (STS and DS-TH-UWB-PPM) across a MIMO wireless link and compares its performance with the equivalent SISO DS-TH-UWB-PPM system. Both schemes implement the MRC detector on a chip by chip basis rather than a symbol by symbol basis. This system is simpler to implement, at the loss of overall channel information in a MIMO system that uses a symbol by symbol decoder. By using the proposed technique, at high E_b/N_o, the data rate can be effectively doubled compared to a SISO based equivalent system using only DS-TH-UWB-PPM. This is achieved, however, at the cost of an increase in observed BER.

This chapter is organised as follows. Section 7.2 outlines the simulation of the DS-TH-UWB two pulse position simulation (as already described in Section 6.2). Section 7.3 proposes how the two pulse position simulation can be modified to three pulse positions using the STS Technique proposed in [9] as applied across two Saleh-Valenzuela channels (one for each transmitting antenna) using UWB PPM. Section 7.4 outlines how the Symbol Energy to Noise (E_b/N_o) ratio was measured in the SIMULINK simulation. Section 7.5 presents the simulation results and compare the results for the same seed value between the SISO and MIMO system proposed here, while Section 7.6 concludes the chapter and leads on to the system in Chapter 8 which shows how to use two transmit antennas without degrading the system and transmit at twice the data rate available with only one transmit antenna, taking advantage of available space diversity.

7.2 DS-TH-UWB with two pulse positions

The Simulation of a SISO DS-TH-UWB-PPM system as described in Section 6.2 was re-used for comparison with the STS dual antenna MIMO system proposed in this chapter. The system described in Section 6.2 used a Rake based receiver to collect the energy of each finger followed by a chip based MRC detector. These simulation results are reproduced from from the simulation study described in Section 6.2, and data with 95% confidence intervals are shown in Figure 6.2-1. However, only one single seed set was used to produce the results shown in this chapter. The same seed set was used so that it was possible to compare the BER performance of the SISO and MIMO systems. The system described in Section 7.3 uses a dual antenna single receiver system (MIMO) whereas the results shown in Figure 6.2-1 used single antenna to single antenna or SISO based system. The system described in Section 6.2 used an outer loop spreading/de-spreading stage on the chip by chip waveforms that were received for the two pulse position systems. The same time hopping pattern was used in all cases which was fixed at [6 0 5 3 6 4 5 3] so each system can be appropriately compared. The spreading/de-spreading sections used a Walsh-Hadamard thirty two chip code. As previously described, the time hopping pattern used was split into 8 slots, numbered 0-7. Each slot was fixed at one hundred nanoseconds. Only one of the eight slots is used to transmit the chip. For example, in the first eight slots, slot number six was used to transmit the two pulse position UWB signal.

Within the simulation for the same seed value, the algorithms used were to look at the first L arriving rays, the first L arriving rays which are one nanosecond away from other multipath, and the strongest L arriving rays which are at least one nanosecond away from other multipath rays. This was simulated in Chapter 6 for L=1 and L=4. The results shown in Figure 6.2-1 are reproduced in Figure 7.2-1 for one seed set only so as to compare these results to those obtained for the non-optimal MIMO system described in Section 7.3. The tabulated data for one seed set only, for this system, are provided in Appendix 11.

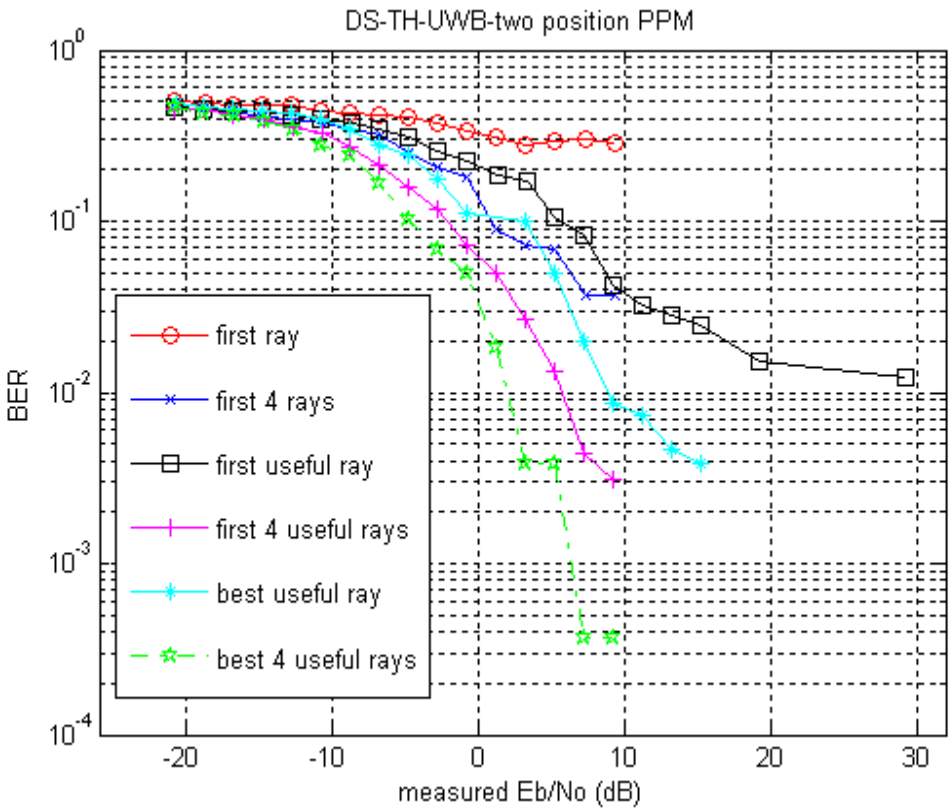

Figure 7.2-1: DS-TH-UWB simulations for 2 position PPM for a single seed set.

7.3 MIMO system

In Section 6.3 it was observed for the STS based modified DS-TH-UWB-PPM simulation that in simulations of the STS baseband systems described in [8] one could represent at the chip level values being sent by -2, 0, 2. It was suggested in Section 6.3 that these could be represented by three time shifts of the Gaussian pulses used for transmission. This added only the addition on one extra time shift. Thus by adding only one extra pulse position it was feasible to send two symbols in the same period that only a single symbol was sent using DS-TH-UWB-two position PPM. This was achieved with perfect knowledge of the channel characterisation and timing at the receiver in the presence of noise on a chip by chip basis. Further, it was observed in the simulation of the STS baseband system [8] that each channel had a different discrete value transmitted. That is, if a -2 was sent on one antenna path a 0 or 2 (but not a -2) was transmitted on the other. For a system based on pulse position modulation, where Gaussian pulses are transmitted at different time shifts to represent -2, 0, and 2, each antenna would transmit a pulse at a slightly different time. If using orthogonal

pulse position modulation and the UWB channel characteristics of each transmitting antenna are uncorrelated, it will lead to the receiver (having perfect CSI) being able to detect and recover the data stream originally transmitted.

With the STS technique applied to DS-TH-UWB PPM it transmits the sum stream on antenna 1 and the difference stream on antenna 2. Since it is now over two antennas this is hence forth referred to as STS-TH-UWB-PPM. Each antenna is assumed to correspond to an uncorrelated SV channel (using two different seed values for each antenna wireless channel). This can provide a diversity of up to two at the transmitters (space diversity). These streams involve the use of two 32 bit spreading sequences. Proceeding similarly to Chapter 6, the individual chips of these spreading sequences are represented by $c_1[j]$ and $c_2[j]$ where these are the two Walsh-Hadamard spreading sequences used in STS and j is the counter for the individual chips within that sequence which here is an integer in the range {1,2,..,32}. Proceeding, as per notation used in Section 6.3, to say that b_1 and b_2 are the two bits to be transmitted across the STS-TH-UWB-PPM MIMO channel. Hence for the addition stream it is given by (as per Section 6.3, Equation 6.3-1):

$$b_1 c_1[j] + b_2 c_2[j] = \left\{ \begin{matrix} 2 \\ 0 \\ -2 \end{matrix} \right\} \quad for \quad j = 1,...,32 \qquad (7.3\text{-}1)$$

while for the difference stream is given by (as per Section 6.3 Equation 6.3-2):

$$b_2 c_1[j] - b_1 c_2[j] = \left\{ \begin{matrix} 2 \\ 0 \\ -2 \end{matrix} \right\} \quad for \quad j = 1,...,32 \qquad (7.3\text{-}2)$$

The stream of Equation 7.3-1 is then transmitted on antenna one. The stream of Equation 7.3-2 is transmitted on antenna two. To normalise the system for a two antenna transmission, each antenna transmits at half the power of a SISO system (that is, multiply the signal amplitudes by $1/\sqrt{2}$ within the simulations). Either of these streams can then be transmitted and demodulated at the single receiver in the presence of Gaussian noise using the Space Time Spreader demodulation technique used in [8]. This means that one symbol now represents two bits instead of the one bit represented per symbol transmitted in a system described in Section 7.2. This is achieved at the cost of an extra PPM time shift. Table 7.3.1 shows the STS codes for individual chip level values for 32 chip spreading sequences c_1 and

c_2 used in the Simulink/MATLAB simulation. This technique can also be applied to MIMO systems with four and eight transmit antennas and a single receive antenna. To apply it to such scenarios requires five pulse position shifts for four antennas and nine pulse positions for eight transmit antennas. These are the only situations (n_T = 2, 4 and 8) where STS full rate systems can be used [11]. This thesis reported earlier implementations of such systems undertaken in this study (see Figure 3.4-2). For these cases it requires n_T+1 pulse positions. The proof that these are also valid can be shown in the same way as the formation of Table 7.3.1. That is, form the chip values sent for each antenna in use and tabulate against possible values for the b_i, where i ranges from 1 to 4 for n_T=4 and 1 to 8 for n_T=8.

Table 7.3.1: Sample of Space Time Spreading codes shown for individual chip level values for a 32 chip spreading sequences c_1 and c_2 used in simulation when transmitting {-1,-1} pairing.

b1	b2	c1i	c2i	b1*c1i	b2*c2i	b2*c1i	b1*c2i	**Antenna One** **b1*c1i + b2*c2i**	**Antenna Two** **b2*c1i - b1c2i**
-1	-1	1	1	-1	-1	-1	-1	**-2**	**0**
-1	-1	-1	1	1	-1	1	-1	**0**	**2**
-1	-1	1	-1	-1	1	-1	1	**0**	**-2**
-1	-1	-1	-1	1	1	1	1	**2**	**0**
-1	-1	1	1	-1	-1	-1	-1	**-2**	**0**
-1	-1	-1	1	1	-1	1	-1	**0**	**2**
-1	-1	1	-1	-1	1	-1	1	**0**	**-2**
-1	-1	-1	-1	1	1	1	1	**2**	**0**
-1	-1	1	1	-1	-1	-1	-1	**-2**	**0**

Using the same UWB channels as described in Section 7.2 the simulations were conducted for the first ray, first useful ray (L=1, Partial Rake), the best useful ray (L=1, Selective Rake), the first four rays, the first four useful rays (L=4, Partial Rake) and the best four useful rays (L=4, Selective Rake). The obtained results for a single seed set are shown in Figure 7.2-1. This was also performed in simulation for n_T=2 using three position PPM and a single receiver case but the channels that were used were two uncorrelated SV channels for each transmit antenna. This was implemented for the same seed values utilised in SISO for one of the antenna channels used; the other channel had a different seed set, of course uncorrelated.

The results for this are shown in Figure 7.3-1. The tabulated data for one seed set only, for this MIMO system, are provided in Appendix 12.

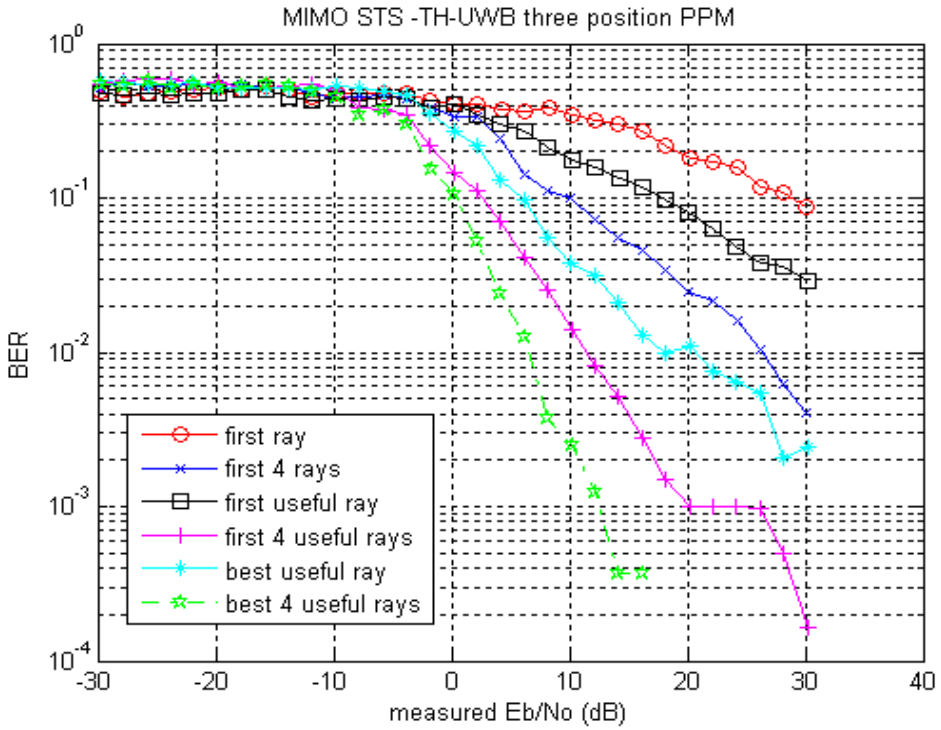

Figure 7.3-1: STS Performance of MIMO TH-UWB-3 position PPM proposed chip based MRC (non-optimal).

7.4 Measured E_b/N_o for MIMO system

The simulator for the MIMO based system incorporated a factor of 0.707 on each antenna as explained in Section 7.3. The mean or average of each antennas total power versus measured noise energy taken over the total slot was then measured (across all multipath in the channel). The result was multiplied by 32 (the number of chips in a symbol) and represented the total energy that was used to transmit two symbols, on average, over one antenna. This was then adjusted for each antenna, considering with STS that each channel transmits both symbols at the same time, one being the sum the other the difference in the case of two transmit antennas. The resulting average measured E_b/N_o for the MIMO system was used in the performance results. No such adjustment is done for the SISO system as it transmits only one symbol at a time. A **dB Gain** SIMULINK module was used in the path of both antennas to change the measured E_b/N_o (dB) in two dB increments for this system. Table 7.5.1 shows sample calculations. All calculations were performed in excel spreadsheets.

Table 7.4.1: Measured Eb/No calculations for MIMO STS UWB system.

SNR (dB)	2Eb/No (dB)	measured Eb/No (dB)
0	-23.76	-29.785
2	-21.77	-27.79

7.5 Comparison of MIMO and SISO

Comparing the results obtained using the two pulse position UWB described in Section 7.2 and the MIMO STS technique described in Section 7.3. Figure 7.5-1 shows the SISO technique outlined in Section 7.2 for the first useful ray and the MIMO system using two antennas outlined in Section 7.3. They show BER versus measured E_b/N_o (dB). Clearly the system described in Section 7.2 provides a lower BER for the same measured E_b/N_o by about 6dB-20dB for high measured E_b/N_o. This should be considered in that the MIMO technique transmits two symbols in the same period that the SISO technique transmits a single symbol. Both techniques used a chip by chip basis for the MRC detector with L=1 finger for the Rake receiver and the de-spreading was performed based on the Walsh Hadamard spreading codes employed. Two orthogonal codes are required for the MIMO system and only one for the SISO system.

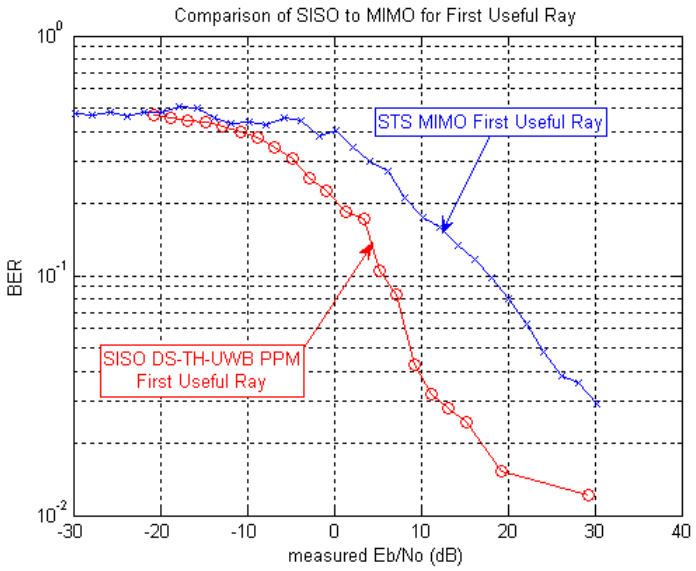

Figure 7.5-1: Comparison of the SISO and MIMO technique for PRake, L=1.

Figure 7.5-2 shows the same data as that for Figure 7.5-1 except now the number of fingers used in the Rake receiver is L=4, for the same seed value. For this situation the STS L=4 MIMO system has a displacement of approximately 3-6 dB for high measured E_b/N_o (dB). The curves are closer than in the case for L=1 but the SISO system still has a better performance.

Figure 7.5-3 shows the results when the best useful rays (or selective rake) are used to detect the symbol sent on a chip by chip basis. Once again the SISO system is 2-5dB's better than the STS based system. Figure 7.5-4 shows the results when the best four (L=4) useful rays are used in the Rake receiver on a chip by chip basis, showing similar performance as in the L=1 situation. From the results the poorer performance of the dual antenna system compared to single antenna system can be attributed to the fact that the chip by chip basis of the decision removes the advantage of knowing the channels exact coefficients and timing over all the energy of the symbol (comprised of 32 Gaussian pulses or chips). This has very little effect on the SISO system as there is only one transmit antenna, however in the MIMO system with two transmit antennas, both uncorrelated channels can interfere with each other. By making a hard decision on a chip by chip basis instead of a symbol by symbol basis, the energy employed in the decision is in fact much smaller than would be used over the whole symbol.

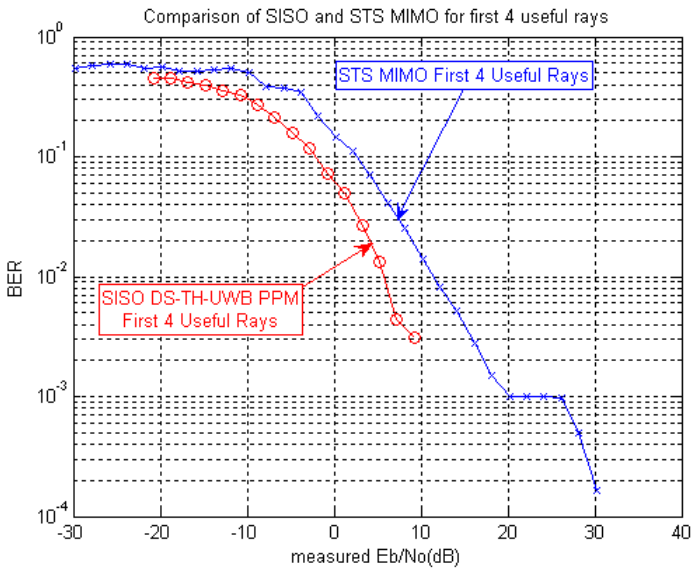

Figure 7.5-2: Comparison of the SISO and MIMO technique for PRake, L=4.

Having two channels (one from each antenna) tends to cause an increase in the probability that a Gaussian pulse on one antenna will coincide with a pulse on the other antenna (as the rays in use will be uncorrelated between the two antennas). Simulations from other studies have shown that much better performance is achievable when all the energy of a symbol is accumulated and used in the hard decision resulting in a symbol being decided upon rather than the chip by chip basis considered here. The major advantage of making a chip by chip hard decision is the fact that the receiver is simpler to implement. It should also be noted that the STS dual antenna system proposed here still enjoys the advantage that two symbols or binary bits are sent in the same period that only one symbol or binary bit is transmitted by the SISO system. Also, if a fade occurs on one antenna it is unlikely to occur on the other and both binary bits are available on either antenna using the STS technique.

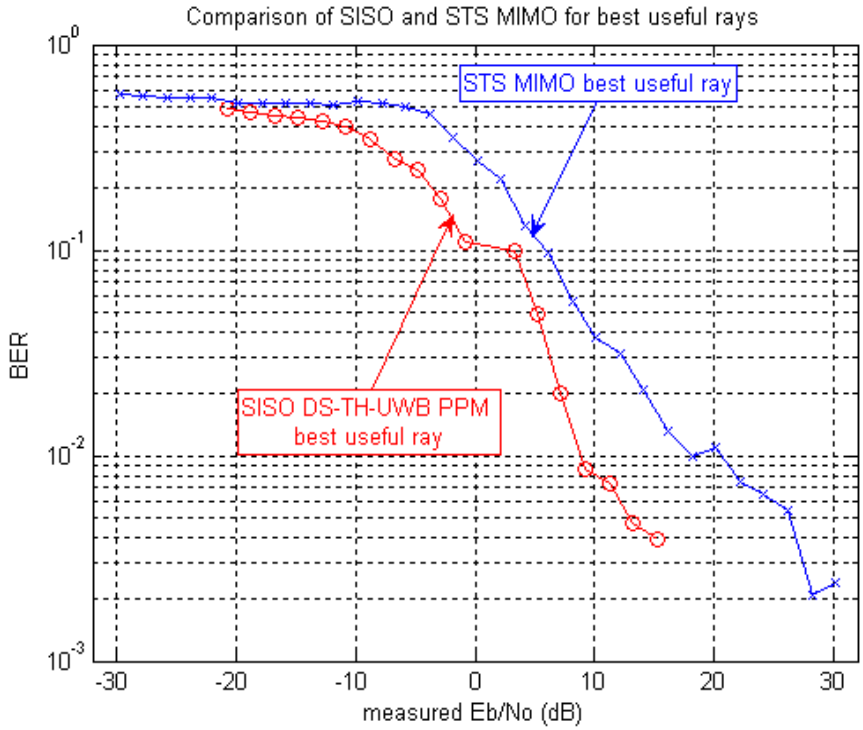

Figure 7.5-3: Comparison of the SISO and MIMO technique for SRake, L=1.

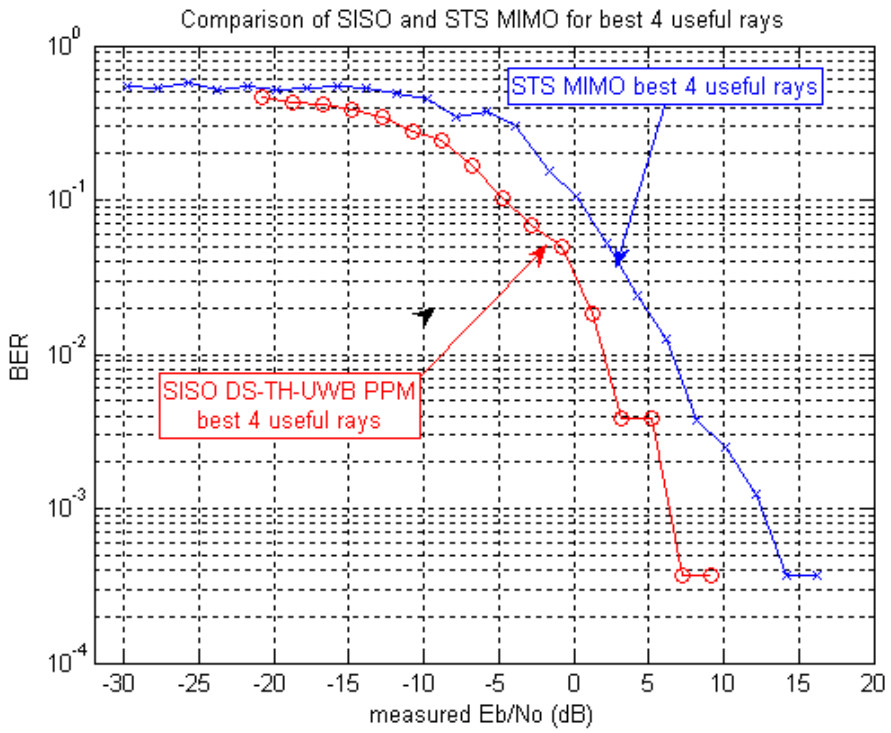

Figure 7.5-4: Comparison of the SISO and MIMO technique for SRake, L=4.

7.6 Conclusion

This chapter illustrates the use of a novel non-optimal technique employing two antennas in a TH UWB PPM MIMO scheme adapted for UWB using an STS technique. This is compared to a SISO based system described in Chapter 6. Both systems make their decisions on a chip by chip basis within a spreading code or codes. It was found that the SISO system had a better performance compared to the MIMO STS based system by between 2dB-20dB depending on the number of fingers used in the Rake receiver and the partial or selective rake techniques employed. This needed to be considered in the light that the MIMO STS based system transmits two symbols in the same time that the SISO system can transmit only one such symbol. In fact, it was pointed out that the MIMO technique employed here can be expanded to systems with four and eight transmit antennas where four and eight symbols respectively could be transmitted in the same time that the SISO transmits one symbol. It was suggested that the MIMO system suffers from extra collisions between each antennas uncorrelated channel coefficients and lower transmit power, as shown in the discussion on how E_b/N_o is measured (Section 7.5). This adversely affects the MIMO system compared to the SISO system which has only one multipath channel to transmit the symbols through. It is

suggested that improvement would be obtained by employing the MRC detector across an entire symbol rather than over a chip period. This is the case that this thesis reports on for the simulation implemented in Chapter 8. However, the presented here non-optimal technique can be used for high measured E_b/N_o to provide a transmission technique to send symbols at BER that decreases as measured E_b/N_o is increased. This is simpler to implement compared to the system which uses an MRC detector across an entire symbol. The simplicity of the demodulator comes at the expense of poorer BER performance.

It should also be remembered that two symbols are transmitted in the same time that one is in a SISO system, though comparing this to the novel SISO based system developed in Chapter 6 , the Modified-DS-TH-UWB BER performance was superior and it also transmits two symbols in one symbol period. However, in the case of the SISO system which was called the Modified-DS-TH-UWB there is only one multipath so space diversity is not available. That is, if there is a deep fade on the multipath channel, the data could be lost or need recovering using other coding techniques (such as Turbo codes [64]).

Chapter 8: Optimal receiver for STS across a TH PPM over UWB S-V MIMO Channel

8.1 Introduction

This chapter outlines a technique which can use multiple transmit antennas to send more than one binary bit using the same number of transmit antennas over a single transmission. It uses Ultra Wideband orthogonal pulse position modulation to achieve this, with the receiver employing a Rake receiver and a Maximum Ratio Combiner optimal detector. This is done over a Space Time Spreading Time Hopping Ultra Wideband Pulse Position Modulation system assuming a rich multipath Saleh-Valenzuela MIMO channel model. Simulation results indicate that a significant gain can be achieved compared with other proposed schemes utilising multiple transmit antennas for Ultra Wide Band Pulse Position communications. The gain is both in terms of transmission rate and the signal to noise ratio required for the simulator bit error rates. This chapter provides a method to employ two transmit antennas to transmit two binary bits using the same energy that would be employed in a SISO based system without degrading the systems performance. This answers the research question formed in the introductory chapter on how to employ multiple antennas (systems with four and eight transmit antennas are realisable) to transmit binary information efficiently over a wireless UWB communication link. This chapter also compares results obtained from the designed Simulink simulator with results reported by Yang and Giannakis [8] showing good agreement. This was done with minor modifications to the Simulink simulation of the TH-DS-UWB-PPM system which forms the basis of this study.

It is not clear how an Ultra Wideband system could use multiple antennas to transmit more than one binary bit in a single transmission period. Yang and Giannakis [8] have proposed techniques which use multiple antennas to transmit a single binary bit using two spreading sequences (see Section 2.10). This is inefficient in terms of the limited number of orthogonal spreading sequences (using two spreading sequences to transmit one binary bit) and they also propose only one such scenario in their contribution which can be shown to use spreading sequences (see Section 8.2). The system developed in this chapter, however, follows [8]

where Pulse Position Modulation is employed to generate a wireless communication data link.

In [8] Yang and Giannakis employ an analog PPM modulation / demodulation technique using two transmit antennas and one receive antenna. They illustrate the use of PAM and PPM, showing through theoretical analysis that the systems are very similar, one employing an amplitude modifier and the other employing a time shift. In [8] they perform their simulations without the use of Time Hopping.

Time Hopping allows multiple users to access the wireless medium without affecting each other provided they do not use the same time hopping pattern and their time hopping patterns are synchronised to some common time. In wireless MAC schemes this is often done by the use of a beacon control packet/frame. In our study it uses a Time Hopping Pattern which [8] does not. This smoothes the spectrum of the UWB system and thus allows the system to appear more like background noise to other wireless communication systems rather than the discrete spectra that would result without its use. For this reason it was decided that the simulated system must incorporate a time hopping pattern, as was done in Chapter 6 and Chapter 7. For PPM the shift in pulse position also smoothes the spectra but its effect is less significant than the use of a time hopping pattern.

It is shown in this chapter that the resultant BER is comparable to that obtained for a Yang Analog ST coding type I scheme [8]. If the system is compared on a per antenna branch basis it is shown that a 3dB improvement is possible over the corresponding Yang ST coding type I scheme which can transmit only one binary bit compared to the two that Space Time Spreading (STS) sends per branch when two transmit antennas are employed. Thus it is shown how multiple antennas may be employed in a Space Time Spreading Time Hopping Ultra Wideband Pulse Position Modulation (STS-TH-UWB-PPM) system to achieve the transmission of multiple binary bits in one transmission period.

This chapter starts by describing briefly a Yang Analog ST coding type I scheme [8] in Section 8.2 and shows how it is in fact using orthogonal Walsh-Hadamard codes on each

antenna. Section 8.3 describes STS and how it is applied to a TH-UWB-PPM system. Section 8.4 describes how the simulator in Simulink for Section 8.3 was modified to provide a Yang Analog ST coding type I scheme and shows the simulation using the Simulink model developed for Yang's ST coding I scheme versus the relevant data from [8]. Section 8.5 then compares Yang's ST coding I scheme in terms of measured E_b/N_o (dB) to the proposed STS-TH-UWB-PPM scheme for Partial and Selective Rake systems for the number of used multipath values (L) of 1 and 4. Section 8.6 is then the conclusion.

8.2 Yang's Analog ST coding I scheme

In [8], one of the proposed techniques to be employed to provide space diversity using two transmit antennas is termed Analog ST coding scheme I. For such a technique Yang and Giannakis [8] propose that at the transmitter a ST encoder is used on each transmitting antenna to form the transmitted signal. The ST encoding occurs over many frames of transmitting Gaussian shaped pulses within short time periods of length T_f. In their simulations and our simulations T_f had a value of 100 ns (nano-seconds). They also deployed the SV channel described in [7], which is a non-line of sight model of the multipath channel. The number of such frames in a symbol is denoted N_f. They indicate that N_f is usually even (as it is for our spreading code in Section 8.3 which uses an N_f=32).

Proceeding, Yang and Giannakis [8] form two signals that are transmitted at the same time from the 0th antenna and the 1st antenna. From the 0th antenna they transmit the waveform (reproduced from [8] equation 10):

$$s_o(t) = s\left(\sqrt{\frac{\varepsilon}{2N_o}}\right)\sum_{n_f=0}^{N_f-1}(-1)^{n_f}\, w\left(t - n_f T_f\right) \qquad (8.2\text{-}1)$$

And from the 1st antenna they transmit the waveform (reproduced from [8] equation 11):

$$s_1(t) = s\left(\sqrt{\frac{\varepsilon}{2N_o}}\right)\sum_{n_f=0}^{N_f-1} w\left(t - n_f T_f\right) \qquad (8.2\text{-}2)$$

The factor of 2 in the denominator is used to normalise the power to that used in a SISO system (as is also described in Section 8.3 for the proposed system). They do not incorporate

a time hopping pattern as described in Section 8.3 and 8.4 of this thesis. The signal w(t) is the Gaussian pulse waveform used or pulse shaper (which is normalised so that the integral over a time period T_f of its squared value is equal to unity, or in other words has unit energy [8]). The term 's' is the coded value of the bit transmitted. The value of s is either -1 representing a '0' or +1 representing a '1'. N_f is the number of frames in a symbol and does not incorporate the time hopping pattern used (the actual period when time hopping is incorporated for one symbol would then be N_f times T_f times the number of slots in the Time Hopping pattern in total, see Section 8.3).

The signal described by Equation 8.2-1 and Equation 8.2-2 are then demodulated over a symbol by multiplication by a template which considers all of the channel multipath gains and appropriately time shifted values of the pulse shaper. This is then combined in an L-finger Rake receiver and then an MRC detector. The procedure is fully described in [8].

These signals described by Equation 8.2-1 and Equation 8.2-2 should be examined closely. In [8] they do not include discussion of spreading codes being used as is done with the STS-TH-UWB-PPM proposed system. However, they are, in fact, using a simple form of Walsh-Hadamard codes to form the difference equation which allows them to demodulate the single bit or symbol transmitted by the ST encoder. The orthogonal Walsh-Hadamard codes used in [8] are the first two:

spreading code 0: +1 -1 +1 -1 +1 -1 +1 -1

spreading code 1: +1 +1 +1 +1 +1 +1 +1 +1

For this reason it is logical that the Analog ST coding I scheme deployed in [8] can be compared to the STS-TH-UWB-PPM system described next in Section 8.3. The STS-TH-UWB-PPM Simulink simulator will be validated and compared against the results found in [8] using the same SV channel parameters in Section 8.4.

8.3 STS-TH-UWB-PPM system

A simulator was designed and is described in Chapter 5 and Chapter 6. The parameters used to model the SV channel were the same as described in [8] Section V. These followed the SV channel descriptor, with rays arriving in clusters given by Poisson process cluster arrival rate,

Λ, such that $\frac{1}{\Lambda} = 2$ ns. The rays within each cluster arrived in a Poisson Process with arrival rate λ, such that $\frac{1}{\lambda} = 0.5$ ns. The amplitudes of each of the arriving rays is found from a Rayleigh distributed random variable having exponentially decaying mean squared value with variables Γ and γ such that Γ =33 ns and γ = 5 ns [8]. The pulse width of the Gaussian pulse (which is the second derivative) was also chosen to be 0.7 ns in accordance with [8].

Further, the real part of the multipath signal was taken, and then a search and marking of useful rays were chosen such that they were one nanosecond or more away from the next nearest multipath ray. This then became the channel model. Many such simulations were run and a database of channel instances was compiled for direct use in the Simulink simulator. These values were not, however, modified for using 0, 1 and 2 ns pulse position modulation. This could have been done to improve the performance of the STS-TH-UWB-PPM by avoiding the possibility of a 2 ns shift corresponding to a pulse position in the alternate PPM shift cases that the MRC needs to calculate when detecting / deciding whether a 0 ns, 1ns or 2ns offset in the chip position was sent in any particular chip (a chip being one bit of a spreading sequence).

It should be noted that the decisions in Chapter 6 were based on the chip level data and de-spreading occurred on the hard decision made at the chip level. In these STS simulations, in accordance with the description in [8], an MRC detector is used after all of the symbols pulses are collected. This is done by accumulating the data at the chip level in accumulators according to a calculated receiver matrix which considers the signals that could possibly be transmitted on the two antennas for the given spreading sequence used in the STS encoder. This needs to be calculated on a spreading sequence basis and will change with a different spreading sequence. It, however, only needs to be done during initialisation and a spreadsheet was employed to check the calculations.

The STS encoder produces spread signals on both antennas in a similar way to the Yang's ST Analog coding I system. The difference, however, is that instead of being based on a

spreading sequence per antenna, it is based on the sum and difference of spreading sequences, as described in Chapter 6 and Chapter 7, according to the equations:

$$b_1 c_1[j] + b_2 c_2[j] = \left\{ \begin{matrix} 2 \\ 0 \\ -2 \end{matrix} \right\} \quad for \quad j = 1,...,32 \qquad (8.3\text{-}1)$$

While for the difference stream it is given by:

$$b_2 c_1[j] - b_1 c_2[j] = \left\{ \begin{matrix} 2 \\ 0 \\ -2 \end{matrix} \right\} \quad for \quad j = 1,...,32 \qquad (8.3\text{-}2)$$

Where the individual chips of the spreading sequences are represented by $c_1[j]$ and $c_2[j]$. These are the two Walsh-Hadamard spreading sequences used in Space Time Spreading and j is the counter for the individual chips within that sequence which here is a integer in the range {1,2,..,32}. The symbols b_1 and b_2 in Equation 8.3-1 and Equation 8.3-2 represent the two binary bits in {-1,+1} coding to be transmitted across the UWB channel. The chip level data on each antenna is then '-2', '0', or '2'. These can be represented by 0ns, 1ns and 2ns shifts respectively in a PPM UWB system. Also, Equation 8.3-1 and Equation 8.3-2 show that the two binary bits to be sent are coded into both the 0^{th} and 1^{st} antenna stream which provides the two fold diversity of STS when using two transmit antennas [9].

The STS-TH-UWB-PPM simulation assumes that each antennas channel or branch is uncorrelated. To model this a different set of channel multipath gains were generated for each antenna and embedded in the simulator. This also means that one channel's multipath could interfere with another, however the decision vector formed at the MRC models all possible combinations of the two channels without the addition of noise making the decision based on an Optimal detector [2;4] when Gaussian noise was added.

A fixed Time Hopping pattern of :

[6 0 5 3 6 4 5 3]

was used throughout all simulations. Each slot was made up of eight one hundred nano second frames and when the time hopping pattern was completed, it was restarted again.

Statistics were only calculated when an active slot was encountered. At all other times the channel was silent as described in Chapter 6.

8.4 Simulation of Yang's Analog ST coding I

The STS-TH-UWB-PPM system described in Section 8.3 was modified by changing the STS encoder to an encoder formed from Equation 8.2-1 and Equation 8.2-2. The STS encoder provides pulse positions for -2, 0, and 2. The modification involved changing the STS coder section to a ST coder that provided only pulse positions -2 and 0, which then represented -1 and +1 for the values of 's' in Equation 8.2-1 and Equation 8.2-2. The MRC detector array was also modified so that only the terms which contributed to the decision were included in the detector module. Thus, apart from modifications in the ST encoder and MRC detector modules the implementation of Yang's Analog ST coding scheme I used the STS-TH-UWB-PPM simulator described in Section 8.3.

The other difference in this simulation is that Yang and Giannakis [8] did not include a time hopping pattern, whereas this is already built into the STS-TH-UWB-PPM simulator so it was also included in the implementation of Yang's Analog ST coding I scheme. This should not have a significant impact on the results as the fixed time hopping pattern is only used in deciding when to measure the statistical data in the simulator and allow for experiments with more than one user into future research as well as smoothing the spectra.

The Simulation of Yang's Analog ST coding I system in Simulink was run for different expected SNR (Signal to Noise Ratio) using three different seed values. An estimate of the corresponding data set (from Figure 7 and Figure 8 of [8]) was plotted versus the data with 95% confidence intervals included. The data from our study was normalised for comparison purposes. Figure 8.4-1 shows the results for L=1 and L=4 for a Partial Rake system. This uses the first L useful rays to form the template in the MRC detector. The tabulated data with 95% confidence intervals is provided in Appendix 13.

Figure 8.4-1 shows similar results for low expected SNR, with our Simulink simulations BER results for the Yang Analog ST coding I schema. For higher expected SNR our simulation

produced lower BER results. The actual simulator data used in [8] for the channel model was unavailable to the author of this thesis, so this study could only use the statistical parameters provided in [8] to generate its own channel model data set. One possible explanation is that for the study in [8] their multipath was richer than that used in this thesis studies simulations as this thesis studies simulated channels multipath were constrained with the maximum number of multipath for any single channel instance to 200 multipath gains (truncating if more were produced).

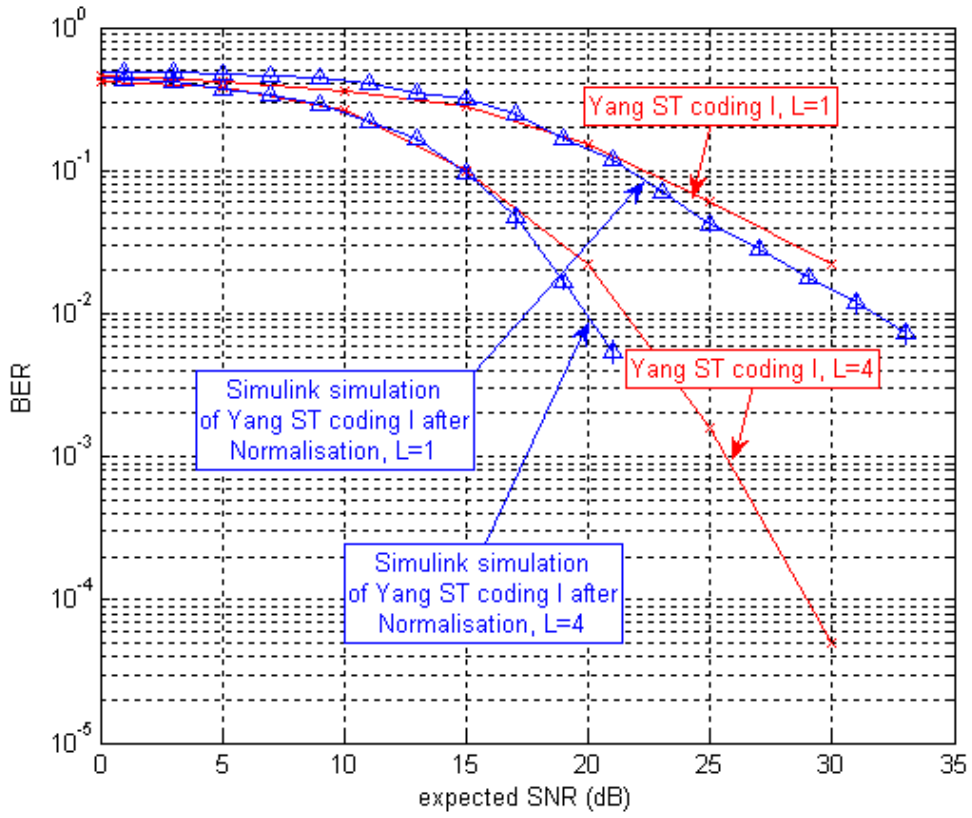

Figure 8.4-1: Yang et al. results from [8] compared to Simulink implementation of [8] 's Analog ST coding I schema with Simulink simulation normalised.

8.5 Comparison with STS system

The Yang et al Analog ST coding type I system [8] (incorporating Time Hopping) was then simulated and the BER versus Eb/No (dB) was measured using the Simulink Simulator. This was then compared to the STS-TH-UWB-PPM proposed system. This was done for L=1,4 and for Partial and Selective Rake detection schemes. Partial rake used the first L useful rays in the template and Selective Rake used the L highest energy useful rays in the template.

Figure 8.5-1 shows the results for the Partial Rake comparison and Figure 8.5-2 shows the results for Selective Rake comparison. It should be noted that the results reported in [8] were only using Partial Rake from our discussion in Section 8.4.

Examining Figure 8.5-1 and Figure 8.5-2 it can be seen that the performance of STS-TH-UWB-PPM was comparable to that found for the Simulink simulation of Yang's Analog ST coding I system. However, it should be noted that the STS system transmits two binary bits within a symbol period whereas Yang's ST coding I system only transmits one binary bit. The tabulated data for the Simulink simulation of Yang's ST coding I systems in terms of measured Eb/No is provided in Appendix 14. That for the developed STS based system is provided in Appendix 15 and Appendix 16.

If one considers the individual transmitting antenna branches of the STS and Yang Analog ST coding I system, the STS system has encoded the two bits to be transmitted (this is the case in both antenna branches) whereas Yang's equivalent technique only has one. If this is considered then the results in Figure 8.5-3 and Figure 8.5-4 are applicable where a significant improvement per antenna can be seen (see Appendix 16).

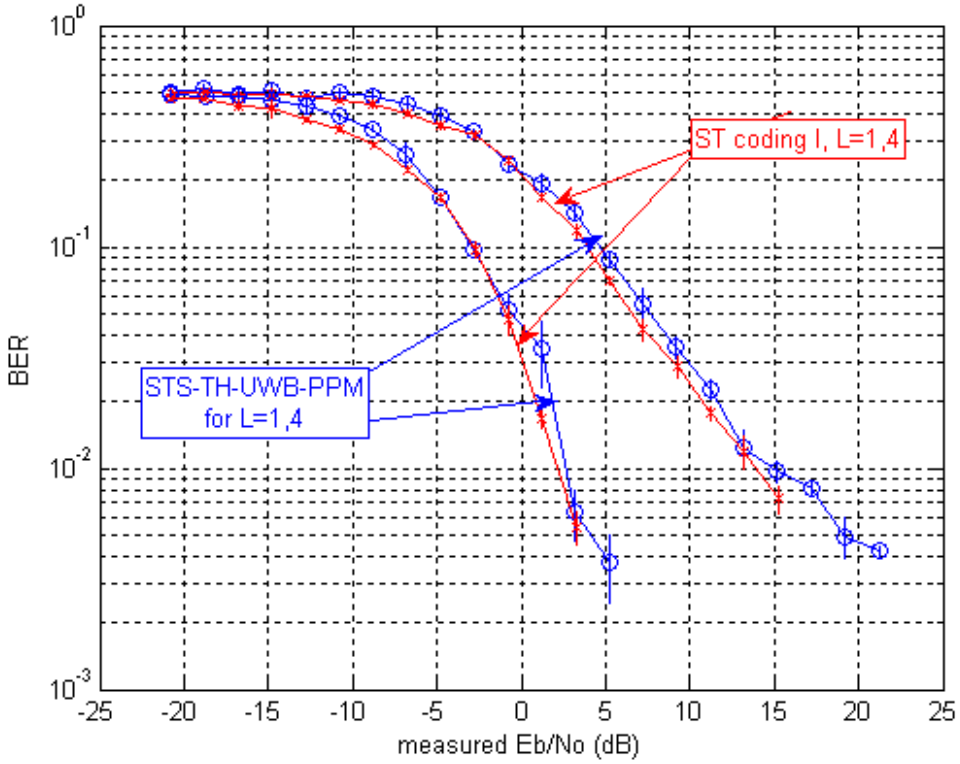

Figure 8.5-1: Simulation of Analog ST coding I and STS-TH-UWB-PPM proposed system for Partial Rake L=1,4.

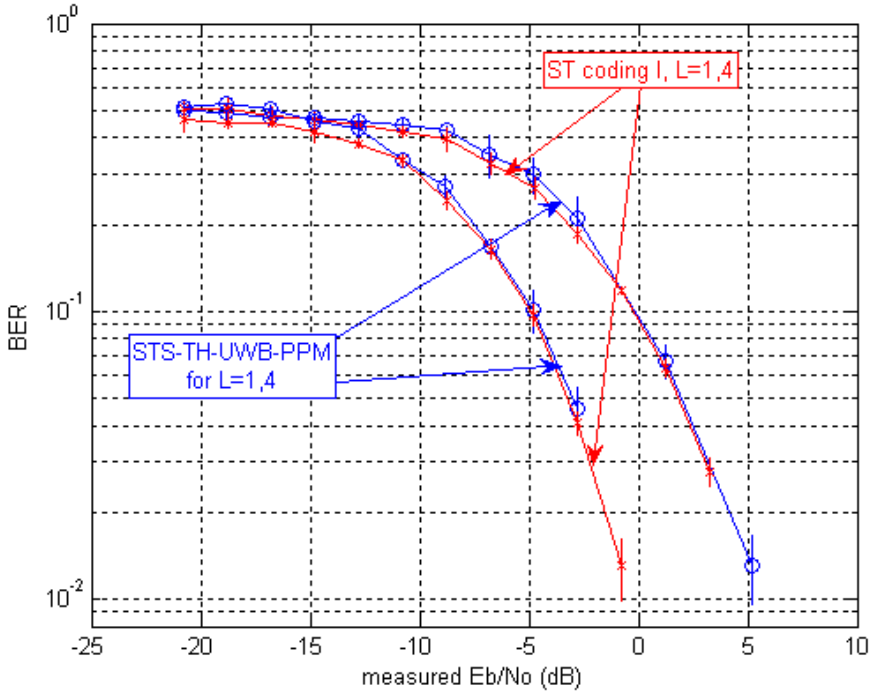

Figure 8.5-2: Simulation of Analog ST coding I and STS-TH-UWB-PPM proposed system for Selective Rake L=1,4.

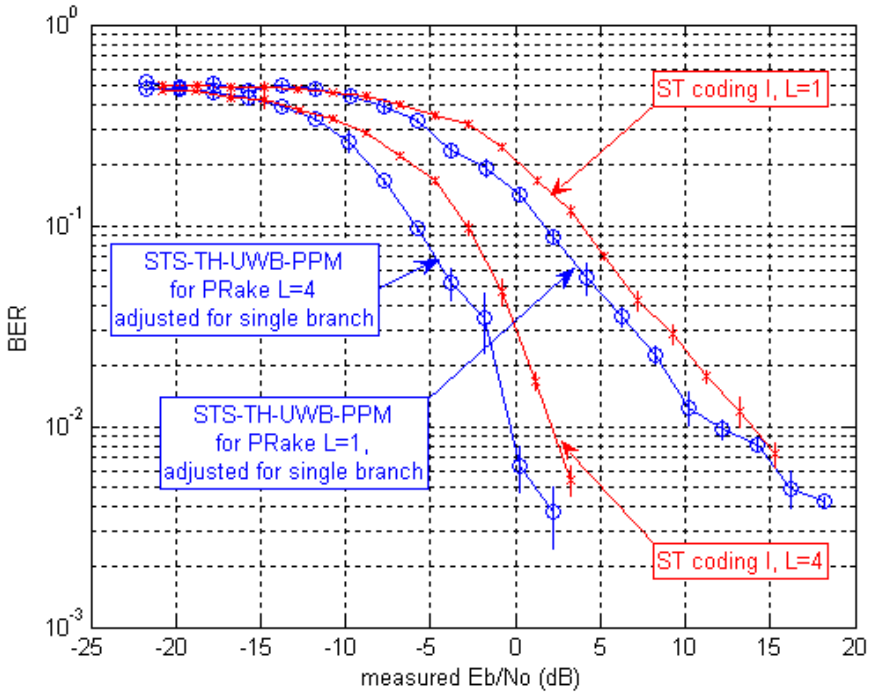

Figure 8.5-3: Simulation of Analog ST coding I and STS-TH-UWB-PPM per antenna branch proposed system for Partial Rake L=1,4.

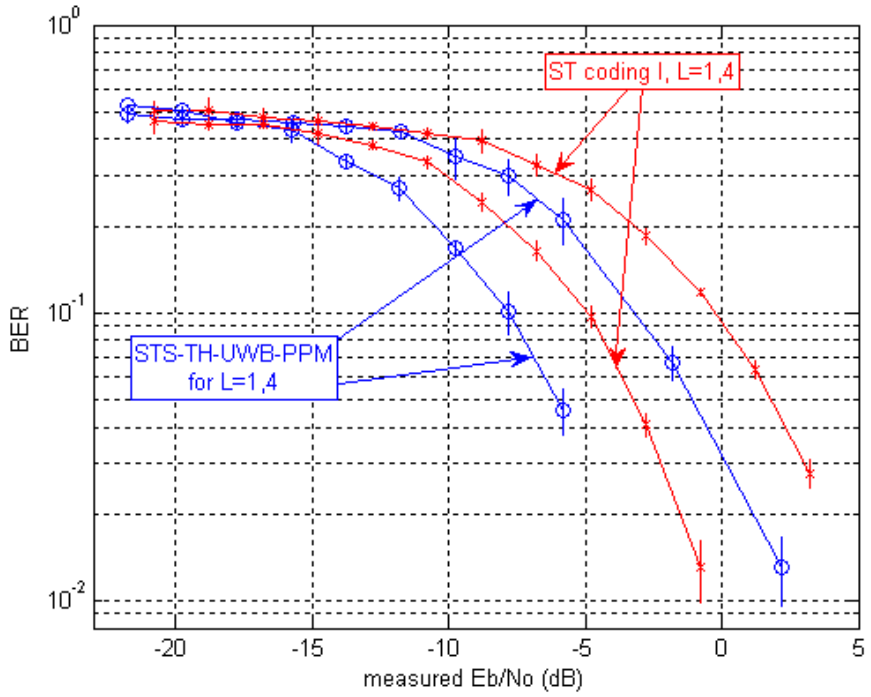

Figure 8.5-4: Simulation of Analog ST coding I and STS-TH-UWB-PPM per antenna branch proposed system for Selective Rake L=1,4.

8.6 Conclusion

This chapter proposed a novel technique to allow transmission of two binary bits using two transmit antennas called STS-TH-UWB-PPM. It has the advantage that the binary bits are available on both antenna signals and requires two spreading sequences to transmit two binary bits. This compares to Yang's Analog ST coding I schema which uses two spreading codes (and only one set allowed) to transmit one binary bit. This proposed system has comparable or significantly better performance to the Analog ST coding I schema described in [8]. It uses multiple pairs of spreading codes to the single pair of spreading codes provided in Yang's Analog ST coding I schema.

This chapter proposed and investigated, through simulation, a system which shows how a UWB PPM system that uses TH and spreading codes can utilise the STS technique and allow the effective use of two transmit antennas (MIMO). It shows a system which transmits two symbols in the same time period that an equivalent SISO system transmits one symbol. In fact, in the case of Yang's Analog ST coding I schema they were using two spreading codes (albeit without, apparently realising it) to transmit a single symbol. The system proposed in this chapter is able to transmit two symbols at the cost of two spreading codes (that is, spreading codes are used efficiently). This is important because the number of available spreading codes (that are orthogonal) is limited to the total size of the spreading code (in chips). In most systems some of these spreading codes will be required for overheads such as estimating the channel coefficients using pilot signals.

It is known that systems that use orthogonal spreading codes that are synchronised with each other will experience a poorer BER performance when other spreading codes are present which are out of phase or unsynchronised. This effect is known as MAI. Chapter 4 investigates the effect of such interference on STS systems. The next chapter investigates the effect of MAI for one, five and ten interferers using Walsh Hadamard spreading codes on the proposed MIMO STS UWB PPM TH system. It also investigates the use of other low correlation codes and their effect in the presence of MAI on the proposed system.

Chapter 9: MAI in STS-TH-UWB-PPM systems

9.1 Introduction

Chapter 8 showed that the resultant BER of the proposed STS over TH UWB PPM system is comparable to that obtained for a Yang Analog ST coding type I scheme [8]. If the system is compared on a per antenna branch basis it was shown that a 3dB improvement is possible over the corresponding Yang ST coding type I scheme which can transmit only one binary bit compared to the two that Space Time Spreading sends per branch when two transmit antennas are employed. It was shown how multiple antennas may be employed in a Space Time Spreading Time Hopping Ultra Wideband Pulse Position Modulation system to achieve the transmission of multiple binary bits in one transmission period. This chapter considers the situation which has multiple STS over TH over UWB PPM systems all offset by random delays from each other in time resulting in multiple access interference. It investigates the degradation that occurs in this situation in terms of BER. It is noted that this situation represents the worse possible case as the interfering sources have the same energy and are aligned within -50ns to +50ns of each other, which is not likely to occur in a realistic implementation (if an implementation were possible with improvements in UWB PPM electronic wireless device production processes). It is found that the system suffers some degradation when this worse case situation is simulated.

This chapter then considers five sets of orthogonal thirty two chip spreading codes. One is the Walsh Hadamard codes used in Chapter 8 to validate the simulations against Yangs ST coder type I [8], and three of the other four are low cross correlation codes. One of these low correlation codes was first proposed in [61], which this thesis refers to as Wysocki codes, and which were used in the study described in Chapter 4. It is found that these spreading codes perform at varying levels of average BER performance when compared to that found when using the Walsh-Hadamard spreading sequence codes or sets. The worse performing code is not the Walsh Hadamard spreading code set but a randomly chosen spreading code set used

to generate another low correlation spreading code set which is also included in this study. A moderate improvement in average BER performance is found when using the Wysocki low correlation spreading code set which was employed in the study described in Chapter 4. The other two low correlation spreading code sets investigated showed a similar or slightly improved BER performance when compared to the BER performance found using the Walsh-Hadamard spreading sequence code set. This chapter concludes by considering the implications of the BER performance of the different spreading sequence sets when MAI is encountered in the proposed STS-TH-UWB-PPM system.

Section 9.2 describes what modifications needed to be made to the system described in Section 8.3 and what alternate Time Hopping vectors were applied. Section 9.3 outlines the experiment which imparts multiple access interference to the desired signal. Section 9.4 reports the results of using the Walsh Hadamard orthogonal codes for different energy subsets using Partial Rake with multipath values (L) chosen as 1 and 4. Section 9.5 reports the result using the lower cross correlation codes proposed in [61], and compares these to results reported in Section 9.4. Finally, Section 9.6 is the conclusion.

9.2 Modifications to STS-TH-UWB-PPM system

The system used was as described in Section 8.3 of Chapter 8. When the low correlation spreading sequence codes are used in Section 9.5 a new decoder needed to be designed for each new pair of spreading codes used in the MAI experiments. This, however, only needs to be done during initialisation and a spreadsheet was employed to check the calculations in all cases.

A fixed Time Hopping pattern of :

[6 0 5 3 6 4 5 3]

was used throughout all the validation simulations with no MAI present as described in Section 8.4. The results of this were presented in Section 8.4 which showed a close agreement between the Simulink simulation and the results for the corresponding system

reported in [8] for Yang's Analog ST coding I scheme. For the MAI simulations the fixed Time Hopping Pattern was slightly modified to:

[6 4 5 3 6 4 5 3]

A different Time Hopping pattern was deployed for the MAI sources offset by a delay chosen from independent uniform time distributions over -50ns to +50ns for each STS source. The Time Hopping Pattern for the MAI experiments for all MAI was fixed at:

[5 3 4 2 5 3 4 2]

This was chosen because it ensured that the MAI sources were delayed by a random offset in time between -50ns and +50ns with the desired STS transmission ensuring that MAI would be experienced by the desired STS source when it was de-spread and a hard decision was made on the two binary bits transmitted in the desired STS transmission period (ie two data bits are transmitted in one STS symbol time period). Each slot was made up of eight one hundred nano second frames and when the time hopping pattern was completed, it was restarted again. Statistics were only calculated when an active slot was encountered. At all other times the channel was silent as described in Chapter 6.

9.3 MAI in STS-TH-UWB-PPM system

The STS-TH-UWB-PPM system described in Section 8.3 was modified to include multiple STS-TH-UWB-PPM systems. The addition of multiple STS-TH-UWB-PPM systems were offset by a random delay in the range -50ns to +50ns, using the fixed Time Hopping pattern:

[5 3 4 2 5 3 4 2]

for each of the STS-TH-UWB-PPM systems that interfered with the desired STS-TH-UWB-PPM. The channel multipaths were chosen from the same set of channel multipaths used for the desired STS-TH-UWB-PPM for antenna 0 and antenna 1 but using different random number sources to select the particular instance of a channel multipath. This made it unlikely that the same channel multipath is chosen for any one of the MAI STS-TH-UWB-PPM systems. Even if one of these MAI STS-TH-UWB-PPM channel multipaths were the same as the desired STS-TH-UWB-PPM, it would be offset in time in all cases except in the unlikely situation that the delay randomly chosen was zero. To have included independent channel sets for each STS-TH-UWB-PPM antenna would have resulted in simulation executables that

were impractical in storage size (using this situation the executable for each system implementation was 32Mbytes) and the variation found in the results of Section 9.4 and Section 9.5 (see Appendix 25 for error bar plots) indicate that this was not required.

The simulations were then setup for the same seed value for the case where there were one MAI, five MAI and ten MAI. These results are presented in Section 9.4 and Section 9.5. As each STS-TH-UWB-PPM requires two spreading codes and the Walsh Hadamard and alternate low correlation orthogonal code sets used were thirty two chips in length, for a system with ten MAI STS-TH-UWB-PPM and the desired STS-TH-UWB-PPM it requires twenty two of the thirty two spreading codes available. A practical implementation will require spreading codes used as pilot channels to estimate the channel coefficients (which in our simulation are perfectly known). It was thought that for a thirty two chip length orthogonal code set that it is unlikely that more than eleven STS-TH-UWB-PPM sources could be deployed which would be aligned with similar Time Hopping patterns.

9.4 MAI in STS-TH-UWB-PPM results using Walsh-Hadamard codes

The STS-TH-UWB-PPM system was setup as described in Section 9.3. For the initial tests it used one desired STS-TH-UWB-PPM system (as described in Section 8.3) and one MAI STS-TH-UWB-PPM system as described in Section 9.3. Only one seed value was used for these experiments (this investigation did not include any 95% confidence intervals for the one MAI systems). It also used the same seed value for the STS-TH-UWB-PPM system described in Section 8.3 for direct comparison. The single MAI interferer was setup with a measured Eb/No of -26.3dB, -16.3dB, -6.3dB and +3.15dB. The number of paths used for these simulations was L=1. The results are shown in Figure 9.4-1 through Figure 9.4-4. Examining the results shown in these four figures, it appears that one MAI STS-TH-UWB-PPM has minimal to no effect on the desired MAI STS-TH-UWB-PPM except for a small improvement in BER for low Eb/No (dB). This improvement does not appear to be a function of the Eb/No of the interfering MAI STS-TH-UWB-PPM source.

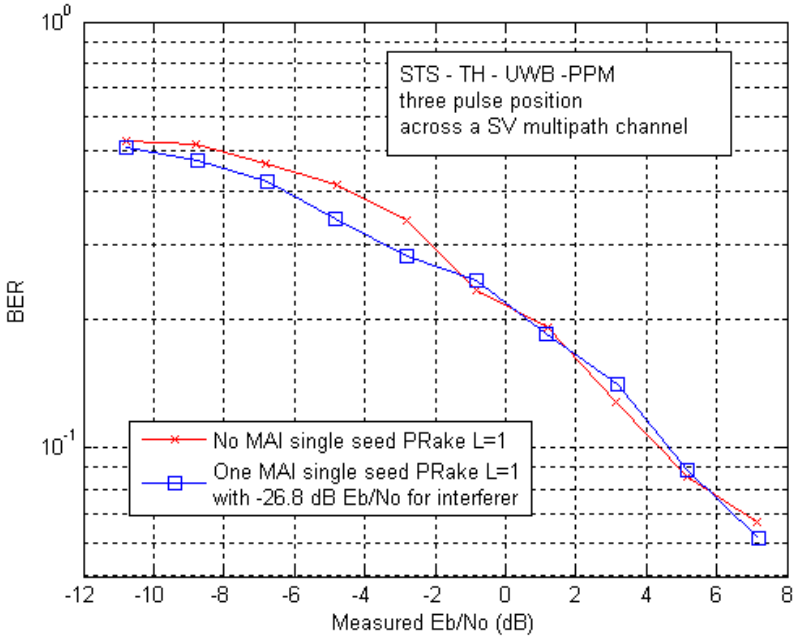

Figure 9.4-1: Shows the effect of one MAI interferer offset by randomly varied time to desired STS-TH-UWB-PPM system for L=1 when interferer has E_b/N_o of -26.8dB, using the same seed set value for the channel and noise sources.

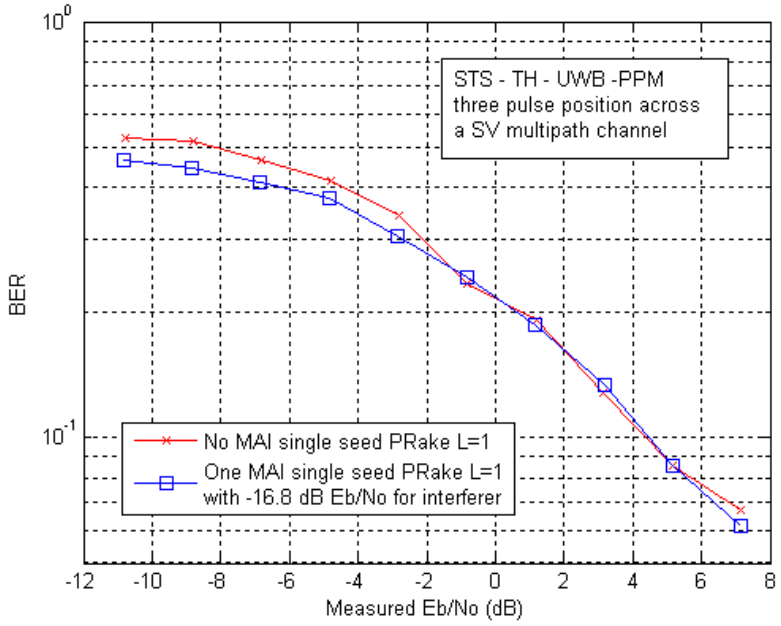

Figure 9.4-2: Shows the effect of one MAI interferer offset by randomly varied time to desired STS-TH-UWB-PPM system for L=1 when interferer has E_b/N_o of -16.8dB, using the same seed set value for the channel and noise sources.

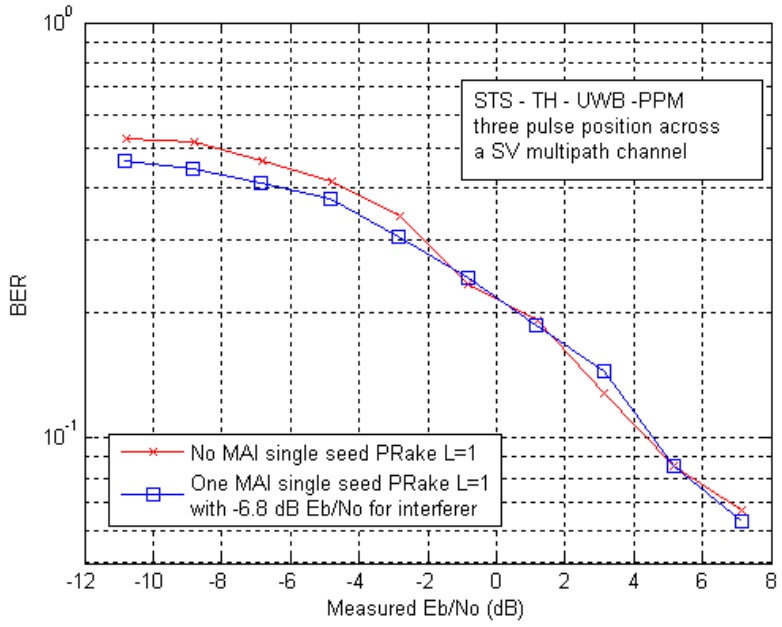

Figure 9.4-3: Shows the effect of one MAI interferer offset by randomly varied time to desired STS-TH-UWB-PPM system for L=1 when interferer has E_b/N_o of -6.8dB, using the same seed set value for the channel and noise sources.

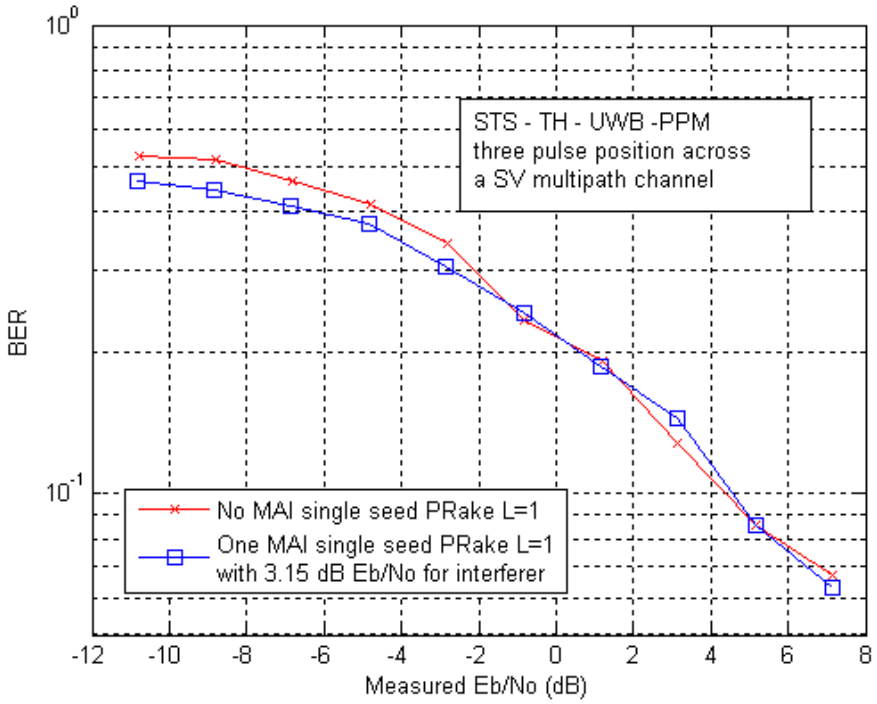

Figure 9.4-4: Shows the effect of one MAI interferer offset by randomly varied time to desired STS-TH-UWB-PPM system for L=1 when interferer has E_b/N_o of +3.15dB using the same seed set value for the channel and noise sources.

The simulator was modified so that five MAI STS-TH-UWB-PPM systems interfered with the desired STS-TH-UWB-PPM system using random delays chosen from a uniform distribution with shifts between -50ns and +50ns. The five MAI interferers were setup all with a measured Eb/No of -26.3dB, -16.3dB, -6.3dB and +3.15dB. Values were also used for the multipath of L=1 and L=4. The results are shown in Figure 9.4-5 through Figure 9.4-8. It is clear that for the first three MAI interferer energy levels, other than for the improvement in BER for low energy levels of MAI, that there is no effect on the desired STS-TH-UWB-PPM system compared to when no MAI sources are present. However, when the measured Eb/No of the MAI sources is increased to +3.15dB, a significant increase in BER is experienced by the desired STS-TH-UWB-PPM system indicating that MAI has resulted in a degradation of its performance.

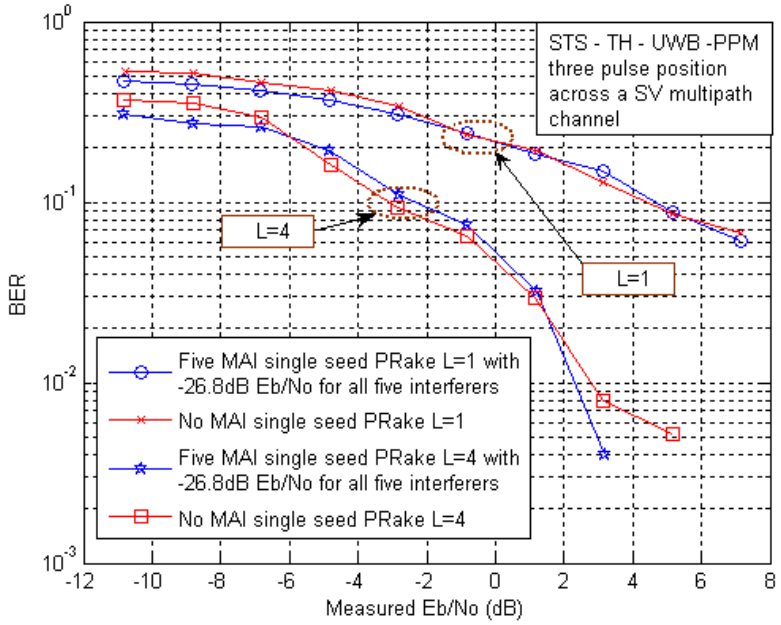

Figure 9.4-5: Shows the effect of five MAI interferers offset by randomly varied time to desired STS-TH-UWB-PPM system for L=1 and L=4 when all interferers have E_b/N_o of -26.8dB using the same seed set value for the channel and noise sources.

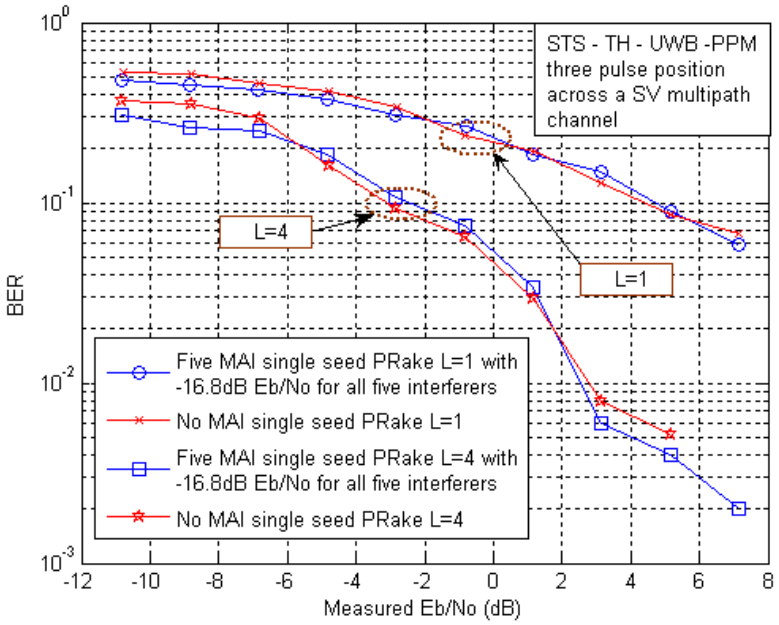

Figure 9.4-6: Shows the effect of five MAI interferers offset by randomly varied time to desired STS-TH-UWB-PPM system for L=1 and L=4 when all interferers have E_b/N_o of -16.8dB using the same seed set value for the channel and noise sources.

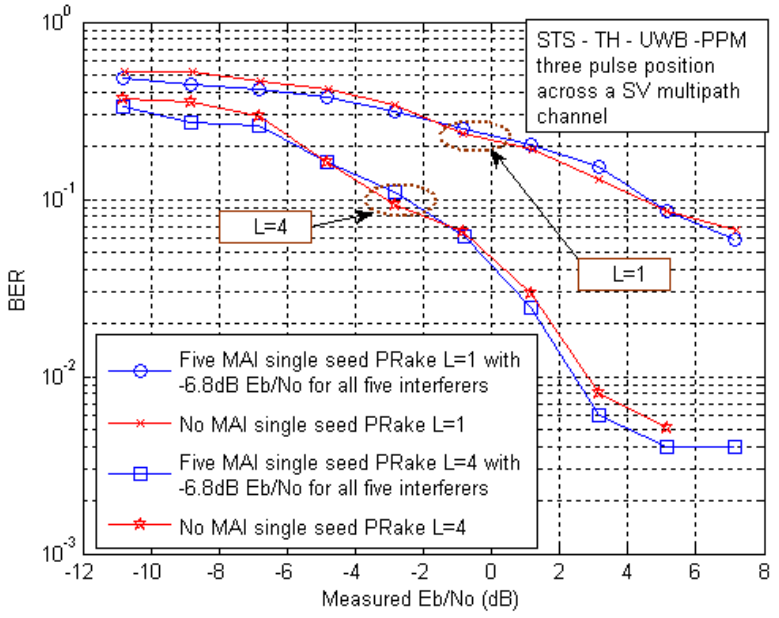

Figure 9.4-7: Shows the effect of five MAI interferers offset by randomly varied time to desired STS-TH-UWB-PPM system for L=1 and L=4 when all interferers have E_b/N_o of -6.8dB using the same seed set value for the channel and noise sources.

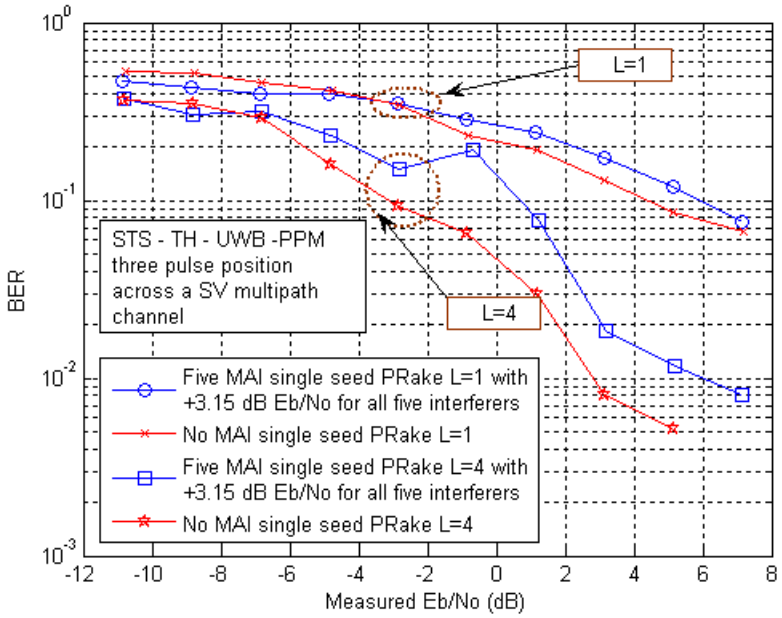

Figure 9.4-8: Shows the effect of five MAI interferers offset by randomly varied time to desired STS-TH-UWB-PPM system for L=1 and L=4 when all interferers have E_b/N_o of +3.15dB using the same seed set value for the channel and noise sources.

The simulator was then modified so that there were now ten MAI STS-TH-UWB-PPM sources interfering with the desired STS-TH-UWB-PPM system. In all other respects the experiment was equivalent to the five MAI experiment. Figure 9.4-9 through Figure 9.4-12 shows the results on a semilog plot. For the cases where Eb/No was -26.3dB and -16.3dB there was no significant deviation from results for the situation where there were no MAI STS-TH-UWB-PPM sources present. For the case where Eb/No was -6.8dB there was a slight increase in the BER for higher Eb/No for the desired STS-TH-UWB-PPM source. For the case where Eb/No was +3.15dB there was a very significant degradation in the BER performance of both the L=1 and L=4 systems. This strongly indicates that when the Eb/No is +3.15dB that MAI from ten sources causes a significant degradation in the STS-TH-UWB-PPM system.

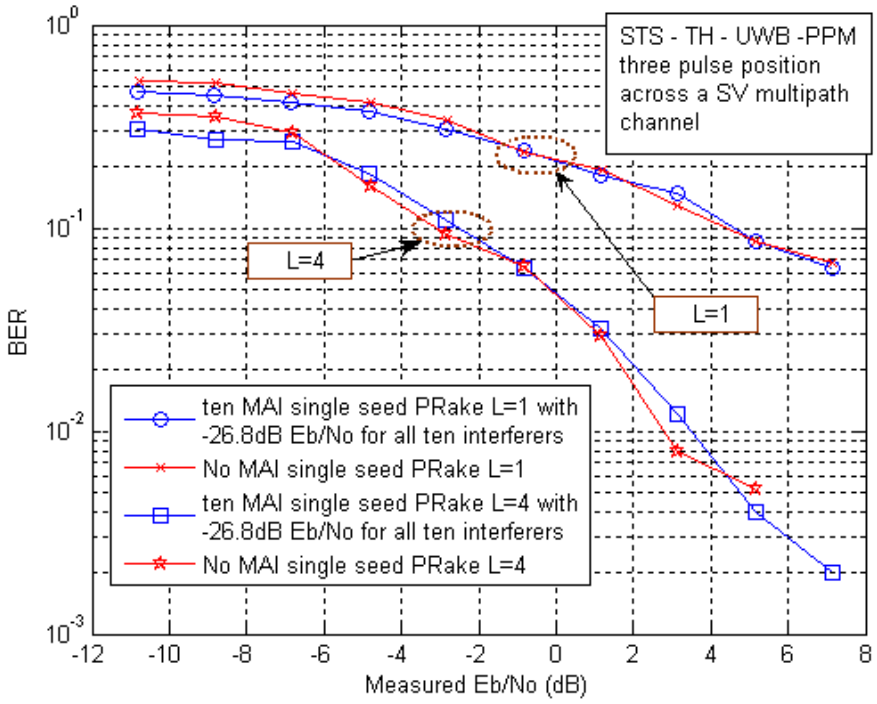

Figure 9.4-9: Shows the effect of ten MAI interferers offset by randomly varied time to desired STS-TH-UWB-PPM system for L=1 and L=4 when all interferers have E_b/N_o of -26.8dB using the same seed set value for the channel and noise sources.

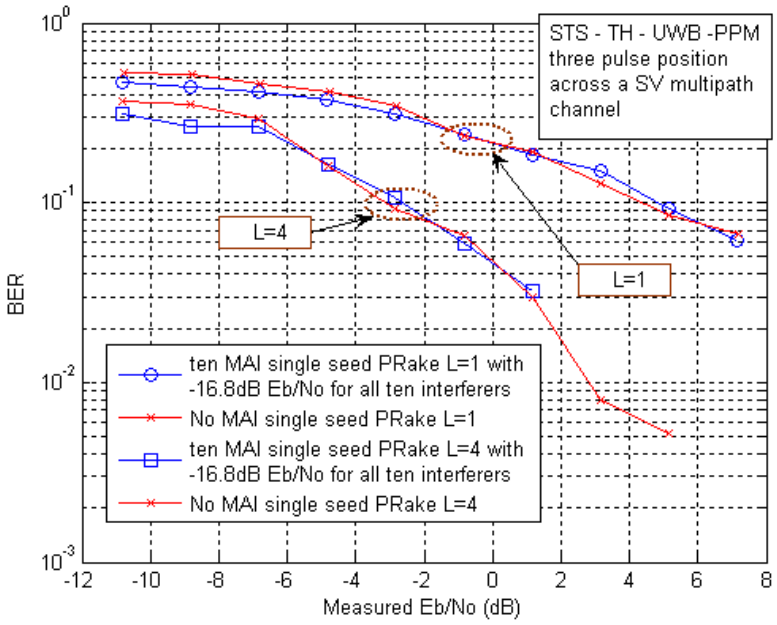

Figure 9.4-10: Shows the effect of ten MAI interferers offset by randomly varied time to desired STS-TH-UWB-PPM system for L=1 and L=4 when all interferers have E_b/N_o of -16.8dB using the same seed set value for the channel and noise sources.

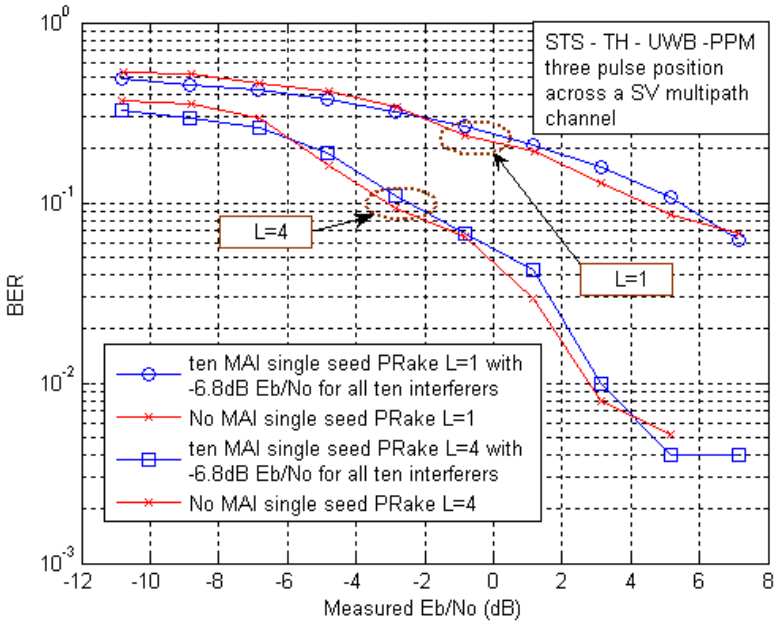

Figure 9.4-11: Shows the effect of ten MAI interferers offset by randomly varied time to desired STS-TH-UWB-PPM system for L=1 and L=4 when all interferers have E_b/N_o of -6.8dB using the same seed set value for the channel and noise sources.

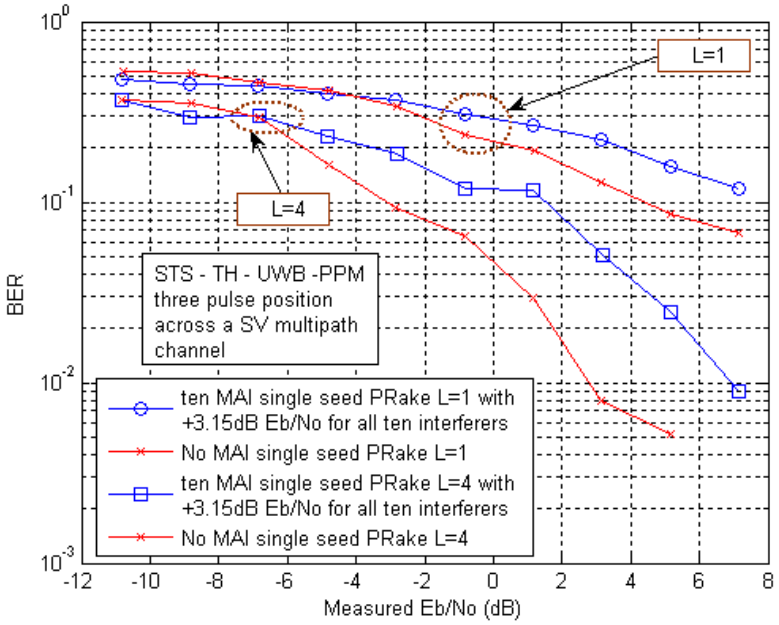

Figure 9.4-12: Shows the effect of ten MAI interferers offset by randomly varied time to desired STS-TH-UWB-PPM system for L=1 and L=4 when all interferers have E_b/N_o of +3.15dB using the same seed set value for the channel and noise sources.

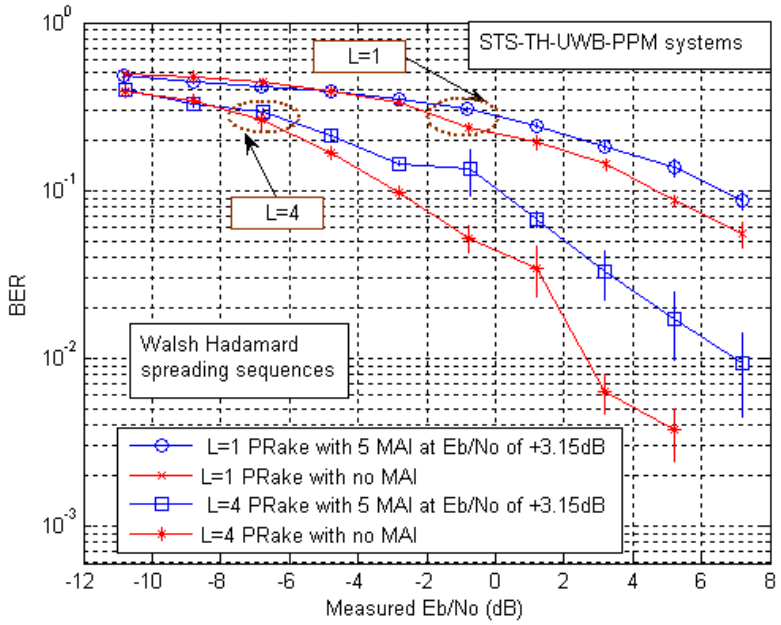

Figure 9.4-13: Shows the effect of five MAI interferers offset by randomly varied time to desired STS-TH-UWB-PPM system for L=1 and L=4 when all interferers have E_b/N_o of +3.15dB with 95% confidence intervals.

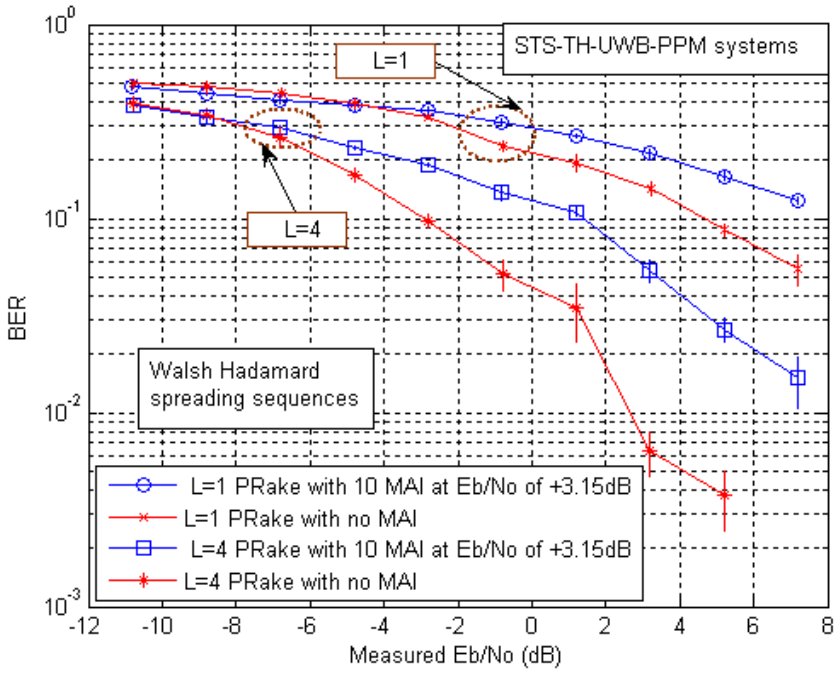

Figure 9.4-14: Shows the effect of ten MAI interferers offset by randomly varied time to desired STS-TH-UWB-PPM system for L=1 and L=4 when all interferers have E_b/N_o of +3.15dB with 95% confidence intervals.

As a result of the measurements for a single seed when E_b/N_o of all the five and ten MAI STS-TH-UWB-PPM interferers was kept constant at +3.15dB, extra seed values were used to form 95% confidence intervals. Figure 9.4-13 shows the results when multipath of L=1 and L=4 are deployed compared to the situation where no MAI is present and E_b/N_o of the five interferers is kept constant at +3.15dB. Figure 9.4-14 shows the results when multipath of L=1 and L=4 are deployed compared to the situation where no MAI is present and E_b/N_o of the ten interferers is kept constant at +3.15dB. The tabulated data is provided in Appendix 17. From these results it can be seen that significant degradation in BER performance is, on average, experienced by the desired STS-TH-UWB-PPM system when five and ten MAI STS-TH-UWB-PPM sources are present. As expected this degradation is more pronounced when ten MAI STS-TH-UWB-PPM are encountered compared to that which is experienced when five MAI STS-TH-UWB-PPM sources are present.

9.5 MAI using low correlation sequences

In [61] they define three measures of correlation. They indicate in [61] that Opperman and Vucetic [65] provided a mathematical expression of the average mean square value of the cross-correlation of all M sequences used in a spreading sequence set of length N as R_{CC} which was defined in [61] as (where $M \leq N$):

$$R_{CC} = \frac{1}{M(M-1)} \sum_{i=1}^{M} \sum_{\substack{k=1 \\ k \neq i}}^{M} \sum_{\tau=1-N}^{N-1} \left| c_{i,k}(\tau) \right|^2$$

(9.5-1)

Where $c_{i,k}(\tau)$ is the discrete aperiodic correlation function which they define (in [61] Equation 11). In [61] they also indicate that a similar measure, also provided by Opperman and Vucetic [65] , for comparing autocorrelation performance can be used which was defined as [61]:

$$R_{AC} = \frac{1}{M} \sum_{i=1}^{M} \sum_{\substack{\tau=1-N \\ \tau \neq 0}}^{N-1} \left| c_{i,i}(\tau) \right|^2$$

(9.5-2)

Wysocki and Wysocki [61] further indicate that, for systems based on DS CDMA, these parameters should be as low as possible and they proceed to use these as optimisation criteria for new spreading sequence sets such as the Wysocki sequences presented in [61] and the

w32dash03 and orthogonal gold spreading sequences presented in [66]. The other criteria applied is the maximum value of the aperiodic cross-correlation functions, denoted C_{max}, as they argue that this is a parameter indicative of the worse case performance of the spreading sequence when DS CDMA is considered. This chapter is interested, for this study, in applying the codes found in [61] and subsequently in [66] for the situation comprised of multiple users who are not synchronised, causing MAI when using STS-TH-UWB-PPM physical layer transmission systems.

From [61] and [66] is found the following properties for the various spreading code sequence sets used in this study. For the Walsh Hadamard spreading sequence set of length N=32 its parameters measured in [61] are:

$$C_{max}=0.9688$$

$$R_{AC}=6.5938$$

$$R_{CC}=0.7873$$

For the Wysocki spreading sequence set [61]:

$$C_{max}=0.4063$$

$$R_{AC}=0.8925$$

$$R_{CC}=0.9738$$

For the w32dash03 spreading sequence set [66]:

$$C_{max}=0.3750$$

$$R_{AC}=0.9682$$

$$R_{CC}=0.9844$$

For the Orthogonal Gold spreading sequence set [66]:

$$C_{max}=0.3750$$

$$R_{AC}=0.9675$$

$$R_{CC}=1.0078$$

The spreading sequence set h32dash03 was derived from the Hall difference set as reported in [66] and is used as a control to contrast against the other four sequence sets employed in this study.

All five spreading sequence sets were simulated and tested in the presence of no noise and no MAI with 1000 symbols transmitted in the simulations with zero errors generated. Then three different seed set values were used with the same set of pairings used for all spreading sequence code sets. The codes c1 and c2, as shown in Appendix 17 through Appendix 21, were used in all experiments as the target spreading codes for the target STS-TH-UWB-PPM system. All the other pairings, forming the MAI, were also kept constant and not varied between spreading code sequence sets. That is, the indexes into the array of spreading sequences of the individual spreading sequence sets were left unchanged as indicated by re-use of the label pairs {c3,c4}, {c5,c6}, …, {c21,c22} as found in Appendix 17 through Appendix 21.

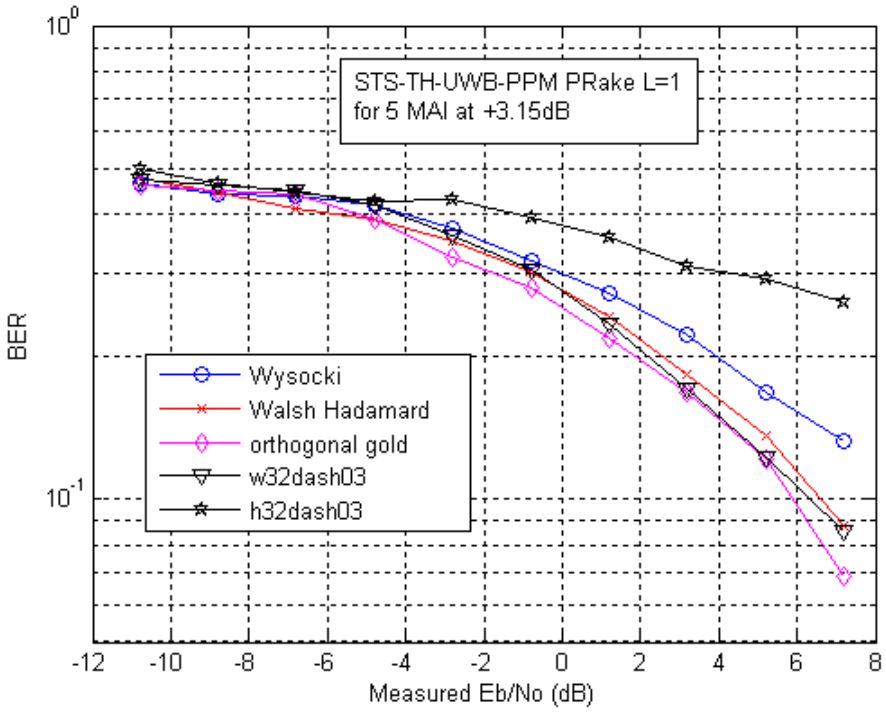

Figure 9.5-1: Comparison of performance of wysocki codes, orthogonal gold codes, w32dash03 codes, h32dash03 codes versus Walsh Hadamard codes in the presence of five MAI interferers at +3.15dB for L=1 of mean BER versus Measured E_b/N_o (dB).

These other four spreading code sequence sets were used to replace the Walsh Hadamard sequences used in the previous sections, Section 9.2 through to Section 9.4. This was done for each spreading code sequence set for the situation where the MAI STS-TH-UWB-PPM interferers had an Eb/No of +3.15dB. It was simulated for the cases where it had five and ten MAI STS-TH-UWB-PPM asynchronous interfering sources. The decoder was modified for each of the new spreading sequences, as the new desired STS-TH-UWB-PPM spreading sequences used different spreading code pairs (since they were different spreading sequence sets).

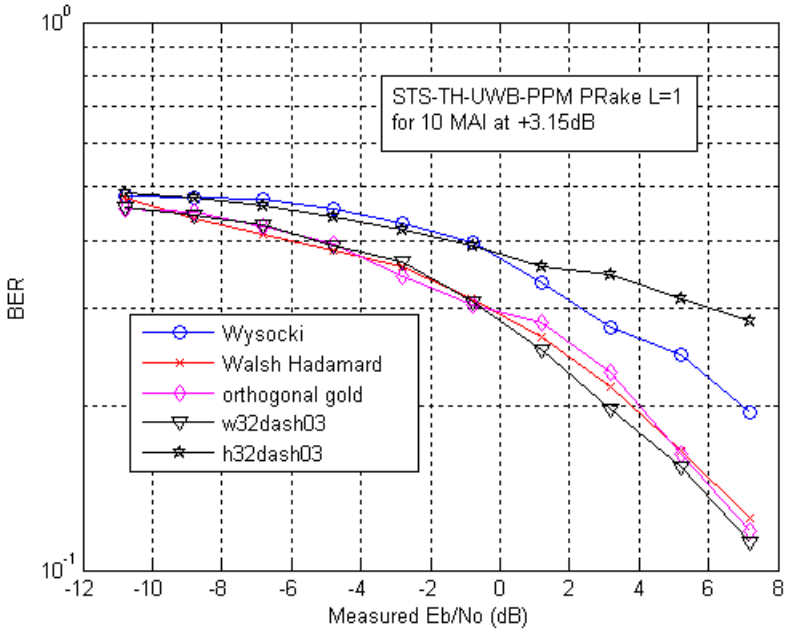

Figure 9.5-2: Comparison of performance of wysocki codes, orthogonal gold codes, w32dash03 codes, h32dash03 codes versus Walsh Hadamard codes in the presence of ten MAI interferers at +3.15dB for L=1 of mean BER versus Measured E_b/N_o (dB).

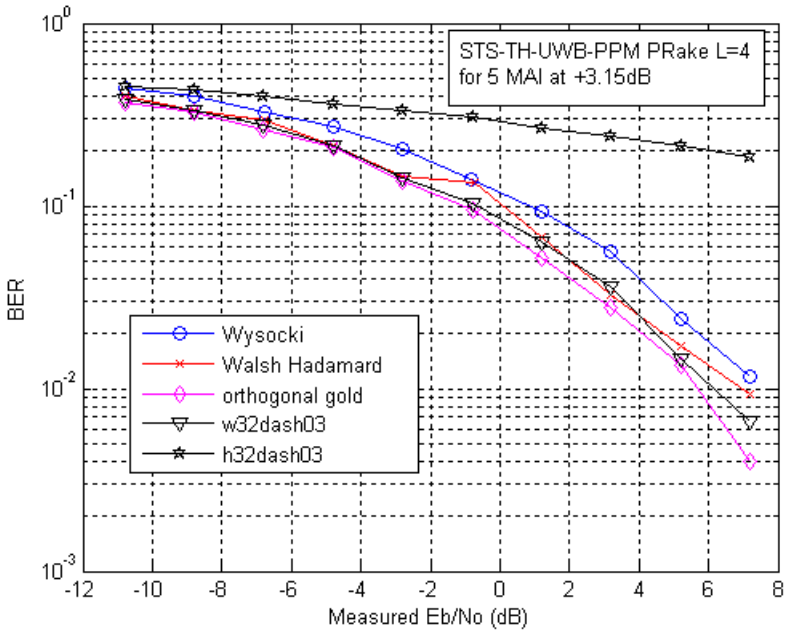

Figure 9.5-3: Comparison of performance of wysocki codes, orthogonal gold codes, w32dash03 codes, h32dash03 codes versus Walsh Hadamard codes in the presence of five MAI interferers at +3.15dB for L=4 of mean BER versus Measured E_b/N_o (dB).

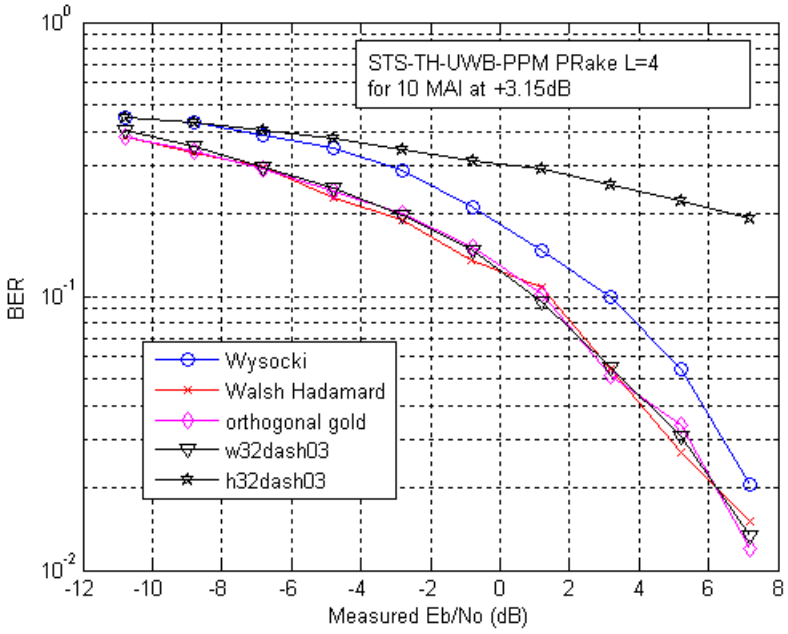

Figure 9.5-4: Comparison of performance of wysocki codes, orthogonal gold codes, w32dash03 codes, h32dash03 codes versus Walsh Hadamard codes in the presence of ten MAI interferers at +3.15dB for L=4 of mean BER versus Measured E_b/N_o (dB).

The results for Partial Rake systems with L=1, 4 in the presence of five and ten MAI sources with measured E_b/N_o of +3.15dB are shown in Figure 9.5-1, Figure 9.5-2, Figure 9.5-3, and Figure 9.5-4 and tabulated values are provided in Appendix 18. Considering the data collected in this study, it is noted that the randomly selected spreading sequence set labelled as h32dash03 shows the poorest BER performance as measured E_b/N_o (in dB) is increased. The next spreading sequence set with a much improved BER performance is the Wysocki spreading sequence set which was employed in the results for STS outlined in Chapter 4 where its superior performance in a BPSK modulated (wideband) Direct Sequence STS system to the Walsh Hadamard spreading sequence set was observed. In the STS-TH-UWB-PPM system proposed it is clear that the Wysocki codes have no advantage or lead to a worse BER performance than the corresponding Walsh Hadamard sequence set. A possible reason for this is that the lower cross correlation Wysocki codes are compared against all the other codes in the Wysocki code sequence (of which there are 32 in total) in calculating the lower cross correlation. Since the STS-TH-UWB-PPM system is already resistant to MAI (since it requires a E_b/N_o of +3.15dB to see any significant effect), and the codes which have been used in the simulation may not be constantly interfering with each other as often as necessary to provide the advantage of the lower cross correlation which was shown to be the case in Chapter 4, the advantages of the Wysocki spreading sequence set are significantly affected. Further, in Chapter 4 where it showed the advantage of the Wysocki codes, the codes were overlayed directly in time, space and frequency with small offset delays.

Considering the data for the final three spreading sequence sets, which are the Walsh Hadamard, w32dash03 and Orthogonal Gold spreading codes, it is evident that they have very similar BER performance as the measured E_b/N_o in dB is increased. Figure 9.5-5 through to Figure 9.5-8 shows the BER performance of these final three spreading sequence sets for high measured E_b/N_o. In general the w32dash03 and Orthogonal Gold spreading sequences perform marginally better than the Walsh Hadamard spreading sequences employed. It is noted, however, that this is not the case for every measured E_b/N_o value with some plots showing that there are occassions when the Walsh Hadamard spreading codes provide a better average BER performance. For example, in Figure 9.5-8, with an E_b/N_o of +5.2dB the Walsh Hadamard spreading sequence set has the best BER performance. There is a clear trend, however, that the w32dash03 and Orthogonal Gold spreading sequences do somewhat improve the average BER performance as the measured E_b/N_o is increased.

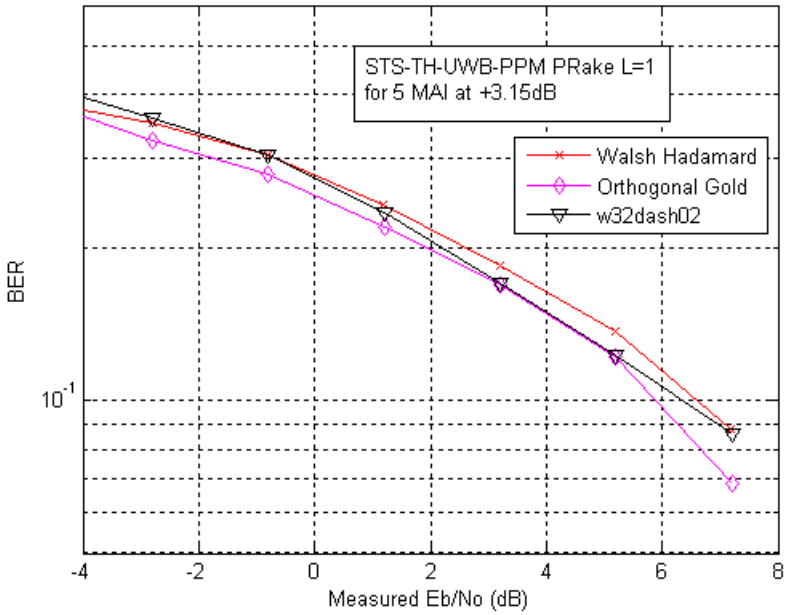

Figure 9.5-5: Comparison of performance of orthogonal gold codes, w32dash03 codes, and Walsh Hadamard codes in the presence of five MAI interferers at +3.15dB for L=1 of mean BER versus Measured E_b/N_o (dB).

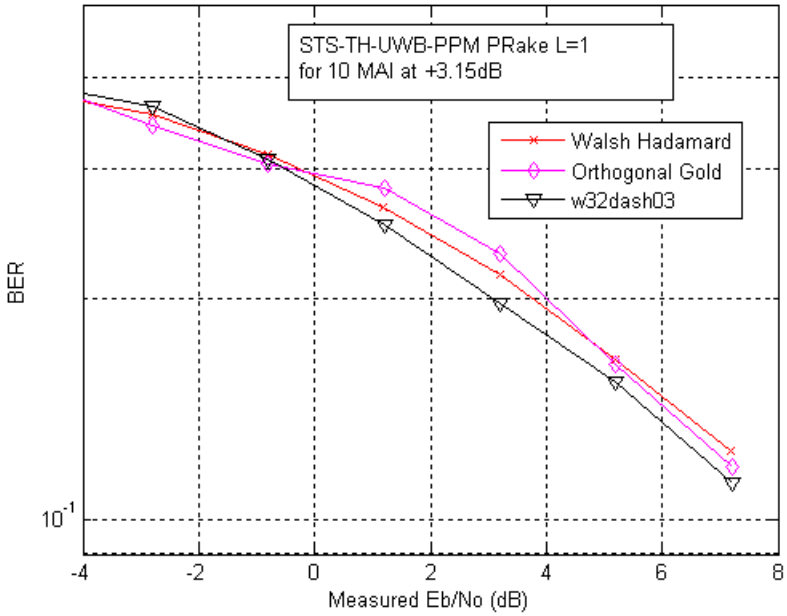

Figure 9.5-6: Comparison of performance of orthogonal gold codes, w32dash03 codes, and Walsh Hadamard codes in the presence of ten MAI interferers at +3.15dB for L=1 of mean BER versus Measured E_b/N_o (dB).

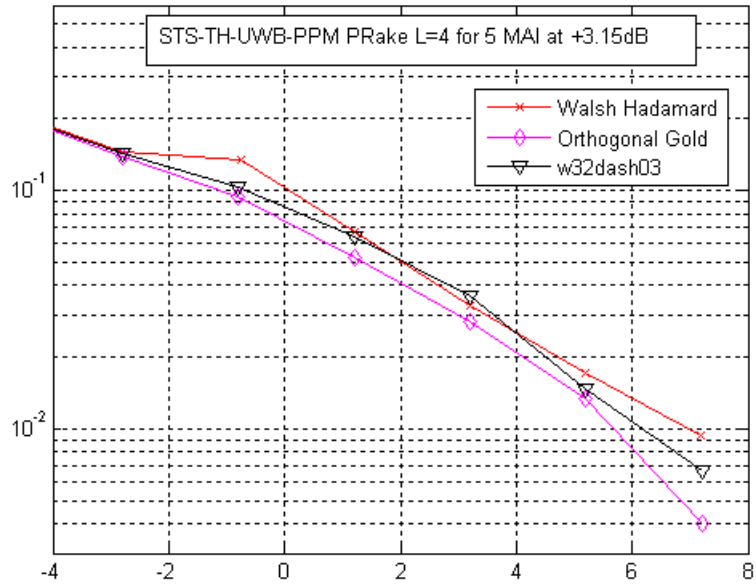

Figure 9.5-7: Comparison of performance of orthogonal gold codes, w32dash03 codes, and Walsh Hadamard codes in the presence of five MAI interferers at +3.15dB for L=4 of mean BER versus Measured E_b/N_o (dB).

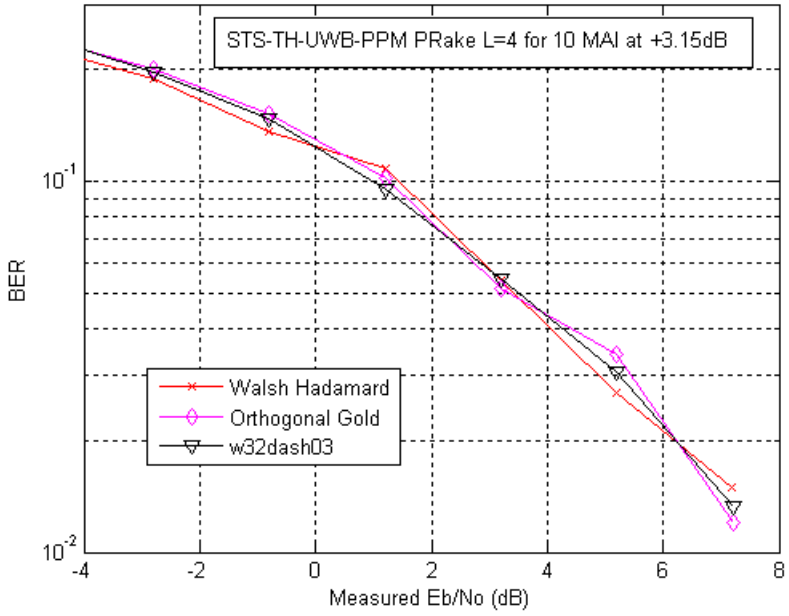

Figure 9.5-8: Comparison of performance of orthogonal gold codes, w32dash03 codes, and Walsh Hadamard codes in the presence of ten MAI interferers at +3.15dB for L=4 of mean BER versus Measured E_b/N_o (dB).

9.6 Conclusion

This chapter presents the results of an investigation into the effect of Multiple Access Interference when the desired STS-TH-UWB-PPM system was co-located with delayed versions of other STS-TH-UWB-PPM systems using Walsh-Hadamard spreading sequences and found that for low E_b/N_o there was no significant degradation in the BER performance. In the presence of only one MAI user the study found no evidence of a significant degradation in BER performance compared to an system with no MAI regardless of the energy level of the interfering MAI source. In the presence of five and ten MAI sources when their energy levels had a measured E_b/N_o of +3.15dB it was found that, for higher E_b/N_o, there was a measurable degradation in BER performance. This is in agreeance with the theoretical calculations provided in Chapter 10.

This chapter then presented a comparison of the BER performance of different spreading sequences with five and ten MAI sources each with a measured E_b/N_o of +3.15dB. It was found that the poorest BER performance was encountered when the randomly chosen spreading sequence h32dash03 (used to obtain the low correlation spreading sequence w32dash03) was employed. Surprisingly it was found that when the Wysocki spreading sequence set proposed in [61] was employed the BER performance was marginally worse than that found using the Walsh Hadamard sequence set. This was an unexpected finding and could be explained by the nature of the UWB PPM system being resistant to MAI since the codes do not correspond for all time space and frequency in the UWB system (with its high level of multipath) as they do in the DS wideband system studied in [10]. It is also possible that a poor choice of the Wysocki spreading sequences was used in the simulation for the desired STS-TH-WUB-PPM pairing (the sequences were chosen purely at random and kept fixed for all spreading sequence simulation sets relative to the family of spreading sequence codes all of length 32 chips). This is possible as the other two low correlation spreading sequences employed, w32dash03 and Orthogonal Gold, displayed marginally improved BER performance at most (but not all) measured E_b/N_o values. This implies that instead of looking for low correlation between individual spreading sequences a criteria that minimises correlation between pairs of sequences should be sought.

The next chapter, Chapter 10, models and analyses mathematically the proposed STS-TH-UWB-PPM system and investigates the effect of MAI on the BER performance of such a system. Then, finally, the thesis is concluded in Chapter 11 as it considers the significant contributions of this study and provides future possible directions for continued research.

Chapter 10: Analysis of STS-TH-UWB-PPM system for All Rake in presence of MAI

10.1 Introduction

This chapter presents an analysis of the proposed STS-TH-UWB-PPM system. Expressions are provided for the average BER in the presence and absence of MAI sources. The system is analysed for the case of perfect knowledge of all the CSI and the multipath energy on both antenna branches available. This is termed an All Rake receiver.

10.2 Description of System parameters

This STS-TH-UWB-PPM system described thus far can be modeled as a sequence of Time Hopping UWB pulses. The system that was simulated in Chapter 8 and Chapter 9 is shown in the schematic of Figure 10.2-1.

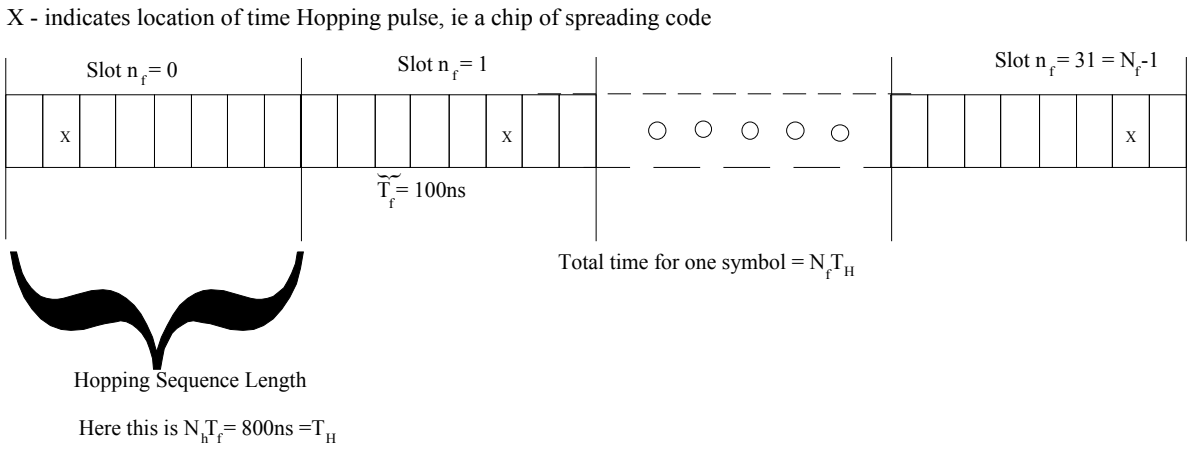

Figure 10.2-1: Shows relationship between terms used to describe a STS-TH-UWB-PPM system.

Lets consider a system with multiple co-located in time STS-TH-UWB-PPM systems. Forming the mathematical equation describing user 'u' in our system with multiple users, the model for the transmitted signal from the two transmit antennas as the signal $s^{(u)}(t)$ is:

$$s^{(u)}(t) = \left(\sqrt{\frac{E_{TX}(u)}{2}}\right) \sum_{n_{f_{(u)}}=0}^{N_f-1} w\left(t - n_{f_{(u)}} T_H - c_{n_{f_{(u)}}}^{(u)} T_f - \Delta_{n_{f_{(u)}}}^{(i)}\right) + \left(\sqrt{\frac{E_{TX}(u)}{2}}\right) \sum_{n_{f_{(u)}}=0}^{N_f-1} w\left(t - n_{f_{(u)}} T_H - c_{n_{f_{(u)}}}^{(u)} T_f - \Delta_{n_{f_{(u)}}}^{(j)}\right) \quad (10.2\text{-}1)$$

Here $E_{TX}(u)$ is the transmitted power of user u, the first term is the signal transmitted on antenna 0, the second term is the signal transmitted simultaneously on antenna 1, and the factor 2 in the denominator of both terms is to normalise the total signal power to that which would be needed for a similar SISO system. The w(t) is the unity power pulse shaper used for all users simultaneously, with width T_w. These pulses are then delayed by the arguments provided. The delay $n_{f_{(u)}} T_H$ is the delay due to the spreading sequence and the Time Hopping slot pattern employed. For example in the simulations of Chapter 8 and Chapter 9 there were 8 slots per Time Hopping cycle. One of these 8 frames would have had the transmitted UWB pulse, referred to for user u as $n_{f_{(u)}}$. The second delay term, $c_{n_{f_{(u)}}}^{(u)} T_f$, refers to the delay due to the time hopping sequence pattern. It determines which of the frames of the Time Hopping slots available will be used to send the gaussian pulse for user u for frame number n_f. The third term is the value of the delay for the actual PPM. This is different depending on which antenna the signal originates on. For antenna 0 the delay is denoted by $\Delta_{n_{f_{(u)}}}^{(i)}$, while for antenna 1 its denoted $\Delta_{n_{f_{(u)}}}^{(j)}$. For our STS-TH-UWB-PPM system for a particular user u it should be noted that $\Delta_{n_{f_{(u)}}}^{(i)} \neq \Delta_{n_{f_{(u)}}}^{(j)}$.

For the symbol s, it is chosen from the set {[1,1], [1,-1],[-1,1],[-1,-1]}. It is then spread using two orthogonal spreading codes as per the STS schema previously described and modulated using UWB three position PPM and transmitted. For our mathematical model the UWB three position PPM results in the delays on each antenna branch for the data being unique (as described above). The processing gain is for our system the value of N_f. In other studies (such

as in [8]), N_f would be the number of times that the single valued symbol chosen from the set {1,-1} was transmitted before being demodulated using a Rake receiver and MRC. The energy of user 'u' is $E_{TX}(u)$ and the relationship between $E_{TX}(u)$ and the total energy for a transmitted symbol for user u, ε_u , over a spreading code period of $N_f T_H$ is:

$$E_{TX}(u) = \frac{\varepsilon_u}{N_f} \qquad (10.2\text{-}2)$$

Which compares to Equation 2.10-6 which is provided from [8]. For the Time Hopping sequence if two users occupy the same frame of duration T_f (actually a chip of our spreading code), then a collision occurs. This collision results in user u experiencing MAI which results in an increase in the instantaneous BER. If this occurs for all chips in the STS spreading codes this will add further to the probability that the SER (Symbol Error Rate) will increase and, hence the actual instantaneous BER, over a symbol period. This would occur if the Time Hopping pattern used by other users to provide multiple accesses to the users overlapped in time (this overlap may occur asynchronously as was done with our simulations where it was allowed to overlap within a time frame of -50ns to +50ns with a delayed frame start time taken from a uniform distribution). These Time Hopping patterns or Time Hopping sequences are characterised, typically, by two attributes which are now introduced for the purposes of this analysis. The first attribute is denoted the periodicity and given the symbol N_p. Here, N_p is an integer and indicates how long the repeating code is before the sequence is repeated or restarted. For our simulations it used an N_p=8. The second attribute is called the Cardinality and this is denoted N_h. This attribute indicates the size of the alphabet used in the Time Hopping code and for our simulations it also used a cardinality of 8 which implies an alphabet ranging from 0 to 7 [67].

Given these definitions the user u's code hopping sequence is now denoted by:

$$c_{n_{f(u)}}^{(u)} \epsilon \mathcal{R}, \quad 0 \le c_{n_{f(u)}}^{(u)} \le N_h - 1 \qquad (10.2\text{-}3)$$

and typically $c_{n_{f(u)}}^{(u)}$ is an integer. For the STS-TH-UWB-PPM system it employs multiple time shifts. It is noted that these time shifts, $\Delta_{n_{f(u)}}^{(i)}$, $\Delta_{n_{f(u)}}^{(j)}$ are taken from the set of time shifts determined by the nominal pulse width of the pulse shaper, that is they are selected

from the set $\{0, T_w, 2T_w\}$. For the system which was simulated in Simulink it had a pulse width of one nanosecond so the possible pulse position time shifts were selected from the set $\{0,1ns, 2ns\}$. If R is used to represent the data rate in bps, and it is noted that for the proposed system, one symbol represents two data binary bits (which is encoded on both antennas), then the data rate R is given by the relationship:

$$R = \frac{2\ data\ bits/symbol}{N_f T_H}$$

(10.2-4)

Or

$$R = \frac{2\ data\ bits/symbol}{N_f N_h T_f}$$

(10.2-5)

For the specific values used in the Simulink simulations it is noted that T_f=100ns, N_f=32, N_h=8, so the data rate of the simulated system would be:

$$R = \frac{2\ data\ bits/symbol}{N_f N_h T_f} = \frac{2}{(32)(8)(100ns)} = 78{,}125\ bps$$

(10.2-6)

The pulse shaper, w(t), is defined by Equation 5.2-2 (page 107). Using the SV model for the UWB channel from Equation 2.11-11 gives:

$$h(t) = \sum_{l=0}^{\infty} \sum_{k=0}^{\infty} \beta_{kl} e^{j\theta_{kl}} \delta(t - T_l - \tau_{kl})$$

(10.2-7)

These channel coefficients are complex, however the analysis models the channels over the time of duration T_f and the channel coefficients are real because the UWB signal is real, so SV channel for antenna 0 for user u can be expressed as:

$$h_{o,u}(t) = \sum_{l_{0,u}=0}^{L_{0,u}-1} \beta_{l_{0,u}}^{(0)}\, \delta\left(t - \tau_{l_{o,u}}^{(0)}\right)$$

(10.2-8)

Where $\beta_{l_{0,u}}^{(0)}$ are the real amplitudes of the UWB system with truncation of its impulse response occurring after a time period of duration T_f seconds for user u (according to the SV model the magnitudes of the arriving clusters decreases with increasing time and in our

model after T_f seconds they should be negligible in magnitude compared to those arriving within the duration T_f; for our simulations and in [8] a duration of 100ns was used for the channel instances of the SV channels). In a similar manner, for the uncorrelated SV channel for antenna 1 for user u, it can be written as:

$$h_{1,u}(t) = \sum_{l_{1,u}=0}^{L_{1,u}-1} \beta_{l_{1,u}}^{(1)} \delta\left(t - \tau_{l_{1,u}}^{(1)}\right)$$

(10.2-9)

Also for this analysis $L_{0,u}$ represents every single multipath for the SV channel between antenna 0 and the receiver and $L_{1,u}$ represents every single multipath for the SV channel between antenna 1 and the receiver. It should be noted that since the channels are uncorrelated then the number of multipath on each channel are not necessarily identical. The analysis does not consider (as was done in the simulations of this thesis and as Yang and Giannakis [8] in theirs), the choice of any particular multipath as this analysis is for an All Rake receiver system.

The channel energy for each antenna path is now defined. For antenna 0 this is given by:

$$E_{H,u}^{(0)} = \sum_{l_{0,u}=0}^{L_{0,u}-1} \left(\beta_{l_{0,u}}^{(0)}\right)^2$$

(10.2-10)

Since the channel coefficients are real valued for the UWB channel, and hence for antenna 1 for user u the channel energy is similarly given by:

$$E_{H,u}^{(1)} = \sum_{l_{1,u}=0}^{L_{1,u}-1} \left(\beta_{l_{1,u}}^{(1)}\right)^2$$

(10.2-11)

Representing the convolution operator by the symbol * allows the expression for the received signal as a result of the transmission of user u's signal at the receiver to be given by:

$$r_u(t) = \left[\left(\sqrt{\frac{E_{TX}(u)}{2}}\right)\sum_{n_{f_{(u)}}=0}^{N_f-1} w\left(t - n_{f_{(u)}}T_H - c_{n_{f_{(u)}}}^{(u)}T_f - \Delta_{n_{f_{(u)}}}^{(i)}\right)\right] * h_{0,u}(t) + \left[\left(\sqrt{\frac{E_{TX}(u)}{2}}\right)\sum_{n_{f_{(u)}}=0}^{N_f-1} w\left(t - n_{f_{(u)}}T_H - c_{n_{f_{(u)}}}^{(u)}T_f - \Delta_{n_{f_{(u)}}}^{(j)}\right)\right] * h_{1,u}(t) + n(t)$$

(10.2-12)

It is assumed that both antenna channels are flat fading or static over the time frame needed to transmit one symbol which here is of duration N_fT_H. This will be allowed to vary later when the expectation of the MRC results are taken. The term *n(t)* is the receivers white gaussian noise with mean zero and variance σ^2. Extending the equation to include multiple users which have been asynchronously added to the system and that have overlapping Time Hopping patterns. It is further assumed that it has N_u such users in total. Then the expression for the received waveform at the receiver is given by:

$$r(t) = \sum_{u=1}^{N_u}\left[\left(\sqrt{\frac{E_{TX}(u)}{2}}\right)\sum_{n_{f_{(u)}}=0}^{N_f-1} w\left(t - n_{f_{(u)}}T_H - c_{n_{f_{(u)}}}^{(u)}T_f - \Delta_{n_{f_{(u)}}}^{(i)}\right)\right] * h_{0,u}(t) + \sum_{u=1}^{N_u}\left[\left(\sqrt{\frac{E_{TX}(u)}{2}}\right)\sum_{n_{f_{(u)}}=0}^{N_f-1} w\left(t - n_{f_{(u)}}T_H - c_{n_{f_{(u)}}}^{(u)}T_f - \Delta_{n_{f_{(u)}}}^{(j)}\right)\right] * h_{1,u}(t) + n(t)$$

(10.2-13)

Taking into account that the impulse response of the channel is a sequence of dirac delta impulses of finite length (essentially an Finite Impulse Response or tapped delay line model) the expression for the signal received at the receiver in the presence of N_u users for one symbol period when the channel is flat fading is given as:

$$r(t) = \sum_{u=1}^{N_u} \left(\sqrt{\frac{E_{TX}(u)}{2}} \right) \sum_{n_{f_{(u)}}=0}^{N_f-1} \sum_{l_{0,u}=0}^{L_{o,u}-1} \beta_{l_{o,u}}^{(0)} w\left(t - n_{f_{(u)}} T_H - c_{n_{f_{(u)}}}^{(u)} T_f - \Delta_{n_{f_{(u)}}}^{(i)} - \tau_{l_{0,u}}^{(0)} - \Delta'_{N_f T_{H_{(u)}}} \right)$$
$$+ \sum_{u=1}^{N_u} \left(\sqrt{\frac{E_{TX}(u)}{2}} \right) \sum_{n_{f_{(u)}}=0}^{N_f-1} \sum_{l_{1,u}=0}^{L_{1,u}-1} \beta_{l_{1,u}}^{(1)} w\left(t - n_{f_{(u)}} T_H - c_{n_{f_{(u)}}}^{(u)} T_f - \Delta_{n_{f_{(u)}}}^{(j)} - \tau_{l_{1,u}}^{(1)} \right.$$
$$\left. - \Delta'_{N_f T_{H_{(u)}}} \right) + n(t)$$

(10.2-14)

Where the term $\Delta'_{N_f T_{H_{(u)}}}$ has been added to model the effect of asynchronous users. If $\Delta'_{N_f T_{H_{(u)}}} = 0$ for all users u then the Time Hopping patterns are synchronised. This term will be allowed to vary between $-T_f/2$ and $+T_f/2$ seconds or in the case our simulated system this was between -50ns and +50ns.

10.3 The STS-TH-UWB-PPM demodulator

The received signal given by Equation 10.2-14 is then used in the demodulation by multiplying it by the signal which would have been received for each of the four different symbols sent, defined by the set s. Any of the u user signals may be chosen as the desired signal. Without loss of generality user 1 (u=1) is chosen as the desired signal. It is normal to multiply by the complex conjugate of the desired signal of the channel, however the UWB signal is purely real so the system uses the templated copy of the desired signal given that with coherent reception uses perfect knowledge of the CSI. For user 1 the desired signal is defined as a continuous time signal composed of gaussian pulses with the term $\Delta'_{N_f T_{H_{(u)}}} = 0$, as user 1 is the desired signal and synchronisation is assumed to be perfect. The demodulator forms the four template signals which are then used to multiply the desired signal to indicate which of the four possibilities were transmitted.

For the symbol s={1,1} it is represented by the templated signal:

$$f_{template}^{(1,1)}(t) = \sum_{n_{f_{(1)}}=0}^{N_f-1} \sum_{l_{0,1}=0}^{L_{0,1}-1} \beta_{l_{0,1}}^{(0)} w\left(t - n_{f_{(1)}} T_H - c_{n_{f_{(1)}}}^{(1)} T_f - \Delta_{n_{f_{(1)}}}^{(1,1)(i)} - \tau_{l_{0,1}}^{(0)}\right) + \sum_{n_{f_{(1)}}=0}^{N_f-1} \sum_{l_{1,1}=0}^{L_{1,1}-1} \beta_{l_{1,1}}^{(1)} w\left(t - n_{f_{(1)}} T_H - c_{n_{f_{(1)}}}^{(1)} T_f - \Delta_{n_{f_{(1)}}}^{(1,1)(j)} - \tau_{l_{1,1}}^{(1)}\right)$$

(10.3-1)

For the symbol s={1,-1} it is represented by the templated signal:

$$f_{template}^{(1,-1)}(t) = \sum_{n_{f_{(1)}}=0}^{N_f-1} \sum_{l_{0,1}=0}^{L_{0,1}-1} \beta_{l_{0,1}}^{(0)} w\left(t - n_{f_{(1)}} T_H - c_{n_{f_{(1)}}}^{(1)} T_f - \Delta_{n_{f_{(1)}}}^{(1,-1)(i)} - \tau_{l_{0,1}}^{(0)}\right) + \sum_{n_{f_{(1)}}=0}^{N_f-1} \sum_{l_{1,1}=0}^{L_{1,1}-1} \beta_{l_{1,1}}^{(1)} w\left(t - n_{f_{(1)}} T_H - c_{n_{f_{(1)}}}^{(1)} T_f - \Delta_{n_{f_{(1)}}}^{(1,-1)(j)} - \tau_{l_{1,1}}^{(1)}\right)$$

(10.3-2)

For the symbol s={-1,1} it is represented by the templated signal:

$$f_{template}^{(-1,1)}(t) = \sum_{n_{f_{(1)}}=0}^{N_f-1} \sum_{l_{0,1}=0}^{L_{0,1}-1} \beta_{l_{0,1}}^{(0)} w\left(t - n_{f_{(1)}} T_H - c_{n_{f_{(1)}}}^{(1)} T_f - \Delta_{n_{f_{(1)}}}^{(-1,1)(i)} - \tau_{l_{0,1}}^{(0)}\right) + \sum_{n_{f_{(1)}}=0}^{N_f-1} \sum_{l_{1,1}=0}^{L_{1,1}-1} \beta_{l_{1,1}}^{(1)} w\left(t - n_{f_{(1)}} T_H - c_{n_{f_{(1)}}}^{(1)} T_f - \Delta_{n_{f_{(1)}}}^{(-1,1)(j)} - \tau_{l_{1,1}}^{(1)}\right)$$

(10.3-3)

For the symbol s={-1,-1} it is represented by the templated signal:

$$f_{template}^{(-1,-1)}(t) = \sum_{n_{f_{(1)}}=0}^{N_f-1} \sum_{l_{0,1}=0}^{L_{0,1}-1} \beta_{l_{0,1}}^{(0)} w\left(t - n_{f_{(1)}} T_H - c_{n_{f_{(1)}}}^{(1)} T_f - \Delta_{n_{f_{(1)}}}^{(-1,-1)(i)} - \tau_{l_{0,1}}^{(0)}\right) + \sum_{n_{f_{(1)}}=0}^{N_f-1} \sum_{l_{1,1}=0}^{L_{1,1}-1} \beta_{l_{1,1}}^{(1)} w\left(t - n_{f_{(1)}} T_H - c_{n_{f_{(1)}}}^{(1)} T_f - \Delta_{n_{f_{(1)}}}^{(-1,-1)(j)} - \tau_{l_{1,1}}^{(1)}\right)$$

(10.3-4)

Forming the generalised form of the template waveform is achieved by taking the individual symbols and replacing them by the generic representation s, where s can be replaced by actual symbol sent in specific instances. Of course all four must be calculated and the maximum value taken for implementation of a MRC decoder integrated over an entire symbol time of $N_f T_H$:

$$f_{template}^{(s)}(t) = \sum_{n_{f_{(1)}}=0}^{N_f-1} \sum_{l_{0,1}=0}^{L_{0,1}-1} \beta_{l_{0,1}}^{(0)} w\left(t - n_{f_{(1)}} T_H - c_{n_{f_{(1)}}}^{(1)} T_f - \Delta_{n_{f_{(1)}}}^{(s)(i)} - \tau_{l_{0,1}}^{(0)}\right) + \sum_{n_{f_{(1)}}=0}^{N_f-1} \sum_{l_{1,1}=0}^{L_{1,1}-1} \beta_{l_{1,1}}^{(1)} w\left(t - n_{f_{(1)}} T_H - c_{n_{f_{(1)}}}^{(1)} T_f - \Delta_{n_{f_{(1)}}}^{(s)(j)} - \tau_{l_{1,1}}^{(1)}\right)$$

(10.3-5)

If the received signal r(t) is then multiplied by the generic template for symbol s the result is denoted $x^{(s)}(t)$. Hence, the expression for the result $x^{(s)}(t)$ after multiplication by the templated signal $f_{template}^{(s)}(t)$ is:

$$\begin{aligned} x^{(s)}(t) = & \left(\sqrt{\frac{E_{TX}(1)}{2}}\right) \sum_{n_{f_{(1)}}=0}^{N_f-1} \sum_{l_{0,1}=0}^{L_{0,1}-1} \left(\beta_{l_{0,1}}^{(0)}\right)^2 w^2\left(t - n_{f_{(1)}} T_H - c_{n_{f_{(1)}}}^{(1)} T_f - \Delta_{n_{f_{(1)}}}^{(s)(i)} - \tau_{l_{0,1}}^{(0)}\right) \\ & + \left\{\left(\sqrt{\frac{E_{TX}(1)}{2}}\right)\left[\sum_{n_{f_{(1)}}=0}^{N_f-1} \sum_{l_{1,1}=0}^{L_{1,1}-1} \beta_{l_{1,1}}^{(1)} w\left(t - n_{f_{(1)}} T_H - c_{n_{f_{(1)}}}^{(1)} T_f - \Delta_{n_{f_{(1)}}}^{(s)(j)} - \tau_{l_{1,1}}^{(1)}\right)\right]\right. \\ & \left. \times \left[\sum_{n_{f_{(1)}}=0}^{N_f-1} \sum_{l_{0,1}=0}^{L_{0,1}-1} \beta_{l_{0,1}}^{(0)} w\left(t - n_{f_{(1)}} T_H - c_{n_{f_{(1)}}}^{(1)} T_f - \Delta_{n_{f_{(1)}}}^{(s)(i)} - \tau_{l_{0,1}}^{(0)}\right)\right]\right\} \\ & + \left(\sqrt{\frac{E_{TX}(1)}{2}}\right) \sum_{n_{f_{(1)}}=0}^{N_f-1} \sum_{l_{1,1}=0}^{L_{1,1}-1} \left(\beta_{l_{1,1}}^{(1)}\right)^2 w^2\left(t - n_{f_{(1)}} T_H - c_{n_{f_{(1)}}}^{(1)} T_f - \Delta_{n_{f_{(1)}}}^{(s)(j)} - \tau_{l_{1,1}}^{(1)}\right) \\ & + \left\{\left(\sqrt{\frac{E_{TX}(1)}{2}}\right)\left[\sum_{n_{f_{(1)}}=0}^{N_f-1} \sum_{l_{0,1}=0}^{L_{0,1}-1} \beta_{l_{0,1}}^{(0)} w\left(t - n_{f_{(1)}} T_H - c_{n_{f_{(1)}}}^{(1)} T_f - \Delta_{n_{f_{(1)}}}^{(s)(i)} - \tau_{l_{0,1}}^{(0)}\right)\right]\right. \\ & \left. \times \left[\sum_{n_{f_{(1)}}=0}^{N_f-1} \sum_{l_{1,1}=0}^{L_{1,1}-1} \beta_{l_{1,1}}^{(1)} w\left(t - n_{f_{(1)}} T_H - c_{n_{f_{(1)}}}^{(1)} T_f - \Delta_{n_{f_{(1)}}}^{(s)(j)} - \tau_{l_{1,1}}^{(1)}\right)\right]\right\} + V_{MAI} + N \end{aligned}$$

(10.3-6)

Where $\times$ represents the continuous time multiplication of two continous time signals or

waveforms, and:

$$V_{MAI} = \left\{ \left[\sum_{u=2}^{N_u} \left(\sqrt{\frac{E_{TX}(u)}{2}} \right) \sum_{n_{f_{(u)}}=0}^{N_f-1} \sum_{l_{0,u}=0}^{L_{o,u}-1} \beta_{l_{o,u}}^{(0)} w\left(t - n_{f_{(u)}} T_H - c_{n_{f_{(u)}}}^{(u)} T_f - \Delta_{n_{f_{(u)}}}^{(i)} - \tau_{l_{0,u}}^{(0)} - \Delta'_{N_f T_{H_{(u)}}} \right) \right. \right.$$

$$+ \sum_{u=2}^{N_u} \left(\sqrt{\frac{E_{TX}(u)}{2}} \right) \sum_{n_{f_{(u)}}=0}^{N_f-1} \sum_{l_{1,u}=0}^{L_{1,u}-1} \beta_{l_{1,u}}^{(1)} w\left(t - n_{f_{(u)}} T_H - c_{n_{f_{(u)}}}^{(u)} T_f - \Delta_{n_{f_{(u)}}}^{(j)} - \tau_{l_{1,u}}^{(1)} \right.$$

$$\left. \left. - \Delta'_{N_f T_{H_{(u)}}} \right) \right] \times \left[\sum_{n_{f_{(1)}}=0}^{N_f-1} \sum_{l_{0,1}=0}^{L_{0,1}-1} \beta_{l_{0,1}}^{(0)} w\left(t - n_{f_{(1)}} T_H - c_{n_{f_{(1)}}}^{(1)} T_f - \Delta_{n_{f_{(1)}}}^{(s)(i)} - \tau_{l_{0,1}}^{(0)} \right) \right] \right\}$$

$$+ \left\{ \left[\sum_{u=2}^{N_u} \left(\sqrt{\frac{E_{TX}(u)}{2}} \right) \sum_{n_{f_{(u)}}=0}^{N_f-1} \sum_{l_{0,u}=0}^{L_{o,u}-1} \beta_{l_{o,u}}^{(0)} w\left(t - n_{f_{(u)}} T_H - c_{n_{f_{(u)}}}^{(u)} T_f - \Delta_{n_{f_{(u)}}}^{(i)} - \tau_{l_{0,u}}^{(0)} \right. \right. \right.$$

$$\left. \left. - \Delta'_{N_f T_{H_{(u)}}} \right) \right.$$

$$+ \sum_{u=2}^{N_u} \left(\sqrt{\frac{E_{TX}(u)}{2}} \right) \sum_{n_{f_{(u)}}=0}^{N_f-1} \sum_{l_{1,u}=0}^{L_{1,u}-1} \beta_{l_{1,u}}^{(1)} w\left(t - n_{f_{(u)}} T_H - c_{n_{f_{(u)}}}^{(u)} T_f - \Delta_{n_{f_{(u)}}}^{(j)} - \tau_{l_{1,u}}^{(1)} \right.$$

$$\left. \left. - \Delta'_{N_f T_{H_{(u)}}} \right) \right] \times \left[\sum_{n_{f_{(1)}}=0}^{N_f-1} \sum_{l_{1,1}=0}^{L_{1,1}-1} \beta_{l_{1,1}}^{(1)} w\left(t - n_{f_{(1)}} T_H - c_{n_{f_{(1)}}}^{(1)} T_f - \Delta_{n_{f_{(1)}}}^{(s)(j)} - \tau_{l_{1,1}}^{(1)} \right) \right] \right\}$$

(10.3-7)

And the noise term is:

$$N = \left\{ [n(t)] \times \left[\sum_{n_{f_{(1)}}=0}^{N_f-1} \sum_{l_{0,1}=0}^{L_{0,1}-1} \beta_{l_{0,1}}^{(0)} w\left(t - n_{f_{(1)}} T_H - c_{n_{f_{(1)}}}^{(1)} T_f - \Delta_{n_{f_{(1)}}}^{(s)(i)} - \tau_{l_{0,1}}^{(0)} \right) \right] \right\}$$

$$+ \left\{ [n(t)] \times \left[\sum_{n_{f_{(1)}}=0}^{N_f-1} \sum_{l_{1,1}=0}^{L_{1,1}-1} \beta_{l_{1,1}}^{(1)} w\left(t - n_{f_{(1)}} T_H - c_{n_{f_{(1)}}}^{(1)} T_f - \Delta_{n_{f_{(1)}}}^{(s)(j)} - \tau_{l_{1,1}}^{(1)} \right) \right] \right\}$$

(10.3-8)

Proceed by integrating the four possible received signals over a full symbol period to get the received signals. This full symbol period is over the time $N_f T_H$, and which provides the outputs at the MRC of:

$$y^{(1,1)} = \int_0^{N_f T_H} x^{(1,1)}(t)dt \quad (10.3\text{-}9)$$

$$y^{(1,-1)} = \int_0^{N_f T_H} x^{(1,-1)}(t)dt \quad (10.3\text{-}10)$$

$$y^{(-1,1)} = \int_0^{N_f T_H} x^{(-1,1)}(t)dt \quad (10.3\text{-}11)$$

$$y^{(-1,-1)} = \int_0^{N_f T_H} x^{(-1,-1)}(t)dt \quad (10.3\text{-}12)$$

The choice of which symbol has been sent is then based on the largest value of $y^{(s)}(t)$. Note that in our simulations waveforms that would be expected were calculated, given knowledge of the path gains and energy of the individual antennas in the absence of MAI or noise, integrate these over a chip period (T_f, only when active for the Hopping pattern) and subtract this from the received signal over the same chip, for each possible case. After all chips have been collected the decision statistic is to choose the symbol whose output has the lowest absolute value. For this analysis it is also assumed that the receiver knows the transmission power or SNR of each user. These need not be the same but it is, for simplicity, assumed that all MAI users have the same SNR later in the analysis.

Using Equation 10.3-6 it is noted that the desired signal for symbol s is:

$$
\begin{aligned}
y^{(s)}{}_{no\ noise}(t) = \int_0^{N_f T_H} \Bigg\{ & \left(\sqrt{\frac{E_{TX}(1)}{2}} \right) \sum_{n_{f_{(1)}}=0}^{N_f-1} \sum_{l_{0,1}=0}^{L_{0,1}-1} \left(\beta_{l_{0,1}}^{(0)} \right)^2 w^2 \left(t - n_{f_{(1)}} T_H - c_{n_{f_{(1)}}}^{(1)} T_f \right. \\
& \left. - \Delta_{n_{f_{(1)}}}^{(s)(i)} - \tau_{l_{0,1}}^{(0)} \right) \\
& + \Bigg\{ \left(\sqrt{\frac{E_{TX}(1)}{2}} \right) \left[\sum_{n_{f_{(1)}}=0}^{N_f-1} \sum_{l_{1,1}=0}^{L_{1,1}-1} \beta_{l_{1,1}}^{(1)} w \left(t - n_{f_{(1)}} T_H - c_{n_{f_{(1)}}}^{(1)} T_f - \Delta_{n_{f_{(1)}}}^{(s)(j)} - \tau_{l_{1,1}}^{(1)} \right) \right] \\
& \times \left[\sum_{n_{f_{(1)}}=0}^{N_f-1} \sum_{l_{0,1}=0}^{L_{0,1}-1} \beta_{l_{0,1}}^{(0)} w \left(t - n_{f_{(1)}} T_H - c_{n_{f_{(1)}}}^{(1)} T_f - \Delta_{n_{f_{(1)}}}^{(s)(i)} - \tau_{l_{0,1}}^{(0)} \right) \right] \Bigg\} \\
& + \left(\sqrt{\frac{E_{TX}(1)}{2}} \right) \sum_{n_{f_{(1)}}=0}^{N_f-1} \sum_{l_{1,1}=0}^{L_{1,1}-1} \left(\beta_{l_{1,1}}^{(1)} \right)^2 w^2 \left(t - n_{f_{(1)}} T_H - c_{n_{f_{(1)}}}^{(1)} T_f - \Delta_{n_{f_{(1)}}}^{(s)(j)} - \tau_{l_{1,1}}^{(1)} \right) \\
& + \Bigg\{ \left(\sqrt{\frac{E_{TX}(1)}{2}} \right) \left[\sum_{n_{f_{(1)}}=0}^{N_f-1} \sum_{l_{0,1}=0}^{L_{0,1}-1} \beta_{l_{0,1}}^{(0)} w \left(t - n_{f_{(1)}} T_H - c_{n_{f_{(1)}}}^{(1)} T_f - \Delta_{n_{f_{(1)}}}^{(s)(i)} - \tau_{l_{0,1}}^{(0)} \right) \right] \\
& \times \left[\sum_{n_{f_{(1)}}=0}^{N_f-1} \sum_{l_{1,1}=0}^{L_{1,1}-1} \beta_{l_{1,1}}^{(1)} w \left(t - n_{f_{(1)}} T_H - c_{n_{f_{(1)}}}^{(1)} T_f - \Delta_{n_{f_{(1)}}}^{(s)(j)} - \tau_{l_{1,1}}^{(1)} \right) \right] \Bigg\} \Bigg\} dt
\end{aligned}
$$

(10.3-13)

It should be noted that the second and fourth terms of this integration are identical. While this integration looks complicated it has, in fact, very many locations in time when its value is zero. Subtracting this from Equation 10.3-6 leaves the noise and MAI terms, for the correct symbol transmitted, that is conditional on s being transmitted and for the other three possibilities there will be the difference between the correct symbol, the noise and the MAI. The absolute value is then taken and one chooses the statistic closest to zero. One or

two bit errors then occur if this is not the signal transmitted due to the variance of the noise or MAI in the system. Using this to form the decision statistics:

$$z^{(1,1)} = abs(y^{(1,1)}(t) - y^{(1,1)}{}_{no\ noise}(t)) \quad (10.3\text{-}14)$$

$$z^{(1,-1)} = abs(y^{(1,-1)}(t) - y^{(1,-1)}{}_{no\ noise}(t)) \quad (10.3\text{-}15)$$

$$z^{(-1,1)} = abs(y^{(-1,1)}(t) - y^{(-1,1)}{}_{no\ noise}(t)) \quad (10.3\text{-}16)$$

$$z^{(-1,-1)} = abs(y^{(-1,-1)}(t) - y^{(-1,-1)}{}_{no\ noise}(t)) \quad (10.3\text{-}17)$$

And choose the symbol which has the lowest value of z.

10.4 The average BER in the presence and absence of MAI

Considering the terms in our expression for $z^{(s)}(t)$ via terms in $x^{(s)}(t)$ and $y^{(s)}(t)$. In fact, the analysis will primarily consider the decision statistic implied by $y^{(s)}(t)$ to determine the average BER for the proposed STS-TH-UWB-PPM system. Start this part of the analysis by considering an estimate for the average SER.

First consider the noise term, N, of Equation 10.3-8 which is integrated over a symbol period of N_fT_H. The term n(t) is white gaussian noise with mean zero and variance σ^2. This is then multiplied by the demodulating channel template (the sum of the templates used to demodulate signals for antenna 0 and antenna 1). As discussed in Yang and Giannakis[8] since n(t) is a zero mean noise variable, the result of the time multiplication will also have zero mean. Since this study and Yang and Giannakis[8] choose a template gaussian pulse with unit energy, the variance will be the sum of the noise terms and channel gain. The templates used in the MRC demodulator is only defined with non-zero terms for N_f periods of duration T_f. It is further noted that the channel does not change its real channel coefficients for the SV UWB channel over a symbol time of N_fT_h (that is its assumed flat fading). From this it is concluded that the variance of the noise term integrated over a symbol time will be given by the formula:

$$N_f\sigma^2\left(E_{H,1}^{(0)} + E_{H,1}^{(1)}\right) \quad (10.4\text{-}1)$$

Where $E_{H,1}^{(0)}$ and $E_{H,1}^{(1)}$ are defined by Equation 10.2-10 and Equation 10.2-11 for user one (u=1).

For the transmitted signal s, which is composed of the first four terms of Equation 10.3-6, proceed by integrating all four terms over a symbol period N_fT_H. Considering the integration of the first and third terms in Equation 10.3-6 gives:

$$\int_0^{N_fT_H}\left\{\left(\sqrt{\frac{E_{TX}(1)}{2}}\right)\sum_{n_{f_{(1)}}=0}^{N_f-1}\sum_{l_{0,1}=0}^{L_{0,1}-1}\left(\beta_{l_{0,1}}^{(0)}\right)^2 w^2\left(t-n_{f_{(1)}}T_H-c_{n_{f_{(1)}}}^{(1)}T_f-\Delta_{n_{f_{(1)}}}^{(s)(i)}-\tau_{l_{0,1}}^{(0)}\right)\right\}dt$$
$$+\int_0^{N_fT_H}\left\{\left(\sqrt{\frac{E_{TX}(1)}{2}}\right)\sum_{n_{f_{(1)}}=0}^{N_f-1}\sum_{l_{1,1}=0}^{L_{1,1}-1}\left(\beta_{l_{1,1}}^{(1)}\right)^2 w^2\left(t-n_{f_{(1)}}T_H-c_{n_{f_{(1)}}}^{(1)}T_f\right.\right.$$
$$\left.\left.-\Delta_{n_{f_{(1)}}}^{(s)(j)}-\tau_{l_{1,1}}^{(1)}\right)\right\}dt$$

(10.4-2)

As the channel is flat fading there will be N_f equivalent integrations over duration T_f, so this reduces to:

$$N_f\left(\sqrt{\frac{E_{TX}(1)}{2}}\right)\left\{\int_0^{T_f}\sum_{l_{0,1}=0}^{L_{0,1}-1}\left(\beta_{l_{0,1}}^{(0)}\right)^2 w^2\left(t-n_{f_{(1)}}T_H-c_{n_{f_{(1)}}}^{(1)}T_f-\Delta_{n_{f_{(1)}}}^{(s)(i)}-\tau_{l_{0,1}}^{(0)}\right)dt\right.$$
$$\left.+\int_0^{T_f}\sum_{l_{1,1}=0}^{L_{1,1}-1}\left(\beta_{l_{1,1}}^{(1)}\right)^2 w^2\left(t-n_{f_{(1)}}T_H-c_{n_{f_{(1)}}}^{(1)}T_f-\Delta_{n_{f_{(1)}}}^{(s)(j)}-\tau_{l_{1,1}}^{(1)}\right)dt\right\}$$

(10.4-3)

Since the real channel coefficients of the SV model used in the UWB signal are real valued and constant and because this study chose to use a unit energy gaussian pulse waveform for the templated signal, where it satisfies:

$$\int_0^{T_f} w^2(t)dt=\int_0^{T_w} w^2(t)dt=1$$

(10.4-4)

Then Equation 10.4-3 becomes:

$$N_f\left(\sqrt{\frac{E_{TX}(1)}{2}}\right)\left\{E_{H,1}^{(0)}+E_{H,1}^{(1)}\right\}$$

(10.4-5)

The other two terms of Equation 10.3-6 are functions of integrals of the autocorrelation function of the unit energy gaussian pulse of the form:

$$\sum_i \int_0^{N_f T_H} \gamma_i w(t-\theta_i) w(t-\varphi_i)$$

(10.4-6)

Where γ_i are the real valued (positive and negative) multiplicative coefficients as a result of the channel coefficients of the uncorrelated channels. The terms $w(t-\theta_i)$ and $w(t-\varphi_i)$ represent the individual multipath multiplying each other, noting that in many cases this product will be zero as these pulses will be orthogonal (they have less than one nanosecond widths, ie they have widths of T_w). As these channels are uncorrelated (and independent) the mean value of the waveform represented by the other two terms will be approximately zero. Simulation of these terms using Simulink for an all rake system showed that this approximation is good to within 10% of the actual exact value of the signal. So, to a good approximation, this analysis ignores the contribution of these two terms in forming the decision metric.

The integration over a symbol period ($N_f T_H$) of the MAI term V_{MAI}, whose expression is shown in Equation 10.3-7 corresponds to both in-phase (perfectly aligned Time Hopping pattern) and out of phase MAI (partially aligned Time Hopping pattern). Since the channels are uncorrelated and independent, the mean value of all the waveforms integrated over a symbol period has the same form as that shown in Equation 10.4-6 with zero mean and some finite variance (directly proportional to the number of MAI sources overlapping with the desired target user ie user 1). The MAI can be modelled as a gaussian noise source with zero mean and finite variance. This model is more valid as more MAI sources are added. Equation 10.3-7 allows each MAI source to have a different signal power.

If it is now required that all MAI sources have the same power as perceived at user 1's receiver the analysis can be re-formulated so that the value for the MAI term becomes:

$$V_{MAI} = \left(\sqrt{\frac{E_{TX_{MAI}}}{2}}\right)\left[\left\{\left[\sum_{u=2}^{N_u}\sum_{n_{f_{(u)}}=0}^{N_f-1}\sum_{l_{0,u}=0}^{L_{o,u}-1}\beta_{l_{o,u}}^{(0)}w\left(t-n_{f_{(u)}}T_H-c_{n_{f_{(u)}}}^{(u)}T_f-\Delta_{n_{f_{(u)}}}^{(i)}-\tau_{l_{0,u}}^{(0)}\right.\right.\right.$$
$$\left.-\Delta'_{N_fT_{H_{(u)}}}\right)$$
$$+\sum_{u=2}^{N_u}\sum_{n_{f_{(u)}}=0}^{N_f-1}\sum_{l_{1,u}=0}^{L_{1,u}-1}\beta_{l_{1,u}}^{(1)}w\left(t-n_{f_{(u)}}T_H-c_{n_{f_{(u)}}}^{(u)}T_f-\Delta_{n_{f_{(u)}}}^{(j)}-\tau_{l_{1,u}}^{(1)}-\Delta'_{N_fT_{H_{(u)}}}\right)\Bigg]$$
$$\left.\times\left[\sum_{n_{f_{(1)}}=0}^{N_f-1}\sum_{l_{0,1}=0}^{L_{0,1}-1}\beta_{l_{0,1}}^{(0)}w\left(t-n_{f_{(1)}}T_H-c_{n_{f_{(1)}}}^{(1)}T_f-\Delta_{n_{f_{(1)}}}^{(s)(i)}-\tau_{l_{0,1}}^{(0)}\right)\right]\right\}$$
$$+\left\{\left[\sum_{u=2}^{N_u}\sum_{n_{f_{(u)}}=0}^{N_f-1}\sum_{l_{0,u}=0}^{L_{o,u}-1}\beta_{l_{o,u}}^{(0)}w\left(t-n_{f_{(u)}}T_H-c_{n_{f_{(u)}}}^{(u)}T_f-\Delta_{n_{f_{(u)}}}^{(i)}-\tau_{l_{0,u}}^{(0)}-\Delta'_{N_fT_{H_{(u)}}}\right)\right.\right.$$
$$+\sum_{u=2}^{N_u}\sum_{n_{f_{(u)}}=0}^{N_f-1}\sum_{l_{1,u}=0}^{L_{1,u}-1}\beta_{l_{1,u}}^{(1)}w\left(t-n_{f_{(u)}}T_H-c_{n_{f_{(u)}}}^{(u)}T_f-\Delta_{n_{f_{(u)}}}^{(j)}-\tau_{l_{1,u}}^{(1)}-\Delta'_{N_fT_{H_{(u)}}}\right)\Bigg]$$
$$\left.\left.\left.\times\left[\sum_{n_{f_{(1)}}=0}^{N_f-1}\sum_{l_{1,1}=0}^{L_{1,1}-1}\beta_{l_{1,1}}^{(1)}w\left(t-n_{f_{(1)}}T_H-c_{n_{f_{(1)}}}^{(1)}T_f-\Delta_{n_{f_{(1)}}}^{(s)(j)}-\tau_{l_{1,1}}^{(1)}\right)\right]\right\}\right]$$

(10.4-7)

Allowing all MAI to have the same signal power, permits calculation of the MAI due to one MAI source. The effect of extra MAI sources can then be calculated using the properties of zero mean gaussian sources (this requires the sources to appear as gaussian random variables with zero mean and some finite variance, but this is a reasonable approximation [67]). The variance for all the N_u-1 MAI sources is then denoted as σ_{MAI}^2.

For one only MAI source Equation 10.4-7 becomes:

$$V_{MAI\,OneSource} = \left(\sqrt{\frac{E_{TX_{MAI}}}{2}}\right)\Bigg[\Bigg\{\Bigg[\sum_{n_{f_{(2)}}=0}^{N_f-1}\sum_{l_{0,2}=0}^{L_{o,2}-1}\beta_{l_{o,2}}^{(0)}w\left(t-n_{f_{(2)}}T_H-c_{n_{f_{(2)}}}^{(2)}T_f-\Delta_{n_{f_{(2)}}}^{(i)}-\tau_{l_{0,2}}^{(0)}-\Delta'_{N_fT_{H_{(2)}}}\right)$$
$$+\sum_{n_{f_{(2)}}=0}^{N_f-1}\sum_{l_{1,2}=0}^{L_{1,2}-1}\beta_{l_{1,2}}^{(1)}w\left(t-n_{f_{(2)}}T_H-c_{n_{f_{(2)}}}^{(2)}T_f-\Delta_{n_{f_{(2)}}}^{(j)}-\tau_{l_{1,2}}^{(1)}-\Delta'_{N_fT_{H_{(2)}}}\right)\Bigg]$$
$$\times\left[\sum_{n_{f_{(1)}}=0}^{N_f-1}\sum_{l_{0,1}=0}^{L_{0,1}-1}\beta_{l_{0,1}}^{(0)}w\left(t-n_{f_{(1)}}T_H-c_{n_{f_{(1)}}}^{(1)}T_f-\Delta_{n_{f_{(1)}}}^{(s)(i)}-\tau_{l_{0,1}}^{(0)}\right)\right]\Bigg\}$$
$$+\Bigg\{\Bigg[\sum_{n_{f_{(2)}}=0}^{N_f-1}\sum_{l_{0,2}=0}^{L_{o,2}-1}\beta_{l_{o,2}}^{(0)}w\left(t-n_{f_{(2)}}T_H-c_{n_{f_{(2)}}}^{(2)}T_f-\Delta_{n_{f_{(2)}}}^{(i)}-\tau_{l_{0,2}}^{(0)}-\Delta'_{N_fT_{H_{(2)}}}\right)$$
$$+\sum_{n_{f_{(2)}}=0}^{N_f-1}\sum_{l_{1,2}=0}^{L_{1,2}-1}\beta_{l_{1,2}}^{(1)}w\left(t-n_{f_{(2)}}T_H-c_{n_{f_{(2)}}}^{(2)}T_f-\Delta_{n_{f_{(2)}}}^{(j)}-\tau_{l_{1,2}}^{(1)}-\Delta'_{N_fT_{H_{(2)}}}\right)\Bigg]$$
$$\times\left[\sum_{n_{f_{(1)}}=0}^{N_f-1}\sum_{l_{1,1}=0}^{L_{1,1}-1}\beta_{l_{1,1}}^{(1)}w\left(t-n_{f_{(1)}}T_H-c_{n_{f_{(1)}}}^{(1)}T_f-\Delta_{n_{f_{(1)}}}^{(s)(j)}-\tau_{l_{1,1}}^{(1)}\right)\right]\Bigg\}\Bigg] \qquad (10.4\text{-}8)$$

Which can be re-written as:

$$V_{MAI\,OneSource} = \left(\sqrt{\frac{E_{TX_{MAI}}}{2}}\right)\Psi_{u=2} \qquad (10.4\text{-}9)$$

The term $\Psi_{u=2}$ is modelled as a random gaussian variable with zero mean and variance $\sigma^2_{MAI_1}$, where this is the variance for a single MAI source. Using a computer simulation of $\Psi_{u=2}$ to provide an ensemble average and variance of the resulting waveform over a period of N_fT_H seconds for a particular value of N_f and T_H over many channel instances, assuming these will be ergodic. This is a reasonable assumption as, in fact, the channel is generated using the SV channel model which is a statistical model as described in Section 2.11.

The decision vector for symbol s (as an approximation) then becomes:

$$\theta^{(s)} \cong N_f \left(\sqrt{\frac{E_{TX}(1)}{2}} \right) \left\{ E_{H,1}^{(0)} + E_{H,1}^{(1)} \right\} + \int_0^{N_f T_H} V_{MAI} dt + \int_0^{N_f T_H} N dt$$

(10.4-10)

The Probability of a symbol error (instantaneous SER) conditioned on the real channel coefficients for antenna 0 and antenna 1, in the presence of MAI, is then:

$$P^{(s)} \left(e | \left\{ E_{H,1}^{(0)}, E_{H,1}^{(1)} \right\} \right) = Q \left(\sqrt{\frac{\left(N_f \left(\sqrt{\frac{E_{TX}(1)}{2}} \right) \left\{ E_{H,1}^{(0)} + E_{H,1}^{(1)} \right\} \right)^2}{\left\{ \left[N_f \sigma^2 \left(E_{H,1}^{(0)} + E_{H,1}^{(1)} \right) \right] + \left[\left(\sqrt{\frac{E_{TX_{MAI}}}{2}} \right)^2 \sigma_{MAI}^2 \right] \right\}} \right)$$

(10.4-11)

Where Q is the gaussian tail function [8] given by:

$$Q(x) = \frac{1}{\sqrt{(2\pi)}} \int_x^{\infty} e^{-\left(\frac{t^2}{2}\right)} dt$$

(10.4-12)

It is noted that by using Equation 10.2-2 that:

$$\varepsilon_1 = E_{TX}(1) N_f$$

(10.4-13)

Then substituting this into Equation 10.4-11 gives:

$$P^{(s)} \left(e | \left\{ E_{H,1}^{(0)}, E_{H,1}^{(1)} \right\} \right) = Q \left(\sqrt{\frac{\frac{N_f \varepsilon_1}{2} \left\{ E_{H,1}^{(0)} + E_{H,1}^{(1)} \right\}^2}{\left\{ \left[N_f \sigma^2 \left(E_{H,1}^{(0)} + E_{H,1}^{(1)} \right) \right] + \left[\left(\frac{E_{TX_{MAI}}}{2} \right) \sigma_{MI}^2 \right] \right\}} \right)$$

(10.4-14)

Re-arranging this gives:

$$P^{(s)}\left(e\middle|\left\{E_{H,1}^{(0)},E_{H,1}^{(1)}\right\}\right)=Q\left(\sqrt{\frac{\frac{N_f\varepsilon_1}{2}\left\{E_{H,1}^{(0)}+E_{H,1}^{(1)}\right\}^2}{N_f\sigma^2\left\{\left[\left(E_{H,1}^{(0)}+E_{H,1}^{(1)}\right)\right]+\left[\left(\frac{E_{TX_{MAI}}}{2N_f\sigma^2}\right)\sigma_{MAI}^2\right]\right\}}}\right)$$

(10.4-15)

Which leads to:

$$P^{(s)}\left(e\middle|\left\{E_{H,1}^{(0)},E_{H,1}^{(1)}\right\}\right)=Q\left(\sqrt{\frac{\frac{\varepsilon_1}{2\sigma^2}\left\{E_{H,1}^{(0)}+E_{H,1}^{(1)}\right\}^2}{\left\{\left[\left(E_{H,1}^{(0)}+E_{H,1}^{(1)}\right)\right]+\left[\left(\frac{E_{TX_{MAI}}}{2N_f\sigma^2}\right)\sigma_{MAI}^2\right]\right\}}}\right)$$

(10.4-16)

Defining the transmit SNR for user 1, in a similar way as done in Yang and Giannakis[8], as:

$$\rho_1=\frac{\varepsilon_1}{\sigma^2}$$

(10.4-17)

Then Equation 10.4-16 becomes:

$$P^{(s)}\left(e\middle|\left\{E_{H,1}^{(0)},E_{H,1}^{(1)}\right\}\right)=Q\left(\sqrt{\frac{\frac{\rho_1}{2}\left\{E_{H,1}^{(0)}+E_{H,1}^{(1)}\right\}^2}{\left\{\left[\left(E_{H,1}^{(0)}+E_{H,1}^{(1)}\right)\right]+\left[\left(\frac{E_{TX_{MAI}}}{2N_f\sigma^2}\right)\sigma_{MAI}^2\right]\right\}}}\right)$$

(10.4-18)

If there is no MAI present then this expression reduces to:

$$P^{(s)}\left(e\middle|\left\{E_{H,1}^{(0)},E_{H,1}^{(1)}\right\}\right)_{No\ MAI}=Q\left(\sqrt{\left(\frac{\rho_1}{2}\left\{E_{H,1}^{(0)}+E_{H,1}^{(1)}\right\}\right)}\right)$$

(10.4-19)

To find the average SER proceed by taking the expectation of Equation 10.4-18 and Equation 10.4-19. It is noted that since the individual channels, while uncorrelated and independent, are taken from the same statistical distribution then the expectation or mean value of their squared coefficients over many instances should be the same. In fact this was

measured in the simulations and found to be true to a close approximation between different seed values. Taking the expectation of Equation 10.4-18 gives:

$$P^{(s)}(e) = P^{(s)}\left(e\middle|\left\{Expectation(E_{H,1}^{(0)}), Expectation(E_{H,1}^{(1)})\right\}\right)$$

$$= Q\left(\sqrt{\frac{\frac{\rho_1}{2}\left\{Expectation(E_{H,1}^{(0)}) + Expectation(E_{H,1}^{(1)})\right\}^2}{\left\{\left[\left(Expectation(E_{H,1}^{(0)}) + Expectation(E_{H,1}^{(1)})\right)\right] + \left[\left(\frac{E_{TX_{MAI}}}{2N_f\sigma^2}\right)\sigma_{MAI}^2\right]\right\}}}\right)$$

(10.4-20)

Where the word **Expectation** is used rather than the normal operator **E** to avoid confusion with the symbol denoting the sum of the squared values of the SV channel coefficients. Those terms where the expectation is not taken are constants for the system.

It is now noted that for the SV channel:

$$Expectation(E_{H,1}^{(0)}) = Expectation(E_{H,1}^{(1)}) = \eta$$

(10.4-21)

Using this in Equation 10.4-20 results in:

$$P^{(s)}(e) = Q\left(\sqrt{\frac{\frac{\rho_1}{2}\{2\eta\}^2}{\left\{2\eta + \left[\left(\frac{E_{TX_{MAI}}}{2N_f\sigma^2}\right)\sigma_{MAI}^2\right]\right\}}}\right)$$

(10.4-22)

When there is no MAI present this reduces to the average SER of:

$$P^{(s)}(e) = Q\left(\sqrt{\rho_1\eta}\right)$$

(10.4-23)

The probability, conditioned on an error having occurred, that there are one bit in error is two chances in three possibilities. The probability, conditioned on an error having occurred, that there are two bits in error is one chance in three possibilities. Proceeding by using the average SER, for high SNR, to determine an expression for the BER. In the presence of MAI the expression for the average BER then becomes:

$$P(e) = \left(\frac{2}{3}\right)P^{(s)}(e) + \left(\frac{1}{3}\right)\left(2P^{(s)}(e)\right) = \frac{4}{3}P^{(s)}(e) = \frac{4}{3}Q\left(\sqrt{\frac{\frac{\rho_1}{2}\{2\eta\}^2}{\left\{2\eta + \left[\left(\frac{E_{TX_{MAI}}}{2N_f\sigma^2}\right)\sigma_{MAI}^2\right]\right\}}}\right)$$

(10.4-24)

In the absence of MAI the average BER is then:

$$P(e) = \left(\frac{2}{3}\right)P^{(s)}(e) + \left(\frac{1}{3}\right)\left(2P^{(s)}(e)\right) = \frac{4}{3}P^{(s)}(e) = \frac{4}{3}Q\left(\sqrt{\rho_1\eta}\right)$$

(10.4-25)

For low SNR the BER approaches the SER. Using an expression for upper and lower bounds for the BER using an M-ary PAM system found in [68] for narrowband systems which states that the BER satisfies (where M=4):

$$\frac{P^{(S)}(e)}{M} = \frac{P^{(S)}(e)}{4} \leq P(e) \leq P^{(S)}(e) \qquad (10.4\text{-}26)$$

Considering the situation where one of the antenna branches suffers a deep fade for all its multipath it is possible to calculate the average BER, conditioned on antenna 1 suffering a deep fade, from Equation 10.4-20 as:

$$P^{(s)}(e) = P^{(s)}\left(e\middle|\left\{Expectation(E_{H,1}^{(0)}), Expectation(E_{H,1}^{(1)})\Big|_{=0}\right\}\right)$$

$$= Q\left(\sqrt{\frac{\frac{\rho_1}{2}\left\{Expectation(E_{H,1}^{(0)}) + Expectation(E_{H,1}^{(1)})\Big|_{=0}\right\}^2}{\left\{\left[\left(Expectation(E_{H,1}^{(0)}) + Expectation(E_{H,1}^{(1)})\Big|_{=0}\right)\right] + \left[\left(\frac{E_{TX_{MAI}}}{2N_f\sigma^2}\right)\sigma_{MAI}^2\right]\right\}}}\right)$$

(10.4-27)

Which reduces to:

$$P^{(s)}(e) = P^{(s)}\left(e\middle|\left\{Expectation(E_{H,1}^{(0)}),0\right\}\right)$$
$$= Q\left(\sqrt{\frac{\frac{\rho_1}{2}\left\{Expectation(E_{H,1}^{(0)})+0\right\}^2}{\left\{\left[\left(Expectation(E_{H,1}^{(0)})+0\right)\right]+\left[\left(\frac{E_{TX_{MAI}}}{2N_f\sigma^2}\right)\sigma_{MAI}^2\right]\right\}}}\right)$$

(10.4-28)

Which leads, in the presence of MAI, to a SER of:

$$P^{(s)}(e) = Q\left(\sqrt{\frac{\frac{\rho_1}{2}\{\eta\}^2}{\left\{\eta+\left[\left(\frac{E_{TX_{MAI}}}{2N_f\sigma^2}\right)\sigma_{MAI}^2\right]\right\}}}\right)$$

(10.4-29)

If MAI is not present, for a deep fade on antenna 1 (or by symmetry on antenna 0), this becomes:

$$P^{(s)}(e) = Q\left(\sqrt{\frac{\rho_1\eta}{2}}\right)$$

(10.4-30)

Using the same arguments as before to convert the average SER to average BER, again for high SNR, the average BER in the presence of a deep fade for an all rake receiver in the presence of MAI becomes:

$$P(e) = \left(\frac{2}{3}\right)P^{(s)}(e) + \left(\frac{1}{3}\right)\left(2P^{(s)}(e)\right) = \frac{4}{3}P^{(s)}(e) = \frac{4}{3}Q\left(\sqrt{\frac{\frac{\rho_1}{2}\{\eta\}^2}{\left\{\eta+\left[\left(\frac{E_{TX_{MAI}}}{2N_f\sigma^2}\right)\sigma_{MAI}^2\right]\right\}}}\right)$$

(10.4-31)

And in the absence of MAI it is:

$$P(e) = \left(\frac{2}{3}\right)P^{(s)}(e) + \left(\frac{1}{3}\right)\left(2P^{(s)}(e)\right) = \frac{4}{3}P^{(s)}(e) = \frac{4}{3}Q\left(\sqrt{\frac{\rho_1\eta}{2}}\right)$$

(10.4-32)

This is the average BER for high SNR in the presence of a deep fade on one antenna link because with the proposed system based on STS, both branches have coded into the PPM

system knowledge of the symbol transmitted. Thus it still receives at the receiver the symbol sent in the event of a deep fade on one of the antenna links with the penalty being an increase in the actual average BER for the duration of the deep fade.

10.5 The average SER versus SNR for All Rake

From measured simulated results the expected value of η for the SV channel used in our study for an all Rake was found to be 1.6145×10^{-6}. It is noted from [4] that a relationship exists between the complementary error function (*erfc*) and Q(x) defined by:

$$erfc(x) = 2Q\left(\left(\sqrt{2}\right)x\right) \tag{10.5-1}$$

Where *erfc(x)* is defined as:

$$erfc(x) \stackrel{\text{def}}{=} \frac{2}{\sqrt{\pi}} \int_x^{\infty} e^{-t^2} dt \tag{10.5-2}$$

Applying some simple algebraic manipulation one can show that:

$$Q(x) = \frac{1}{2} erfc\left(\frac{x}{\sqrt{2}}\right) \tag{10.5-3}$$

The function *erfc(x)* is provided in Mathematica 4.0, which was then used to produce the plot of the theoretical results for SER in the absence of MAI of Equation 10.4-23 as shown in Figure 10.5-1. Normalising the SNR of 54dB to be the expected SNR of 0dB. This is where this study found that its SER response for the STS-TH-UWB-PPM system is comparable to that reported for BER in Figure 2 of [8] for a UWB rake receiver using 16 fingers, reproduced in Figure 2.10-1. The SER begins to improve (so called waterfall effect) significantly in the SER versus expected SNR plot after this actual SNR of 54dB. This study does this for the no MAI case and keeps this constant for the MAI present cases. In [8] they do not provide an estimate of the channels mean energy, as defined by the expectations of Equation 10.2-10 or Equation 10.2-11, as has been done in this study. The assumption is that they also must have normalised to provide their expected SNR in their plotted results, or they used a much larger value for the channel energy than is found from our simulations (which used the same parameters used in validation against their model in Chapter 8 and which [8] stated they used). Appendix 22 shows the calculations used to plot the data of Figure 10.5-1 .

Considering the effect of MAI on the SER versus expected SNR. Defining the SNR of the MAI (assuming all MAI sources have the same expected SNR) as:

$$\rho_{mai} = \frac{\varepsilon_{mai}}{\sigma^2} = \frac{E_{TX_{MAI}} N_f}{\sigma^2}$$

(10.5-4)

Combining this with Equation 10.4-22 gives an expression for the SER in the presence of MAI as:

$$P^{(s)}(e) = Q\left(\sqrt{\frac{\frac{\rho_1}{2}\{2\eta\}^2}{\left\{2\eta + \left[\left(\frac{\rho_{mai}}{2N_f}\right)\sigma_{MAI}^2\right]\right\}}}\right)$$

(10.5-5)

In our simulations a spreading sequence length of 32 chips is used, and it was fixed to the expected SNR of the MAI at 10dB, and allow there to be five and ten interfering MAI sources. From simulations of one MAI using the developed Simulink model it was found that the interference of one MAI source had a gaussian like distribution (done over 2000 symbols, with channel varied every two symbol periods) with values oscillating around zero (mean was slightly negative at -4.1874×10^{-8}) and variance of 4.531×10^{-12}.

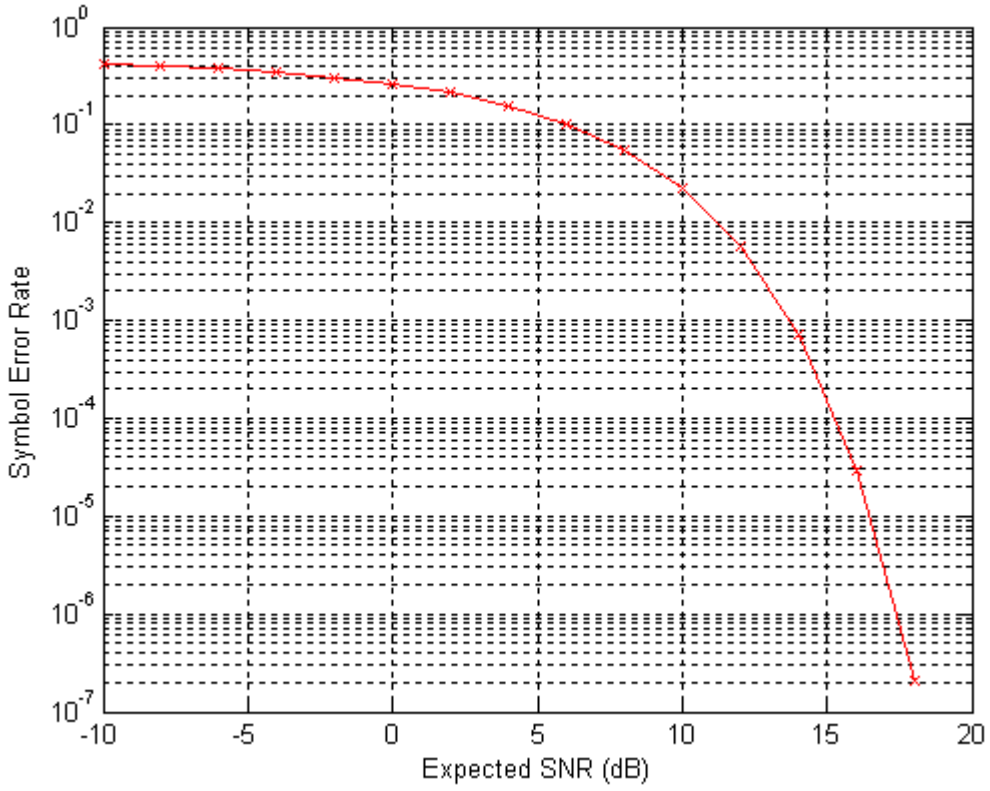

Figure 10.5-1: Symbol Error Rate versus Expected SNR (dB) for all rake of an STS-TH-UWB-PPM system.

The variance for a single source, assuming it's a zero mean gaussian, can be used to calculate the variance of five and ten MAI sources by simply multiplying it by the number of MAI sources used in the theory calculations based on the measured simulation value for one MAI source [56]. The results of the calculations involved for five and ten MAI using the formula of Equation 10.5-5 are shown in Appendix 23 and Appendix 24. These results are plotted in Figure 10.5-2 and Figure 10.5-3.

Shown in Figure 10.5-4 is a comparison of the no MAI, 5 MAI and 10 MAI for the All Rake STS-TH-UWB-PPM system with all the MAI sources being at an expected SNR of 10dB. It shows that the SER increases (and hence the BER) for high expected SNR as extra MAI sources are added. These results are a confirmation of a similar observation for the simulated systems described in Chapter 9 where the MAI were also randomly moved uniformly over a chip period of time with overlapping TH patterns.

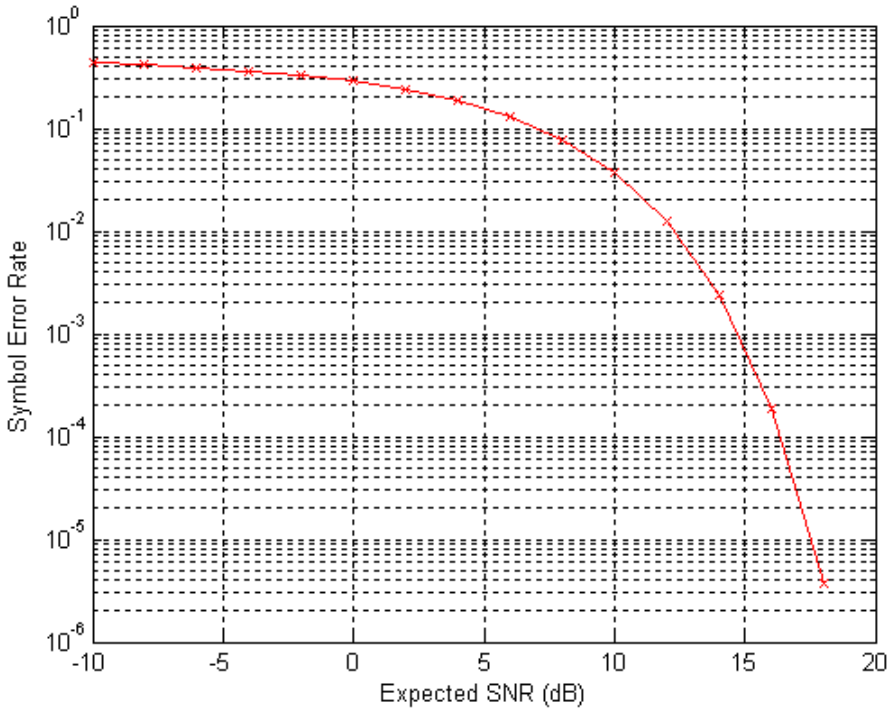

Figure 10.5-2: Symbol Error Rate versus Expected SNR (dB) for all rake in the presence of 5 MAI sources with expected SNR of 10dB of an STS-TH-UWB-PPM system.

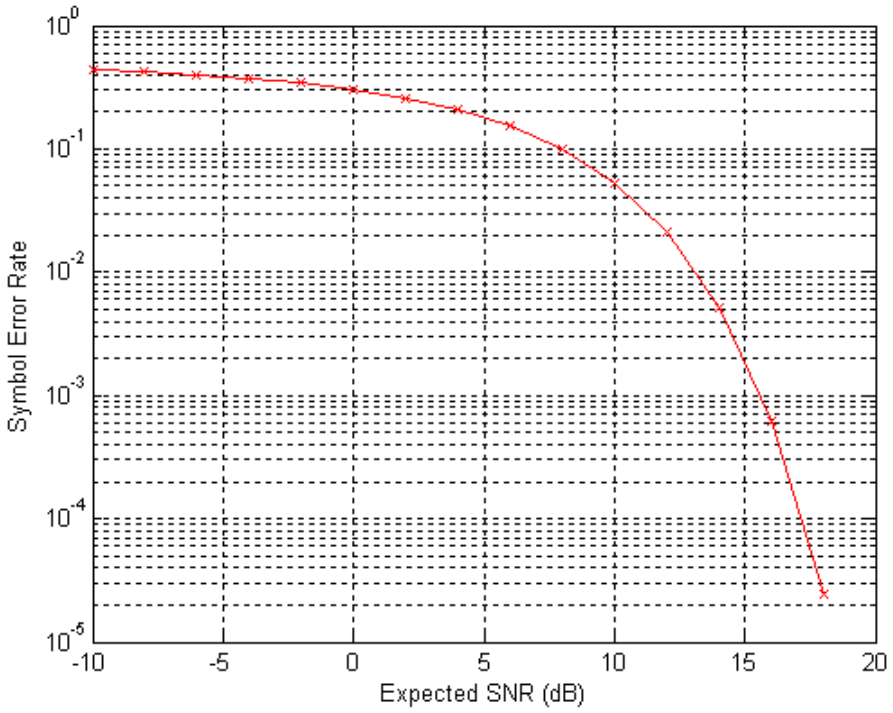

Figure 10.5-3: Symbol Error Rate versus Expected SNR (dB) for all rake in the presence of 10 MAI sources with expected SNR of 10dB of an STS-TH-UWB-PPM system.

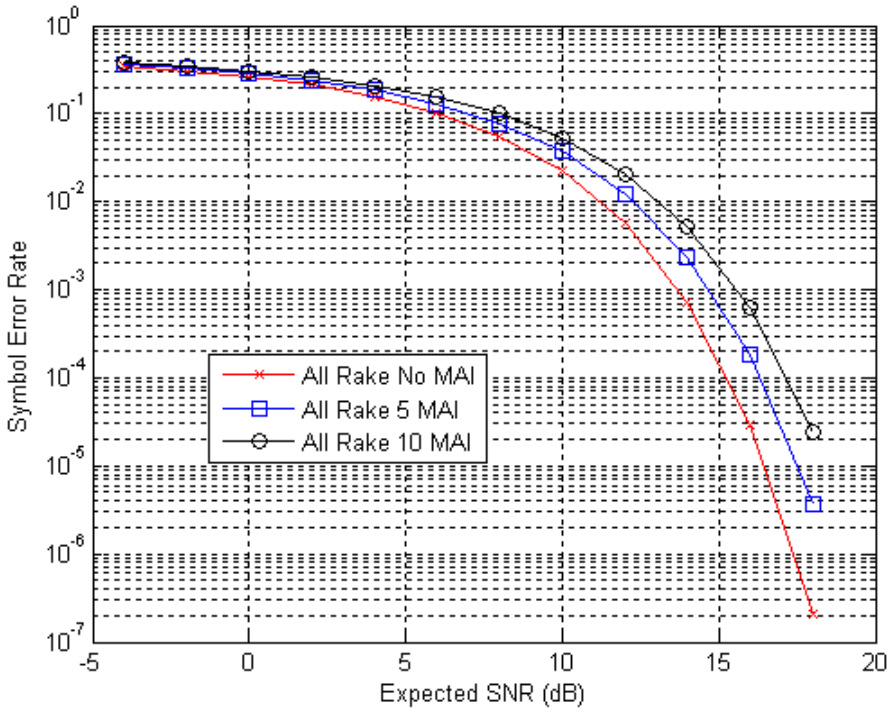

Figure 10.5-4: Symbol Error Rate versus Expected SNR (dB) for all rake in the presence of no MAI, 5 MAI and 10 MAI sources with expected SNR of 10dB of an STS-TH-UWB-PPM system.

10.6 Conclusion

This chapter has presented the analysis of the STS-TH-UWB-PPM proposed system in the presence of MAI. An expression for the SER and for the BER at high expected SNR was provided. It confirmed the measured simulation results obtained in Chapter 9 which showed that the STS-TH-UWB-PPM system is affected by the presence of MAI when the TH patterns overlay in an asynchronous manner. The calculations based on the theoretical formula derived for the system under the assumption that MAI appears to be zero mean gaussian interference has verified the observed simulated study which examined the system in the presence of MAI performed in Chapter 9. Chapter 11 concludes the thesis and provides some areas of future research.

Chapter 11: Conclusion

11.1 Introduction

This thesis started with the question of how to use space diversity, using multiple antennas or MIMO, in a system that uses TH UWB PPM. An investigation was conducted on an implementation of a STS and the effects of MAI on such systems, showing how to mitigate against the MAI by using low correlation codes. Attention was then turned to the development of an UWB PPM simulation and this simulation was used to develop a proposed approach to providing a MIMO system in an UWB PPM TH physical wireless communication link. This concluding chapter will consider all of the contributions which have been outlined and investigated in this thesis. It will look at the significant contributions that this thesis has made in the area of UWB PPM MIMO systems and then outline future areas of possible research.

11.2 Significant Contributions of the thesis

This study looked at the application of the STS technique proposed in [9] to a two transmit, single receiver antenna wireless physical layer application using a TH UWB PPM system. In Chapter 1 the research question was asked how to transmit two symbols using two transmit antennas (MIMO) in the same time that a system with one transmit antenna (SISO) would transmit one symbol when using an Ultra Wideband PPM based transmission mechanism (that is a series of baseband pulses with ultra large bandwidth). The question also asked is how to do this without causing significant degradation of the performance compared to a single antenna system. The contributions of the thesis were outlined in developing tools (simulations) which helped us to answer this question by investigating the performance of systems developed along the way. This was the methodology this study adopted. This same methodology was adopted in similar studies such as the original STS study in [9] and the Analog Ultra Wideband systems proposed by Yang in [8]. Proceeding by examining, once again, the systems developed in this study. Aiming to highlight their importance in answering the primary research question which forms the significant contribution of this thesis to

literature. It is emphasized that the work provided in this dissertation has been peer reviewed and the list of peer reviewed publications was provided at the front of this thesis (page vi). The simulations provided in this thesis were validated against peer reviewed publications three different times, once for the original STS simulations and twice for the UWB PPM (once for the SISO and the MIMO UWB PPM simulations). Using these foundations the thesis proceeded to provide an answer to its research questions. In Chapter 2 a review was provided of the available literature concerning the analysis of MIMO systems and in particular on the STS technique as well as on UWB PPM systems and their implementations in simulation studies.

In Chapter 3 Simulink was used to develop a simulation of a Space Time Spreading MIMO system which was validated against simulation results found in [9]. Results were shown for two, four and eight antenna systems in terms of their BER performance. It was in developing these systems, followed by studying UWB PPM systems, that the genesis for the application of STS to form a MIMO UWB PPM system was formed. It is well known that spread spectrum systems suffer from MAI when the codes are mis-aligned [69;70], so in Chapter 4 a study into the effect of MAI using Walsh Hadamard spreading sequences was undertaken and it found that a significant degradation in BER performance was observed. Spreading sequences were then used which, while still orthogonal, were known to have improved cross-correlation properties and showed that it could improve the BER performance of our STS system if the Walsh-Hadamard sequences were replaced with the low cross correlation codes (Wysocki spreading sequences found in [61]). While these two chapters did not answer the primary research question, they provided the background necessary to setup the proposed solution in later chapters. They also were a significant contribution in that a simulation, validated against original work, was produced using Simulink and using this simulation it was shown how STS could suffer from MAI and how use of a low cross-correlation spreading sequence can mitigate against the degradation caused in BER performance as a result.

In Chapter 5 a UWB PPM system was implemented in Simulink. The Saleh-Valenzuela multipath channel described in [7] was used, using the same statistical channel parameters assigned in [8]. The Simulink SISO UWB PPM system was validated against the

corresponding BER performance provided in [8]. Thus Chapter 5 presented the development and validation of a Simulink simulation of the UWB PPM wireless communication link. A situation was also found, while checking the no noise simulation, that the chosen simulations channel model can induce errors and it was demonstrated the mechanism that causes these errors (see Section 5.5).

In Chapter 6 a technique for SISO transmission was proposed that uses the STS technique but applies it to three pulse positions. It is here that it is first observed that the STS system at the physical wireless layer presents discrete values of -2, 0, and 2 which can be used to model by the position of individual pulses in our UWB PPM. The Simulink simulation was also modified so that it used a fixed Time Hopping pattern, allowing for smoothing of the UWB spectral footprint and for the possibility of multiple uses (using different Time Hopping patterns). It was shown that the system improved its BER performance when using the three pulse positions applying a STS based system which this thesis named DS-modified-TH-UWB-PPM. It was also noted that this system transmits two symbols in the same time that the two pulse position system transmits one symbol. Chapter 2 considered M-ary PPM, where it was found that four pulse positions to represent two symbols, assuming that a pulse is always transmitted (see page 45). The system proposed and investigated in Chapter 6 only required three pulse positions. It was shown that this performance improvement in a channel that was initially optimised to choose paths which were separated from other multipath by at least one nanosecond, which for three pulse positions should have been changed to two nanoseconds (ie to optimise for the use of three pulse positions). This change was not done to the channel data so a comparison in performance could be made even when the proposed three pulse system was disadvantaged. In fact, the same channel coefficients are used in all the UWB PPM system simulations from Chapter 5 onwards.

In Chapter 7 a MIMO three pulse position system was proposed that used two transmit antennas and one receive antenna. The system proposed was non-optimal in that the receiver made a decision on a chip by chip basis, essentially losing most of the information contained in perfect knowledge of the channels coefficients (CSI). It was compared to the corresponding SISO based system and found to have a poorer BER performance. However, it was noted that it transmitted two symbols in the same time that the SISO system transmitted

one symbol. Its receiver is also simpler to design (no need to store all the information about each received chip of a full spreading code before making a hard decision). This simplicity of the receiver design is then traded off against the poorer BER performance that results. This system does provide an answer to the first part of our research question: it shows that it is possible to use two transmit antennas with direct sequence spreading codes to transmit two symbols in the same time an equivalent SISO system transmits one. Its disadvantage is that it does so in a way which does result in noticeable degradation of the BER performance of the system.

In Chapter 8 the TH-UWB-PPM simulator was modified to implement the MIMO Analog ST Type I schema proposed in [8] and it showed similar BER performance to that reported in [8]. Thus the MIMO simulation of the UWB PPM system was validated. The STS-TH-UWB-PPM system was simulated which used all of the CSI information over the 32 chips of one transmission period (in which it transmitted two symbols in the same time that the MIMO Analog ST Type I schema transmitted one symbol). The BER performance was compared on a branch basis, given that the STS schema transmits two symbols on each antenna, allowing for the recovery of both symbols even if a major fade occurs on one of the antenna branches, at the cost of an increase in BER performance. It was shown that this system can transmit the two symbols without degrading the BER performance experienced across the wireless channel. The system proposed and investigated in Chapter 8 answers both parts of our primary research question. That is the two transmit antennas were successfully used to transmit two symbols across the wireless communications link in a TH UWB PPM system, and it was done in such a way as to not degrade the performance compared to the SISO equivalent system. This is the major contribution of this dissertation.

In Chapter 9 the effect of MAI on the system proposed and investigated in Chapter 8 was investigated. MAI was simulated that overlapped with the target system within a 100ns time window, and with a Time Hopping pattern for the interfering MAI which ensured that this overlapping was guaranteed to occur. It was found that when there was only one MAI present the proposed system exhibited no significant degradation in BER performance. When five and ten MAI sources were introduced each with a E_b/N_o of +3.15dB, it was found that BER performance for the target STS-TH-UWB-PPM system was significantly impacted. Using the

same set of low correlation codes used in Chapter 4 it was found there was no significant improvement over using the Walsh-Hadamard spreading sequences, and in fact the Walsh Hadamard sequences provided better BER performance. This is attributed to the fact the properties of these low correlation spreading codes are calculated on chip delays against every other member of the spreading sequence code family. In the STS technique proposed in Chapter 8 each communication link requires two synchronised spreading codes. It may be that a criterion that optimises the cross-correlation between pairs of spreading codes needs to be found. The use of three other spreading sequences sets was investigated and it was found that the worst BER performance was observed when using the h32dash03 randomly selected sequence set. The Wysocki spreading sequence showed significant improvement in BER performance when compared to the h32dash03 spreading sequence set BER performance for high Eb/No. The Walsh Hadamard, w32dash03 and Orthogonal Gold spreading sequence sets had comparable BER performance with a marginal improvement observed for the two low correlation codes for most of the measured E_b/N_o values observed.

In Chapter 10 the proposed system of Chapter 8 was analysed with and without the presence of MAI sources. This chapter provided an analytical expression for the average BER as a function of average SNR with and without the presence of MAI sources. It was also shown that should there be a major fade on one of the two antennas links that both transmitted bits can still be recovered at the expense of a higher average BER. It then compared the derived expression for average BER versus expected SNR to similar plotted results found in [8] (see page 196). These theoretical results were then graphed in terms of average SER versus expected SNR.

11.3 Future Work

From the results for STS-TH-UWB-PPM systems in the presence of MAI using different spreading sequence sets with low correlation as presented in Chapter 9 there was some marginal improvement in BER performance for some of the low correlation spreading sequence codes. These low correlation spreading sequence code sets were chosen on the basis of cross correlation and auto correlation between individual members of the spreading code sequence set. In the case of STS based systems it is required that each STS user must utilise two orthogonal spreading sequences. Thus each of the pairs of spreading sequences used will

be orthogonal to each other and induce no MAI for a single user. The MAI of interest is that caused between pairs of spreading sequences. Thus a new criteria needs to be developed which minimises the cross correlation and auto correlation between pairs of spreading sequences rather than between individual spreading sequences. This could be done by starting with the identified low correlation spreading codes and the Walsh Hadamard spreading codes, finding the best eleven orthogonal spreading sequence sets (possibly by brute force techniques) and then investigating if the simulator in the study shows any improvement in BER performance.

As a large percentage of the total received UWB PPM signal energy of a SV channels' resolvable multipath rays arrive, on average, in the first 50ns (especially for the case where one uses a Partial Rake receiver structure) there is no reason that the energy collected using the receivers signal template could be collected on a 50ns boundary and then recombined later at the symbol decoder. This system may possibly have a worse BER performance as it may be more likely that the MAI channels have signal energy components in the same small time epochs. It would thus be interesting to modify the Simulink simulations of this study so that the energy is collected at these 50ns boundaries while allowing all channels to span the existing 100ns time frame. This may also have the advantage of being slightly more realistic as the length of the channels multipath can in some situations (for example in a metal vessel such as a Submarine or Aircraft Carrier) exceed 100ns. It should be noted that the SV study on which the channel model was based was done in office buildings as described in Section 2.11 with channel characteristics of about 50-100ns in most cases.

The original study reported by Saleh and Valenzuela [7] on the SV channel model used polarised antennas. A technique has recently been suggested that is able to allow polarised diversity to be harnessed. This study used the theory of Quaternions [71] orthogonal designs to show how to use polarised antennas to obtain diversity across a wireless channel. It may be possible to combine the theory of Quaternions with two dual polarised antennas in an UWB system to achieve an increased diversity effect over the UWB channel. This, however, would require a major modification to the models used in the Simulink simulations and further development of theoretical considerations to the polarisation of the UWB signals.

The Simulink simulation was designed to be adaptable to different channel models and different pulse shapes for the UWB PPM system. Volterra series could be used to model non-linear systems and it may be possible to adapt the Simulink simulator to investigate the use of Volterra series in modeling the effects of different pulse shapes. It also is possible to adapt the simulator to use different channel models for different wireless scenarios such as those proposed in the various IEEE working groups on the application of UWB channels in different wireless environments (see [44]). The system modelled here was based on a non-line of sight model for the communications channel, however the Simulation could be adapted to incorporate UWB line of sight models and study the effects of MAI in such systems.

It is known that, at the expense of increased latency, use of Gallagher or Turbo codes can improve significantly the average BER performance as shown in [64] for wideband STS. The Simulink simulation combined with a turbo code could be used to investigate the possible improvement in average BER.

This study looks at a system which is based on pico-cellular scenarios. The doppler effect, which would effect results, is not considered as all mobile devices are considered to be stationary between the receiver and the transmitter. This is in agreeance with the model used for the UWB channel by Saleh-Valenzuela who formed their statistical model in a typical office location [7].

References

[1] Liberti and Rappaport, *Smart Antennas for wireless communications: IS-95 and Third Generation CDMA Applications* Prentice Hall, Communications Engineering and Emerging Technologies, 1999.

[2] J. G. Proakis, *Digital Communications*, 4 ed McGraw-Hill, 2001.

[3] T. S. Rappaport, *Wireless Communications: Principles and Practice*, 2 ed Prentice Hall, 2002.

[4] Sergio Verdu, *Multiuser Detection*, 1 ed Cambridge Press, 1998.

[5] Rooyen, Lotter, and Wyk, *Space Time Processing for CDMA Mobile Communications* Kluwer, International Series in Engineering and Computer Science, 2000.

[6] N. J. August and S. H. Dong, "Operation, system architectures, and physical Layer design considerations of distributed MAC protocols for UWB," *Microwave Theory and Techniques, IEEE Transactions on*, vol. 54, no. 7, pp. 3001-3012, 2006.

[7] A. Saleh and R. Valenzuela, "A Statistical Model for Indoor Multipath Propagation," *Selected Areas in Communications, IEEE Journal on*, vol. 5, no. 2, pp. 128-137, 1987.

[8] Y. Liuqing and G. B. Giannakis, "Analog space-time coding for multiantenna ultra-wideband transmissions," *Communications, IEEE Transactions on*, vol. 52, no. 3, pp. 507-517, 2004.

[9] B. Hochwald, T. L. Marzetta, and C. B. Papadias, "A transmitter diversity scheme for wideband CDMA systems based on space-time spreading," *Selected Areas in Communications, IEEE Journal on*, vol. 19, no. 1, pp. 48-60, 2001.

[10] G. Ganesan and P. Stoica, "Space-time block codes: a maximum SNR approach," *Information Theory, IEEE Transactions on*, vol. 47, no. 4, pp. 1650-1656, 2001.

[11] Geramita and J. R. Seberry, *Orthogonal Designs: Quadratic Forms and Hadamard Matrices, Lecture Notes in Pure and Applied Mathematics volume 43* Marcel Dekker Inc New York and Basel, 1979.

[12] V. Tarokh, H. Jafarkhani, and A. R. Calderbank, "Space-time block codes from orthogonal designs," *Information Theory, IEEE Transactions on*, vol. 45, no. 5, pp. 1456-1467, 1999.

[13] H. Jafarkhani, "A quasi-orthogonal space-time block code," *Communications, IEEE Transactions on*, vol. 49, no. 1, pp. 1-4, 2001.

[14] S. M. Alamouti, "A simple transmit diversity technique for wireless communications," *Selected Areas in Communications, IEEE Journal on*, vol. 16, no. 8, pp. 1451-1458, 1998.

[15] J. K. Cavers, "An analysis of pilot symbol assisted modulation for Rayleigh fading channels [mobile radio]," *Vehicular Technology, IEEE Transactions on*, vol. 40, no. 4, pp. 686-693, 1991.

[16] S. Sampei and T. Sunaga, "Rayleigh fading compensation method for 16QAM in digital land mobile radio channels," *in Conference Proceedings of the 39th IEEE Vehicular Technology Conference,* San Francisco,CA,USA, vol. 2,pp. 640-646,May 1989.

[17] A. Wittneben, "Basestation modulation diversity for digital simulcast," *in Conference Proceedings of the 41st IEEE Vehicular Technology Conference,* St.Louis, MO,USA,pp. 848-853,May 1991.

[18] A. Wittneben, "A new bandwidth efficient transmit antenna modulation diversity scheme for linear digital modulation," *in Conference Proceedings of IEEE International Conference on Communications, 1993 (ICC 93),* Geneva, Switzerland, vol. 3,pp. 1630-1634,May 1993.

[19] N. Seshadri and J. H. Winters, "Two signaling schemes for improving the error performance of frequency-division-duplex (FDD) transmission systems using transmitter antenna diversity," *in Conference Proceedings of the 43rd IEEE Vehicular Technology Conference,* Secaucus, NJ, USA,pp. 508-511,May 1993.

[20] J. H. Winters, "The diversity gain of transmit diversity in wireless systems with Rayleigh fading," *in Conference Proceedings of IEEE International Conference on Communications, 1994 (SUPERCOMM/ICC '94),* New Orleans, LA, USA, vol. 2,pp. 1121-1125,May 1994.

[21] V. Weerackody, "Diversity for the direct-sequence spread spectrum system using multiple transmit antenna," *AT&T Technical Memo*, 1993.

[22] H. Huang, "Increasing IS-95 downlink capacity with transmit and receive diversity," *Bell Labs Tech Memo*, 1997.

[23] K. Rohani and L. Jalloul, "Orthogonal transmit diversity for direct spread CDMA," *in Conference Proceedings of ETSI SMG2,* Stockholm, Sweden,Sept. 1997.

[24] K. Rohani, M. Harrison, and K. Kuchi, "A comparison of base station transmit diversity methods for third generation cellular standards," *in Conference Proceedings of the 49th IEEE Vehicular Technology Conference,* Houston, Texas, USA, vol. 1,pp. 351-355,May 1999.

[25] A. Stamoulis, L. Zhiqiang, and G. B. Giannakis, "Space-time block-coded OFDMA with linear precoding for multirate services," *Signal Processing, IEEE Transactions on*, vol. 50, no. 1, pp. 119-129, 2002.

[26] X. Hao, V. Kukshya, and T. S. Rappaport, "Spatial and temporal characteristics of 60-GHz indoor channels," *Selected Areas in Communications, IEEE Journal on*, vol. 20, no. 3, pp. 620-630, 2002.

[27] B. M. Hochwald and T. L. Marzetta, "Unitary space-time modulation for multiple-antenna communications in Rayleigh flat fading," *Information Theory, IEEE Transactions on*, vol. 46, no. 2, pp. 543-564, 2000.

[28] B. Hochwald, T. Marzetta, and C. Papadias, "A novel space time spreading scheme for wireless CDMA systems," *in Conference Proceedings of the 37th Annual Allerton Conference on Communications and Computing,* Monticello, IL, USA,Sept. 1999.

[29] T. L. Marzetta and B. M. Hochwald, "Capacity of a mobile multiple-antenna communication link in Rayleigh flat fading," *Information Theory, IEEE Transactions on*, vol. 45, no. 1, pp. 139-157, 1999.

[30] V. Tarokh, N. Seshadri, and A. R. Calderbank, "Space-time codes for high data rate wireless communication: performance criterion and code construction," *Information Theory, IEEE Transactions on*, vol. 44, no. 2, pp. 744-765, 1998.

[31] V. Tarokh, A. Naguib, N. Seshadri, and A. R. Calderbank, "Combined array processing and space-time coding," *Information Theory, IEEE Transactions on*, vol. 45, no. 4, pp. 1121-1128, 1999.

[32] R. Kohno, H. Imai, M. Hatori, and S. Pasupathy, "Combinations of an adaptive array antenna and a canceller of interference for direct-sequence spread-spectrum multiple-access system," *Selected Areas in Communications, IEEE Journal on*, vol. 8, no. 4, pp. 675-682, 1990.

[33] A. F. Naguib, A. Paulraj, and T. Kailath, "Capacity improvement with base-station antenna arrays in cellular CDMA," *Vehicular Technology, IEEE Transactions on*, vol. 43, no. 3, pp. 691-698, 1994.

[34] A. J. Paulraj and C. B. Papadias, "Space-time processing for wireless communications," *Signal Processing Magazine, IEEE*, vol. 14, no. 6, pp. 49-83, 1997.

[35] D. Gerlach and A. Paulraj, "Adaptive transmitting antenna arrays with feedback," *Signal Processing Letters, IEEE*, vol. 1, no. 10, pp. 150-152, 1994.

[36] G. G. Raleigh, S. N. Diggavi, V. K. Jones, and A. Paulraj, "A blind adaptive transmit antenna algorithm for wireless communication," *in Conference Proceedings of IEEE International Conference on Communications, 1995 (ICC '95),* Seattle, WA, USA, vol. 3,pp. 1494-1499,June 1995.

[37] F. Rashid-Farrokhi and L. Tassiulas, "Power control and space-time diversity for CDMA systems," *in Conference Proceedings of IEEE Global Telecommunications Conference, 1998 (GLOBECOM '98),* Sydney, Australia, vol. 4,pp. 2134-2140,November 1998.

[38] P. Ligdas and N. Farvadin, "Optimizing the transmit power for slow fading channels," *Information Theory, IEEE Transactions on*, vol. 46, no. 2, pp. 565-576, 2000.

[39] R. A. Soni, R. M. Buchrer, and T. Jiann, "Open-loop transmit diversity in IS-20000 systems," *in Conference Proceedings of the Thirty-Third Asilomar Conference on Signals, Systems, and Computers,* Pacific Grove, CA, USA, vol. 1,pp. 654-658,October 1999.

[40] H. Jafarkhani and V. Tarokh, "Multiple transmit antenna differential detection from generalized orthogonal designs," *Information Theory, IEEE Transactions on*, vol. 47, no. 6, pp. 2626-2631, 2001.

[41] P. Li, "A combined OFDM-CsDMA approach to cellular mobile communications," *Communications, IEEE Transactions on*, vol. 47, no. 7, pp. 979-982, 1999.

[42] S. Madden, R. Szewczyk, M. J. Franklin, and D. Culler, "Supporting aggregate queries over ad-hoc wireless sensor networks," *in Conference Proceedings of the 4th IEEE Workshop on Mobile Computing Systems and Applications,* Callicoon, New York, USA,pp. 49-58,June 2002.

[43] Oppermann, Hamalainen, and linatti, *UWB: Theory and application* Wiley, 2005.

[44] Di Benedetto and Giancola, *Understanding Ultra Wide Band: Radio Fundamentals* Prentice Hall, Communications Engineering and Emerging Technologies, 2004.

[45] R. Harjani, J. Harvey, and R. Sainati, "Analog/RF physical layer issues for UWB systems," *in Conference Proceedings of the 17th International Conference on VLSI Design, IEEE Computer Society,* Mumbai, India,pp. 941-948,January 2004.

[46] M. Speth, S. A. Fechtel, G. Fock, and H. Meyr, "Optimum receiver design for wireless broad-band systems using OFDM. I," *Communications, IEEE Transactions on*, vol. 47, no. 11, pp. 1668-1677, 1999.

[47] Y. Lie-Liang and L. Hanzo, "Residue number system assisted fast frequency-hopped synchronous ultra-wideband spread-spectrum multiple-access: a design alternative to impulse radio," *Selected Areas in Communications, IEEE Journal on*, vol. 20, no. 9, pp. 1652-1663, 2002.

[48] D. Gerakoulis and P. Salmi, "Link performance of an ultra wide bandwidth wireless in-home network," *in Conference Proceedings of the 7th International Symposium on Computers and Communications,* Taormina-Giardini Naxos, Italy,pp. 699-704,July 2002.

[49] Y. Liuqing and G. B. Giannakis, "Ultra-wideband communications: an idea whose time has come," *Signal Processing Magazine, IEEE*, vol. 21, no. 6, pp. 26-54, 2004.

[50] A. Mehbodniya and S. Aissa, "Coexistence Between DS-UWB and MB-OFDM: Analysis and Interference Mitigation," *in Conference Proceedings of IEEE Global Telecommunications Conference 2007 (GLOBECOM '07),* Washington, DC, USA,pp. 5200-5204,November 2007.

[51] F. Ramirez-Mireles, "Performance of ultrawideband SSMA using time hopping and M-ary PPM," *Selected Areas in Communications, IEEE Journal on*, vol. 19, no. 6, pp. 1186-1196, 2001.

[52] N. J. August, L. Hyung-Jin, and D. S. Ha, "An efficient multi-user UWB receiver for distributed medium access in ad hoc and sensor networks," *in Conference Proceedings of IEEE Radio and Wireless Conference,* Atlanta, Georgia, USA,pp. 455-458,September 2004.

[53] "Personal Communication in Wireless Winter School,ACORN,Australian National University, Canberra, Australia,July 2005," 2005.

[54] D. Cassioli, M. Z. Win, F. Vatalaro, and A. F. Molisch, "Performance of low-complexity RAKE reception in a realistic UWB channel," *in Conference Proceedings of the IEEE International Conference on Communications 2002 (ICC 2002),* New York, NY, USA, vol. 2,pp. 763-767,April 2002.

[55] M. C. Jeruchim, P. Balaban, and K. S. Shanmugan, *Simulation of Communication Systems: Modeling, Methodology and Techniques* Kluwer, 2000.

[56] Papoulis and Athanasios, *Probability, Random Variables, and Stochastic Processes*, 3 ed McGraw Hill International Editions, 1991.

[57] R. Scholtz, "Multiple access with time-hopping impulse modulation," *in Conference Proceedings of the IEEE Military Communications Conference 1993 (MILCOM '93),* Boston, MA, USA, vol. 2,pp. 447-450,October 1993.

[58] J. D. Choi and W. E. Stark, "Performance of ultra-wideband communications with suboptimal receivers in multipath channels," *Selected Areas in Communications, IEEE Journal on*, vol. 20, no. 9, pp. 1754-1766, 2002.

[59] L. Hojoon, H. Byungchil, S. Yoan, and I. Sungbin, "Multipath characteristics of impulse radio channels," *in Conference Proceedings of the 51st IEEE Vehicular Technology Conference,* Tokyo, Japan, vol. 3,pp. 2487-2491,May 2000.

[60] J. Fuhl, A. F. Molisch, and E. Bonek, "Unified channel model for mobile radio systems with smart antennas," *Radar, Sonar and Navigation, IEE Proceedings* -, vol. 145, no. 1, pp. 32-41, 1998.

[61] B. Wysocki and T. Wysocki, "Modified Walsh-Hadamard sequences for DS CDMA wireless systems," *International Journal of Adaptive Control and Signal Processing*, vol. 16, pp. 589-602, 2002.

[62] R. A. Soni and R. M. Buehrer, "On the performance of open-loop transmit diversity techniques for IS-2000 systems: a comparative study," *Wireless Communications, IEEE Transactions on*, vol. 3, no. 5, pp. 1602-1615, 2004.

[63] J. D. Choi and W. E. Stark, "Performance analysis of RAKE receivers for ultra-wideband communications with PPM and OOK in multipath channels," *in Conference Proceedings of the IEEE International Conference on Communications 2002 (ICC 2002),* New York, NY, USA, vol. 3,pp. 1969-1973,April 2002.

[64] I. S. Raad, P. J. Vial, and T. A. Wysocki, "A study of Turbo Codes across Space Time Spreading Channel," *in Conference Proceedings of the 14th International Czech - Slovak Scientific Conference,* Bratislava, Slovak Republic,pp. 64-67,April 2004.

[65] J. Oppermann and B. S. Vucetic, "Complex spreading sequences with a wide range of correlation properties," *Communications, IEEE Transactions on*, vol. 45, no. 3, pp. 365-375, 1997.

[66] J. R. Seberry, B. Wysocki, and T. Wysocki, "Performance Comparison of Sequences designed from the Hall Difference Set and Orthogonal Gold Sequences of Length 32," *in Conference Proceedings of the 8th International Symposium on Communication Theory and Applications (ISCTA'05),* United Kingdom,pp. 104-107, 2005.

[67] K. Popovski, B. Wysocki, and T. Wysocki, "Modelling and Comparative Performance Analysis of a Time-Reversed UWB System," *EURASIP Journal on Wireless Communications and Networking*, 2007.

[68] S. Benedetto, E. Biglieri, and V. Castellani, *Digital Transmission Theory*, 1 ed. Turin: Prentice Hall International, 1987, p. 639.

[69] M. Pursley, "Performance Evaluation for Phase-Coded Spread-Spectrum Multiple-Access Communication--Part I: System Analysis," *Communications, IEEE Transactions on*, vol. 25, no. 8, pp. 795-799, 1977.

[70] M. Pursley and D. Sarwate, "Performance Evaluation for Phase-Coded Spread-Spectrum Multiple-Access Communication--Part II: Code Sequence Analysis," *Communications, IEEE Transactions on*, vol. 25, no. 8, pp. 800-803, 1977.

[71] J. Seberry, K. Finlayson, S. S. Adams, T. A. Wysocki, X. Tianbing, and B. J. Wysocki, "The Theory of Quaternion Orthogonal Designs," *Signal Processing, IEEE Transactions on*, vol. 56, no. 1, pp. 256-265, 2008.

[72] Golub and Loan, *Matrix Computations* John Hopkins University Press, 1996.

[73] Y. Liuqing and G. B. Giannakis, "Space-time coding for impulse radio," *in Conference Proceedings of the IEEE Conference on Ultra Wideband Systems and Technologies,* Wyndham Baltimore Inner Harbour, USA,pp. 235-239,May 2002.

[74] M. Z. Win and R. A. Scholtz, "On the energy capture of ultrawide bandwidth signals in dense multipath environments," *Communications Letters, IEEE*, vol. 2, no. 9, pp. 245-247, 1998.

[75] Z. Fang, W. Zhiqiang, and C. R. Nassar, "Generalized fading channel model with application to UWB," *in Conference Proceedings of the IEEE Conference on Ultra Wideband Systems and Technologies,* Wyndham Baltimore Inner Harbour, USA,pp. 13-17,May 2002.

[76] A. Muqaibel, A. Safaai-Jazi, B. Woerner, and S. Riad, "UWB channel impulse response characterization using deconvolution techniques," *in Conference Proceedings of the 45th Midwest Symposium on Circuits and Systems 2002 (MWSCAS-2002),* Tulsa, Oklahoma,USA, vol. 3,p. III-8,August 2002.

[77] W. Di, P. Spasojevic, and I. Seskar, "Multipath beamforming for UWB: channel unknown at the receiver," *in Conference Proceedings of the 36th Asilomar conference on Signals, Systems and Computers,* Pacific Grove, Califomia,USA, vol. 1,pp. 599-603,November 2002.

[78] T. Zhi, Y. Liuqing, and G. B. Giannakis, "Symbol timing estimation in ultra wideband communications," *in Conference Proceedings of the 36th Asilomar conference on Signals, Systems and Computers,* Pacific Grove, Califomia,USA, vol. 2,pp. 1924-1928,November 2002.

[79] R. A. Scholtz and L. Joon-Yong, "Problems in modeling UWB channels," *in Conference Proceedings of the 36th Asilomar conference on Signals, Systems and Computers,* Pacific Grove, Califomia,USA, vol. 1,pp. 706-711,November 2002.

[80] J. Keignart and N. Daniele, "Subnanosecond UWB channel sounding in frequency and temporal domain," *in Conference Proceedings of the IEEE Conference on Ultra Wideband Systems and Technologies,* Wyndham Baltimore Inner Harbour, USA,pp. 25-30,May 2002.

[81] L. Ray-Rong, T. Jenn-Hwan, and H. Chiuder, "Transmission coefficients measurement of building materials for UWB systems in 3 -10 GHz," *in Conference Proceedings of the 57th IEEE Semiannual Vehicular Technology Conference 2003 (VTC 2003-Spring),* Jeju, Korea, vol. 1,pp. 11-14,April 2003.

[82] B. Denis and J. Keignart, "Post-processing framework for enhanced UWB channel modeling from band-limited measurements," *in Conference Proceedings of the IEEE Conference on Ultra Wideband Systems and Technologies,* Reston, Virginia, USA,pp. 260-264,November 2003.

[83] S. S. Ghassemzadeh, R. Jana, C. W. Rice, W. Turin, and V. Tarokh, "A statistical path loss model for in-home UWB channels," *in Conference Proceedings of the IEEE Conference on Ultra Wideband Systems and Technologies,* Wyndham Baltimore Inner Harbour, USA,pp. 59-64,May 2002.

[84] C. Prettie, D. Cheung, L. Rusch, and M. Ho, "Spatial correlation of UWB signals in a home environment," *in Conference Proceedings of the IEEE Conference on Ultra Wideband Systems and Technologies,* Wyndham Baltimore Inner Harbour, USA,pp. 65-69,May 2002.

[85] T. B. Welch, R. L. Musselman, B. A. Emessiene, P. D. Gift, D. K. Choudhury, D. N. Cassadine, and S. M. Yano, "The effects of the human body on UWB signal propagation in an indoor environment," *Selected Areas in Communications, IEEE Journal on*, vol. 20, no. 9, pp. 1778-1782, 2002.

[86] M. Z. Win and R. A. Scholtz, "On the robustness of ultra-wide bandwidth signals in dense multipath environments," *Communications Letters, IEEE*, vol. 2, no. 2, pp. 51-53, 1998.

[87] L. Joon-Yong and R. A. Scholtz, "Ranging in a dense multipath environment using an UWB radio link," *Selected Areas in Communications, IEEE Journal on*, vol. 20, no. 9, pp. 1677-1683, 2002.

[88] N. Boubaker and K. B. Letaief, "A low complexity MMSE-RAKE receiver in a realistic UWB channel and in the presence of NBI," *in Conference Proceedings of the IEEE Wireless Communications and Networking Conference 2003 (WCNC 2003),* New Orleans, LA, USA , vol. 1,pp. 233-237,March 2003.

[89] M. Z. Win and R. A. Scholtz, "Characterization of ultra-wide bandwidth wireless indoor channels: a communication-theoretic view," *Selected Areas in Communications, IEEE Journal on*, vol. 20, no. 9, pp. 1613-1627, 2002.

[90] T. Taniguchi and T. Kobayashi, "An omnidirectional and low-VSWR antenna for the FCC-approved UWB frequency band," *in Conference Proceedings of the IEEE Antennas and Propagation Society International Symposium,* Columbus, Ohio,USA, vol. 3,pp. 460-463,June 2003.

[91] T. Taniguchi and T. Kobayashi, "An omnidirectional and low-VSWR antenna for ultra-wideband wireless systems," *in Conference Proceedings of the IEEE Radio and Wireless Conference 2002 (RAWCON 2002),* Boston, Massachusetts,USA,pp. 145-148,August 2002.

[92] B. Parr, C. ByungLok, K. Wallace, and D. Zhi, "A novel ultra-wideband pulse design algorithm," *Communications Letters, IEEE*, vol. 7, no. 5, pp. 219-221, 2003.

[93] M. Z. Win, "Spectral density of random UWB signals," *Communications Letters, IEEE*, vol. 6, no. 12, pp. 526-528, 2002.

[94] L. Huaping, "Error performance of a pulse amplitude and position modulated ultra-wideband system over lognormal fading channels," *Communications Letters, IEEE*, vol. 7, no. 11, pp. 531-533, 2003.

[95] W. Turin, R. Jana, S. S. Ghassemzadeh, C. W. Rice, and T. Tarokh, "Autoregressive modeling of an indoor UWB channel," *in Conference Proceedings of the IEEE Conference on Ultra Wideband Systems and Technologies,* Wyndham Baltimore Inner Harbour, USA,pp. 71-74,21st May 2002.

[96] J. M. Cramer, R. A. Scholtz, and M. Z. Win, "On the analysis of UWB communication channels," *in Conference Proceedings of the IEEE Military Communications Conference 1999 (MILCOM 1999),* Atlantic City, NJ, USA, vol. 2,pp. 1191-1195,October 1999.

[97] T. Jin, X. Zhengyuan, and L. Ping, "Mean and covariance based estimation of multiple access UWB channels," *in Conference Proceedings of the IEEE Conference on Ultra Wideband Systems and Technologies,* Reston, Virginia, USA,pp. 458-462,November 2003.

[98] J. A. Tsai and B. D. Woerner, "A new orthogonal transmit waveform with space-time diversity (OTW-STD) for wireless CDMA downlink systems," *in Conference Proceedings of the Thirty-Fifth Asilomar Conference on Signals, Systems and Computers,* Pacific Grove, California, USA, vol. 1,pp. 241-245,November 2001.

[99] T. Jiann-An and B. D. Woerner, "Performance of orthogonal transmit waveforms for CDMA uplink systems in MIMO Rayleigh channels," *in Conference Proceedings of the IEEE Wireless Communications and Networking Conference 2002 (WCNC 2002),* vol. 1,pp. 206-209,Orlando, FL, USA, 2002.

[100] T. Jiann-An, H. Chang-Lung, and I. Chih-Lin, "BER analysis of a modified space-time spreading code for CDMA systems in MIMO Ricean channels," *in Conference Proceedings of the IEEE Global Telecommunications Conference 2003 (GLOBECOM '03),* San Francisco, USA, vol. 1,pp. 307-311,December 2003.

[101] G. Taricco and E. Biglieri, "Exact pairwise error probability of space-time codes," *Information Theory, IEEE Transactions on*, vol. 48, no. 2, pp. 510-513, 2002.

[102] E. Biglieri and G. Taricco, "Exact pairwise error probability of space-time codes," *in Conference Proceedings of the IEEE International Conference on Communications 2002 (ICC 2002),* New York, NY, USA, vol. 3,pp. 1373-1376,April 2002.

[103] Q. Yongquan and L. Daoben, "Performance analysis of several open-loop transmit diversity schemes for IMT-2000 systems," *in Conference Proceedings of the International Conference on Communication Technology 2003 (ICCT 2003),* Beijng, China, vol. 2,pp. 1107-1110,April 2003.

[104] R. Doostnejad, J. L. Teng, and E. S. Sousa, "Impact of power control on the performance of space-time spreading systems with suboptimal detectors," *in Conference Proceedings of the IEEE Pacific Rim Conference on Communications, Computers and signal Processing 2003 (PACRIM. 2003),* Victoria, BC, Canada, vol. 1,pp. 506-509,August 2003.

[105] M. Hamalainen, R. Tesi, and J. Iinatti, "UWB coexistence with IEEE 802.11a and UMTS in modified Saleh-Valenzuela channel," *in Conference Proceedings of the International Workshop on Ultra Wideband Systems,* Kyoto, Japan,pp. 45-49,May 2004.

[106] J. I. Jamp and L. E. Larson, "A coding technique for spectral shaping ultra-wideband pulse position modulated signals," *in Conference Proceedings of the IEEE 60th Vehicular Technology Conference - Fall 2004 (VTC2004-Fall),* Los Angeles, USA, vol. 2,pp. 1188-1191,September 2004.

[107] H. Joo and C. KyungHi, "Exploitation of extra diversity in UWB MB-OFDM system," *in Conference Proceedings of the IEEE/ACES International Conference on Wireless Communications and Applied Computational Electromagnetics,* Honolulu, Hawaii, USA,pp. 9-12,April 2005.

[108] W. Li-Chun, L. Wei-Cheng, and S. Kuan-Jiin, "On the performance of using multiple transmit and receive antennas in pulse-based ultrawideband systems," *Wireless Communications, IEEE Transactions on*, vol. 4, no. 6, pp. 2738-2750, 2005.

[109] W. Jianjun, X. Haige, and T. Zhi, "Weighted noncoherent receivers for UWB PPM signals," *Communications Letters, IEEE*, vol. 10, no. 9, pp. 655-657, 2006.

[110] T. Zasowski, F. Troesch, and A. Wittneben, "Partial Channel State Information and Intersymbol Interference in Low Complexity UWB PPM Detection," *in Conference Proceedings of the IEEE International Conference on Ultra-Wideband,* Waltham, MA, USA,pp. 369-374,September 2006.

[111] M. Kamoun and L. Mazet, "Optimal Bandwidth for UWB PPM in Poisson Arriving Multipath Channel and Jitter Context," *in Conference Proceedings of the 7th IEEE Workshop on Signal Processing Advances in Wireless Communications 2006 (SPAWC '06),* Cannes,France,pp. 1-5,July 2006.

[112] L. Junsheng, M. Ghavami, C. Xiaoli, B. Allen, and W. Malik, "Diversity Analysis of Multi-Antenna UWB Impulse Radio Systems with Correlated Propagation Channels," *in*

Conference Proceedings of the IEEE Wireless Communications and Networking Conference 2007 (WCNC 2007), Kowloon,Hong Kong,pp. 1593-1598,March 2007.

[113] L. Wei-Cheng and W. Li-Chun, "BER Analysis in A Generalized UWB Frequency Selective Fading Channel With Randomly Arriving Clusters and Rays," *in Conference Proceedings of the IEEE International Conference on Communications 2007 (ICC '07),* Glasgow, Scotland,pp. 4281-4286,June 2007.

[114] A. M. Kuzminskiy, F. J. Mullany, and C. B. Papadias, "Semi-blind channel estimation at the receiver for steered-STS transmit antenna architecture in cdma2000," *in Conference Proceedings of the IEEE International Conference on Acoustics, Speech, and Signal Processing 2005 (ICASSP '05),* Philadelphia, Pennsylvania, USA, vol. 3,p. iii/565-iii/568,March 2005.

[115] S. M. Razavizadeh, A. K. Khandani, V. T. Vakili, and T. Wen, "Space-Time Precoding for Downlink Transmission in Multiple Antenna CDMA Systems," *Vehicular Technology, IEEE Transactions on*, vol. 56, no. 5(part 1), pp. 2590-2602, 2007.

[116] H. Wicaksana, M. H. Island, and Y. L. Guan, "Performance of open loop transmit diversity schemes in the downlink multicell CDMA system," *in Conference Proceedings of the 6th International Conference on Information, Communications & Signal Processing,* Singapore,pp. 1-5,December 2007.

[117] L. L. Yang, "Performance of multiantenna multicarrier direct-sequence code division multiple access using orthogonal variable spreading factor codes-assisted space-+time spreading in time-selective fading channels," *Communications, IET*, vol. 2, no. 5, pp. 708-719, 2008.

[118] M. Z. Win and R. A. Scholtz, "Ultra-wide bandwidth time-hopping spread-spectrum impulse radio for wireless multiple-access communications," *Communications, IEEE Transactions on*, vol. 48, no. 4, pp. 679-689, 2000.

[119] N. J. August and S. H. Dong, "An efficient UWB radio architecture for busy signal MAC protocols," *in Conference Proceedings of the first Annual IEEE Communications Society Conference on Sensor and Ad Hoc Communications and Networks 2004 (SECON 2004),* Santa Clara, California, USA,pp. 325-334,October 2004.

[120] C. Dianjun and T. Hashimoto, "Transmit diversity schemes for an overloaded space-time spreading system over a flat Rayleigh fading channel," *in Conference Proceedings of the 15th IEEE International Symposium on Personal, Indoor and Mobile Radio Communications 2004 (PIMRC 2004),* Barcelona, Spain, vol. 4,pp. 2664-2668,September 2004.

[121] C. Xiaodong, G. B. Giannakis, and M. D. Zoltowski, "Space-time spreading and block coding for correlated fading channels in the presence of interference," *Communications, IEEE Transactions on*, vol. 53, no. 3, pp. 515-525, 2005.

Appendix 1: Utility MATLAB scripts used in study for plotting

MATLAB script: error_bars_utility.m

```
function [X, Y] = error_bars_utility(data)

%author: Peter Vial 7/2/04
% data should be in form Xin upper_95%_limit mean lower_95%_limit with the first row having the maximum value of X
% which is the same format as in  the excel spreadsheets used in the study

% test example:
% dB        upper                   mean                    lower
% 5.000     0.141062673650493   0.137751862248138   0.134441050845783
% 4.500     0.139821588742416   0.136757488242512   0.133693387742607
% 4.000     0.138548308721366   0.135492614507385   0.132436920293405
% 3.500     0.137439419018110   0.134387115612884   0.131334812207659
% 3.000     0.136405516371326   0.133346491653508   0.130287466935690
% 2.500     0.135480409657448   0.132442242557757   0.129404075458067
% 2.000     0.134662150618591   0.131589743410257   0.128517336201922
% 1.500     0.133947062208652   0.130842744157256   0.127738426105860
% 1.000     0.133216947388281   0.130139619860380   0.127062292332479
% 0.500     0.132617971165128   0.129557620442380   0.126497269719631
% 0.000     0.132063371758853   0.129015245984754   0.125967120210655
% -0.500    0.131574159907272   0.128539121460879   0.125504083014485
% -1.000    0.131140775998204   0.128117621882378   0.125094467766553
% -1.500    0.130758080628729   0.127724372275628   0.124690663922526
% -2.000    0.130435618470944   0.127394372605627   0.124353126740311
% -2.500    0.130121671223416   0.127079622920377   0.124037574617338
% -3.000    0.129833143215664   0.126781248218752   0.123729353221840
% -3.500    0.129580109027922   0.126537248462752   0.123494387897581
% -4.000    0.129352233582315   0.126318248681751   0.123284263781188
% -4.500    0.129144392187375   0.126115373884626   0.123086355581877
%-5.000     0.128949360119942   0.125925249074751   0.122901138029560

% first create X

[a,b] = size(data)

if b~=4
   error('must have 4 columns')
end

X=[];
s1=1
c1=a
for i=1:a
   X(s1) = data(c1,1)
   s1=s1+1
   X(s1) = data(c1,1)
   s1=s1+1
   X(s1) = data(c1,1)
   s1=s1+1
   X(s1) = data(c1,1)
   s1=s1+1
   c1=c1-1
end

y=[];
s1=1
c1=a
for i=1:a
   Y(s1) = data(c1,3)
   s1=s1+1
   Y(s1) = data(c1,4)
   s1=s1+1
   Y(s1) = data(c1,2)
```

```
   s1=s1+1
   Y(s1) = data(c1,3)
   s1=s1+1
   c1=c1-1
end
```

MATLAB script: calculate_area_under_positive_curve.m

```
function area = calculate_area_under_positive_curve(curve,time)

% curve - vector of curve values, expect only positive as
%         want this to calculate a real squared function
% time - sample of time epochs, expected

area=0;
curve=curve(:);
time=time(:);
for n=1:max(size(curve)-1)
   area=area+(curve(n).*( time(n+1)-time(n) ));
end
```

Appendix 2: STS Simulink results for m=4, 8 tabulated data

STS for Four Transmit Antennas

A Simulink simulation of a Space Time Spreading system was produced and the following results for 95% confidence intervals for **m=4** for expected SNR of 0dB through 16dB are shown here which are graphed in Figure 3.4-2:

Exp. SNR (dB)	Lower 95% value	Mean BER	Upper 95% value
0	0.107488669	0.107983	0.108477331
1	0.084670736	0.085147833	0.085624931
2	0.063965993	0.064689667	0.06541334
3	0.046451858	0.047271	0.048090142
4	0.032155805	0.033047833	0.033939862
5	0.021218512	0.022078167	0.022937821
6	0.013300187	0.014028	0.014755813
7	0.00794779	0.008510167	0.009072543
8	0.004511517	0.004856	0.005200483
9	0.002467543	0.002625333	0.002783124
10	0.0012037	0.001304083	0.001404466
11	0.000563116	0.000612667	0.000662217
12	0.000309544	0.000327967	0.000346389
13	0.000134836	0.000147767	0.000160697
14	0.00005200	0.00006140	0.00007080
15	0.00001821	0.00002496	0.00003170
16	0.00000578	0.00000923	0.00001268

STS for Eight Transmit Antennas

A Simulink simulation of a Space Time Spreading system was produced and the following results for 95% confidence intervals for **m=8** for expected SNR of 0dB through 16dB are shown here which are graphed in Figure 3.4-2:

Exp. SNR (dB)	Lower 95% value	Mean BER	Upper 95% value
0	0.097300048	0.098469167	0.099638285
1	0.074294766	0.07523225	0.076169734
2	0.054060518	0.054810333	0.055560148
3	0.037304973	0.037847417	0.03838986
4	0.024199102	0.024504083	0.024809065
5	0.014650878	0.014781667	0.014912456
6	0.008186666	0.008201333	0.008216001
7	0.004137795	0.004172833	0.004207872
8	0.001764193	0.001878375	0.001992557
9	0.000720783	0.000786167	0.000851551
10	0.0002555831	0.0002964167	0.0003372502
11	0.0000888637	0.0000961875	0.0001035113
12	0.0000241075	0.0000282083	0.0000323092
13	0.0000065308	0.0000080175	0.0000095043
14	0.0000010848	0.0000015088	0.0000019327

Appendix 3: MAI in STS tabulated data

Case study 1: Single MAI interferer – Walsh-Hadamard for 0dB

STS MAI study User 1 fixed at 0dB, MAI interference User 2 varies from -5dB to +5dB for two Transmit Antennas 95% confidence interval tabulated data using 128 chip Walsh-Hadamard code set:

User 1 expected SNR kept constant at 0dB			
expected SNR dB for User 2 at User 1's receiver	**upper bound 95% confidence interval**	**Mean BER**	**lower bound 95% confidence interval**
5.000	0.145108078591442	0.142448190885142	0.139788303178843
4.500	0.143518339397799	0.140769525897141	0.138020712396482
4.000	0.142002017037609	0.139184027482639	0.136366037927669
3.500	0.140725504573672	0.137817528849138	0.134909553124603
3.000	0.139446583455299	0.136502030164636	0.133557476873974
2.500	0.138287820873447	0.135309531357135	0.132331241840824
2.000	0.137291513087967	0.134263199070134	0.131234885052301
1.500	0.136352165300210	0.133278533388133	0.130204901476056
1.000	0.134001771125625	0.131910068026488	0.129818364927350
0.500	0.133017108581973	0.130869635930142	0.128722163278311
0.000	0.132310847084591	0.130144025311530	0.127977203538470
-0.500	0.131696673858969	0.129467359122530	0.127238044386090
-1.000	0.131121537271114	0.128870692857863	0.126619848444611
-1.500	0.130625813536334	0.128362193197362	0.126098572858391
-2.000	0.130144189333537	0.127883637963807	0.125623086594076
-2.500	0.129735874554963	0.127451027149862	0.125166179744761
-3.000	0.129394192082872	0.127089694064861	0.124785196046851
-3.500	0.129036308602873	0.126713138768972	0.124389968935072
-4.000	0.128764809889991	0.126419638974805	0.124074468059620
-4.500	0.128474038027211	0.126121972512805	0.123769906998399
-5.000	0.128254163919387	0.125884917121750	0.123515670324112

Case study 2: Two MAI interferers – Walsh-Hadamard for 0dB

STS MAI study User 1 fixed at 0dB, another MAI Interferer User 2a kept at 0dB, MAI interference User 2b varies from -5dB to +0.5dB for two Transmit Antennas single seed set value used, tabulated data using 128 chip Walsh-Hadamard code set:

User 1 expected SNR kept constant at 0dB, and another MAI interferers' SNR also kept constant at 0dB at User 1's receiver	
expected SNR dB for User 2 at User 1's receiver	**BER**
0.500	0.145671
0.000	0.144889
-0.500	0.144157
-1.000	0.1434655
-1.500	0.142857
-2.000	0.1422935
-2.500	0.141854
-3.000	0.141388
-3.500	0.1409795
-4.000	0.140646
-4.500	0.1403015
-5.000	0.1400345

Case study 3: One MAI interferers – Walsh-Hadamard for 4dB

STS MAI study User 1 fixed at 4dB, MAI interference User 2 varies from -5dB to +5dB for two Transmit Antennas single seed set value used, tabulated data using 128 chip Walsh-Hadamard code set:

User 1 expected SNR kept constant at 4dB,	
expected SNR dB for User 2 at User 1's receiver	**BER**
5.000	0.065749434250566
4.000	0.063532436467564
3.000	0.061653938346062
2.000	0.06021143978856
1.000	0.058922441077559
0.000	0.057893442106558
-1.000	0.0570939429060507
-2.000	0.056489943510057
-2.500	0.056237943762056
-3.000	0.056029443970556
-3.500	0.055817944182056
-4.000	0.055623444376556
-4.500	0.055491444508556
-5.000	0.055320944679055

Appendix 4: MAI in STS 95% confidence intervals tabulated data for low correlation codes

Case study 1: Single MAI interferer – alternating pairs of orthogonal 32 chip low correlation codes

User 1 kept constant at 0dB using the same pair of low correlation orthogonal code and User 2 uses alternating pairs of low correlation orthogonal codes, but in the same sequence for each random simulation.

User 1 expected SNR kept constant at 0dB			
expected SNR dB for User 2 at User 1's receiver	**upper bound 95% confidence interval**	**Mean BER**	**lower bound 95% confidence interval**
5.000	0.143418137831033	0.140113484886515	0.136808831941998
4.500	0.141889573085413	0.138578486421514	0.135267399757615
4.000	0.140380523577045	0.137094237905762	0.133807952234479
3.500	0.139040558352373	0.135811239188761	0.132581920025148
3.000	0.137883392612462	0.134650115349885	0.131416838087308
2.500	0.136829792025103	0.133618241381759	0.130406690738415
2.000	0.135894394439485	0.132676117323883	0.129457840208281
1.500	0.135005200958533	0.131815243184757	0.128625285410981
1.000	0.134229551448892	0.131057618942381	0.127885686435870
0.500	0.133540181283302	0.130387494612505	0.127234807941709
0.000	0.132928613016855	0.129760370239630	0.126592127462405
-0.500	0.132355488401597	0.129203370796629	0.126051253191662
-1.000	0.131851952489180	0.128710871289129	0.125569790089077
-1.500	0.131408448159123	0.128268246731753	0.125128045304383
-2.000	0.130975201442032	0.127860497139503	0.124745792836974
-2.500	0.130600742534290	0.127492122507878	0.124383502481465
-3.000	0.130256576604689	0.127153622846377	0.124050669088065
-3.500	0.129956643558425	0.126874998125002	0.123793352691578
-4.000	0.129690268613777	0.126615248384752	0.123540228155726
-4.500	0.129445983598329	0.126373373626626	0.123300763654923
-5.000	0.129241154851577	0.126166498833501	0.123091842815425

Case study 2: Single MAI interferer one set only of 32 chip low correlation code pairs used

User 1 kept constant at 0dB and both User 1 and User 2 uses same fixed pairs of low correlation orthogonal codes

User 1 expected SNR kept constant at 0dB			
expected SNR dB for User 2 at User 1's receiver	**upper bound 95% confidence interval**	**Mean BER**	**lower bound 95% confidence interval**
5.000	0.141150708896800	0.138099986900013	0.135049264903226
4.500	0.139821590613947	0.136757488242512	0.133693385871076
4.000	0.138548310587763	0.135492614507385	0.132436918427008
3.500	0.137439420882435	0.134387115612884	0.131334810343333
3.000	0.136405518239757	0.133346491653508	0.130287465067259
2.500	0.135480411513139	0.132442242557757	0.129404073602376
2.000	0.134662152495196	0.131589743410257	0.128517334325317
1.500	0.133947064104747	0.130842744157256	0.127738424209765
1.000	0.133216949267892	0.130139619860380	0.127062290452868
0.500	0.132617973034369	0.129557620442380	0.126497267850390
0.000	0.132063373620626	0.129015245984754	0.125967118348882
-0.500	0.131574161761052	0.128539121460879	0.125504081160705
-1.000	0.131140777844726	0.128117621882378	0.125094465920031
-1.500	0.130758082481698	0.127724372275628	0.124690662069558
-2.000	0.130435620328516	0.127394372605627	0.124353124882739
-2.500	0.130121673081478	0.127079622920377	0.124037572759276
-3.000	0.129833145079740	0.126781248218752	0.123729351357764
-3.500	0.129580110886481	0.126537248462752	0.123494386039022
-4.000	0.129352235435451	0.126318248681751	0.123284261928051
-4.500	0.129144394037478	0.126115373884626	0.123086353731774
-5.000	0.128949361967048	0.125925249074751	0.122901136182454

Appendix 5: MATLAB script to generate STS wideband system plot for m=1, 2, 4 and 8

MATLAB script: mequals124and8resultsforstsinPhdappendix.m

```
%Author: P J Vial, Originally May 2004, modified May 2008
% requires the use of error_bars_utility()
X=[ 0 2 4 6 8 10 12 14 16];
Xmequals4=[ 0 1 2 3 4 5 6 7 8 9 10 11 12 13 14 15 16];
Ymequals4oneseed = [ 0.107983   0.085147833 0.064689667 0.047271    0.033047833 0.022078167 0.014028    0.008510167
0.004856    0.002625333 0.001304083 0.000612667 0.000327967 0.000147767 0.00006140  0.00002496  0.00000923];

datasetm4 = [
0   0.108477331 0.107983    0.107488669
1   0.085624931 0.085147833 0.084670736
2   0.065413339 0.064689667 0.063965994
3   0.048090141 0.047271    0.046451859
4   0.033939861 0.033047833 0.032155805
5   0.022937821 0.022078167 0.021218513
6   0.014755813 0.014028    0.013300187
7   0.009072543 0.008510167 0.00794779
8   0.005200483 0.004856    0.004511517
9   0.002783124 0.002625333 0.002467543
10  0.001404466 0.001304083 0.001203701
11  0.000662217 0.000612667 0.000563116
12  0.000346389 0.000327967 0.000309544
13  0.000160697 0.000147767 0.000134836
14  0.00007080  0.00006140  0.00005200
15  0.00003170  0.00002496  0.00001821
16  0.00001268  0.00000923  0.00000578 ];

[ XM4, YEBm4 ] =  error_bars_utility(datasetm4);

Xmequals8=[ 0 1  2  3 4 5 6 7 8 9 10 11 12 13 14];
Ymequals8oneseed=[0.098469167 0.07523225 0.054810333 0.037847417  0.024504083 0.014781667  0.008201333
0.004172833  0.001878375  0.000786167  0.0002964167  0.0000961875 0.0000282083  0.0000080175  0.0000015088 ];

datasetm8 = [
0  0.099638284  0.098469167 0.097300049
1  0.076169733  0.07523225  0.074294767
2  0.055560148  0.054810333 0.054060519
3  0.03838986   0.037847417 0.037304974
4  0.024809064  0.024504083 0.024199102
5  0.014912456  0.014781667 0.014650878
6  0.008216001  0.008201333 0.008186666
7   0.004207872 0.004172833 0.004137795
8  0.001992557  0.001878375     0.001764193
9  0.000851551  0.000786167     0.000720783
10 0.0003372502 0.0002964167    0.0002555832
11 0.0001035113 0.0000961875    0.0000888637
12 0.0000323092 0.0000282083    0.0000241075
13 0.0000095043 0.0000080175    0.0000065308
14 0.0000019327 0.0000015088    0.0000010848];

[ XM8, YEBm8 ] =  error_bars_utility(datasetm8);

Y1=[ 0.125378159007337 0.083223656219481 0.050328740274745  0.027694538505235 0.013990262226069
0.006600901808268 0.002944581230601 0.001271150437474 0.000540645680033 ];

% now add 95% confidence intervals

Y1SNR0dB =[ 0.125266516165150 0.125489801849524 ];
X1SNR0dB = [ 0 0];

Y1SNR2dB =[ 0.083121501929891 0.083325810509071 ];
X1SNR2dB = [ 2 2];

Y1SNR4dB =[ 0.050243720701582 0.050413759847907 ];
```

```
X1SNR4dB = [ 4 4]

Y1SNR6dB =[ 0.027620258953674 0.027768818056796 ];
X1SNR6dB = [ 6 6 ]

Y1SNR8dB =[ 0.013945780478867 0.014034743973272 ];
X1SNR8dB = [ 8 8 ]

Y1SNR10dB =[ 0.006578180484769 0.006623623131767 ];
X1SNR10dB = [ 10 10];

Y1SNR12dB =[ 0.002931742263961 0.002957420197241 ];
X1SNR12dB = [ 12 12];

Y1SNR14dB =[ 0.001265409769043 0.001276891105904 ];
X1SNR14dB = [ 14 14];

Y1SNR16dB =[ 0.000537289716432 0.000544001643634 ];
X1SNR16dB = [ 16 16 ];

Y6=[ 0.155950995088823 0.116664249602711 0.083611672818767 0.057870579157700 0.038893809150341
0.025587135751369 0.016618229599695 0.010685776142332 0.006826734026273 ];

% now add 95% confidence intervals

Y6SNR0dB =[ 0.155797528433079 0.156104461744567 ];
X6SNR0dB = [ 0 0];

Y6SNR2dB =[ 0.116494457907024 0.116834041298399 ];
X6SNR2dB = [ 2 2];

Y6SNR4dB =[ 0.083535303195218   0.083688042442316];
X6SNR4dB = [ 4 4]

Y6SNR6dB =[ 0.0577641314469508  0.057977023845893 ];
X6SNR6dB = [ 6 6]

Y6SNR8dB =[ 0.038809774460520  0.0389778438440162 ];
X6SNR8dB = [ 8 8]

Y6SNR10dB =[ 0.025527504130381 0.025646767372357 ];
X6SNR10dB = [ 10 10]

Y6SNR12dB =[ 0.016567167784670 0.016669291414720 ];
X6SNR12dB = [ 12 12]

Y6SNR14dB =[ 0.010639673159616  0.010731879125048 ];
X6SNR14dB = [ 14 14]

Y6SNR16dB =[ 0.006782004815251  0.006871463237295 ];
X6SNR16dB = [ 16 16]

semilogy( X,Y6,'-kx',X,Y1, '-rx', Xmequals4, Ymequals4oneseed, '-gx', Xmequals8, Ymequals8oneseed,'-bx')
xlabel('SNR (dB)')
ylabel('BER')

legend('m=1','m=2','m=4','m=8','Location','NorthEast')
hold

semilogy( X1SNR0dB, Y1SNR0dB, 'r', X1SNR2dB, Y1SNR2dB, 'r', X1SNR4dB, Y1SNR4dB, 'r', X1SNR6dB,
Y1SNR6dB, 'r', X1SNR8dB, Y1SNR8dB, 'r', X1SNR10dB, Y1SNR10dB, 'r', X1SNR12dB, Y1SNR12dB, 'r', X1SNR14dB,
Y1SNR14dB, 'r', X1SNR16dB, Y1SNR16dB, 'r',X6SNR0dB, Y6SNR0dB, 'k', X6SNR2dB, Y6SNR2dB, 'k', X6SNR4dB,
Y6SNR4dB, 'k', X6SNR6dB, Y6SNR6dB, 'k', X6SNR8dB, Y6SNR8dB, 'k', X6SNR10dB, Y6SNR10dB, 'k', X6SNR12dB,
Y6SNR12dB, 'k', X6SNR14dB, Y6SNR14dB, 'k', X6SNR16dB, Y6SNR16dB, 'k', XM4, YEBm4, 'k', XM8, YEBm8, 'k')

grid
```

Appendix 6: MATLAB scripts to generate SV channel matrices

MATLAB script: cp0802_IEEEuwbpvialsv.m

```
%
%
% Programmed by Peter Vial 6/12/2004
%
% Generates a multipath profile of the Saleh-Valenzula model used in
% ST-coding paper targetted for UWB Simulink Simulation validation tests
%
% History and accreditation:
% Modified a program by Guerino Giancola called:
%           FUNCTION 8.8 : "cp0802_IEEEuwb"
% from the book "Understanding UWB Radio Fundamentals" by Di Benedetto
% which Generated the channel impulse response for a multi-path
% channel according to statistical model proposed by the IEEE 802.15.SG3a
% to provide the S-V model used in ST-coding
%
% Another difference is I do not normalise the coefficients at this stage
%

% Use this one for testing:
% function [ NC h0realmagnitude h0real h0 h0phase rmsdelayspread ITMPG HAweaksqsum OT HLocalMean CAT HT
HA HAweak h HPhase phase omega rdt PT dt ts LAMBDA lambda GAMMA gamma  ] = cp0802_IEEEuwbpvialsv();
%
% Returned Variables:
%
% SortDatatestdatt: An array of 200 rows (maximum) which contains all
%         the multipath taps found whether within 1.4ns or not.
%         Useable multipath is a subset of this larger data pool
%         generated by the S-V algorithm
%
% SortData: An array containing the useable multipath starting at the time
%         of arrival and going to the last strongest multipath
%         which could be used by the RAKE receiver and that are
%         separated in time by at least 1.4ns
%
% NewData : An array containing the multipath starting at the strongest
%         multipath and heading to the weakest that can be used
%         by the RAKE receiver
%
% LNewData :    The Total number of useable (ie greater than 1.4ns time
%           difference between points) multipath
%
function [ SortDatatestdatt SortData NewData LNewData ] = cp0802_IEEEuwbpvialsv(losTime);


% ------------------------------------------------------------------------
%         Step Zero    -    Input parameters
% ------------------------------------------------------------------------

% losTime = 7e-9;          % Time of arrival of first pulse
                    % assuming 2 metre separation

OT = 98e-9 - losTime;     % observation time [s]- setting to two nano-
                    % seconds less than actual of 100ns
                    % to consider pulse width and also PPM delay
                    % less time of arrival of first pulse which
                    % using speed of light as 3 X 10^8 is 7ns over
                    % 2 metres.
                    %
ts = 1e-12;              % time resolution [s]; same as used in
                    % Simulink target model
```

```
fc = 1/ts;              % sampling frequency

LAMBDA = 0.5*1e9;       % cluster arrival rate (1/s)
lambda = 2e9;           % ray arrival rate (1/s)
GAMMA = 33e-9;          % cluster decay factor
gamma =  5e-9;          % ray decay factor

% ray decay threshold
% setting to 0.9 so get 100-300 multipath
% originally was set to 0.001 where we get 2000-4000 multipath
% note using 0.0001 gives similar numbers to 0.001 pvial 9/12/4
rdt = 0.9;
% rays are neglected whn exp(-t/gamma) < rdt

% peak threshold [dB]
PT = 50;
% rays are considered if their amplitude is
% within the -PT range with respect to the peak

G=0;
% G = 1 graphical output
% G = 0 no graphical output

verbose=0;
% verbose = 1 Prints out all data and messages
% verbose = 0 No data printed out on execution

% ------------------------------------------------------------------
%        Step One    -   Cluster characterization
% ------------------------------------------------------------------

dt = 1 / fc;    % sampling time

T = 1 / LAMBDA; % average cluster inter-arrival time
            % [s]
t = 1 / lambda; % average ray inter-arrival time

i = 1;
CAT(i) = 0;
next = 0;

if verbose
   % Print out the simulation details
   disp('Time of first arrival is the so called losTime')
   losTime
   disp('Observation Time (OT) given by 100ns-2ns-losTime')
   OT
   disp('Time Resolution time, ts, should be same as used in Simulink for its overall smalled discrete sampling time')
   ts
   disp('The Cluster exponential interarrival time (poisson arrival rate LAMBDA) 1/LAMBDA is (seconds):')
   T
   disp('The ray exponential interarrival time (poisson arrival rate lambda) 1/lamda is (seconds):')
   t
   disp('The Cluster decay factor time GAMMA (seconds)is:')
   GAMMA
   disp('The ray decay factor time gamma (seconds) is:')
   gamma
   disp('The ray decay threshold has been set to (rdt):')
   rdt
   disp('The Peak Threshold (how far below peak is acceptable) (PT) is')
   PT
end



while next < OT
```

```
   i = i + 1;
   next = next + expinv( rand, T);
   if next < OT
      CAT(i) = next;
   end
end   % while remaining > 0

% ----------------------------------------------------------------
%    Step Two - Path characterization
% ----------------------------------------------------------------

NC = length(CAT);    % number of observed clusters

if verbose
   disp('The Number of Observed Clusters is (NC):');
   NC
end

omega = 7.0207e-8;  % mean energy (squared value of the voltage) of first
        % arriving cluster and ray B(0,0)
        % Calculated a Go and G and using a 2 metre with exponent 3.5
        % calculated the value of 7.0207e-8 for omega (which is mean of
        % B(0,0) squared and should not change over a simulation run.
        % Modified pvial 7/12/4

pc = 0;                    % path counter

for i = 1 : NC
   % do first arriving ray of the cluster i
   pc = pc + 1;
   CT = CAT(i);    % cluster time
              % note for the first cluster this should be time 0

   HT(pc) = CT;    % store time of cluster i's first ray
   HPhase(pc)=2*pi*rand; % phase is a random number zero to 2pi
                 % uniformly distributed
   HLocalMean(pc)= omega * exp(-1*(CT/GAMMA)); % local mean of first ray
                                  % of cluster i for the
                                  % first ray of the
                                  % first cluster this should
                                  % be omega!
   GAMMALocalMean(i)=HLocalMean(pc);
   GAMMALocalMeanT(i)=HT(pc);
   next = 0;

   HA(pc) = 0; % create the amplitude vector but leave as zero till later

   % exp(-next/gamma)
   % rdt
   while ( ( exp(-next/gamma) > rdt)&&( (CT+next<OT) ) )
         % exp(-next/gamma)
         % rdt
      pc = pc + 1;
      next = next + expinv(rand, t);
      HT(pc) = CT + next; %record time of following ray in cluster i

      HA(pc) = 0; % create the amplitude vector but leave as
              % zero till later

      HPhase(pc)=2*pi*rand;      % phase is a random number zero to 2pi
                        % uniformly distributed

      HLocalMean(pc)= omega * exp(-1*(CT/GAMMA)) * exp(-1*(next/gamma));
                     % local mean of first ray
                     % of cluster i for the
                     % first ray of the
```

```
                    % first cluster this should
                    % be omega! It is a mean squared value
                    % as per S-V model

  end  % end when magnitude is exponentially smaller than 'rdt'
end % for i = 1 : NC

for i = 1 : pc
  tmp=HLocalMean(i); %These means have the squared power values
  LocalMeanVariance=tmp/2;
  LocalMeanStdDev=sqrt(LocalMeanVariance);
  X1gaussian=LocalMeanStdDev*randn;
  X2gaussian=LocalMeanStdDev*randn;
  X1gaussianSquared=X1gaussian.^2;
  X2gaussianSquared=X2gaussian.^2;
  sum1=X1gaussianSquared+X2gaussianSquared;
  CurrentVoltageAmplitude=sqrt(sum1);  % now has a voltage / amplitude
                          % with the requiste statistical
                          % variation for S-V model
  HA(i)=CurrentVoltageAmplitude;
end % for i = 1 : pc

%check, do any of the times coincide
%if so emit a warning and use largest amplitude for both
for i=1:pc
  for zz = 1 : pc
    itk1 = floor( HT(i)/dt );
    itk2 = floor( HT(zz)/dt );
    if (i~=zz)
      if (itk1==itk2)
        warning('Have found the same relative arrival time for two different multipath')
        % use the largest magnitude path and ignore the smallest
        % one (could also add them assuming constructive signals)
        % note that one event will cause two warning messages!
        if HA(i)>=HA(zz)
          HA(zz)=HA(i);
        else
          HA(i)=HA(zz);
        end
      end
    end
  end
end

HAweak=HA;
HAweaksqsum=sum(HA.^2);
%Weak peak filtering
%
%peak =  max(HA.*cos(HPhase)) ; % no need to take absolute value as all values are > 0
%limit = peak /10^(PT/10);
%HA = HA .* ( (HA.*cos(HPhase)) > (limit .*ones(1,length(HA)))); %only
%interested in real part for UWB, did this but no discernable difference in
%results so have gone back to original methodology by Guerino Giancola
%
%
% Weak peak filtering
peak =  max(HA) ; % no need to take absolute value as all values are > 0
limit = peak /10^(PT/10);
HA = HA .* ( HA > (limit .*ones(1,length(HA))));


for i = 1 : pc
  itk = floor( HT(i)/dt ); % adjust to nearest multiple of delta t (dt)
  h(itk+1) = HA(i); % now place the pulses in the correct time bin
  phase(itk+1) = HPhase(i); % and phase of each pulse
end
```

```
ITMPG = sum(h.^2);  % calculate the Instantaneous total multipath power
                % gain for the current set of multipaths

%To calculate rms delay spread should include time of arrival of first
%pulse as this is losTime here we need to adjust times accordingly (Tad???)
tempsum1=0;
tempsum2=0;
for xx=1:length(h)
   if (h(xx)>0)
      time=losTime+(xx-1)*dt;
      timesq=time^2;
      hsq=h(xx)^2;
      tempsum1=tempsum1 + (  time*hsq   );
      tempsum2=tempsum2 + ( timesq*hsq  );
   end
end
secondmoment=tempsum2/ITMPG;
firstmoment=tempsum1/ITMPG;
firstmomentsq=firstmoment^2;
rmsdelayspread=sqrt(secondmoment-firstmomentsq);

% ------------------------------------------------------------------
%      Step Three -  Generate Amplitude and Phase Channel (time)
%                  impulse response
% ------------------------------------------------------------------

N = floor(ts/dt);
L = N * ceil(length(h)/N);
h0 = zeros(1,L);
h0phase = zeros(1,L);
%hf = h0;
h0(1:length(h)) = h;
h0phase(1:length(phase)) = phase;

% energy normalization
%E_tot=sum(h.^2);
%h0 = h0 / sqrt(E_tot);
%E_tot = sum(hf .^ 2);
%hf = hf / sqrt(E_tot);

% ------------------------------------------------------------------
%      Step Four -   Generate Real part of Channel (time)
%                  impulse response
% ------------------------------------------------------------------

for i=1:length(h0)
   h0real(i)=h0(i)*cos(h0phase(i)); % now hreal can be negative as well!
end
h0realmagnitude=abs(h0real);
% ------------------------------------------------------------------
%      Step Five -   Generate Power Delay Profile of Real part of
%                  Channel (time) impulse response
% ------------------------------------------------------------------

h0realpdp=h0real.^2;

% ------------------------------------------------------------------
%    Step Six - Graphical output
% ------------------------------------------------------------------

if G
   Tmax = dt*length(h0);
   time = (0:dt:Tmax-dt);

   figure(1);
```

```
   S1 = stem(time,h0);
   AX=gca;
   set(AX,'FontSize',14);
   T=title('Channel Impulse Response: Amplitude');
   set(T,'FontSize',14);
   x=xlabel('Time [s]');
   set(x,'FontSize',14);
   y=ylabel('Amplitude Gain');
   set(y,'FontSize',14);
   figure(2);
   S2=stairs(time,h0phase);
   AX=gca;
   set(AX,'FontSize',14);
   T=title('Channel Impulse Response: Phase');
   set(T,'FontSize',14);
   x=xlabel('Time [s]');
   set(x,'FontSize',14);
   y=ylabel('Phase');
   set(y,'FontSize',14);
   figure(3);
   S2=stairs(time,h0real);
   AX=gca;
   set(AX,'FontSize',14);
   T=title('Channel Impulse Response: Real Part Only (UWB is a real signal)');
   set(T,'FontSize',14);
   x=xlabel('Time [s]');
   set(x,'FontSize',14);
   y=ylabel('Amplitude');
   set(y,'FontSize',14);
   figure(4);
   S2=stairs(time,h0realmagnitude);
   AX=gca;
   set(AX,'FontSize',14);
   T=title('Channel Impulse Response: Absolute value of Real Part');
   set(T,'FontSize',14);
   x=xlabel('Time [s]');
   set(x,'FontSize',14);
   y=ylabel('Magnitude');
   set(y,'FontSize',14);
   figure(5);
   S2=stairs(time,h0realpdp);
   AX=gca;
   set(AX,'FontSize',14);
   T=title('Channel Impulse Response: Power Delay Profile of Real Part');
   set(T,'FontSize',14);
   x=xlabel('Time [s]');
   set(x,'FontSize',14);
   y=ylabel('Power referenced to 1 Ohm resistor');
   set(y,'FontSize',14);
   hold on
   plot(GAMMALocalMeanT,GAMMALocalMean,'r',GAMMALocalMeanT,GAMMALocalMean,'o');
   hold off
end

if verbose
   disp('print Instantaneous Total Mean Power Gain of Amplitudes')
   ITMPG
   ITMPGreal=h0real.^2;
   disp('print Instantaneous Total Mean Power Gain for Real Part of Channel')
   ITMPGreal=sum(ITMPGreal)
end

% ------------------------------------------------------------------
%    Step Seven - Sort on Real Data
% ------------------------------------------------------------------
```

```
% This section uses the real signal component and provides an ordered list
%

DataToSort = h0real;  % Data to be sorted
DataSortedValue = []; % Value in ascending order from largest to lowest that is not zero
DataSortedIndex = []; % Time index of these nonzero values
DataSortedTime  = []; % Contains relative time values, excluding losTime
TempStorageValue = [];
TempStorageIndex = [];

indexptr=0;
% First find all non zero values
for cnt=1:length(h0real)
   if (DataToSort(cnt)~=0)
      indexptr = indexptr + 1;
      TempStorageValue(indexptr) = DataToSort(cnt);
      TempStorageIndex(indexptr) = cnt;
   end
end

indexptr=0;
max_value=max(abs(TempStorageValue)); % consider that values will be negative!
while (max_value~=0)

   for cnt=1:length(TempStorageValue)
      if ( abs(TempStorageValue(cnt) ) == max_value )
         indexptr = indexptr + 1;
         % store both the value and time index
         DataSortedValue(indexptr) = TempStorageValue(cnt);
         DataSortedIndex(indexptr) = TempStorageIndex(cnt);
         % zero out the temporary storage data
         TempStorageValue(cnt)=0;
         TempStorageIndex(cnt)=0;
         break; % start search for next largest value
      end
   end
   max_value=max(abs(TempStorageValue));
end

for cnt=1:length(DataSortedValue)
   DataSortedTime(cnt)=ts*(DataSortedIndex(cnt)-1);
end

% should now be sorted in ascending order
testdatt = [ DataSortedValue' DataSortedIndex' DataSortedTime'];

if verbose
   disp('Priniting out Data Values and Index')
   testdatt
   disp('print number of detected multipath')
   size(DataSortedValue) % print number of detected multipath
end

% ------------------------------------------------------------------
%    Step Eight - Using Sort on Real Data Create input Arrays
%                 to Simulink!!!
% ------------------------------------------------------------------


% want all pulses that are less than 2 pulse widths apart to be removed
% from the list that is used to select the best time periods to perform
% selective rake reception on. Note that these pulses will still be present
% in the waveform and will form a type of current symbol interference which
% will probably re-inforce the correct answer rather than generate extra
% errors which may explain the better error rate at lower SNR's in ST
% coding paper!!
```

```
testdatt=testdatt;
testdattstore=testdatt; % needed for all multipath in ascending time order
for outerloop=1:max(length(testdatt))
   if (testdatt(outerloop,3)>=0)
      for cnt =1:max(length(testdatt))
         if (outerloop~=cnt)
            if (testdatt(cnt,3)>=0)
               if (abs(testdatt(cnt,3)-testdatt(outerloop,3))<1.4e-9)
                  testdatt(cnt,1)=0; % remove entry
                  testdatt(cnt,2)=0;
                  testdatt(cnt,3)=-1; %set the time to negative
               end
            end
         end
      end
   end
end

if verbose
   disp('Printing sorted data with all unusable multipath removed, ie any that is within 1.4ns of major peak')
   testdatt
end

NewData=[];
indexptr=0;
for cnt=1:max(length(testdatt))
   if (testdatt(cnt,3)>=0)
      indexptr=indexptr+1;
      NewData(indexptr,1)=testdatt(cnt,1);
      NewData(indexptr,2)=testdatt(cnt,2);
      NewData(indexptr,3)=testdatt(cnt,3);
   end
end
if verbose
   disp('Display Useable multipath starting at largest magnitude and working to smallest')
   NewData % contains the multipath in descending order of magnitude and
         % time index and time in seconds, with best magnitude path and
         % time first row, and next best after that ...
end

LNewData = size(NewData); % indicates number of useable multipath

if verbose
   disp('The maximum number of useable multipath for this data run of multipaths is:(LNewData) ')
   LNewData
end

if G
   figure(6);
   stem(NewData(:,1)); % plot the useable multipath
end

% now try and re-sort data into another array which is in ascending time
% order. Do this by first finding maximum times and creat a matrix which
% starts at the end then this matrix is fed into another sort which simply
% flips the matrix so time is in ascending order
TempStorageValue = NewData;
TempStorageSort = [];   % a temporary storage area
SortData=[];          % The targetted Final sorted data

indexptr=0;
max_time=max(TempStorageValue(:,3)); % find maximum time
while (max_time>=0)
   for cnt=1:length(TempStorageValue)
      if (TempStorageValue(cnt,3)>=0)
         if ( (TempStorageValue(cnt,3) ) == max_time )
```

```
            indexptr = indexptr + 1;
            % store all values in the row and make time -1
            TempStorageSort(indexptr,1) = TempStorageValue(cnt,1);
            TempStorageSort(indexptr,2) = TempStorageValue(cnt,2);
            TempStorageSort(indexptr,3) = TempStorageValue(cnt,3);
            % zero out the temporary storage data and set time negative
            TempStorageValue(cnt,1)=0;
            TempStorageValue(cnt,2)=0;
            TempStorageValue(cnt,3)=-1;
            break; % start search for next largest time value
          end
        end
    end

    max_time=max(TempStorageValue(:,3)); % find maximum time
end

if verbose
    disp('TempStorageValue is:')
    TempStorageValue
    disp('TempStorageSort is:')
    TempStorageSort
end

indexptr=0;
for cnt=length(TempStorageSort):-1:1
    indexptr=indexptr+1;
    SortData(indexptr,1)=TempStorageSort(cnt,1);
    SortData(indexptr,2)=TempStorageSort(cnt,2);
    SortData(indexptr,3)=TempStorageSort(cnt,3);
end

if verbose
    disp('printing SortData, useable multipath in order of time of arrival')
    SortData % Useable multipath in order of time arrival
end

if G
    figure(7);
    stem(SortData(:,3),SortData(:,1));   % plot the time versus magnitude of
                                % useable multipath
end

% need another element which fills out a two hundred multipath array. To
% tell simulink if the path exists during this period then use a value of
% '1' for exists and '0' for non existent - then can calculate the expected
% SNR for all paths and summing the instantaeous values and then taking the
% mean of these over many symbols. The value 200 is chosen only because
% this is reasonable compared to what papers have said on the number of
% multipath

% First put the available list of testdatt in chronological order of
% arrival

% now try and re-sort data into another array which is in ascending time
% order. Do this by first finding maximum times and creat a matrix which
% starts at the end then this matrix is fed into another sort which simply
% flips the matrix so time is in ascending order
TempStorageValue = testdattstore; % get original matrix data
TempStorageSort = [];   % a temporary storage area
SortDatatestdatt=[];          % The targetted Final sorted data

indexptr=0;
max_time=max(TempStorageValue(:,3)); % find maximum time
while (max_time>=0)
    for cnt=1:length(TempStorageValue)
```

```
    if (TempStorageValue(cnt,3)>=0)
      if ( (TempStorageValue(cnt,3) ) == max_time )
        indexptr = indexptr + 1;
        % store all values in the row and make time -1
        TempStorageSort(indexptr,1) = TempStorageValue(cnt,1);
        TempStorageSort(indexptr,2) = TempStorageValue(cnt,2);
        TempStorageSort(indexptr,3) = TempStorageValue(cnt,3);
        % zero out the temporary storage data and set time negative
        TempStorageValue(cnt,1)=0;
        TempStorageValue(cnt,2)=0;
        TempStorageValue(cnt,3)=-1;
        break; % start search for next largest time value
      end
    end
  end

  max_time=max(TempStorageValue(:,3)); % find maximum time
end


% TempStorageValue
% TempStorageSort

indexptr=0;
for cnt=length(TempStorageSort):-1:1
  indexptr=indexptr+1;
  SortDatatestdatt(indexptr,1)=TempStorageSort(cnt,1);
  SortDatatestdatt(indexptr,2)=TempStorageSort(cnt,2);
  SortDatatestdatt(indexptr,3)=TempStorageSort(cnt,3);
end

if verbose
  disp('printing SortDatatestdatt')
  SortDatatestdatt
end

if G
  figure(8);
  stem(SortDatatestdatt(:,3),SortDatatestdatt(:,1));
end

% now create a new array that spans 200 multipath
length_testdatt=length(SortDatatestdatt);
if length(SortDatatestdatt)>200
  warning('trucating testdatt as it is larger than 200 multipath; truncating to first 200 rows')
  SortDatatestdatt=SortDatatestdatt(1:200,:);
  length_testdatt=200;
end

if length(SortDatatestdatt)<200
  if verbose
    disp('increasing length of testdatt to 200')
  end
  tempArray=zeros(200,3);
  tempArray(1:length(SortDatatestdatt),1:3)=SortDatatestdatt;
  SortDatatestdatt=tempArray; % now should be 200 in length
end

if verbose
  disp('The length of the Sorted Data is:')
  length(SortDatatestdatt)
end

tempArray=zeros(200,4);
for cnt=1:200
  if (cnt<=length_testdatt)
```

```
      tempArray(cnt,1)=SortDatatestdatt(cnt,1);
      tempArray(cnt,2)=SortDatatestdatt(cnt,2);
      tempArray(cnt,3)=SortDatatestdatt(cnt,3);
      tempArray(cnt,4)=1; % add the multipath presence indicator
    else
      break; % quit for loop
    end
end

SortDatatestdatt=tempArray;
if verbose
   disp('printing SortDatatestdatt with 200 rows, if multipath present 4th row is 1 if not present its zero')
   SortDatatestdatt
end
```

MATLAB script: createinputdatavectors.m

```
% Author: P J Vial
%
% Date: 5/1/05
%
% Rev: 0.0
%
% Inputs:
%         losTime: Time of arriving first (line of sight or non line of sight) ray
%         NoOfRaysUsed: Indicates how many rays used in decoding (usually
%                   denoted 'L'
%
% Outputs:
%      GetOneRecVector: A Vector sampled at Simulink Sample rate of
%      1 by 10^-12 which would represent all multipath events using SV
%      model over all time with a constant stream of one's sent which
%      includes phases and gains for ALL multipath without noise
%
%      GetZeroRecVector: A Vector sampled at Simulink Sample rate of
%      1 by 10^-12 which would represent all multipath events using SV
%      model over all time with a constant stream of zero's sent which
%      includes phases and gains for ALL multipath without noise
%
%      GetOneRecTemplate: A Vector sampled at Simulink Sample rate of
%      1 by 10^-12 which would represent all useful multipath events used
%      using SV model over all time with a constant stream of one's sent
%      which includes phases and gains for ALL useful multipath ie those
%      separated by 1.4ns or more in this model
%
%      GetZeroRecTemplate: A Vector sampled at Simulink Sample rate of
%      1 by 10^-12 which would represent all useful multipath events used
%      using SV model over all time with a constant stream of one's sent
%      which includes phases and gains for ALL useful multipath ie those
%      separated by 1.4ns or more in this model
%
%      GetRakeOneRecTemplate: A Vector sampled at Simulink Sample rate of
%      1 by 10^-12 which would represent the multipath used in the Rake
%      receiver - Here initially this will be the case L=1 for a series of
%      all one's transmitted
%
%      GetRakeZeroRecTemplate: A Vector sampled at Simulink Sample rate of
%      1 by 10^-12 which would represent the multipath used in the Rake
%      receiver - Here initially this will be the case L=1 for a series of
%      all zero's transmitted
%
function [ GetOneRecVector GetZeroRecVector GetOneRecTemplate GetZeroRecTemplate GetRakeOneRecTemplate
GetRakeZeroRecTemplate ] = createinputdatavectors(losTime,NoOfRaysUsed);
```

```
%
G=0;
% G = 1 graphical output
% G = 0 no graphical output
%
% declare simulink sampling time - must match simulink sampling time which
% has been currently set to 1e-12:
simulinksamplingtime = 1e-12;
% Get the sampled data
[ SortDatatestdatt SortData NewData LNewData ] = cp0802_IEEEuwbpvialsv(losTime);
            %load SortDatatestdatt  %used for debugging only

if LNewData<NoOfRaysUsed
   NoOfRaysUsed=LNewData;      % ensure that there is enough useful rays!
end

% Now SortDatatestdatt has the following structure. It starts with
% reference to the first 'losTime' so this offset needs to be incorporated
% into its received structure
% The first column is the real magnitude (either poistive or negative)
% which gives a phase of 0 or 180 degrees (pi)
% The second column is the index into the signal relative to a sampling
% rate of 1 by 10^-12 so this gives a time location over 100ns period. As
% losTime is considered in the calculation no multipath should result in
% InterSymbol Interference (none present after 100ns at all). The third
% column is the actual time of arrival relative to the losTime (first ray
% arrives at losTime and is indexed with '1' in the second column). The
% fourth column tells us if there is an entry. The maximum numbe of entries
% is 200 (the length of the matrix)
% So summarising we have:
%   real amplitude    array index    relative time of arrival   ray present
%                                          1 yes 0 no
%
% %%%%%%%%%%%%%%%%%%%%%%%%%%%%%%%%%%%%%%%%%%%%%%%%%%%%%%%%%%%%%%%%%%%%%%% %
%                                          %
%    First do All ones case, ie generate GetOneRecVector        %
%                                          %
% %%%%%%%%%%%%%%%%%%%%%%%%%%%%%%%%%%%%%%%%%%%%%%%%%%%%%%%%%%%%%%%%%%%%%%% %
%
% Get the secondgaussianderivative template for a '1':
[onepulse,timeonepulse] = generateonepulse2();
%
% Now move this pulse in time to consider the losTime:
offset = losTime/simulinksamplingtime;
offset=fix(offset); %ensure its an interger, note it should be!
onepulseoffset=zeros(1,length(onepulse));
for cnt=1:(length(onepulse)-offset)
   onepulseoffset(cnt+offset)=onepulse(cnt);
end

if G
   figure(9);
   plot(timeonepulse,onepulse,timeonepulse,onepulseoffset);
end

% There is no need to calculate the offset for the other rays
% as this information is contained in the array index less 1
% this last operation adjusts for the fact that the first ray occurs
% at time 0 or index 1 ;so to calibrate subtraction of 1 is required
%
% First create the needed vector which will have all the One
% sent multipath:
GetOneRecVector = zeros(1,length(onepulse));
```

```
%
% onepulseoffset is our template as it will have the required losTime
% plus be the first arriving ray
%
offset=0;

if G
   figure(10);
end

for cnt=1:200   % The maximum number of possible multipath is limited
            % to 200
   if (SortDatatestdatt(cnt,4)==1) %check that there is a ray
      offset=SortDatatestdatt(cnt,2)-1; % adjust for indexing
      tempVector=zeros(1,length(onepulse));
      for cnt1=1:(length(onepulseoffset)-offset)
         tempVector(cnt1+offset)=SortDatatestdatt(cnt,1)*onepulseoffset(cnt1);
      end
      GetOneRecVector=GetOneRecVector+tempVector;
      if G
         plot(timeonepulse,GetOneRecVector);
      end
   end
end

% %%%%%%%%%%%%%%%%%%%%%%%%%%%%%%%%%%%%%%%%%%%%%%%%%%%%%%%%%%%%%%%%%%%%%
%
%                                                    %
%      Now do All zeros case, ie generate GetZeroRecVector          %
%                                                    %
% %%%%%%%%%%%%%%%%%%%%%%%%%%%%%%%%%%%%%%%%%%%%%%%%%%%%%%%%%%%%%%%%%%%%%
%
%
% Get the secondgaussianderivative template for a '1':
[zeropulse,timezeropulse] = generatezeropulse2();
%
% Now move this pulse in time to consider the losTime:
offset = losTime/simulinksamplingtime;
offset=fix(offset); %ensure its an interger, note it should be!
zeropulseoffset=zeros(1,length(zeropulse));
for cnt=1:(length(onepulse)-offset)
   zeropulseoffset(cnt+offset)=zeropulse(cnt);
end

if G
   figure(11);
   plot(timezeropulse,zeropulse,timezeropulse,zeropulseoffset);
end

% There is no need to calculate the offset for the other rays
% as this information is contained in the array index less 1
% this last operation adjusts for the fact that the first ray occurs
% at time 0 or index 1 ;so to calibrate subtraction of 1 is required
%
% First create the needed vector which will have all the Zero
% sent multipath:
GetZeroRecVector = zeros(1,length(onepulse));

%
% zeropulseoffset is our template as it will have the required losTime
% plus be the first arriving ray
%
```

```
offset=0;

if G
   figure(12);
end

for cnt=1:200   % The maximum number of possible multipath is limited
            % to 200
   if (SortDatatestdatt(cnt,4)==1) %check that there is a ray
      offset=SortDatatestdatt(cnt,2)-1; % adjust for indexing
      tempVector=zeros(1,length(zeropulse));
      for cnt1=1:(length(zeropulseoffset)-offset)
         tempVector(cnt1+offset)=SortDatatestdatt(cnt,1)*zeropulseoffset(cnt1);
      end
      GetZeroRecVector=GetZeroRecVector+tempVector;
      if G
         plot(timezeropulse,GetZeroRecVector);
      end
   end
end

if G
   figure(13);
   subplot(211),plot(timeonepulse,GetOneRecVector);
   grid;
   subplot(212),plot(timezeropulse,GetZeroRecVector);
   grid;
end

         % load SortData %% used for debugging only
%
% %%%%%%%%%%%%%%%%%%%%%%%%%%%%%%%%%%%%%%%%%%%%%%%%%%%%%%%%%%%%%%%%%%%%%%% %
%                                          %
%  Now do All useful ones case, ie generate GetOneRecTemplate     %
%                                          %
% %%%%%%%%%%%%%%%%%%%%%%%%%%%%%%%%%%%%%%%%%%%%%%%%%%%%%%%%%%%%%%%%%%%%%%% %
%
% First create the needed vector which will have all the useful One
% sent multipath:
GetOneRecTemplate = zeros(1,length(onepulse));
%
% onepulseoffset is our template as it will have the required losTime
% plus be the first arriving ray
%
offset=0;
if G
   figure(14);
end

for cnt=1:length(SortData)
   offset=SortData(cnt,2)-1; % adjust for indexing
   tempVector=zeros(1,length(onepulse));
   for cnt1=1:(length(onepulseoffset)-offset)
      tempVector(cnt1+offset)=SortData(cnt,1)*onepulseoffset(cnt1);
   end
   GetOneRecTemplate=GetOneRecTemplate+tempVector;
   if G
      plot(timeonepulse,GetOneRecTemplate);
   end
end

%
% %%%%%%%%%%%%%%%%%%%%%%%%%%%%%%%%%%%%%%%%%%%%%%%%%%%%%%%%%%%%%%%%%%%%%%% %
```

```
%                                          %
%  Now do All useful zeros case, ie generate GetZeroRecTemplate   %
%                                          %
% %%%%%%%%%%%%%%%%%%%%%%%%%%%%%%%%%%%%%%%%%%%%%%%%%%%%%%%%%%%%%%%%%%%%%%% %
%
% First create the needed vector which will have all the useful Zero
% sent multipath:
GetZeroRecTemplate = zeros(1,length(zeropulse));
%
% zeropulseoffset is our template as it will have the required losTime
% plus be the first arriving ray
%
offset=0;
if G
   figure(15);
end

for cnt=1:length(SortData)
   offset=SortData(cnt,2)-1; % adjust for indexing
   tempVector=zeros(1,length(zeropulse));
   for cnt1=1:(length(zeropulseoffset)-offset)
      tempVector(cnt1+offset)=SortData(cnt,1)*zeropulseoffset(cnt1);
   end
   GetZeroRecTemplate=GetZeroRecTemplate+tempVector;
   if G
      plot(timeonepulse,GetZeroRecTemplate);
   end
end

if G
   figure(16);
   subplot(211),plot(timeonepulse,GetOneRecTemplate);
   grid;
   subplot(212),plot(timezeropulse,GetZeroRecTemplate);
   grid;
end

            %load NewData %% used for debugging only
%
% %%%%%%%%%%%%%%%%%%%%%%%%%%%%%%%%%%%%%%%%%%%%%%%%%%%%%%%%%%%%%%%%%%%%%%% %
%                                          %
% Now do RAKE receiver ones case, ie generate GetRakeOneRecTemplate %
%                                          %
% %%%%%%%%%%%%%%%%%%%%%%%%%%%%%%%%%%%%%%%%%%%%%%%%%%%%%%%%%%%%%%%%%%%%%%% %
%
% First create the needed vector which will have all the RAKE One
% sent multipath:
GetRakeOneRecTemplate = zeros(1,length(onepulse));
%
% onepulseoffset is our template as it will have the required losTime
% plus be the first arriving ray
%
offset=0;
if G
   figure(17);
end
               % NoOfRaysUsed=length(NewData); % debug
               % NoOfRaysUsed=10; % debug

for cnt=1:NoOfRaysUsed
   offset=NewData(cnt,2)-1; % adjust for indexing
   tempVector=zeros(1,length(onepulse));
   for cnt1=1:(length(onepulseoffset)-offset)
```

```
    tempVector(cnt1+offset)=NewData(cnt,1)*onepulseoffset(cnt1);
  end
  GetRakeOneRecTemplate=GetRakeOneRecTemplate+tempVector;
  if G
    plot(timeonepulse,GetRakeOneRecTemplate);
  end
end

%
% %%%%%%%%%%%%%%%%%%%%%%%%%%%%%%%%%%%%%%%%%%%%%%%%%%%%%%%%%%%%%%%%%%%%%%%%%% %
%                                     %
% Now do RAKE receiver zeros case, ie generate GetRakeZeroRecTemplate %
%                                     %
% %%%%%%%%%%%%%%%%%%%%%%%%%%%%%%%%%%%%%%%%%%%%%%%%%%%%%%%%%%%%%%%%%%%%%%%%%% %
%
% First create the needed vector which will have all the RAKE Zero
% sent multipath:
GetRakeZeroRecTemplate = zeros(1,length(zeropulse));
%
% zeropulseoffset is our template as it will have the required losTime
% plus be the first arriving ray
%
offset=0;
if G
  figure(18);
end
for cnt=1:NoOfRaysUsed
  offset=NewData(cnt,2)-1; % adjust for indexing
  tempVector=zeros(1,length(zeropulse));
  for cnt1=1:(length(zeropulseoffset)-offset)
    tempVector(cnt1+offset)=NewData(cnt,1)*zeropulseoffset(cnt1);
  end
  GetRakeZeroRecTemplate=GetRakeZeroRecTemplate+tempVector;
  if G
    plot(timeonepulse,GetRakeZeroRecTemplate);
  end
end

if G
  figure(19);
  subplot(211),plot(timeonepulse,GetRakeOneRecTemplate);
  grid;
  subplot(212),plot(timezeropulse,GetRakeZeroRecTemplate);
  grid;
end

% now truncate or vectors by 1 element to have exactly 100ns
% intervals for simulation input data
GetOneRecVector        =  GetOneRecVector(1:100000);
GetZeroRecVector       =  GetZeroRecVector(1:100000);
GetOneRecTemplate      =     GetOneRecTemplate(1:100000);
GetZeroRecTemplate     =  GetZeroRecTemplate(1:100000);
GetRakeOneRecTemplate   =  GetRakeOneRecTemplate(1:100000);
GetRakeZeroRecTemplate  =  GetRakeZeroRecTemplate(1:100000);
```

MATLAB script: createSDTotal.m

```
function [ SDTotal ] = createSDTotal(NoOfChannels,losTime)
%testing only:
%function [SDTotal SortDatatestdatt SortData NewData LNewData ] = createSDTotal(NoOfChannels,losTime)

% SDTotal has 5 columns, every 200 rows represents 1 channel
% The first column is the gain (real number , not complex)
% The second column is an index in relative time
% The third column is calculated relative time
% The fourth column indicates the presence or absence of an entry 0 none 1
%                                          ray present
% The fifth column is a ranking of usefulness of ray 1 best, to n worse
% useful ray!

% Recommend use 7e-9 for losTime, as this is used in cp0802_IEEEuwbpvialsv()

NoOfChannels=fix(NoOfChannels);
if (NoOfChannels>=1)
   lenOfSDTotal=200*NoOfChannels;
   SDTotal=zeros(lenOfSDTotal,5);
   for cnt=1:NoOfChannels
      [ SortDatatestdatt SortData NewData LNewData ] = cp0802_IEEEuwbpvialsv(losTime)
      startpt =   ((cnt-1)*200)+1;
      endpt   =   cnt*200;
      SDTotal(startpt:endpt,1:4)=SortDatatestdatt;
      NoOfUsefulRays=max(LNewData);
      for cnt1=1:NoOfUsefulRays
         for cnt2=startpt:endpt
            if (SDTotal(cnt2,2)==NewData(cnt1,2))
               SDTotal(cnt2,5)=cnt1
            end
         end
      end
   end
end
```

Appendix 7: UWB PPM with 95% confidence intervals tabulated data for validation simulations

UWB PPM L=1 First Useful arriving ray (Partial Rake) Simulink simulation data

expected SNR dB	upper bound 95% confidence interval	Mean BER	lower bound 95% confidence interval
0	0.480364812078	0.4689	0.457435187922
2	0.473581688863	0.4612	0.448818311137
4	0.464413053748	0.4516	0.438786946252
6	0.454318576311	0.4417	0.429081423689
8	0.435766023307	0.4248	0.413833976693
10	0.418191174051	0.4054	0.392608825949
12	0.391847830849	0.3811	0.370352169151
14	0.36284441266	0.3548	0.34675558734
16	0.33015913033	0.3225	0.31484086967
18	0.29313678688	0.2858	0.27846321312
20	0.256295379915	0.2468	0.237304620085
22	0.213395657252	0.2042	0.195004342748
24	0.172628965472	0.1624	0.152171034528
25	0.155581913863	0.1454	0.135218086137
26	0.13677965787	0.1284	0.12002034213
28	0.106664978906	0.0989	0.091135021094
30	0.077165075476	0.0726	0.068034924524

UWB PPM L=4 First Useful arriving ray (Partial Rake) Simulink simulation data

expected SNR dB	upper bound 95% confidence interval	Mean BER	lower bound 95% confidence interval
0	0.44689275	0.4398	0.43270725
2	0.431640928	0.42382	0.415999072
4	0.411852712	0.4025	0.393147288
6	0.391660688	0.38	0.368339312
8	0.363612466	0.3525	0.341387534
10	0.330109387	0.3199	0.309690613
12	0.29066067	0.2805	0.27033933
14	0.245095204	0.2358	0.226504796
16	0.197535349	0.1881	0.178664651
18	0.144910938	0.1341	0.123289062
20	0.100487293	0.0908	0.081112707
22	0.057493296	0.0536	0.049706704
24	0.031854758	0.0288	0.025745242
25	0.019459783	0.0179	0.016340217
26	0.013075101	0.0115	0.009924899
28	0.006239123	0.0047	0.003160877
30	0.002993409	0.0024	0.001806591

Appendix 8: UWB PPM with 95% confidence intervals tabulated data for first arriving rays and best arriving rays (Selective Rake)

UWB PPM L=1 First arriving ray Simulink simulation data

expected SNR dB	upper bound 95% confidence interval	Mean BER	lower bound 95% confidence interval
0	0.4763700000	0.4649500000	0.4535200000
2	0.4703400000	0.4599700000	0.4496100000
4	0.4627100000	0.4520700000	0.4414200000
6	0.4549600000	0.4444400000	0.4339200000
8	0.4358500000	0.4293500000	0.4228400000
10	0.4261700000	0.4170800000	0.4079900000
12	0.4054100000	0.3977600000	0.3901100000
14	0.3814200000	0.3741200000	0.3668200000
16	0.3544600000	0.3491700000	0.3438700000
18	0.3254800000	0.3227100000	0.3199400000
20	0.2996500000	0.2958800000	0.2921100000
22	0.2741600000	0.2691000000	0.2640400000
24	0.2428800000	0.2366600000	0.2304400000
26	0.2165400000	0.2097900000	0.2030300000
28	0.2021300000	0.1939000000	0.1856700000
30	0.1870700000	0.1788400000	0.1706100000

UWB PPM L=4 First four arriving rays Simulink simulation data

expected SNR dB	upper bound 95% confidence interval	Mean BER	lower bound 95% confidence interval
0	0.4471900000	0.4409100000	0.4346300000
2	0.4332900000	0.4261900000	0.4190800000
4	0.4147600000	0.4093200000	0.4038900000
6	0.3876600000	0.3843000000	0.3809400000
8	0.3612200000	0.3592300000	0.3572500000
10	0.3308100000	0.3274200000	0.3240300000
12	0.2956100000	0.2887600000	0.2819200000
14	0.2558100000	0.2485600000	0.2413000000
16	0.2051100000	0.2031300000	0.2011400000
18	0.1594400000	0.1558500000	0.1522600000
20	0.1182100000	0.1150300000	0.1118500000
22	0.0832320000	0.0812300000	0.0792280000
24	0.0585270000	0.0550200000	0.0515130000
26	0.0403900000	0.0369640000	0.0335370000
28	0.0283330000	0.0256300000	0.0229270000
30	0.0216470000	0.0199050000	0.0181630000

UWB PPM L=1 best arriving ray (Selective Rake) Simulink simulation data

expected SNR dB	upper bound 95% confidence interval	Mean BER	lower bound 95% confidence interval
0	0.4455200000	0.4404500000	0.4353800000
2	0.4310800000	0.4246800000	0.4182700000
4	0.4131000000	0.4059700000	0.3988400000
6	0.3888700000	0.3799900000	0.3711100000
8	0.3582700000	0.3494400000	0.3406000000
10	0.3229900000	0.3131900000	0.3033900000
12	0.2804900000	0.2686300000	0.2567700000
14	0.2362700000	0.2220300000	0.2078000000
16	0.1862200000	0.1727200000	0.1592300000
18	0.1377700000	0.1260000000	0.1142200000
20	0.0917820000	0.0834030000	0.0750240000
22	0.0570470000	0.0521310000	0.0472160000
24	0.0313760000	0.0286150000	0.0258540000
26	0.0200940000	0.0182210000	0.0163470000
28	0.0149700000	0.0130790000	0.0111880000
30	0.0118390000	0.0099128000	0.0079866000

UWB PPM L=4 best arriving ray (Selective Rake) Simulink simulation data

expected SNR dB	upper bound 95% confidence interval	Mean BER	lower bound 95% confidence interval
0	0.4013900000	0.3950100000	0.3886300000
2	0.3720600000	0.3669000000	0.3617400000
4	0.3429100000	0.3372300000	0.3315400000
6	0.2998200000	0.2966100000	0.2933900000
8	0.2556400000	0.2528600000	0.2500700000
10	0.2056300000	0.2027300000	0.1998400000
12	0.1545200000	0.1508500000	0.1471700000
14	0.1057900000	0.1018100000	0.0978200000
16	0.0575150000	0.0553990000	0.0532830000
18	0.0306020000	0.0288470000	0.0270920000
20	0.0115030000	0.0110730000	0.0106440000
22	0.0039391000	0.0037049000	0.0034707000
24	0.0020016000	0.0014426000	0.0008835800
26	0.0005573100	0.0003820200	0.0002067400
28	0.0002152560	0.0001285440	0.0000418325

Appendix 9: DS TH UWB PPM with 95% confidence intervals tabulated data for first arriving rays (Partial Rake) and best arriving rays (Selective Rake)

DS TH UWB PPM two pulse system for Partial Rake, L=1

Measured Eb/No dB	upper bound 95% confidence interval	Mean BER	lower bound 95% confidence interval
-20.7410004	0.51757	0.49187	0.46617
-18.7322004	0.49532	0.47624	0.45716
-16.7364004	0.48051	0.46571	0.4509
-14.7496004	0.46613	0.44958	0.43303
-12.7478004	0.43616	0.42826	0.42036
-10.7488004	0.4164	0.40556	0.39472
-8.72640043	0.39158	0.37824	0.36489
-6.73180043	0.35668	0.3412	0.32573
-4.73740043	0.32012	0.30571	0.29129
-2.75000043	0.27533	0.26528	0.25524
-0.75620043	0.23708	0.22662	0.21616
3.277999566	0.2201	0.18913	0.15815
5.278999566	0.15699	0.1297	0.10241
7.285799566	0.10577	0.089184	0.072597
9.286799566	0.077033	0.061869	0.046706

DS TH UWB PPM two pulse system for Partial Rake, L=4

Measured Eb/No dB	upper bound 95% confidence interval	Mean BER	lower bound 95% confidence interval
-20.7526004	0.46243	0.44599	0.42955
-18.7492004	0.45449	0.43683	0.41916
-16.7370004	0.43727	0.41599	0.39471
-14.7352004	0.40626	0.38624	0.36622
-12.7302004	0.3528	0.34393	0.33506
-10.7324004	0.32611	0.3068	0.28748
-8.73980043	0.27167	0.25595	0.24022
-6.75300043	0.22096	0.20449	0.18803
-4.74860043	0.16183	0.15232	0.14281
-2.75220043	0.11367	0.10741	0.10115
-0.75987391	0.074968	0.071433	0.067899
1.269199566	0.042914	0.036797	0.03068
3.257999566	0.021049	0.015541	0.010032
5.230399566	0.010366	0.0079485	0.0055314
7.239199566	0.0040714	0.0035491	0.0030268
9.246525174	0.002314	0.0016384	0.00096284

DS TH UWB PPM two pulse system Selective Rake, L=1

Measured Eb/No dB	upper bound 95% confidence interval	Mean BER	lower bound 95% confidence interval
-20.7320004	0.52139	0.49745	0.47351
-18.7380004	0.50447	0.47919	0.45392
-16.7438004	0.49243	0.46062	0.42881
-14.7422004	0.47515	0.44493	0.41471
-12.7386004	0.427	0.41156	0.39612
-10.7404004	0.40327	0.38489	0.3665
-8.72840043	0.36072	0.33918	0.31763
-6.74340043	0.29968	0.28102	0.26235
-4.74840043	0.25556	0.24026	0.22495
-2.75820043	0.19043	0.17869	0.16696
-0.74340043	0.13224	0.12135	0.11047
3.282599566	0.081415	0.062738	0.044061
7.250399566	0.030107	0.019357	0.0086065
9.225599566	0.032107	0.015359	0

DS TH UWB PPM two pulse system Selective Rake, L=4

Measured Eb/No dB	upper bound 95% confidence interval	Mean BER	lower bound 95% confidence interval
-20.7548004	0.46114	0.45506	0.44898
-18.7446004	0.43506	0.43181	0.42855
-16.7476004	0.41009	0.40431	0.39852
-14.7364004	0.38611	0.36587	0.34563
-12.7290004	0.35462	0.32802	0.30142
-10.7478004	0.28358	0.27037	0.25715
-8.75380043	0.23541	0.22518	0.21494
-6.74757267	0.16955	0.15443	0.13932
-4.75037884	0.10344	0.098087	0.092735
-2.76000118	0.064208	0.059287	0.054366
-0.74600043	0.039735	0.031604	0.023473
1.254999566	0.015186	0.011928	0.0086703
3.239399566	0.0041868	0.0031944	0.0022021

Appendix 10: DS Modified TH UWB PPM with 95% confidence intervals tabulated data for first arriving rays (Partial Rake) and best arriving rays (Selective Rake)

DS Modified TH UWB PPM three pulse system for Partial Rake, L=1

Measured Eb/No dB	upper bound 95% confidence interval	Mean BER	lower bound 95% confidence interval
-20.7278003	0.51812	0.48975	0.46138
-18.7320003	0.51132	0.4795	0.44767
-16.7258003	0.50334	0.46996	0.43658
-14.7198003	0.48986	0.45505	0.42024
-12.7342003	0.47648	0.43686	0.39725
-10.7350003	0.44611	0.40994	0.37377
-8.73920035	0.42385	0.38369	0.34353
-6.74520035	0.3753	0.34135	0.3074
-4.76000035	0.34221	0.31437	0.28652
-2.76960035	0.30041	0.27889	0.25738
-0.77120035	0.24497	0.22868	0.2124
1.160399653	0.23936	0.19346	0.14757
3.220399653	0.21306	0.16133	0.10959
5.242999653	0.17835	0.11421	0.050072
7.300599653	0.17436	0.10721	0.040052
9.300599653	0.16818	0.095606	0.023032

DS Modified TH UWB PPM three pulse system for Partial Rake, L=4

Measured Eb/No dB	upper bound 95% confidence interval	Mean BER	lower bound 95% confidence interval
-20.7298003	0.43103	0.40874	0.38645
-18.7394003	0.4057	0.38745	0.36921
-16.7470003	0.39657	0.37107	0.34557
-14.7374003	0.36602	0.34665	0.32727
-12.7542003	0.33094	0.3154	0.29987
-10.7570003	0.29661	0.28095	0.26529
-8.76660035	0.26667	0.24409	0.22151
-6.75360035	0.21524	0.20519	0.19513
-4.74600035	0.23952	0.17827	0.11702
-2.77260035	0.10387	0.093613	0.083354
-0.77800035	0.054521	0.049785	0.045049
1.216399653	0.02589	0.021933	0.017977
3.219999653	0.013213	0.011425	0.0096369
5.239599653	0.0068383	0.0045571	0.002276
7.235799653	0.0042456	0.0025297	0.00081383
9.244799653	0.0040061	0.002033	0.0000599830

DS Modified TH UWB PPM three pulse system Selective Rake, L=1

Measured Eb/No dB	upper bound 95% confidence interval	Mean BER	lower bound 95% confidence interval
-20.7304003	0.47376	0.45549	0.43722
-18.7196003	0.46178	0.43964	0.4175
-16.7214003	0.44421	0.4239	0.40359
-14.7352003	0.42305	0.40467	0.38628
-12.7360003	0.40774	0.38437	0.36101
-10.7606003	0.36438	0.34775	0.33113
-8.74880035	0.32122	0.30667	0.29212
-6.77120035	0.28649	0.26877	0.25104
-4.77100035	0.21832	0.21176	0.20521
-2.75940035	0.16576	0.15687	0.14797
-0.77440035	0.11194	0.10748	0.10302
1.275399653	0.082215	0.060746	0.039277
3.258199653	0.044145	0.037879	0.031613
5.243599653	0.044624	0.022597	0.0005697
7.239799653	0.012854	0.010406	0.0079587
9.213599653	0.01118	0.0081684	0.0051567

DS Modified TH UWB PPM three pulse system Selective Rake, L=4

Measured Eb/No dB	upper bound 95% confidence interval	Mean BER	lower bound 95% confidence interval
-20.7226003	0.44823	0.42785	0.40747
-18.7336003	0.41787	0.40176	0.38566
-16.7428003	0.39034	0.37249	0.35464
-14.7632003	0.35834	0.34241	0.32648
-12.7578003	0.31666	0.29735	0.27804
-10.7592003	0.26406	0.25441	0.24476
-8.76120035	0.21132	0.19889	0.18647
-6.76500035	0.16618	0.1528	0.13943
-4.74860035	0.10425	0.093077	0.081904
-2.76600035	0.054014	0.047464	0.040914
-0.77120035	0.021165	0.018729	0.016292
1.223399653	0.0098044	0.0072651	0.0047259
3.208599653	0.0035624	0.0022776	0.00099291

Appendix 11: Single seed data (seedc) for SISO DS TH UWB PPM for first rays, for first useful arriving rays (Partial Rake) and best arriving rays (Selective Rake)

DS TH UWB PPM two pulse system for first arriving ray, L=1

Measured Eb/No dB	Mean BER
-20.78900043	0.49751
-18.76800043	0.48544
-16.77900043	0.48077
-14.78900043	0.47847
-12.79300043	0.4717
-10.78100043	0.44444
-8.778000434	0.42373
-6.780000434	0.41152
-4.782000434	0.40323
-2.768000434	0.37175
-0.761000434	0.33223
1.252999566	0.3125
3.220999566	0.28169
5.252999566	0.29412
7.335999566	0.29851
9.389999566	0.28571

DS TH UWB PPM two pulse system for first four arriving rays, L=4

Measured Eb/No dB	Mean BER
-20.80100043	0.45872
-18.78700043	0.44843
-16.78400043	0.4386
-14.78900043	0.40984
-12.76000043	0.39063
-10.76400043	0.37313
-8.761000434	0.34364
-6.754000434	0.31646
-4.779000434	0.25253
-2.808000434	0.2045
-0.797000434	0.18215
1.237999566	0.09009
3.246999566	0.071942
5.255999566	0.068182
7.344999566	0.037037
9.344999566	0.037037

DS TH UWB PPM two pulse system for first useful arriving rays (PRake), L=1

Measured Eb/No dB	Mean BER
-20.79600043	0.46948
-18.79900043	0.45662
-16.78100043	0.44444
-14.78200043	0.43478
-12.78000043	0.42194
-10.77100043	0.4
-8.759000434	0.37594
-6.775000434	0.3413
-4.756000434	0.30769
-2.786000434	0.25575
-0.810000434	0.22727
1.344999566	0.18519
3.394999566	0.17241
5.242999566	0.10417
7.238999566	0.083333
9.215999566	0.042553
11.24199957	0.031847
13.22099957	0.028169
15.20799957	0.02457
19.19399957	0.015244
29.22118957	0.012092

DS TH UWB PPM two pulse system for first four useful arriving rays (PRake), L=4

Measured Eb/No dB	Mean BER
-20.79900043	0.45662
-18.78800043	0.45045
-16.78000043	0.42194
-14.76600043	0.3937
-12.76900043	0.35211
-10.76300043	0.32787
-8.773000434	0.26738
-6.810000434	0.21277
-4.811000434	0.15601
-2.782000434	0.11669
-0.784367789	0.073099415
1.226999566	0.049261
3.226999566	0.026738
5.204999566	0.013141
7.204999566	0.0044379
9.222627606	0.003061224

DS TH UWB PPM two pulse system for best useful arriving rays (SRake), L=1

Measured Eb/No dB	Mean BER
-20.76800043	0.48544
-18.80100043	0.46729
-16.78700043	0.44843
-14.77900043	0.44053
-12.78400043	0.42553
-10.76800043	0.39841
-8.763000434	0.34483
-6.781000434	0.27855
-4.790000434	0.24631
-2.812000434	0.17668
-0.783000434	0.11025
3.246999566	0.09901
5.220999566	0.04902
7.182999566	0.019881
9.206999566	0.0085763
11.21599957	0.0072886
13.19599957	0.0046992
15.20662258	0.00387597

DS TH UWB PPM two pulse system for best four useful arriving rays (PRake), L=4

Measured Eb/No dB	Mean BER
-20.80100043	0.46729
-18.78400043	0.43103
-16.77700043	0.41322
-14.75800043	0.3861
-12.76100043	0.34364
-10.78100043	0.27855
-8.790000434	0.24631
-6.80986164	0.168350168
-4.777892471	0.1017294
-2.785004181	0.068399453
-0.753000434	0.049505
1.212999566	0.018182
3.201999566	0.003861
5.201999566	0.003861
7.213999566	0.00036463
9.213999566	0.00036463

Appendix 12: Single seed data (seedc) for MIMO Non-Optimal STS TH UWB PPM (chip by chip decision) for first rays, for first useful arriving rays (Partial Rake) and best arriving rays (Selective Rake)

MIMO Non-optimal STS TH UWB PPM two pulse system for first arriving ray, L=1

Measured Eb/No dB	Mean BER
-29.77760035	0.49261
-27.79560035	0.45455
-25.78060035	0.4717
-23.77760035	0.48544
-21.79960035	0.50761
-19.79060035	0.51282
-17.79960035	0.50761
-15.79160035	0.53191
-13.80460035	0.50505
-11.80960035	0.44643
-9.787600347	0.47619
-7.787600347	0.47619
-5.787600347	0.47619
-3.785600347	0.47847
-1.808600347	0.43103
0.245399653	0.40486
2.253399653	0.40161
4.210399653	0.37175
6.207399653	0.369
8.230399653	0.38168
10.18939965	0.34965
12.19239965	0.31546
14.15439965	0.29851
16.17749965	0.26882
18.18019965	0.21692
20.19979965	0.18282
22.19019965	0.17123
24.21882965	0.15601
26.16519965	0.11614
28.15419965	0.10799
30.15309965	0.088417

MIMO Non-optimal STS TH UWB PPM two pulse system for first four arriving rays, L=4

Measured Eb/No dB	Mean BER
-29.80260035	0.52083
-27.78860035	0.55556
-25.79760035	0.53763
-23.79160035	0.53191
-21.78960035	0.55249
-19.79560035	0.54054
-17.79260035	0.54348
-15.79360035	0.5102
-13.78660035	0.51546
-11.78060035	0.4717
-9.815600347	0.44053
-7.810600347	0.44843
-5.796600347	0.45872
-3.812600347	0.4386
-1.765600347	0.38314
0.169399653	0.33445
2.168399653	0.33557
4.186399653	0.24155
6.187399653	0.14144
8.159399653	0.11198
10.14839965	0.099502
12.17639965	0.071429
14.18579965	0.055617
16.17059965	0.045269
18.18219965	0.034435
20.15859965	0.024516
22.15419965	0.021598
24.20512965	0.016103
26.15269965	0.010363
28.18919965	0.00625
30.15159965	0.0040816

MIMO Non-optimal STS TH UWB PPM two pulse system for first useful arriving rays (PRake), L=1

Measured Eb/No dB	Mean BER
-29.78060035	0.4717
-27.79260035	0.46729
-25.78460035	0.48077
-23.79660035	0.45872
-21.78060035	0.48309
-19.78060035	0.48309
-17.79960035	0.50761
-15.79560035	0.50251
-13.80460035	0.45249
-11.80560035	0.42918
-9.812600347	0.4386
-7.798600347	0.42553
-5.795600347	0.45455
-3.814600347	0.44444
-1.769600347	0.38168
0.245399653	0.40486
2.183399653	0.34247
4.159399653	0.3012
6.177399653	0.27397
8.185399653	0.21186
10.19939965	0.17452
12.20639965	0.15949
14.19449965	0.13387
16.17209965	0.11682
18.20389965	0.098276
20.15659965	0.080451
22.17169965	0.063012
24.15622265	0.047768
26.17079965	0.038158
28.18359965	0.035676
30.16219965	0.029223

MIMO Non-optimal STS TH UWB PPM two pulse system for first four useful arriving rays (PRake), L=4

Measured Eb/No dB	Mean BER
-29.79160035	0.54945
-27.77760035	0.56818
-25.72660035	0.59524
-23.72660035	0.5988
-21.79560035	0.54054
-19.78260035	0.56497
-17.79060035	0.51282
-15.79060035	0.51282
-13.79760035	0.53763
-11.79260035	0.54645
-9.784600347	0.49751
-7.760600347	0.3876
-5.783600347	0.37736
-3.820600347	0.34602
-1.812600347	0.2193
0.215399653	0.14771
2.155399653	0.11099
4.173399653	0.070225
6.167399653	0.041068
8.165399653	0.025113
10.16439965	0.014
12.16439965	0.00825
14.18549965	0.005168
16.17819965	0.0027996
18.16429965	0.0015
20.16429965	0.001
22.16429965	0.001
24.16428265	0.001
26.18019965	0.00098296
28.16429965	0.0005
30.17509965	0.00016667

MIMO Non-optimal STS TH UWB PPM two pulse system for best useful arriving rays (SRake), L=1

Measured Eb/No dB	Mean BER
-29.75060035	0.57803
-27.78260035	0.56497
-25.79260035	0.54645
-23.79260035	0.54645
-22.04260035	0.55556
-19.78660035	0.51546
-17.79660035	0.52356
-15.78660035	0.51546
-13.78660035	0.51546
-11.79960035	0.50761
-9.791600347	0.52632
-7.796600347	0.52356
-5.781600347	0.49505
-3.800600347	0.46083
-1.802600347	0.35587
0.177399653	0.27397
2.186399653	0.22124
4.190399653	0.13245
6.137399653	0.097561
8.137399653	0.055741
10.13739965	0.0375
12.13739965	0.0315
14.13739965	0.021
16.16829965	0.013055
18.17819965	0.0098348
20.17819965	0.011
22.17819965	0.0075245
24.17239965	0.0064392
26.17239965	0.0053996
28.17239965	0.0020776
30.17239965	0.0024301

MIMO Non-optimal STS TH UWB PPM two pulse system for best four useful arriving rays (PRake), L=4

Measured Eb/No dB	Mean BER
-29.79560035	0.54054
-27.79160035	0.53191
-25.75060035	0.57803
-23.79660035	0.52356
-21.78960035	0.55249
-19.79660035	0.52356
-17.79160035	0.52632
-15.79260035	0.54645
-13.79160035	0.52632
-11.77760035	0.48544
-9.804600347	0.45249
-7.821600347	0.34722
-5.765600347	0.37736
-3.857600347	0.29851
-1.685600347	0.15504
0.208399653	0.10582
2.205399653	0.051813
4.186399653	0.024155
6.184399653	0.012469
8.175399653	0.0037481
10.16539965	0.0025107
12.16539965	0.0012553
14.17199965	0.00036534
16.17199965	0.00036534

Appendix 13: MIMO DS UWB PPM with 95% confidence intervals tabulated data for validation simulations of Yang Analog ST coding I schema from Yang [9]

MIMO DS UWB PPM L=1 First Useful arriving ray (Partial Rake) Simulink simulation data

Normalised SNR dB	upper bound 95% confidence interval	Mean BER	lower bound 95% confidence interval
1	0.5119	0.48891	0.46592
3	0.51616	0.49002	0.46387
5	0.48795	0.47576	0.46357
7	0.46276	0.45671	0.45065
9	0.4567	0.44111	0.42552
11	0.41303	0.40193	0.39082
13	0.36613	0.35303	0.33993
15	0.3342	0.31919	0.30418
17	0.25614	0.2465	0.23687
19	0.17477	0.16832	0.16187
21	0.12741	0.11899	0.11057
23	0.073239	0.070667	0.068095
25	0.046455	0.042	0.037545
27	0.0319	0.028667	0.025433
29	0.018947	0.017695	0.016443
31	0.013884	0.011902	0.0099198
33	0.0082983	0.0072409	0.0061836

MIMO DS UWB PPM L=4 First Useful arriving ray (Partial Rake) Simulink simulation data

Normalised SNR dB	upper bound 95% confidence interval	Mean BER	lower bound 95% confidence interval
1	0.45948	0.43605	0.41262
3	0.4555	0.42119	0.38689
5	0.38201	0.37468	0.36735
7	0.35223	0.34091	0.32958
9	0.29246	0.28879	0.28512
11	0.22952	0.22261	0.2157
13	0.17254	0.16739	0.16223
15	0.10479	0.097347	0.089899
17	0.054190505	0.047055667	0.039920828
19	0.018368331	0.016711	0.015053669
21	0.006401264	0.005433333	0.004465403
23	0.001399796	0.001066667	0.000733537

MIMO DS UWB PPM L=1 best Useful arriving ray (Selective Rake) Simulink simulation data

This data was measured from the Simulink Simulator but was not used in the thesis report or any publication.

Normalised SNR dB	upper bound 95% confidence interval	Mean BER	lower bound 95% confidence interval
1	0.5128	0.47599	0.43918
3	0.49283	0.46467	0.43651
5	0.45631	0.44413	0.43195
7	0.43797	0.41874	0.39951
9	0.42929	0.3942	0.35912
11	0.35286	0.32553	0.2982
13	0.29018	0.26764	0.2451
15	0.19602	0.18449	0.17296
17	0.12123	0.11823	0.11524
19	0.06774	0.063333	0.058926
21	0.0309	0.027667	0.024433

MIMO DS UWB PPM L=4 best four Useful arriving rays (Selective Rake) Simulink simulation data

This data was measured from the Simulink Simulator but was not used in the thesis report or any publication.

Normalised SNR dB	upper bound 95% confidence interval	Mean BER	lower bound 95% confidence interval
1	0.4706	0.45318	0.43576
3	0.45449	0.42026	0.38603
5	0.39814	0.38282	0.36751
7	0.34821	0.3326	0.31699
9	0.25818	0.24175	0.22532
11	0.17623	0.16413	0.15203
13	0.10454	0.096717	0.088894
15	0.044275	0.040667	0.037059
17	0.016201	0.013	0.009799

Appendix 14: MIMO DS UWB PPM with 95% confidence intervals tabulated data for validation simulations of Yang Analog ST coding I schema from Yang [9] in terms of measured Eb/No

MIMO DS UWB PPM L=1 First Useful arriving ray (Partial Rake) Simulink simulation data for measured Eb/No

Measured Eb/No (dB)	upper bound 95% confidence interval	Mean BER	lower bound 95% confidence interval
-20.783	0.52689	0.49989	0.47289
-18.778	0.51945	0.49919	0.47893
-16.779	0.5119	0.48891	0.46592
-14.783	0.51616	0.49002	0.46387
-12.773	0.48795	0.47576	0.46357
-10.776	0.46276	0.45671	0.45065
-8.7763	0.4567	0.44111	0.42552
-6.7741	0.41303	0.40193	0.39082
-4.7612	0.36613	0.35303	0.33993
-2.755	0.3342	0.31919	0.30418
-0.76756	0.25614	0.2465	0.23687
1.23837691	0.17477	0.16832	0.16187
3.24119062	0.12741	0.11899	0.11057
5.24285902	0.073239	0.070667	0.068095
7.24285902	0.046455	0.042	0.037545
9.24285902	0.0319	0.028667	0.025433
11.2358578	0.018947	0.017695	0.016443
13.2375192	0.013884	0.011902	0.00992
15.2373408	0.008298	0.007241	0.006184

MIMO DS UWB PPM L=4 First Useful arriving ray (Partial Rake) Simulink simulation data for measured Eb/No

Measured Eb/No (dB)	upper bound 95% confidence interval	Mean BER	lower bound 95% confidence interval
-20.782	0.47512	0.46742	0.45972
-18.779	0.47314	0.46526	0.45738
-16.776	0.45948	0.43605	0.41262
-14.779	0.4555	0.42119	0.38689
-12.76	0.38201	0.37468	0.36735
-10.756	0.35223	0.34091	0.32958
-8.754	0.29246	0.28879	0.28512
-6.7667	0.22952	0.22261	0.2157
-4.7656	0.17254	0.16739	0.16223
-2.7645	0.10479	0.097347	0.089899
-0.76747278	0.054190505	0.04705567	0.03992083
1.231643986	0.018368331	0.016711	0.01505367
3.228810777	0.006401264	0.00543333	0.0044654
5.243657321	0.001399796	0.00106667	0.00073354

MIMO DS UWB PPM L=1 best Useful arriving ray (Selective Rake) Simulink simulation data for measured Eb/No

Measured Eb/No (dB)	upper bound 95% confidence interval	Mean BER	lower bound 95% confidence interval
-20.772	0.54831	0.50604	0.46378
-18.766	0.5543	0.50275	0.4512
-16.77	0.5128	0.47599	0.43918
-14.771	0.49283	0.46467	0.43651
-12.775	0.45631	0.44413	0.43195
-10.774	0.43797	0.41874	0.39951
-8.7641	0.42929	0.3942	0.35912
-6.7585	0.35286	0.32553	0.2982
-4.7532	0.29018	0.26764	0.2451
-2.7608	0.19602	0.18449	0.17296
-0.75765	0.12123	0.11823	0.11524
1.24285902	0.06774	0.063333	0.058926
3.24285902	0.0309	0.027667	0.024433

MIMO DS UWB PPM L=4 best four Useful arriving rays (Selective Rake) Simulink simulation data for measured Eb/No

Measured Eb/No (dB)	upper bound 95% confidence interval	Mean BER	lower bound 95% confidence interval
-20.771	0.50796	0.46478	0.42159
-18.779	0.46717	0.44981	0.43245
-16.774	0.4706	0.45318	0.43576
-14.78	0.45449	0.42026	0.38603
-12.77	0.39814	0.38282	0.36751
-10.745	0.34821	0.3326	0.31699
-8.7567	0.25818	0.24175	0.22532
-6.7608	0.17623	0.16413	0.15203
-4.759	0.10454	0.096717	0.088894
-2.7571	0.044275	0.040667	0.037059
-0.75714	0.016201	0.013	0.009799

Appendix 15: Optimal MIMO STS TH UWB PPM with 95% confidence intervals tabulated data in terms of measured Eb/No

MIMO STS TH UWB PPM L=1 First Useful arriving ray (Partial Rake) Simulink simulation data for measured Eb/No

Measured Eb/No (dB)	upper bound 95% confidence interval	Mean BER	lower bound 95% confidence interval
-26.808	0.50123	0.49868	0.49613
-24.793	0.50694	0.4969	0.48686
-22.788	0.53742	0.50842	0.47943
-20.781	0.52825	0.50004	0.47184
-18.794	0.53827	0.5197	0.50114
-16.778	0.51398	0.48705	0.46011
-14.778	0.54236	0.50683	0.47129
-12.76	0.51172	0.47335	0.43498
-10.779	0.51678	0.49519	0.47359
-8.7838	0.51063	0.4765	0.44237
-6.7866	0.46467	0.44415	0.42363
-4.7714	0.41798	0.392	0.36601
-2.7965	0.34137	0.33248	0.32359
-0.7911	0.24952	0.2351	0.22068
1.2211	0.21305	0.19429	0.17554
3.2133	0.15355	0.142	0.13046
5.2122	0.093837	0.087	0.080163
7.214	0.064483	0.054758	0.045032
9.214	0.039369	0.035303	0.031237
11.213	0.025004	0.022818	0.020632
13.218	0.014964	0.012486	0.010009
15.206	0.010724	0.0096681	0.0086123
17.203	0.0085804	0.0080499	0.0075195
19.208	0.0059205	0.0048992	0.0038778
21.208	0.0044286	0.0042257	0.0040228

MIMO STS TH UWB PPM L=4 First four Useful arriving rays (Partial Rake) Simulink simulation data for measured Eb/No

Measured Eb/No (dB)	upper bound 95% confidence interval	Mean BER	lower bound 95% confidence interval
-26.782	0.517	0.49595	0.47491
-24.788	0.50479	0.49214	0.47948
-22.784	0.51337	0.49645	0.47954
-20.781	0.51367	0.49125	0.46883
-18.775	0.48892	0.4751	0.46127
-16.795	0.50622	0.47865	0.45107
-14.785	0.48959	0.46255	0.4355
-12.776	0.45575	0.43179	0.40783
-10.791	0.39954	0.38703	0.37452
-8.7956	0.35116	0.34085	0.33054
-6.8069	0.29243	0.26225	0.23207
-4.7755	0.17007	0.16612	0.16217
-2.7875	0.099118	0.0961	0.093082
-0.78782	0.060941	0.051667	0.042393
1.1807	0.046077	0.034546	0.023015
3.2059	0.0079883	0.0063256	0.0046629
5.2109	0.0049998	0.0037174	0.0024349

MIMO STS TH UWB PPM L=1 best Useful arriving ray (Selective Rake) Simulink simulation data for measured Eb/No

Measured Eb/No (dB)	upper bound 95% confidence interval	Mean BER	lower bound 95% confidence interval
-26.806	0.52149	0.49568	0.46987
-24.805	0.52856	0.49649	0.46442
-22.804	0.5211	0.49136	0.46161
-20.797	0.54753	0.50043	0.45333
-18.804	0.52481	0.491	0.4572
-16.786	0.49083	0.47175	0.45267
-14.764	0.49292	0.47058	0.44823
-12.761	0.48498	0.45647	0.42795
-10.766	0.46427	0.4453	0.42632
-8.7735	0.43979	0.42377	0.40776
-6.7959	0.40897	0.35041	0.29185
-4.7979	0.34006	0.29781	0.25556
-2.7906	0.24844	0.20989	0.17135
1.2122	0.076088	0.067	0.057912
5.2122	0.016488	0.013	0.009512

MIMO STS TH UWB PPM L=4 best four Useful arriving rays (Selective Rake) Simulink simulation data for measured Eb/No

Measured Eb/No (dB)	upper bound 95% confidence interval	Mean BER	lower bound 95% confidence interval
-26.794	0.54707	0.51033	0.4736
-24.794	0.51076	0.49944	0.48811
-22.799	0.5111	0.50104	0.49098
-20.802	0.52554	0.51481	0.50408
-18.799	0.52971	0.52275	0.51578
-16.798	0.52124	0.50317	0.4851
-14.784	0.47404	0.45533	0.43663
-12.788	0.4666	0.42902	0.39144
-10.803	0.35124	0.33593	0.32062
-8.8014	0.29509	0.27016	0.24524
-6.7693	0.17447	0.16684	0.1592
-4.7933	0.11749	0.10091	0.084335
-2.7878	0.054468	0.046	0.037532

Appendix 16: Optimal MIMO STS TH UWB PPM with 95% confidence intervals tabulated data in terms of measured Eb/No adjusted for two symbols and one branch as each branch has both transmitted symbols

MIMO STS TH UWB PPM L=1 First Useful arriving ray (Partial Rake) Simulink simulation data for measured Eb/No

Measured Eb/No (dB) (Single branch)	upper bound 95% confidence interval	Mean BER	lower bound 95% confidence interval
-29.75	0.50123	0.49868	0.49613
-27.74	0.50694	0.4969	0.48686
-25.735	0.53742	0.50842	0.47943
-23.736	0.52825	0.50004	0.47184
-21.741	0.53827	0.5197	0.50114
-19.731	0.51398	0.48705	0.46011
-17.746	0.54236	0.50683	0.47129
-15.725	0.51172	0.47335	0.43498
-13.73	0.51678	0.49519	0.47359
-11.745	0.51063	0.4765	0.44237
-9.7456	0.46467	0.44415	0.42363
-7.7366	0.41798	0.392	0.36601
-5.7559	0.34137	0.33248	0.32359
-3.7693	0.24952	0.2351	0.22068
-1.7539	0.21305	0.19429	0.17554
0.24873	0.15355	0.142	0.13046
2.2221	0.093837	0.087	0.080163
4.2284	0.064483	0.054758	0.045032
6.2284	0.039369	0.035303	0.031237
8.2264	0.025004	0.022818	0.020632
10.225	0.014964	0.012486	0.010009
12.21	0.010724	0.0096681	0.0086123
14.198	0.0085804	0.0080499	0.0075195
16.204	0.0059205	0.0048992	0.0038778
18.205	0.0044286	0.0042257	0.0040228

MIMO STS TH UWB PPM L=4 First four Useful arriving rays (Partial Rake) Simulink simulation data for measured Eb/No

Measured Eb/No (dB) (Single branch)	upper bound 95% confidence interval	Mean BER	lower bound 95% confidence interval
-29.734	0.517	0.49595	0.47491
-27.736	0.50479	0.49214	0.47948
-25.735	0.51337	0.49645	0.47954
-23.735	0.51367	0.49125	0.46883
-21.726	0.48892	0.4751	0.46127
-19.729	0.50622	0.47865	0.45107
-17.743	0.48959	0.46255	0.4355
-15.731	0.45575	0.43179	0.40783
-13.75	0.39954	0.38703	0.37452
-11.75	0.35116	0.34085	0.33054
-9.8116	0.29243	0.26225	0.23207
-7.7503	0.17007	0.16612	0.16217
-5.7793	0.099118	0.0961	0.093082
-3.7779	0.060941	0.051667	0.042393
-1.7849	0.046077	0.034546	0.023015
0.22707	0.0079883	0.0063256	0.0046629
2.2096	0.0049998	0.0037174	0.0024349

MIMO STS TH UWB PPM L=1 best Useful arriving ray (Selective Rake) Simulink simulation data for measured Eb/No

Measured Eb/No (dB) (Single branch)	upper bound 95% confidence interval	Mean BER	lower bound 95% confidence interval
-29.745	0.52149	0.49568	0.46987
-27.752	0.52856	0.49649	0.46442
-25.745	0.5211	0.49136	0.46161
-23.726	0.54753	0.50043	0.45333
-21.744	0.52481	0.491	0.4572
-19.738	0.49083	0.47175	0.45267
-17.714	0.49292	0.47058	0.44823
-15.708	0.48498	0.45647	0.42795
-13.725	0.46427	0.4453	0.42632
-11.751	0.43979	0.42377	0.40776
-9.7699	0.40897	0.35041	0.29185
-7.7836	0.34006	0.29781	0.25556
-5.7796	0.24844	0.20989	0.17135
-1.7779	0.076088	0.067	0.057912
2.2221	0.016488	0.013	0.009512

MIMO STS TH UWB PPM L=4 best four Useful arriving rays (Selective Rake) Simulink simulation data for measured Eb/No

Measured Eb/No (dB) (Single branch)	upper bound 95% confidence interval	Mean BER	lower bound 95% confidence interval
-29.726	0.54707	0.51033	0.4736
-27.726	0.51076	0.49944	0.48811
-25.731	0.5111	0.50104	0.49098
-23.745	0.52554	0.51481	0.50408
-21.748	0.52971	0.52275	0.51578
-19.734	0.52124	0.50317	0.4851
-17.746	0.47404	0.45533	0.43663
-15.755	0.4666	0.42902	0.39144
-13.76	0.35124	0.33593	0.32062
-11.794	0.29509	0.27016	0.24524
-9.7473	0.17447	0.16684	0.1592
-7.7809	0.11749	0.10091	0.084335
-5.7779	0.054468	0.046	0.037532

Appendix 17: Optimal MIMO STS TH UWB PPM in presence of MAI using 32 chip Walsh Hadamard spreading sequences with 95% confidence intervals tabulated data

Table of Walsh Hadamard Code set assignments for 10 MAI case study

Note: Codes c23 through c32 are not used in MAI studies for MAI with 10 interferes, c1 and c2 are formed for targeted user, other pairs are MAI

Code label	Walsh Hadamard code set for 32 chips																													
c3	1	1	1	1	1	1	1	1	1	1	1	1	1	1	1	1	1	1	1	1	1	1	1	1	1	1	1	1	1	1
c1	1	-1	1	-1	1	-1	1	-1	1	-1	1	-1	1	-1	1	-1	1	-1	1	-1	1	-1	1	-1	1	-1	1	-1	1	-1
c2	1	1	-1	-1	1	1	-1	-1	1	1	-1	-1	1	1	-1	-1	1	1	-1	-1	1	1	-1	-1	1	1	-1	-1	1	-1
c5	1	-1	-1	1	1	-1	-1	1	1	-1	-1	1	1	-1	-1	1	1	-1	-1	1	1	-1	-1	1	1	-1	-1	1	1	-1
c7	1	1	1	1	-1	-1	-1	-1	1	1	1	1	-1	-1	-1	-1	1	1	1	1	-1	-1	-1	-1	1	1	1	1	-1	-1
c9	1	-1	1	-1	-1	1	-1	1	1	-1	1	-1	-1	1	-1	1	1	-1	1	-1	-1	1	-1	1	1	-1	1	-1	-1	1
c11	1	1	-1	-1	-1	-1	1	1	1	1	-1	-1	-1	-1	1	1	1	1	-1	-1	-1	-1	1	1	1	1	-1	-1	-1	-1
c13	1	-1	-1	1	-1	1	1	-1	1	-1	-1	1	-1	1	1	-1	1	-1	-1	1	-1	1	1	-1	1	-1	-1	1	-1	1
c15	1	1	1	1	1	1	1	1	-1	-1	-1	-1	-1	-1	-1	-1	1	1	1	1	1	1	1	1	-1	-1	-1	-1	-1	-1
c17	1	-1	1	-1	1	-1	1	-1	-1	1	-1	1	-1	1	-1	1	1	-1	1	-1	1	-1	1	-1	-1	1	-1	1	-1	1
c19	1	1	-1	-1	1	1	-1	-1	-1	-1	1	1	-1	-1	1	1	1	1	-1	-1	1	1	-1	-1	-1	-1	1	1	-1	-1
c21	1	-1	-1	1	1	-1	-1	1	-1	1	1	-1	-1	1	1	-1	1	-1	-1	1	1	-1	-1	1	-1	1	1	-1	-1	1
c23	1	1	1	1	-1	-1	-1	-1	-1	-1	-1	-1	1	1	1	1	1	1	1	1	-1	-1	-1	-1	-1	-1	-1	-1	1	1
c25	1	-1	1	-1	-1	1	-1	1	-1	1	-1	1	1	-1	1	-1	1	-1	1	-1	-1	1	-1	1	-1	1	-1	1	1	-1
c27	1	1	-1	-1	-1	-1	1	1	-1	-1	1	1	1	1	-1	-1	1	1	-1	-1	-1	-1	1	1	-1	-1	1	1	1	1
c29	1	-1	-1	1	-1	1	1	-1	-1	1	1	-1	1	-1	-1	1	1	-1	-1	1	-1	1	1	-1	-1	1	1	-1	1	-1
c4	1	1	1	1	1	1	1	1	1	1	1	1	1	1	1	1	-1	-1	-1	-1	-1	-1	-1	-1	-1	-1	-1	-1	-1	-1
c31	1	-1	1	-1	1	-1	1	-1	1	-1	1	-1	1	-1	1	-1	-1	1	-1	1	-1	1	-1	1	-1	1	-1	1	-1	1
c32	1	1	-1	-1	1	1	-1	-1	1	1	-1	-1	1	1	-1	-1	-1	-1	1	1	-1	-1	1	1	-1	-1	1	1	-1	-1
c30	1	-1	-1	1	1	-1	-1	1	1	-1	-1	1	1	-1	-1	1	-1	1	1	-1	-1	1	1	-1	-1	1	1	-1	-1	1
c28	1	1	1	1	-1	-1	-1	-1	1	1	1	1	-1	-1	-1	-1	-1	-1	-1	-1	1	1	1	1	-1	-1	-1	-1	1	1
c26	1	-1	1	-1	-1	1	-1	1	1	-1	1	-1	-1	1	-1	1	-1	1	-1	1	1	-1	1	-1	-1	1	-1	1	1	-1
c24	1	1	-1	-1	-1	-1	1	1	1	1	-1	-1	-1	-1	1	1	-1	-1	1	1	1	1	-1	-1	-1	-1	1	1	1	1
c22	1	-1	-1	1	-1	1	1	-1	1	-1	-1	1	-1	1	1	-1	-1	1	1	-1	1	-1	-1	1	-1	1	1	-1	1	-1
c20	1	1	1	1	1	1	1	1	-1	-1	-1	-1	-1	-1	-1	-1	-1	-1	-1	-1	-1	-1	-1	-1	1	1	1	1	1	1
c18	1	-1	1	-1	1	-1	1	-1	-1	1	-1	1	-1	1	-1	1	-1	1	-1	1	-1	1	-1	1	1	-1	1	-1	1	-1
c16	1	1	-1	-1	1	1	-1	-1	-1	-1	1	1	-1	-1	1	1	-1	-1	1	1	-1	-1	1	1	1	1	-1	-1	1	1
c14	1	-1	-1	1	1	-1	-1	1	-1	1	1	-1	-1	1	1	-1	-1	1	1	-1	-1	1	1	-1	1	-1	-1	1	1	-1
c12	1	1	1	1	-1	-1	-1	-1	-1	-1	-1	-1	1	1	1	1	-1	-1	-1	-1	1	1	1	1	1	1	1	1	-1	-1
c10	1	-1	1	-1	-1	1	-1	1	-1	1	-1	1	1	-1	1	-1	-1	1	-1	1	1	-1	1	-1	1	-1	1	-1	-1	1
c8	1	1	-1	-1	-1	-1	1	1	-1	-1	1	1	1	1	-1	-1	-1	-1	1	1	1	1	-1	-1	1	1	-1	-1	1	1
c6	1	-1	-1	1	-1	1	1	-1	-1	1	1	-1	1	-1	-1	1	-1	1	1	-1	1	-1	-1	1	1	-1	-1	1	-1	1

MIMO STS TH UWB PPM L=1 using 32 chip Walsh Hadamard spreading sequences First useful arriving ray (Partial Rake) Simulink simulation data for measured Eb/No in presence of 5 MAI at measured Eb/No of 3.15dB

Measured Eb/No (dB)	upper bound 95% confidence interval	Mean BER	lower bound 95% confidence interval
-10.8046552	0.50183	0.47833	0.45484
-8.80465517	0.45874	0.44633	0.43393
-6.80465517	0.42327	0.41167	0.40006
-4.80465517	0.41258	0.39	0.36742
-2.80465517	0.36128	0.35167	0.34205
-0.80465517	0.316173974	0.303666667	0.291159359
1.195344827	0.2523	0.24367	0.23504
3.195344827	0.19247	0.184	0.17553
5.195344827	0.15222	0.13633	0.12044
7.195344827	0.09853	0.087667	0.076803

MIMO STS TH UWB PPM L=4 using 32 chip Walsh Hadamard spreading sequences First four useful arriving rays (Partial Rake) Simulink simulation data for measured Eb/No in presence of 5 MAI at measured Eb/No of 3.15dB

Measured Eb/No (dB)	upper bound 95% confidence interval	Mean BER	lower bound 95% confidence interval
-10.794	0.41263	0.39684	0.38105
-8.7937	0.34792	0.33029	0.31266
-6.7925	0.3087	0.29583	0.28296
-4.8015	0.22859	0.21188	0.19517
-2.7962	0.15013	0.14494	0.13976
-0.75131	0.17464	0.1341	0.093571
1.2155	0.074756	0.067274	0.059792
3.1987	0.043263	0.032851	0.022439
5.1964	0.024689	0.017214	0.0097379
7.1953	0.014222	0.0093333	0.0044443

MIMO STS TH UWB PPM L=1 using 32 chip Walsh Hadamard spreading sequences First useful arriving ray (Partial Rake) Simulink simulation data for measured Eb/No in presence of 10 MAI at measured Eb/No of 3.15dB

Measured Eb/No (dB)	upper bound 95% confidence interval	Mean BER	lower bound 95% confidence interval
-10.805	0.49147	0.477	0.46253
-8.8047	0.4495	0.43933	0.42917
-6.8047	0.42924	0.41033	0.39143
-4.8047	0.40423	0.382	0.35977
-2.8047	0.37496	0.35733	0.33971
-0.80466	0.3265	0.314	0.3015
1.1953	0.27275	0.26633	0.25992
3.1953	0.22823	0.21567	0.20311
5.19534	0.17444	0.16567	0.15689
7.1953	0.12978	0.12433	0.11889

MIMO STS TH UWB PPM L=4 using 32 chip Walsh Hadamard spreading sequences First four useful arriving rays (Partial Rake) Simulink simulation data for measured Eb/No in presence of 10 MAI at measured Eb/No of 3.15dB

Measured Eb/No (dB)	upper bound 95% confidence interval	Mean BER	lower bound 95% confidence interval
-10.7936242	0.38918075	0.381456667	0.373732583
-8.80232161	0.35809439	0.332913333	0.307732277
-6.80115537	0.299608072	0.295066667	0.290525261
-4.80248687	0.235047865	0.2297	0.224352135
-2.80127372	0.192662027	0.189176667	0.185691306
-0.8034841	0.148525589	0.13593	0.123334411
1.198678697	0.113695722	0.108403333	0.103110945
3.196011263	0.061038033	0.054134333	0.047230634
5.196525108	0.030435957	0.026877	0.023318043
7.195344827	0.019455057	0.015	0.010544943

Appendix 18: Optimal MIMO STS TH UWB PPM in presence of MAI using 32 chip Wysocki (low cross-correlation) spreading sequences with 95% confidence intervals tabulated data

Table of Wysocki Code set assignments for 10 MAI case study

Note: Codes c23 through c32 are not used in MAI studies for MAI with 10 interferes, c1 and c2 are formed for targeted user, other pairs are MAI

Code label				Wysocki low correlation code set for 32 chips																											
c3	1	1	-1	-1	1	-1	1	-1	-1	1	-1	-1	-1	1	1	1	1	-1	-1	1	1	1	1	1	1	1	1	1	1	1	1
c1	1	-1	-1	1	1	1	1	1	-1	-1	-1	1	-1	-1	1	-1	1	1	-1	-1	1	-1	1	-1	1	-1	1	-1	1	-1	1	-1
c2	1	1	1	1	1	-1	-1	1	-1	1	1	1	-1	1	-1	-1	1	-1	1	-1	1	1	-1	-1	1	1	-1	-1	1	1	-1	-1
c5	1	-1	1	-1	1	1	-1	-1	-1	-1	1	-1	-1	-1	-1	1	1	1	1	1	1	-1	-1	1	1	-1	-1	1	1	-1	-1	1
c7	1	1	-1	-1	-1	1	-1	1	-1	1	-1	-1	1	-1	-1	-1	1	-1	-1	1	-1	-1	-1	-1	1	1	1	1	-1	-1	-1	-1
c9	1	-1	-1	1	-1	-1	-1	-1	-1	-1	-1	1	1	1	-1	1	1	1	-1	-1	-1	1	-1	1	1	-1	1	-1	-1	1	-1	1
c11	1	1	1	1	-1	1	1	-1	-1	1	1	1	1	-1	1	1	1	-1	1	-1	-1	-1	1	1	1	1	-1	-1	-1	-1	1	1
c13	1	-1	1	-1	-1	-1	1	1	-1	-1	1	-1	1	1	1	-1	1	1	1	1	-1	1	1	-1	1	-1	-1	1	-1	1	1	-1
c15	1	1	-1	-1	1	-1	1	-1	1	-1	1	1	1	-1	-1	-1	1	-1	-1	1	1	1	1	1	-1	-1	-1	-1	-1	-1	-1	-1
c17	1	-1	-1	1	1	1	1	1	1	1	1	-1	1	1	-1	1	1	1	-1	-1	1	-1	1	-1	-1	1	-1	1	-1	1	-1	1
c19	1	1	1	1	1	-1	-1	1	1	-1	-1	-1	1	-1	1	1	1	-1	1	-1	1	1	-1	-1	-1	-1	1	1	-1	-1	1	1
c21	1	-1	1	-1	1	1	-1	-1	1	1	-1	1	1	1	1	-1	1	1	1	1	1	-1	-1	1	-1	1	1	-1	-1	1	1	-1
c23	1	1	-1	-1	-1	1	-1	1	1	-1	1	1	-1	1	1	1	1	-1	-1	1	-1	-1	-1	-1	-1	-1	-1	-1	-1	1	1	1	1
c25	1	-1	-1	1	-1	-1	-1	-1	1	1	1	-1	-1	-1	1	-1	1	1	-1	-1	-1	1	-1	1	-1	1	-1	1	1	-1	1	-1
c27	1	1	1	1	-1	1	1	-1	1	-1	-1	-1	-1	1	-1	-1	1	-1	1	-1	-1	-1	1	1	-1	-1	1	1	1	1	-1	-1
c29	1	-1	1	-1	-1	-1	1	1	1	1	-1	1	-1	-1	-1	1	1	1	1	1	-1	1	1	-1	-1	1	1	-1	1	-1	-1	1
c4	1	1	-1	-1	1	-1	1	-1	-1	1	-1	-1	-1	1	1	1	-1	1	1	-1	-1	-1	-1	-1	-1	-1	-1	-1	-1	-1	-1	-1
c31	1	-1	-1	1	1	1	1	1	-1	-1	-1	1	-1	-1	1	-1	-1	-1	1	1	-1	1	-1	1	-1	1	-1	1	-1	1	-1	1
c32	1	1	1	1	1	-1	-1	1	-1	1	1	1	-1	1	-1	-1	-1	1	-1	1	-1	-1	1	1	-1	-1	1	1	-1	-1	1	1
c30	1	-1	1	-1	1	1	-1	-1	-1	-1	1	-1	-1	-1	-1	1	-1	-1	-1	-1	-1	1	1	-1	-1	1	1	-1	-1	1	1	-1
c28	1	1	-1	-1	-1	1	-1	1	-1	1	-1	-1	1	-1	-1	-1	-1	1	1	-1	1	1	1	1	-1	-1	-1	-1	1	1	1	1
c26	1	-1	-1	1	-1	-1	-1	-1	-1	-1	-1	1	1	1	-1	1	-1	-1	1	1	1	-1	1	-1	-1	1	-1	1	1	-1	1	-1
c24	1	1	1	1	-1	1	1	-1	-1	1	1	1	1	-1	1	1	-1	1	-1	1	1	1	-1	-1	-1	-1	1	1	1	1	-1	-1
c22	1	-1	1	-1	-1	-1	1	1	-1	-1	1	-1	1	1	1	-1	-1	-1	-1	-1	1	-1	-1	1	-1	1	1	-1	1	-1	-1	1
c20	1	1	-1	-1	1	-1	1	-1	1	-1	1	1	1	-1	-1	-1	-1	1	1	-1	-1	-1	-1	-1	1	1	1	1	1	1	1	1
c18	1	-1	-1	1	1	1	1	1	1	1	1	-1	1	1	-1	1	-1	-1	1	1	-1	1	-1	1	1	-1	1	-1	1	-1	1	-1
c16	1	1	1	1	1	-1	-1	1	1	-1	-1	-1	1	-1	1	1	-1	1	-1	1	-1	-1	1	1	1	1	-1	-1	1	1	-1	-1
c14	1	-1	1	-1	1	1	-1	-1	1	1	-1	1	1	1	1	-1	-1	-1	-1	-1	-1	1	1	-1	1	-1	-1	1	1	-1	-1	1
c12	1	1	-1	-1	-1	1	-1	1	1	-1	1	1	-1	1	1	1	-1	1	1	-1	1	1	1	1	1	1	1	1	-1	-1	-1	-1
c10	1	-1	-1	1	-1	-1	-1	-1	1	1	1	-1	-1	-1	1	-1	-1	-1	1	1	1	-1	1	-1	1	-1	1	-1	-1	1	-1	1
c8	1	1	1	1	-1	1	1	-1	1	-1	-1	-1	-1	1	-1	-1	-1	1	-1	1	1	1	-1	-1	1	1	-1	-1	-1	-1	1	1
c6	1	-1	1	-1	-1	-1	1	1	1	1	-1	1	-1	-1	-1	1	-1	-1	-1	-1	1	-1	-1	1	1	-1	-1	1	-1	1	1	-1

MIMO STS TH UWB PPM L=1 using 32 chip Wysocki (low cross-correlation) spreading sequences First useful arriving ray (Partial Rake) Simulink simulation data for measured Eb/No in presence of 5 MAI at measured Eb/No of 3.15dB

Measured Eb/No (dB)	upper bound 95% confidence interval	Mean BER	lower bound 95% confidence interval
-10.79564	0.48127	0.46600	0.45073
-8.7956	0.45204	0.44267	0.43329
-6.7956	0.45988	0.43667	0.41346
-4.79564	0.45108	0.41667	0.38226
-2.7956	0.40614	0.37333	0.34052
-0.79564	0.35491	0.318	0.28109
1.2044	0.31261	0.27133	0.23006
3.2044	0.26635	0.222	0.17765
5.2044	0.20655	0.16867	0.13079
7.2044	0.15649	0.13333	0.11018

MIMO STS TH UWB PPM L=4 using 32 chip Wysocki (low cross-correlation) spreading sequences First four useful arriving rays (Partial Rake) Simulink simulation data for measured Eb/No in presence of 5 MAI at measured Eb/No of 3.15dB

Measured Eb/No (dB)	upper bound 95% confidence interval	Mean BER	lower bound 95% confidence interval
-10.79098	0.45892	0.44357	0.42822
-8.7813	0.41449	0.39654	0.37859
-6.7922	0.32883	0.32585	0.32286
-4.7995	0.28097	0.26949	0.25801
-2.7961	0.2121	0.20356	0.19502
-0.80482	0.15644	0.13933	0.12222
1.2038	0.098233	0.093167	0.088101
3.20385	0.05768	0.05567	0.05365
5.2038	0.029544	0.024	0.018456
7.20385	0.01448	0.01167	0.00886

MIMO STS TH UWB PPM L=1 using 32 chip Wysocki (low cross-correlation) spreading sequences First useful arriving ray (Partial Rake) Simulink simulation data for measured Eb/No in presence of 10 MAI at measured Eb/No of 3.15dB

Measured Eb/No (dB)	upper bound 95% confidence interval	Mean BER	lower bound 95% confidence interval
-10.796	0.50454	0.48133	0.45812
-8.79564082	0.502635636	0.478666667	0.454697697
-6.7956	0.48554	0.474	0.46246
-4.7956	0.48162	0.45733	0.43305
-2.7956	0.46152	0.42867	0.39582
-0.79564	0.41682	0.39533	0.37384
1.2044	0.35347	0.334	0.31453
3.2044	0.30148	0.27667	0.25186
5.2044	0.27298	0.24667	0.22035
7.2044	0.22203	0.19467	0.16731

MIMO STS TH UWB PPM L=4 using 32 chip Wysocki (low cross-correlation) spreading sequences First four useful arriving rays (Partial Rake) Simulink simulation data for measured Eb/No in presence of 10 MAI at measured Eb/No of 3.15dB

Measured Eb/No (dB)	upper bound 95% confidence interval	Mean BER	lower bound 95% confidence interval
-10.785	0.46664	0.4505	0.43436
-8.7956	0.44614	0.42933	0.41252
-6.7956	0.40222	0.38467	0.36711
-4.79564	0.36112	0.34533	0.32955
-2.7956	0.29177	0.286	0.28023
-0.79564	0.22289	0.21067	0.19844
1.2044	0.17413	0.146	0.11787
3.2044	0.10999	0.099333	0.088678
5.2044	0.056772	0.054	0.051228
7.2044	0.028879	0.020667	0.012455

Appendix 19: Optimal MIMO STS TH UWB PPM in presence of MAI using 32 chip Gold orthogonal spreading sequences with 95% confidence intervals tabulated data

Table of Gold orthogonal Code set assignments for 10 MAI case study

Note: Codes c23 through c32 are not used in MAI studies for MAI with 10 interferes, c1 and c2 are formed for targeted user, other pairs are MAI

Code label	gold orthogonal code set for 32 chips																															
c3	1	-1	-1	-1	1	-1	1	-1	1	1	-1	1	-1	-1	-1	-1	1	1	-1	-1	1	-1	-1	1	1	1	1	1	-1	1	1	1
c1	1	-1	-1	-1	-1	-1	-1	1	-1	-1	1	1	1	1	-1	-1	-1	-1	1	-1	1	-1	-1	-1	-1	1	-1	1	1	1	1	-1
c2	1	1	-1	-1	1	1	1	1	-1	-1	1	-1	-1	1	1	-1	1	-1	1	1	1	-1	-1	1	-1	-1	1	-1	-1	-1	1	1
c5	1	-1	1	-1	1	-1	-1	-1	-1	-1	1	-1	1	-1	1	1	1	1	1	1	-1	-1	-1	1	1	-1	-1	1	1	1	-1	1
c7	1	-1	-1	1	1	-1	1	1	1	-1	1	-1	1	1	-1	1	-1	1	-1	1	-1	1	-1	1	1	1	-1	-1	-1	-1	1	-1
c9	1	1	-1	-1	-1	-1	1	-1	-1	1	1	-1	1	1	1	-1	-1	-1	-1	-1	-1	1	1	1	1	1	1	-1	1	1	-1	1
c11	1	-1	1	-1	1	1	1	-1	1	-1	-1	-1	1	1	1	1	1	-1	1	-1	1	1	1	-1	1	1	1	1	1	-1	1	-1
c13	1	1	-1	1	1	-1	-1	-1	1	1	1	1	1	1	1	1	-1	1	1	1	1	-1	1	-1	-1	1	1	1	-1	-1	-1	1
c15	1	-1	1	-1	-1	-1	1	1	1	1	-1	-1	-1	1	1	1	-1	-1	-1	1	-1	-1	-1	-1	-1	-1	1	1	-1	1	-1	-1
c17	1	1	-1	1	1	1	1	-1	-1	1	-1	1	1	-1	1	1	-1	-1	1	-1	-1	1	-1	1	-1	-1	-1	1	-1	1	1	-1
c19	1	1	1	-1	-1	-1	-1	-1	1	-1	-1	1	-1	1	-1	1	-1	-1	1	1	1	1	1	1	1	-1	-1	-1	-1	1	1	1
c21	1	-1	1	1	1	1	1	1	1	1	1	1	-1	-1	1	-1	-1	-1	1	1	-1	-1	1	-1	1	1	-1	-1	1	1	1	1
c23	1	-1	-1	1	-1	-1	-1	-1	-1	1	-1	-1	-1	-1	-1	1	1	-1	1	1	-1	1	-1	-1	-1	1	1	-1	1	-1	1	1
c25	1	-1	-1	-1	-1	1	1	1	1	-1	-1	1	1	-1	-1	-1	-1	1	1	1	-1	1	1	1	-1	-1	1	1	1	-1	-1	1
c27	1	-1	-1	-1	1	1	-1	-1	-1	1	1	1	-1	1	-1	-1	1	-1	-1	1	-1	1	1	-1	1	-1	-1	1	-1	-1	-1	-1
c29	1	1	-1	-1	1	-1	-1	1	1	-1	-1	-1	-1	-1	1	-1	1	1	1	-1	-1	1	1	-1	-1	1	-1	-1	-1	1	-1	-1
c4	1	1	1	-1	1	-1	1	1	-1	1	1	1	1	-1	-1	1	1	1	-1	1	1	1	1	-1	-1	-1	1	-1	1	1	1	-1
c31	1	1	1	1	1	-1	1	-1	-1	-1	-1	-1	-1	1	-1	-1	-1	1	-1	-1	-1	-1	1	-1	-1	-1	-1	1	1	-1	1	1
c32	1	-1	1	1	-1	-1	1	-1	1	-1	1	1	1	-1	1	-1	1	-1	-1	-1	1	1	-1	-1	-1	-1	-1	-1	-1	-1	-1	1
c30	1	-1	-1	1	-1	1	1	-1	1	1	1	-1	-1	1	-1	1	1	1	1	-1	1	-1	1	1	-1	-1	-1	-1	1	1	-1	-1
c28	1	1	-1	-1	-1	1	-1	-1	1	1	-1	-1	1	-1	1	-1	-1	1	-1	1	1	-1	-1	-1	1	-1	-1	-1	1	-1	1	-1
c26	1	1	1	-1	1	1	-1	1	1	1	-1	1	1	1	-1	1	1	-1	-1	-1	-1	-1	-1	1	-1	1	-1	-1	1	-1	-1	1
c24	1	-1	1	1	1	-1	-1	1	-1	1	-1	1	-1	1	1	-1	-1	1	1	-1	1	1	-1	1	1	-1	1	-1	1	-1	-1	-1
c22	1	1	-1	1	-1	-1	1	1	-1	-1	-1	1	-1	-1	1	1	1	-1	-1	1	1	-1	1	1	1	1	-1	1	1	-1	-1	-1
c20	1	1	1	-1	-1	1	1	-1	-1	-1	1	1	-1	-1	-1	1	-1	1	1	-1	-1	-1	-1	-1	1	1	1	-1	-1	-1	-1	-1
c18	1	1	1	1	1	1	-1	-1	1	-1	1	-1	-1	-1	-1	-1	-1	-1	-1	1	1	1	-1	1	-1	1	1	1	1	1	-1	-1
c16	1	1	1	1	-1	-1	-1	1	1	1	1	-1	1	-1	-1	-1	1	-1	1	-1	-1	-1	1	1	1	-1	1	1	-1	-1	1	-1
c14	1	1	1	1	-1	1	1	1	-1	1	-1	-1	1	1	-1	-1	1	1	1	1	1	1	-1	-1	1	1	-1	1	-1	1	-1	1
c12	1	-1	1	1	-1	1	-1	-1	-1	-1	-1	1	1	1	1	-1	1	1	-1	1	-1	-1	1	1	-1	1	1	-1	-1	1	1	-1
c10	1	1	-1	1	-1	1	-1	1	1	-1	1	1	-1	1	1	1	1	1	-1	-1	-1	1	-1	-1	1	-1	1	1	1	1	1	1
c8	1	-1	1	-1	-1	1	-1	1	-1	1	1	-1	-1	-1	1	1	-1	1	-1	-1	1	1	1	1	-1	1	-1	1	-1	-1	1	1
c6	1	-1	-1	1	1	1	-1	1	-1	-1	-1	-1	1	-1	-1	1	-1	-1	-1	-1	1	-1	1	-1	1	-1	1	-1	-1	1	-1	1

MIMO STS TH UWB PPM L=1 using 32 chip gold (low cross-correlation) spreading sequences First useful arriving ray (Partial Rake) Simulink simulation data for measured Eb/No in presence of 5 MAI at measured Eb/No of 3.15dB

Measured Eb/No (dB)	upper bound 95% confidence interval	Mean BER	lower bound 95% confidence interval
-10.795	0.47687	0.45867	0.44047
-8.7992	0.47187	0.44818	0.42449
-6.7955	0.46399	0.44067	0.41735
-4.7955	0.40504	0.38933	0.37363
-2.7955	0.3402	0.32533	0.31046
-0.79547	0.30274	0.27867	0.25459
1.2045	0.24045	0.21867	0.19688
3.2045	0.1815	0.16867	0.15583
5.2045	0.13173	0.122	0.11227
7.2045	0.087893	0.068667	0.049441

MIMO STS TH UWB PPM L=4 using 32 chip gold (low cross-correlation) spreading sequences First four useful arriving rays (Partial Rake) Simulink simulation data for measured Eb/No in presence of 5 MAI at measured Eb/No of 3.15dB

Measured Eb/No (dB)	upper bound 95% confidence interval	Mean BER	lower bound 95% confidence interval
-10.795	0.3888	0.368	0.3472
-8.7955	0.34327	0.328	0.31273
-6.7955	0.26266	0.25933	0.256
-4.7955	0.22899	0.208	0.18701
-2.7955	0.15531	0.138	0.12069
-0.79547	0.11109	0.094667	0.078242
1.2045	0.065951	0.052	0.038049
3.2045	0.031201	0.028	0.024799
5.2045	0.017029	0.013333	0.0096376
7.2045	0.0072006	0.004	0.00079939

MIMO STS TH UWB PPM L=1 using 32 chip gold (low cross-correlation) spreading sequences First useful arriving ray (Partial Rake) Simulink simulation data for measured Eb/No in presence of 10 MAI at measured Eb/No of 3.15dB

Measured Eb/No (dB)	upper bound 95% confidence interval	Mean BER	lower bound 95% confidence interval
-10.795	0.46415	0.45533	0.44652
-8.7955	0.46501	0.45067	0.43632
-6.7955	0.4371	0.424	0.4109
-4.7955	0.40804	0.39267	0.37729
-2.7955	0.36203	0.344	0.32597
-0.79547	0.32104	0.30533	0.28963
1.2045	0.30029	0.28267	0.26504
3.2045	0.24527	0.23	0.21473
5.2045	0.17446	0.16267	0.15087
7.2045	0.13582	0.118	0.10018

MIMO STS TH UWB PPM L=4 using 32 chip gold (low cross-correlation) spreading sequences First four useful arriving rays (Partial Rake) Simulink simulation data for measured Eb/No in presence of 10 MAI at measured Eb/No of 3.15dB

Measured Eb/No (dB)	upper bound 95% confidence interval	Mean BER	lower bound 95% confidence interval
-10.795	0.41162	0.38333	0.35505
-8.7955	0.37339	0.338	0.30261
-6.7955	0.32618	0.29067	0.25516
-4.7955	0.28102	0.24267	0.20431
-2.7955	0.22377	0.20067	0.17757
-0.79547	0.16889	0.15133	0.13378
1.2045	0.10777	0.102	0.09623
3.2045	0.069881	0.051333	0.032785
5.204527	0.042910	0.034000	0.025090
7.2045	0.015201	0.012	0.0087994

Appendix 20: Optimal MIMO STS TH UWB PPM in presence of MAI using 32 chip w32dash03 low correlation orthogonal spreading sequences with 95% confidence intervals tabulated data

Table of w32dash03 orthogonal Code set assignments for 10 MAI case study

Note: Codes c23 through c32 are not used in MAI studies for MAI with 10 interferes, c1 and c2 are formed for targeted user, other pairs are MAI

Code assignment						W32dash03 low correlation orthogonal code set for 32 chips																									
c3	-1	1	-1	1	-1	1	1	1	1	-1	-1	-1	1	-1	-1	1	1	1	-1	1	1	1	1	1	1	1	1	1	1	1	1
c1	-1	-1	-1	1	-1	1	-1	1	-1	-1	1	1	-1	-1	1	-1	1	1	-1	-1	-1	-1	-1	-1	1	1	-1	-1	1	-1	1	1
c2	-1	1	1	1	-1	1	1	-1	1	1	-1	1	-1	1	-1	-1	-1	1	-1	1	-1	-1	-1	-1	-1	1	1	-1	-1	1	-1	1
c5	-1	1	-1	-1	-1	1	1	1	-1	-1	1	-1	-1	1	1	1	-1	-1	-1	1	1	-1	-1	-1	-1	-1	1	1	-1	-1	1	-1
c7	-1	-1	-1	1	1	1	1	1	1	1	-1	1	1	1	1	-1	1	-1	1	1	1	1	-1	-1	-1	-1	-1	1	1	-1	-1	1
c9	-1	1	1	1	-1	-1	1	1	1	-1	1	-1	-1	-1	1	-1	-1	1	1	-1	1	1	1	-1	-1	-1	-1	-1	1	1	-1	-1
c11	-1	-1	-1	-1	-1	1	-1	1	1	-1	-1	1	1	1	-1	-1	-1	-1	-1	-1	-1	-1	1	1	1	-1	-1	-1	-1	-1	1	1	-1
c13	-1	-1	1	1	1	1	1	-1	1	-1	-1	-1	-1	-1	1	1	-1	-1	1	1	-1	-1	1	1	1	-1	-1	-1	-1	-1	1	1
c15	-1	1	1	-1	-1	-1	1	1	-1	-1	-1	-1	1	1	-1	-1	1	-1	1	-1	1	-1	-1	1	1	1	-1	-1	-1	-1	-1	1
c17	-1	1	-1	-1	1	1	-1	1	1	1	-1	-1	1	-1	1	1	-1	1	1	-1	-1	1	-1	-1	1	1	1	-1	-1	-1	-1	-1
c19	-1	-1	-1	1	1	-1	1	-1	1	-1	1	-1	1	-1	-1	-1	1	-1	-1	-1	-1	-1	1	-1	-1	1	1	1	-1	-1	-1	-1
c21	-1	-1	1	1	-1	-1	-1	1	-1	-1	-1	1	1	-1	-1	1	-1	1	1	1	-1	-1	-1	1	-1	-1	1	1	1	-1	-1	-1
c23 - u	-1	-1	1	-1	-1	1	-1	-1	1	1	-1	-1	-1	-1	-1	1	1	-1	-1	-1	1	-1	-1	-1	1	-1	-1	1	1	1	-1	-1
c25 - u	-1	-1	1	-1	1	1	1	-1	-1	-1	1	-1	1	1	-1	1	1	1	1	1	-1	1	-1	-1	-1	1	-1	-1	1	1	1	-1
c27 - u	-1	-1	1	-1	1	-1	1	1	-1	1	-1	1	1	-1	1	1	1	1	-1	-1	1	-1	1	-1	-1	-1	1	-1	-1	1	1	1
c29 - u	-1	1	1	-1	1	-1	-1	1	1	1	1	-1	-1	-1	-1	-1	1	1	-1	1	-1	1	-1	1	-1	-1	-1	1	-1	-1	1	1
c4	-1	1	-1	-1	1	-1	-1	-1	1	-1	1	1	1	1	-1	1	-1	1	-1	1	1	-1	1	-1	1	-1	-1	-1	1	-1	-1	1
c31 - u	-1	1	-1	1	1	-1	-1	-1	-1	-1	-1	1	-1	-1	1	1	1	-1	-1	1	1	1	-1	1	-1	1	-1	-1	-1	1	-1	-1
c32 - u	-1	-1	-1	1	-1	-1	-1	-1	-1	1	-1	-1	-1	1	-1	-1	1	1	1	1	1	1	1	-1	1	-1	1	-1	-1	-1	1	-1
c30 - u	-1	-1	1	1	-1	1	-1	-1	-1	1	1	-1	1	1	1	1	-1	1	-1	-1	1	1	1	1	-1	1	-1	1	-1	-1	-1	1
c28 - u	-1	1	1	-1	-1	1	1	-1	-1	1	1	1	1	-1	1	-1	1	-1	-1	1	-1	1	1	1	1	-1	1	-1	1	-1	-1	-1
c26 - u	-1	-1	-1	-1	1	1	1	1	-1	1	1	1	-1	-1	-1	-1	-1	1	1	1	1	-1	1	1	1	1	-1	1	-1	1	-1	-1
c24 - u	-1	-1	1	1	1	-1	1	1	1	1	1	1	-1	1	-1	1	-1	-1	-1	-1	1	1	-1	1	1	1	1	-1	1	-1	1	-1
c22	-1	-1	1	-1	-1	-1	-1	1	1	-1	1	1	-1	1	1	1	1	-1	1	1	-1	1	1	-1	1	1	1	1	-1	1	-1	1
c20	-1	1	1	-1	1	1	-1	-1	1	-1	-1	1	-1	1	1	-1	1	1	1	-1	1	-1	1	1	-1	1	1	1	1	-1	1	-1
c18	-1	-1	-1	-1	1	-1	1	-1	-1	-1	-1	-1	-1	1	1	-1	-1	1	-1	-1	-1	1	-1	1	1	-1	1	1	1	1	-1	1
c16	-1	1	1	1	1	-1	-1	1	-1	1	-1	-1	1	1	1	-1	-1	-1	-1	1	-1	-1	1	-1	1	1	-1	1	1	1	1	-1
c14	-1	-1	-1	-1	-1	-1	-1	-1	1	1	1	-1	1	-1	1	-1	-1	-1	1	1	1	-1	-1	1	-1	1	1	-1	1	1	1	1
c12	-1	1	1	1	1	1	-1	-1	-1	-1	1	1	1	-1	-1	-1	-1	-1	1	-1	1	1	-1	-1	1	-1	1	1	-1	1	1	1
c10	-1	1	-1	-1	-1	-1	1	-1	-1	1	-1	1	-1	-1	-1	1	-1	-1	1	-1	-1	1	1	-1	-1	1	-1	1	1	-1	1	1
c8	-1	1	-1	1	1	1	-1	1	-1	1	1	-1	-1	1	-1	1	1	-1	1	-1	-1	-1	1	1	-1	-1	1	-1	1	1	-1	1
c6	-1	1	-1	1	-1	-1	1	-1	1	1	1	1	1	1	1	1	1	1	1	-1	-1	-1	-1	1	1	-1	-1	1	-1	1	1	-1

MIMO STS TH UWB PPM L=1 using 32 chip w32dash03 (low cross-correlation) spreading sequences First useful arriving ray (Partial Rake) Simulink simulation data for measured Eb/No in presence of 5 MAI at measured Eb/No of 3.15dB

Measured Eb/No (dB)	upper bound 95% confidence interval	Mean BER	lower bound 95% confidence interval
-10.795	0.50172	0.474	0.44628
-8.7955	0.4831	0.4613	0.4396
-6.7955	0.45844	0.44867	0.43889
-4.7955	0.4317	0.41867	0.40563
-2.7955	0.36823	0.36067	0.3531
-0.79547	0.31373	0.304	0.29427
1.2045	0.24786	0.234	0.22014
3.2045	0.19886	0.17067	0.14248
5.2045	0.14451	0.12267	0.10082
7.2045	0.10286	0.086	0.06914

MIMO STS TH UWB PPM L=4 using 32 chip w32dash03 (low cross-correlation) spreading sequences First four useful arriving rays (Partial Rake) Simulink simulation data for measured Eb/No in presence of 5 MAI at measured Eb/No of 3.15dB

Measured Eb/No (dB)	upper bound 95% confidence interval	Mean BER	lower bound 95% confidence interval
-10.795	0.3872	0.384	0.3808
-8.7955	0.34865	0.33467	0.32068
-6.7955	0.28588	0.27867	0.27145
-4.7955	0.23018	0.212	0.19382
-2.7955	0.15204	0.14267	0.13329
-0.79547	0.11155	0.10333	0.095121
1.2045	0.073602	0.064	0.054398
3.2045	0.042401	0.036	0.029599
5.2045	0.018362	0.014667	0.010971
7.2045	0.011556	0.0066667	0.0017777

MIMO STS TH UWB PPM L=1 using 32 chip w32dash03 (low cross-correlation) spreading sequences First useful arriving ray (Partial Rake) Simulink simulation data for measured Eb/No in presence of 10 MAI at measured Eb/No of 3.15dB

Measured Eb/No (dB)	upper bound 95% confidence interval	Mean BER	lower bound 95% confidence interval
-10.795	0.48042	0.46067	0.44092
-8.7955	0.45785	0.44333	0.42881
-6.7955	0.43968	0.42533	0.41099
-4.7955	0.40313	0.39133	0.37954
-2.7955	0.37333	0.366	0.35867
-0.79547	0.32113	0.30933	0.29754
1.2045	0.25359	0.25267	0.25174
3.2045	0.20103	0.19733	0.19364
5.2045	0.17826	0.15467	0.13107
7.2045	0.13451	0.11267	0.090822

MIMO STS TH UWB PPM L=4 using 32 chip w32dash03 (low cross-correlation) spreading sequences First four useful arriving rays (Partial Rake) Simulink simulation data for measured Eb/No in presence of 10 MAI at measured Eb/No of 3.15dB

Measured Eb/No (dB)	upper bound 95% confidence interval	Mean BER	lower bound 95% confidence interval
-10.795	0.42086	0.404	0.38714
-8.7955	0.36247	0.354	0.34553
-6.7955	0.31287	0.294	0.27513
-4.7955	0.27812	0.24667	0.21521
-2.7955	0.22074	0.19667	0.17259
-0.79547	0.16422	0.14667	0.12911
1.2045	0.10599	0.095333	0.084678
3.2045	0.061329	0.054667	0.048004
5.2045	0.038058	0.030667	0.023275
7.2045	0.017029	0.013333	0.0096376

Appendix 21: Optimal MIMO STS TH UWB PPM in presence of MAI using 32 chip h32dash03 orthogonal spreading sequences with 95% confidence intervals tabulated data

Table of h32dash03 orthogonal Code set assignments for 10 MAI case study

Note: Codes c23 through c32 are not used in MAI studies for MAI with 10 interferes, c1 and c2 are formed for targeted user, other pairs are MAI

Code assignment	h32dash03 orthogonal code set for 32 chips																															
c3	1	1	1	1	1	1	1	1	1	1	1	1	1	1	1	1	1	1	1	1	1	1	1	1	1	1	1	1	1	1	1	1
c1	1	-1	1	1	1	1	-1	1	-1	1	-1	-1	-1	1	-1	-1	1	1	1	-1	-1	-1	-1	-1	1	1	-1	-1	1	-1	1	1
c2	1	1	-1	1	1	1	1	-1	1	-1	1	-1	-1	-1	1	-1	-1	1	1	1	-1	-1	-1	-1	-1	1	1	-1	-1	1	-1	1
c5	1	1	1	-1	1	1	1	1	-1	1	-1	1	-1	-1	-1	1	-1	-1	1	1	1	-1	-1	-1	-1	-1	1	1	-1	-1	1	-1
c7	1	-1	1	1	-1	1	1	1	1	-1	1	-1	1	-1	-1	-1	1	-1	-1	1	1	1	-1	-1	-1	-1	-1	1	1	-1	-1	1
c9	1	1	-1	1	1	-1	1	1	1	1	-1	1	-1	1	-1	-1	-1	1	-1	-1	1	1	1	-1	-1	-1	-1	-1	1	1	-1	-1
c11	1	-1	1	-1	1	1	-1	1	1	1	1	-1	1	-1	1	-1	-1	-1	1	-1	-1	1	1	1	-1	-1	-1	-1	-1	1	1	-1
c13	1	-1	-1	1	-1	1	1	-1	1	1	1	1	-1	1	-1	1	-1	-1	-1	1	-1	-1	1	1	1	-1	-1	-1	-1	-1	1	1
c15	1	1	-1	-1	1	-1	1	1	-1	1	1	1	1	-1	1	-1	1	-1	-1	-1	1	-1	-1	1	1	1	-1	-1	-1	-1	-1	1
c17	1	1	1	-1	-1	1	-1	1	1	-1	1	1	1	1	-1	1	-1	1	-1	-1	-1	1	-1	-1	1	1	1	-1	-1	-1	-1	-1
c19	1	-1	1	1	-1	-1	1	-1	1	1	-1	1	1	1	1	-1	1	-1	1	-1	-1	-1	1	-1	-1	1	1	1	-1	-1	-1	-1
c21	1	-1	-1	1	1	-1	-1	1	-1	1	1	-1	1	1	1	1	-1	1	-1	1	-1	-1	-1	1	-1	-1	1	1	1	-1	-1	-1
c23 -	1	-1	-1	-1	1	1	-1	-1	1	-1	1	1	-1	1	1	1	1	-1	1	-1	1	-1	-1	-1	1	-1	-1	1	1	1	-1	-1
c25 -	1	-1	-1	-1	-1	1	1	-1	-1	1	-1	1	1	-1	1	1	1	1	-1	1	-1	1	-1	-1	-1	1	-1	-1	1	1	1	-1
c27 -	1	-1	-1	-1	-1	-1	1	1	-1	-1	1	-1	1	1	-1	1	1	1	1	-1	1	-1	1	-1	-1	-1	1	-1	-1	1	1	1
c29 -	1	1	-1	-1	-1	-1	-1	1	1	-1	-1	1	-1	1	1	-1	1	1	1	1	-1	1	-1	1	-1	-1	-1	1	-1	-1	1	1
c4	1	1	1	-1	-1	-1	-1	-1	1	1	-1	-1	1	-1	1	1	-1	1	1	1	1	-1	1	-1	1	-1	-1	-1	1	-1	-1	1
c31 -	1	1	1	1	-1	-1	-1	-1	-1	1	1	-1	-1	1	-1	1	1	-1	1	1	1	1	-1	1	-1	1	-1	-1	-1	1	-1	-1
c32 -	1	-1	1	1	1	-1	-1	-1	-1	-1	1	1	-1	-1	1	-1	1	1	-1	1	1	1	1	-1	1	-1	1	-1	-1	-1	1	-1
c30 -	1	-1	-1	1	1	1	-1	-1	-1	-1	-1	1	1	-1	-1	1	-1	1	1	-1	1	1	1	1	-1	1	-1	1	-1	-1	-1	1
c28 -	1	1	-1	-1	1	1	1	-1	-1	-1	-1	-1	1	1	-1	-1	1	-1	1	1	-1	1	1	1	1	-1	1	-1	1	-1	-1	-1
c26 -	1	-1	1	-1	-1	1	1	1	-1	-1	-1	-1	-1	1	1	-1	-1	1	-1	1	1	-1	1	1	1	1	-1	1	-1	1	-1	-1
c24 -	1	-1	-1	1	-1	-1	1	1	1	-1	-1	-1	-1	-1	1	1	-1	-1	1	-1	1	1	-1	1	1	1	1	-1	1	-1	1	-1
c22	1	-1	-1	-1	1	-1	-1	1	1	1	-1	-1	-1	-1	-1	1	1	-1	-1	1	-1	1	1	-1	1	1	1	1	-1	1	-1	1
c20	1	1	-1	-1	-1	1	-1	-1	1	1	1	-1	-1	-1	-1	-1	1	1	-1	-1	1	-1	1	1	-1	1	1	1	1	-1	1	-1
c18	1	-1	1	-1	-1	-1	1	-1	-1	1	1	1	-1	-1	-1	-1	-1	1	1	-1	-1	1	-1	1	1	-1	1	1	1	1	-1	1
c16	1	1	-1	1	-1	-1	-1	1	-1	-1	1	1	1	-1	-1	-1	-1	-1	1	1	-1	-1	1	-1	1	1	-1	1	1	1	1	-1
c14	1	-1	1	-1	1	-1	-1	-1	1	-1	-1	1	1	1	-1	-1	-1	-1	-1	1	1	-1	-1	1	-1	1	1	-1	1	1	1	1
c12	1	1	-1	1	-1	1	-1	-1	-1	1	-1	-1	1	1	1	-1	-1	-1	-1	-1	1	1	-1	-1	1	-1	1	1	-1	1	1	1
c10	1	1	1	-1	1	-1	1	-1	-1	-1	1	-1	-1	1	1	1	-1	-1	-1	-1	-1	1	1	-1	-1	1	-1	1	1	-1	1	1
c8	1	1	1	1	-1	1	-1	1	-1	-1	-1	1	-1	-1	1	1	1	-1	-1	-1	-1	-1	1	1	-1	-1	1	-1	1	1	-1	1
c6	1	1	1	1	1	-1	1	-1	1	-1	-1	-1	1	-1	-1	1	1	1	-1	-1	-1	-1	-1	1	1	-1	-1	1	-1	1	1	-1

MIMO STS TH UWB PPM L=1 using 32 chip h32dash03 spreading sequences First useful arriving ray (Partial Rake) Simulink simulation data for measured Eb/No in presence of 5 MAI at measured Eb/No of 3.15dB

Measured Eb/No (dB)	upper bound 95% confidence interval	Mean BER	lower bound 95% confidence interval
-10.796	0.52576	0.498	0.47024
-8.7956	0.49494	0.46533	0.43572
-6.7956	0.46799	0.44467	0.42135
-4.7956	0.47838	0.42733	0.37629
-2.7956	0.49211	0.43067	0.36922
-0.79564	0.48469	0.39267	0.30065
1.2044	0.45997	0.356	0.25203
3.2044	0.43734	0.31067	0.184
5.2044	0.42386	0.29333	0.16281
7.2044	0.40788	0.26133	0.11479

MIMO STS TH UWB PPM L=4 using 32 chip h32dash03 spreading sequences First four useful arriving rays (Partial Rake) Simulink simulation data for measured Eb/No in presence of 5 MAI at measured Eb/No of 3.15dB

Measured Eb/No (dB)	upper bound 95% confidence interval	Mean BER	lower bound 95% confidence interval
-10.796	0.48934	0.45333	0.41732
-8.7956	0.48862	0.43267	0.37672
-6.7956	0.48322	0.4	0.31678
-4.7956	0.46681	0.36333	0.25985
-2.7956	0.46428	0.334	0.20372
-0.79564	0.44855	0.30667	0.16479
1.2044	0.40383	0.26467	0.1255
3.2044	0.38327	0.23933	0.095392
5.2044	0.3568	0.214	0.071196
7.2044	0.31376	0.18533	0.056906

MIMO STS TH UWB PPM L=1 using 32 chip h32dash03 spreading sequences First useful arriving ray (Partial Rake) Simulink simulation data for measured Eb/No in presence of 10 MAI at measured Eb/No of 3.15dB

Measured Eb/No (dB)	upper bound 95% confidence interval	Mean BER	lower bound 95% confidence interval
-10.796	0.52115	0.48667	0.45218
-8.7956	0.52375	0.47933	0.43492
-6.7956	0.5166	0.462	0.4074
-4.7956	0.50704	0.44067	0.37429
-2.7956	0.49291	0.418	0.34309
-0.79564	0.47957	0.39133	0.30309
1.2044	0.45825	0.35733	0.25642
3.2044	0.45849	0.346	0.23351
5.2044	0.43638	0.31333	0.19028
7.2044	0.42318	0.284	0.14482

MIMO STS TH UWB PPM L=4 using 32 chip h32dash03 spreading sequences First four useful arriving rays (Partial Rake) Simulink simulation data for measured Eb/No in presence of 10 MAI at measured Eb/No of 3.15dB

Measured Eb/No (dB)	upper bound 95% confidence interval	Mean BER	lower bound 95% confidence interval
-10.796	0.49277	0.45067	0.40856
-8.7956	0.47978	0.42867	0.37755
-6.7956	0.47341	0.40067	0.32792
-4.7956	0.47641	0.37867	0.28093
-2.7956	0.46371	0.34267	0.22162
-0.79564	0.4516	0.314	0.1764
1.2044	0.43092	0.292	0.15308
3.2044	0.39584	0.25333	0.11082
5.2044	0.35443	0.224	0.093568
7.2044	0.32176	0.19333	0.064906

Appendix 22: Tabulation of the Theoretical Symbol Error Rate versus Expected SNR with no MAI for STS-TH-UWB-PPM system

Expected SNR (dB)	Actual SNR (dB)	Actual SNR	Symbol Error Rate (SER)
-34	20	100	0.494931
-32	22	158.4893192	0.493619
-30	24	251.1886432	0.491967
-28	26	398.1071706	0.489887
-26	28	630.9573445	0.487269
-24	30	1000	0.483974
-22	32	1584.893192	0.479828
-20	34	2511.886432	0.474612
-18	36	3981.071706	0.468051
-16	38	6309.573445	0.459803
-14	40	10000	0.449445
-12	42	15848.93192	0.436455
-10	44	25118.86432	0.4202
-8	46	39810.71706	0.399932
-6	48	63095.73445	0.3748
-4	50	100000	0.343913
-2	52	158489.3192	0.306482
0	54	251188.6432	0.26212
2	56	398107.1706	0.211359
4	58	630957.3445	0.156416
6	60	1000000	0.10193
8	62	1584893.192	0.0548406
10	64	2511886.432	0.0220146
12	66	3981071.706	0.00561852
14	68	6309573.445	0.000707245
16	70	10000000	0.0000293366
18	72	15848931.92	0.000000211319
20	74	25118864.32	0.0000000000956084

Appendix 23: Tabulation of Theoretical Symbol Error Rate versus Expected SNR with 5 MAI sources each with an actual SNR of 64dB (expected SNR of 10dB) for STS-TH-UWB-PPM system

Expected SNR (dB)	Actual SNR (dB)	Actual SNR of Target source 1	Actual SNR of each of the 5 MAI sources (dB)	Variance of all 5 MAI sources combined	N_f	Symbol Error Rate (SER)
-34	20	100	64	2.2655E-11	32	0.495511
-32	22	158.4893192	64	2.2655E-11	32	0.494349
-30	24	251.1886432	64	2.2655E-11	32	0.492886
-28	26	398.1071706	64	2.2655E-11	32	0.491045
-26	28	630.9573445	64	2.2655E-11	32	0.488727
-24	30	1000	64	2.2655E-11	32	0.485809
-22	32	1584.893192	64	2.2655E-11	32	0.482137
-20	34	2511.886432	64	2.2655E-11	32	0.477516
-18	36	3981.071706	64	2.2655E-11	32	0.471703
-16	38	6309.573445	64	2.2655E-11	32	0.464393
-14	40	10000	64	2.2655E-11	32	0.455209
-12	42	15848.93192	64	2.2655E-11	32	0.44368
-10	44	25118.86432	64	2.2655E-11	32	0.429236
-8	46	39810.71706	64	2.2655E-11	32	0.411187
-6	48	63095.73445	64	2.2655E-11	32	0.388735
-4	50	100000	64	2.2655E-11	32	0.360997
-2	52	158489.3192	64	2.2655E-11	32	0.327105
0	54	251188.6432	64	2.2655E-11	32	0.286412
2	56	398107.1706	64	2.2655E-11	32	0.238881
4	58	630957.3445	64	2.2655E-11	32	0.185736
6	60	1000000	64	2.2655E-11	32	0.130268
8	62	1584893.192	64	2.2655E-11	32	0.078322
10	64	2511886.432	64	2.2655E-11	32	0.0372766
12	66	3981071.706	64	2.2655E-11	32	0.0123866
14	68	6309573.445	64	2.2655E-11	32	0.00235528
16	70	10000000	64	2.2655E-11	32	0.000186874
18	72	15848931.92	64	2.2655E-11	32	0.000003746070000
20	74	25118864.32	64	2.2655E-11	32	0.000000008552740

Appendix 24: Tabulation of Theoretical Symbol Error Rate versus Expected SNR with 10 MAI sources each with an actual SNR of 64dB (expected SNR of 10dB) for STS-TH-UWB-PPM system

Expected SNR (dB)	Actual SNR (dB)	Actual SNR of Target source 1	Actual SNR of each of the 10 MAI sources (dB)	Variance of all 10 MAI sources combined	N_f	Symbol Error Rate (SER)
-34	20	100	64	4.531E-11	32	0.495929
-32	22	158.4893192	64	4.531E-11	32	0.494876
-30	24	251.1886432	64	4.531E-11	32	0.493549
-28	26	398.1071706	64	4.531E-11	32	0.491879
-26	28	630.9573445	64	4.531E-11	32	0.489776
-24	30	1000	64	4.531E-11	32	0.48713
-22	32	1584.893192	64	4.531E-11	32	0.483799
-20	34	2511.886432	64	4.531E-11	32	0.479608
-18	36	3981.071706	64	4.531E-11	32	0.474334
-16	38	6309.573445	64	4.531E-11	32	0.467701
-14	40	10000	64	4.531E-11	32	0.459364
-12	42	15848.93192	64	4.531E-11	32	0.448895
-10	44	25118.86432	64	4.531E-11	32	0.435765
-8	46	39810.71706	64	4.531E-11	32	0.419338
-6	48	63095.73445	64	4.531E-11	32	0.398859
-4	50	100000	64	4.531E-11	32	0.373475
-2	52	158489.3192	64	4.531E-11	32	0.342294
0	54	251188.6432	64	4.531E-11	32	0.30454
2	56	398107.1706	64	4.531E-11	32	0.259853
4	58	630957.3445	64	4.531E-11	32	0.208828
6	60	1000000	64	4.531E-11	32	0.153781
8	62	1584893.192	64	4.531E-11	32	0.0994755
10	64	2511886.432	64	4.531E-11	32	0.0529232
12	66	3981071.706	64	4.531E-11	32	0.0208818
14	68	6309573.445	64	4.531E-11	32	0.00518851
16	70	10000000	64	4.531E-11	32	0.000626279
18	72	15848931.92	64	4.531E-11	32	0.000024317600000
20	74	25118864.32	64	4.531E-11	32	0.000000157813000

Appendix 25: Plots of BER versus Eb/No for different spreading sequence sets with 95% confidence interval error bars for 5 and 10 MAI for STS-TH-UWB-PPM system

L=1 5 MAI BER versus measured Eb/No (dB) plots

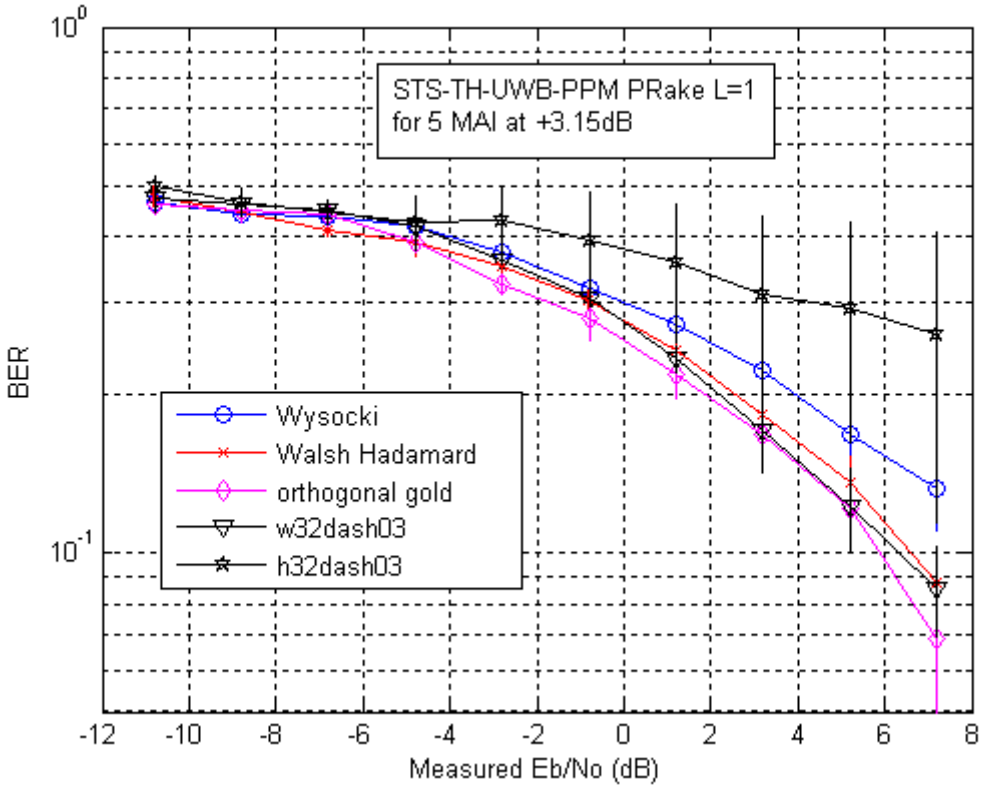

Figure A25-1: Comparison of performance of wysocki codes, orthogonal gold codes, w32dash03 codes, h32dash03 codes versus Walsh Hadamard codes in the presence of five MAI interferers at +3.15dB for L=1 of mean BER versus Measured Eb/No (dB) with 95% confidence intervals shown.

L=4 5 MAI BER versus measured Eb/No (dB) plots

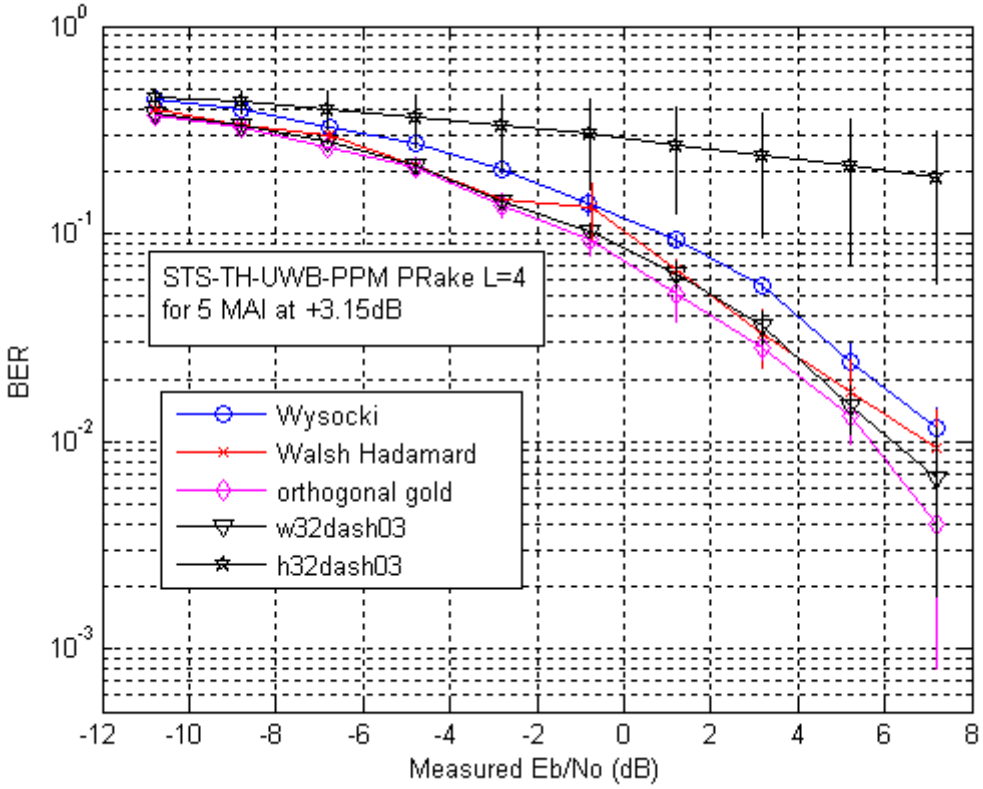

Figure A25-2: Comparison of performance of wysocki codes, orthogonal gold codes, w32dash03 codes, h32dash03 codes versus Walsh Hadamard codes in the presence of five MAI interferers at +3.15dB for L=4 of mean BER versus Measured Eb/No (dB) with 95% confidence intervals shown.

L=1 10 MAI BER versus measured Eb/No (dB) plots

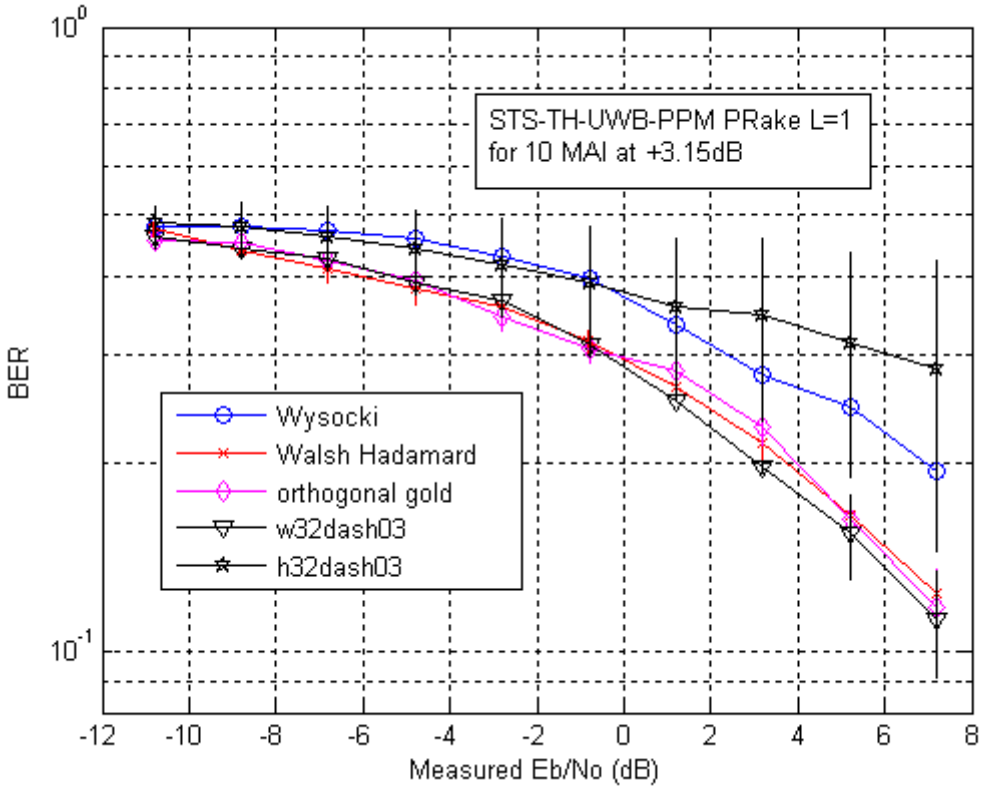

Figure A25-3: Comparison of performance of wysocki codes, orthogonal gold codes, w32dash03 codes, h32dash03 codes versus Walsh Hadamard codes in the presence of ten MAI interferers at +3.15dB for L=1 of mean BER versus Measured Eb/No (dB) with 95% confidence intervals shown.

L=4 10 MAI BER versus measured Eb/No (dB) plots

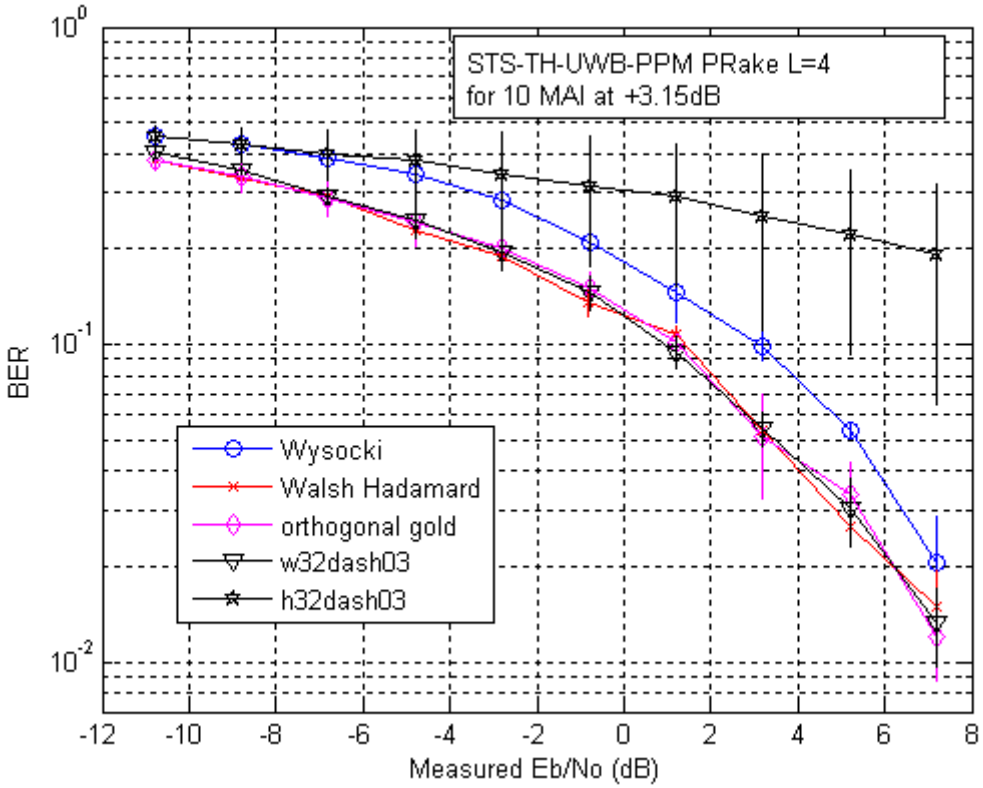

Figure A25-4: Comparison of performance of wysocki codes, orthogonal gold codes, w32dash03 codes, h32dash03 codes versus Walsh Hadamard codes in the presence of ten MAI interferers at +3.15dB for L=4 of mean BER versus Measured Eb/No (dB) with 95% confidence intervals shown.

Appendix 26: Relationship between Expected SNR and measured Eb/No for simulations using database excell spreadsheet

The relationship between Expected SNR (based on the value used in the simulations for the gain) and the measured Eb/No taken across a single branch of the antenna is given by the expression:

$$Expected(SNR) = measured\ \left(\frac{E_b}{N_0}\right) + 30 \quad \text{dB}$$

The relationship between Expected SNR (based on the value used in the simulations for the gain) and the measured Eb/No taken across a two branches of the antenna is given by the expression:

$$Expected(SNR) = measured\ \left(\frac{E_b}{N_0}\right) + 27 \quad \text{dB}$$